

**EXPERIMENTAL INVESTIGATION OF LOCAL
DISTRIBUTION OF HEAT TRANSFER AND FLUID FLOW
CHARACTERISTICS OF IMPINGING SLOT AIR JET**

**A Thesis
Submitted by**

ADIMURTHY M

For the award of the degree of

DOCTOR OF PHILOSOPHY

In

Mechanical Engineering

Under the guidance of

Dr. VADIRAJ V KATTI,

M Tech. Ph.D. (I I T, Bombay)

Principal, KLS Vishwanathrao Deshpande Institute of Technology, Haliyal



DEPARTMENT OF MECHANICAL ENGINEERING

**SRI SIDDHARTHA INSTITUTE OF TECHNOLOGY
TUMAKURU**

**SRI SIDDHARTHA ACADEMY OF HIGHER
EDUCATION**

(Declared U/S 3 of the UGC Act, 1956)

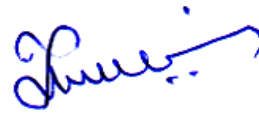
AGALAKOTE, TUMAKURU

2021

SUPERVISOR'S CERTIFICATE

Certified that this thesis titled "**Experimental Investigation of Local Distribution of Heat Transfer and Fluid Flow Characteristics of Impinging Slot Air Jet**" is the bonafide work of Mr. **Adimurthy M(12PH1ME001)** who has carried out this research work under my supervision.

Certified further, that to the best of my knowledge the work reported herein does not form part of any other thesis or dissertation on the basis of which a degree or award was conferred on an earlier occasion on this or to any other candidate.



Dr. Vadiraj V Katti

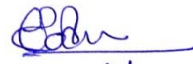
Research supervisor,
Principal,
KLS Vishwanathrao Deshpande
Institute of Technology,
Haliyal, Karnataka

Place: Haliyal

Date: 14-07-2021

DECLARATION

I declare that the thesis entitled **“Experimental Investigation of Local Distribution of Heat Transfer and Fluid Flow Characteristics of Impinging Slot Air Jet”** submitted by me for the award of the degree of Doctor of Philosophy under the guidance of **Dr. Vadiraj V Katti**, Principal, KLS Vishwanathrao Deshpande Institute of Technology, Haliyal, Karnataka, and has not formed the basis earlier for acquiring any degree, diploma, associate ship, fellowship in this university or similar institution of higher learning.



Adimurthy M

(12PH1ME001)

Research Scholar,

Department of Mechanical Engineering,

Sri Siddhartha Institute of Technology,

Kunigal Road, Maralur, Tumakuru,

Karnataka, India.

ABSTRACT

Jet impingement cooling has received considerable attention due to its inherent characteristics of high heat transfer rate. Impinging flow devices allow for short flow paths and relatively high rate of cooling from comparatively small surface area. Few industrial processes that employ impinging jets are drying of food products, textiles, films and papers, processing of some metals and glass, cooling of gas turbine blades and outer wall of the combustion chamber, cooling of electronic equipment, etc. Air will continue to be used as the working fluid due to its low cost, easy availability and reliability.

The requirement for increased gas turbine engine performance has led to the use of much higher turbine entry temperature. The higher gas temperatures require active cooling of the turbine blade using compressor bleed air. Heat transfer enhancement by jet impingement has significant potential to increase the local heat transfer coefficient. Arrays of impinging jets are one of the methods currently used to reduce the blade temperature on the mid-chord and leading-edge regions. The present study focuses on one of the thermal issues of uniformity of distribution of heat transfer. The influence of various geometric and flow parameters of the impingement system on the local distribution of heat transfer coefficients are investigated. The local heat transfer characteristics are studied experimentally using a thin foil heater and an infrared thermal imaging technique.

The local heat transfer and fluid flow distribution on smooth flat surface impinged by a single slot air jet is studied for different jet-to-plate distances ($0.5D_h-10 D_h$) and Reynolds numbers (2500-20000). Semi-empirical correlations for local heat transfer coefficients in the stagnation region are obtained. Further, local heat transfer enhancements on rough flat surface (detached ribs) impinged by a single slot air jet is examined for different geometric parameters of ribs at various jet-to-plate distances. The influence of confinement and inclination angle of the jet with reference to impingement plate on the fluid and thermal characteristics of the single slot air jet are studied experimentally. Finally, the combined effect of confinement and surface roughness is evaluated for the local distribution of the heat transfer and the pressure on the impingement plate.

ACKNOWLEDGEMENT

I thank Shri Siddhartha University (SSU), Tumakuru and Shri Siddhartha Institute of Technology (SSIT), Tumakuru in particular, the Department of Mechanical Engineering, for giving me an opportunity to do my Ph.D. and the support extended.

I would like to express my utmost gratitude to my beloved supervisor Dr. Vadiraj V Katti, who has always been a source of inspiration for me. I consider myself a privileged one, of his research students. Words are inadequate to express appreciation for his parenthood support, guidance and encouragement during this work. His worthy comments, suggestions and valuable guidance successfully enabled and improved my research ability. Without his generous help and support, it was not possible for me to complete this work. I shall ever remain indebted to him. I also thank Dr. Vadiraj V Katti's family for their hospitality and moral support during my research period.

It is my privilege to thank Dr. K N Harishkumar, Head, Department of Mechanical Engineering and Member, Research Progress Review committee for his support and for providing the essential facilities during the research period.

I extend my sincere thanks to Dr. Abdul Shariff, Principal, P.A College of Engineering, Mangaluru for being a member of the Research Progress Review committee and devoting his precious time in providing valuable suggestions and encouragement on this work.

My thanks are also due to Dr. M. Siddappa, Dean, SSIT, Tumakuru for the suggestions and support provided from time to time during my research tenure at SSIT.

I am greatly indebted to Sri M. B. Patil President, BLDE Association, Vijayapura (Karnataka) for his encouragement in pursuing my research work. Profound and heartfelt thanks are due to Dr. V. P. Huggi, former Principal and Dr. Atul Ayare, Principal, BLDEA's Vachana Pitamaha DR. P.G Halakatti college of Engineering and Technology, Vijayapura for providing the infrastructure and facilities for carrying out my research work at the campus otherwise it wouldn't have happened.

I would also like to express my gratitude to my colleagues Dr. M I Sakri, Dr.B.R. Hosamani, S.D. Kulkarni, S.B Koulagi, P.S Kori, and V.V Nagathan for their support and companionship.

I am also thankful to all faculty members and non-teaching staff of the department of Automobile and Mechanical Engineering departments at BLDEA's Vachana Pitamaha DR. P.G Halakatti college of Engineering and Technology, Vijayapura for their support.

I must acknowledge the help rendered by my students Ashwini Tamagond, Pavankumar Sureban and Venkatesh Dinni at various stages of my research work.

I owe special thanks to my parents, who have been my role models in striving for success through hard work and taught me that Honesty is the best policy of life. Words fail to express appreciation to my wife Sow. Nidhi Murthy (Savita) who has always been an endless source of love, and support who single-handedly managed all the chores of family and work, making me free to focus on my work without any worry. Her patience is extremely appreciable. I cannot finish without expressing my heartiest feelings to my son Dr. Akshay M.A and daughter Dr. Akshata M.A for their love and support.

I must also thank my younger brother Sreedharamurthy and family, my younger sister Satyalakshmi and her family who always received me with full affection and love whenever I visited Tumakuru on my work.

Heartfelt thanks to the entire Meda family, brothers, sisters and their family members for their constant encouragement

Finally, I would like to thank everyone who was important and contributed directly or indirectly to the successful realization of this thesis. I express my apologies as I could not mention everyone personally by name.



Adimurthy M

TABLE OF CONTENTS

Serial No.	Particulars	Page No.
	Table of Contents	VII
	List of figures	XI
	List of tables	XIX
	Nomenclature	XX
1	Introduction	1
	1.1 Introduction	1
	1.1.1 Cooling of gas turbine blades	1
	1.1.2 Combustion chamber wall cooling	4
	1.1.3 Cooling of electronic components	5
	1.2 Classification of impinging submerged jets	5
	1.2.1 Structure of free jet	6
	1.2.2 Structure of impinging jet	7
	1.3 Scope of the present work	8
	1.4 Organization of the report	9
2	Literature review on heat transfer and fluid flow distribution of impinging air jets	10
	2.1 Heat transfer and fluid flow over a smooth flat plate interacting with an unconfined single jet	10
	2.2 Heat transfer and fluid flow over a rough flat plate interacting with an unconfined single jet	20
	2.3 Heat transfer and fluid flow over a smooth flat plate interacting with a confined single jet	31
	2.4 Heat transfer and fluid flow over a rough flat (Ribbed) plate interacting with a confined single jet	35
	2.5 Conclusions drawn from literature review	39
	2.6 Objectives of the current work	42
3	Local distribution of wall static pressure and heat transfer on a smooth flat surface due to an impinging slot air jet	44
	3.1 Introduction	44

3.2	Experimental set up	45
3.3	Data Reduction	49
3.4	Results and discussions	50
3.4.1	Validation of the experiment set up	50
3.4.2	Free jet characteristics of unconfined Single slot jet	51
3.4.3	Structure details of the jet when impinges on a target surface	52
3.4.4	Centerline velocity profiles of a turbulent slot jet	52
3.4.5	Local distributions of C_p due to unconfined jet impingement	54
3.4.6	Heat transfer characteristics of an unconfined single slot jet orthogonally impinging over a smooth flat surface	57
3.5	Conclusions	59
4	Local distribution of wall static pressure and heat transfer on a rough(ribbed)surface interacting with an orthogonally impinging slot air jet	61
4.0	Introduction	61
4.1	Experimental setup and methodology	64
4.2	Results and discussions	65
4.2.1	C_p over the target surface mounted with a 4mm detached rib for J2P spacing (Z/D_h) at $Re=2500$ to 20000.	65
4.2.2	C_p over the target surface mounted with a 6 mm detached rib for J2P spacing (Z/D_h) at $Re=2500$ to 20000.	65
4.2.3	C_p over the target surface mounted with a 8 mm detached rib for J2P spacing (Z/D_h) at $Re=2500$ to 20000.	69
4.2.4	C_p on the “Target plate” mounted with a 12 mm detached rib for J2P spacing (Z/D_h) at $Re=2500$ to 20000.	71
4.2.5	Variation of stagnation point C_p on the “Target plate” mounted with detached rib for J2P spacing (Z/D_h) 0.5 to 10, at $Re=2500$ to 20000.	72
4.3	Heat transfer between a rough surface and a slot jet	85

4.4	Comparison of “heat transfer” behavior of the jet on smooth and rough surfaces	98
4.5	Enhancement in the “Average Nusselt number” ($Nu_{2.0}$) with Ribbed surface.	111
4.6	Conclusions	113
5	Influence of confinement on local C_p and Nu distribution	115
5.1	Introduction	115
5.2	Literature review	115
5.3	Objectives of the experiments	119
5.4	Experimental set up and methodology for fluid flow characteristics study	119
5.5	Data reduction	121
5.6	Results and discussion	121
5.6.1	Independency test	121
5.6.2	Lateral Distribution of C_p on a flat surface interacting with a Slot air Jet.	121
5.6.3	Influence of confinement ratio on the C_p	127
5.7	Experimental set up and methodology for heat transfer characteristics studies	129
5.7.1	Methodology for heat transfer characteristics study with a confined slot jet.	129
5.7.2	Data reduction	131
5.7.3	Results and discussion	131
5.7.3.1	Heat transfer estimation for the target plate	131
5.7.3.2	Heat transfer characteristics of an unconfined slot Jet	133
5.7.3.3	Heat transfer characteristics of a confined slot Jet: Effect of the nozzle to target spacing on Heat transfer distribution	135
5.7.3.4	Effect of confinement ratio (L_c/D_h) on Heat transfer distribution	135
5.8	Conclusions	144

6	Influence of confinement on local C_p and heat transfer between a rough(ribbed) flat surface and a slot-air jet	144
6.1	Introduction	144
6.2	Literature review	144
6.2.1	Objectives of the work	145
6.3	Experimental set up and methodology	146
6.3.1	Data reduction	146
6.3.2	Validation of the experimental set up	146
6.4	Results and discussion	147
6.4.1	Rough surface flow study: Influence of Z/D_h on WSP distribution for various “Reynolds number” along the “streamwise direction” for 4mm rib and confinement ratio (L_c/D_h) of 6.8.	147
6.4.2	Influence of Z/D_h on “wall static pressure” distribution for various “Reynolds number” along the “streamwise direction” for 4mm rib and confinement ratio (L_c/D_h) of 10.2	149
6.4.3	Influence of Z/D_h on “wall static pressure” distribution for various “Reynolds number” along the “streamwise direction” for 4mm rib and confinement ratio (L_c/D_h) of 13.6	150
6.4.4	Influence of Z/D_h on “wall static pressure” distribution for various “Reynolds number” along the “streamwise direction” for 6mm rib and confinement ratio (L_c/D_h) of 6.8	151
6.4.5	Influence of Z/D_h on “wall static pressure” distribution for various “Reynolds number” along the “streamwise direction” for 6mm rib and confinement ratio (L_c/D_h) of 10.2	152
6.4.6	Influence of Z/D_h on “wall static pressure” distribution for various “Reynolds number” along the “streamwise direction” for 6mm rib and confinement ratio (L_c/D_h) of 13.6	153

		XI
	6.4.7 Influence of J2P spacing on stagnation point wall static pressure for different Rib and confinement configurations.	154
6.5	Comparison of fluid flow characteristics of confined smooth and confined rough surface	156
	6.5.1 Influence surface roughness and confinement on wall static pressure distribution at $Re=2500$	156
	6.5.2 Influence of confinement ratio on “stagnation point wall static pressure”	158
6.6	Heat transfer study on a Confined rough surface with 4mm rib	161
6.7	Heat transfer study on a Confined rough surface with 6 mm rib	165
6.8	Influence of confinement ratio on stagnation “Nusselt number”	168
6.9	Correlations for stagnation “Nusselt number” of $Re=2500$	174
6.10	conclusions	174
7	Conclusions drawn from the work	175
	Scope for the Future work	179
8	Appendices	
	A1 Calibration of emissivity of the painted surface of target plate	180
	A2 Estimation of energy loss in thin foil heater technique with jet impinging on one surface	182
	A3 Uncertainty analysis of heat transfer and flow parameters	185
9	Bibliography	189
10	List of publications	197

LIST OF FIGURES

Fig. No.	Title	Page No.
1.1	Variation in the turbine entry temperature over recent years (Han <i>et al.</i> , 2000)	2
1.2	Some methods of turbine blade cooling (Colladay, 1975)	3
1.3	Turbine cooling effectiveness (Van Treuren, 1994)	4

1.4	Combustion chamber wall cooling (Gao, 2001)	4
1.5	Structure of submerged jet (Viskanta, 1993)	6
2.1	Correlation of heat transfer coefficients at stagnation point (Gardon, Akfirat 1966)	12
2.2	Lateral variation of local heat transfer coefficients between a plate and an impinging 2-dimensional jet (Gardon, Akfirat 1966)	12
2.3	Combined plot of dimensionless heat transfer coefficient, mean and RMS pressure, and near-wall fluctuating velocity variance distributions on impingement surface for the $Y_n = D_h \frac{1}{4} 0:5$ slot jet nozzle along the minor axis of the nozzle, at centerline, $z/D_h = 0:00$.	14
2.4	Dependence of wall shear stress on Reynolds number for H/D close to 4.0. Actual H/D and Re given in figure.	16
2.5	Variation of velocity and turbulence along the center line of a 2-D jet (Gardon, Akfirat 1966)	21
2.6	Distributions of mean velocity and RMS velocity fluctuations for $Re = 11000$ (Lytle and Webb, 1994)	22
2.7	Radial variations of the Nusselt number (Lytle and Webb, 1994)	23
2.8	Effect of nozzle diameter on stagnation point Nusselt number (Lee <i>et al.</i> , 2004)	24
2.9	Schematic of rough surfaces (Hansen and Webb, 1993)	25
2.10	Variation in average Nusselt number with Reynolds number for rough surfaces (Hansen and Webb, 1993)	26
2.11	Variation in \bar{Nu} as a function of z/d (Hansen and Webb, 1993)	26
2.12	Schematic diagram of the rough surface and plate with its heating pad (Chakroun <i>et al.</i> , 1998)	27
2.13	Distribution of local Nusselt number for $Re = 6500$ (Chakroun <i>et al.</i> , 1998)	28
3.1 a)	Experimental setup for measuring the heat transfer coefficients	47
3.1 b)	Experimental setup for measuring the wall static pressure	47
3.2	Experimental set up for Free jet characteristics study	47
3.3 (a)	Target plate arrangement for heat transfer experiment	48

3.3 (b)	Target plate arrangement for wall static pressure measurement	48
3.4	Influence of Re on C_{pat} at various lateral positions from SP for $Z/D_h=4.0$	49
3.5	WSP variation along with the plate for the various J2P spacing (Z/D_h) at $Re=5000$	49
3.6 (a)	comparison of results with the published work on pressure distribution	51
3.6 (b)	comparison of results with the published work on “Nusselt number” distribution	51
3.7	Structure of submerged jet (Viskanta, 1993)	53
3.8	Normalized centerline velocity profiles of a free jet at various Reynolds number	53
3.9	Variation in the velocity profiles of an unconfined single turbulent slot jet with a nozzle to probe spacing at $Re=10000$	55
3.10	Influence of Re on C_{pat} at various lateral positions from “stagnation point” for $Z/D_h=4.0$	55
3.11	wall static pressure distribution along the width of the plate for the various J2P spacing (Z/D_h) at $Re=5000$	56
3.12(a)	Influence of Re on C_{p0} at the various J2P spacing distances	56
3.12(b)	Influence of Z/D_h on C_{p0} at the various J2P spacing distances	57
3.13	lateral Variation of the Nu for $Z/D_h=0.5$ at various Reynolds number	58
3.14	Distribution of Normalized Nu in the stagnation region for $Z/D_h=0.5$ at different Re	58
3.15	Comparison of the Normalized Nusselt number data from the expt. and from the correlation developed	59
3.16	Distribution of Normalized “Nusselt number” (Nu/Nu_0) in the “stagnation region” for $Z/D_h=1.0$ at different Re	59
3.17	Comparison of the Normalized “Nusselt number” (Nu/Nu_0) from the expt. and the from the correlation developed for $Z/D_h=1.0$	60
4.1	Details of the detached rib (representative)	65
4.2	Details of the “Target plate” with detached rib mounted	65
4.3	wall static pressure variation along the plate for the various J2P	67

	spacing (Z/D_h) at $Re=2500$ to 20000 for Rib size= 4mm	
4.4	wall static pressure variation on the plate at various J2P spacing(Z/D_h) at $Re=2500$ to 20000 for Rib size= 6mm	69
4.5	wall static pressure variation on the plate at various J2P spacing(Z/D_h) at $Re=2500$ to 20000 for Rib size= 8mm	70
4.6	wall static pressure variation on the plate at various J2P spacing(Z/D_h) at $Re=2500$ to 20000 for Rib size= 12mm	72
4.7	Variation of Cp_0 for the different J2P spacing at various Reynolds number for different Rib configuration	73
4.8	wall static pressure variation along the plate for the various J2Pspacing(Z/D_h) at $Re=2500$ for different rib size	75
4.9	wall static pressure variation along the plate for the various J2Pspacing(Z/D_h) at $Re=5000$ for different rib size	77
4.10	wall static pressure variation along the plate for the various J2Pspacing(Z/D_h) at $Re=7500$ for different rib size	78
4.11	wall static pressure variation along the plate for the various J2Pspacing(Z/D_h) at $Re=10000$ for different rib size	79
4.12	wall static pressure variation along the plate for the various J2Pspacing(Z/D_h) at $Re=12500$ for different rib size	80
4.13	wall static pressure variation along the plate for the various J2Pspacing(Z/D_h) at $Re=15000$ for different rib size	81
4.14	wall static pressure variation along the plate for the various J2Pspacing(Z/D_h) at $Re=17500$ for different rib size	82
4.15	wall static pressure variation along the plate for the various J2Pspacing(Z/D_h) at $Re=20000$ for different rib size	83
4.16	Variation of Cp_0 for the different J2P spacing at various Reynolds number and different Rib configurations	85
4.17	Variation of the Nusselt number along the length of the plate for the different J2P spacing (Z/D_h) at $Re =2500$ to 20000 for Rib size= 4mm	87
4.18	Variation of Nu along with the length of the plate at different Reynolds numbers for $Z/D_h=0.5$ to 10 for Rib size= 4mm	89
4.19	Variation of the Nu along the length of the plate for the different	90

	J2P spacing (Z/D_h) at $Re = 2500$ to 20000 for Rib size = 6mm	
4.20	Variation of Nu along with the length of the plate at different Reynolds numbers for $Z/D_h = 0.5$ to 10 for Rib size = 6mm	91
4.21	Variation of the Nu along the length of the plate for the different J2P spacing (Z/D_h) at $Re = 2500$ to 20000 for Rib size = 8mm	93
4.22	Variation of Nu along with the length of the plate at different Reynolds numbers for $Z/D_h = 0.5$ to 10 for Rib size = 8mm	95
4.23	Variation of the Nu along the length of the plate for the different J2P spacing (Z/D_h) at $Re = 2500$ to 20000 for Rib size = 12mm	96
4.24	Variation of Nu along with the plate at different Reynolds numbers for $Z/D_h = 0.5$ to 10 for Rib size = 12mm	97
4.25	Variation of stagnation point Nu for the different J2P spacing at various Reynolds number for different Rib sizes	98
4.26	Variation of the Nu along with the plate for the different J2P spacing (Z/D_h) at $Re = 2500$ for different sizes	100
4.27	Variation of the Nu along with the plate for the different J2P spacing (Z/D_h) at $Re = 5000$ for different sizes	101
4.28	Variation of the Nu along with the plate for the different J2P spacing (Z/D_h) at $Re = 5500$ for different sizes	103
4.29	Variation of the Nu along with the plate for the different J2P spacing (Z/D_h) at $Re = 10000$ for different sizes	104
4.30	Variation of the Nu along with the plate for the different J2P spacing (Z/D_h) at $Re = 12500$ for different sizes	105
4.31	Variation of the Nu along with the plate for the different J2P spacing (Z/D_h) at $Re = 15000$ for different sizes	107
4.32	Variation of the Nu along with the plate for the different J2P spacing (Z/D_h) at $Re = 17500$ for different sizes	108
4.33	Variation of the Nu along with the plate for the different J2P spacing (Z/D_h) at $Re = 20000$ for different sizes	109
4.34	Variation of “stagnation point” “Nusselt number” for the different J2P spacing at various Rib sizes for particular “Reynolds number”	111
4.35	Variation of average $Nu_{2,0}$ with Z/D_h for different ribs at $Re = 2500$	112
4.36	Variation of average $Nu_{2,0}$ with Z/D_h for different ribs at $Re = 10000$	112

5.1	Details of the confinement plate(sample)	120
5.2	Details of mounting the confinement plate at nozzle exit	120
5.3	Variation of C_{p0} with Reynolds number at $Z/D_h=0.5$.	121
5.4	Local C_p distribution along the streamwise direction at Reynolds number of 10000 for the unconfined jet.	123
5.5	Effect of the Z/D_h on lateral distribution of C_p for confinement ratio $L_c/D_h=6.8$ at $Re=10000$	124
5.6	Effect of the Z/D_h ratio on pressure distribution for confined jet size $L_c/D_h=10.2$.	124
5.7	Effect of the Z/D_h ratio on pressure distribution for confined jet size $L_c/D_h=13.6$	125
5.8	Effect of the Z/D_h ratio on pressure distribution for confined jet size $L_c/D_h=17.0$	125
5.9	Effect of the Z/D_h ratio on pressure distribution for confined jet size $L_c/D_h=20.4$	126
5.10	Effect of the Z/D_h ratio on pressure distribution for confined jet size $L_c/D_h=27.2$	126
5.11	Local wall static pressure distribution for $Z/D_h = 0.5$ at $Re=10000$	127
5.12	Local wall static pressure distribution for $Z/D_h = 1.0$ at $Re=10000$	128
5.13	Local wall static pressure distribution for $Z/D_h = 2.0$ at $Re=10000$	128
5.14	Experimental set up for Heat transfer distribution on Confined Slot Air Jet.	129
5.15	Image of Experimental Set Up for Heat Transfer studies	130
5.16	Image of set up showing the position of Slot Jet, Target Plate, and IR Camera.	130
5.17	Sample IR image taken at $Z/D_h=0.25$, $L_c/D_h=6.8$ & Re of 10000.	130
5.18	Sample IR image taken at $Z/D_h=0.25$, $L_c/D_h=27.23$ & Re of 10000.	131
5.19	Local heat transfer distribution for $Z/D_h=0.25-8.0$ at $Re=10000$ and $L_c/D_h=0.0$	133
5.20	Effect of the Z/D_h ratio on Local heat transfer distribution for Confined Slot Jet size $L_c/D_h=6.8$ to $L_c/D_h=10.2$ at $Re=10000$	135
5.21	Effect of the L_c/D_h ratio on Local heat transfer distribution for	136

	Confined Slot air Jet at Re 10000 and Z/D_h at 0.25.	
5.22	Effect of the L_c/D_h ratio on Local heat transfer distribution for Confined Slot air Jet at Re 10000 and Z/D_h at 0.5	137
5.23	Effect of the L_c/D_h ratio on Local heat transfer distribution for Confined Slot air Jet at Re 10000 and Z/D_h at 1.0	138
5.24	Effect of the L_c/D_h ratio on Local heat transfer distribution for Confined Slot air Jet at Re 10000 and Z/D_h at 2.0	139
5.25	Effect of the L_c/D_h ratio on Local heat transfer distribution for Confined Slot air Jet at Re 10000 and Z/D_h at 4.0	140
5.26	Effect of the L_c/D_h ratio on Local heat transfer distribution for Confined Slot air Jet at Re 10000 and Z/D_h at 6.0	141
5.27	Effect of the L_c/D_h ratio on Local heat transfer distribution for Confined Slot air Jet at Re 10000 and Z/D_h at 8.0	142
5.28	Variation of Stagnation Point Pressure and Nusselt Number with Confinement ratio and jet to plate distance at $Re = 10000$	143
5.29	Variation of Stagnation Point Pressure and Nusselt Number with and jet to plate distance and Confinement ratio at $Re = 10000$	143
6.1(a)	Comparison of current results with the results of Akansu (2008)	147
6.1(b)	Comparison of current results with the results of Nirmal <i>et al.</i> (2011)	147
6.2	Variation of wall static pressure along streamwise direction for various Z/D_h at Reynolds number 2500 to 20000	148
6.3	Variation of wall static pressure along the streamwise direction of various Z/D_h at Reynolds number 2500 to 20000 for 4mm rib and $L_c/D_h=10.2$.	149
6.4	Variation of wall static pressure along the streamwise direction of various Z/D_h at Reynolds number 2500 to 20000 for 4mm rib and $L_c/D_h=13.6$.	151
6.5	Variation of wall static pressure along the streamwise direction of various Z/D_h at Reynolds number 2500 to 20000 for 4mm rib and $L_c/D_h=6.8$	152
6.6	Variation of wall static pressure along the streamwise direction of various Z/D_h at Reynolds number 2500 to 20000 for 6mm rib	153

and $L_c/D_h=10.2$.

- 6.7** Variation of wall static pressure along the streamwise direction of various Z/D_h at Reynolds number 2500 to 20000 for 6mm rib and $L_c/D_h=13.6$. 154
- 6.8** Variation of Cp_0 for the different J2P spacing at various Reynolds number for a rough surface. 156
- 6.9** Comparison of wall static pressure of different width and confinement ratios Influence of Confinement on the smooth and rough surface (4mm rib) 157
- 6.10** Effect of confinement on the wall static pressure coefficient over the smooth and rough surface (4mm rib) at $Re =2500$ for various J2P distances 158
- 6.11** Influence of confinement ratio on stagnation point wall static pressure with 4 mm rib at various Reynolds numbers 160
- 6.12** Lateral variation of Nusselt number for the different J2P spacing (Z/D_h) at $Re =2500$ to 20000 for confined rough surface (4mm rib, $L_c/D_h=6.8$) 162
- 6.13** Lateral distribution of Nusselt number for the different J2P spacing (Z/D_h) at $Re =2500$ to 20000 for confined rough surface (4mm rib, $L_c/D_h=10.2$) 163
- 6.14** Lateral distribution of Nusselt number for the different J2P spacing (Z/D_h) at $Re =2500$ to 20000 for confined rough surface (4mm rib, $L_c/D_h=13.6$) 164
- 6.15** Lateral variation of Nusselt number for the different J2P spacing (Z/D_h) at $Re =2500$ to 20000 for confined rough surface (6mm rib, $L_c/D_h=6.8$) 165
- 6.16** Lateral distribution of Nusselt number for the different J2P spacing (Z/D_h) at $Re =2500$ to 20000 for confined rough surface (6mm rib, $L_c/D_h=10.2$) 166
- 6.17** Lateral distribution of Nusselt number for the different J2P spacing (Z/D_h) at $Re =2500$ to 20000 for confined rough surface (6mm rib, $L_c/D_h=13.6$) 167
- 6.18** Influence of confinement ratio on Nu_0 at various Reynolds 169

	numbers with 4mm rib and 6mm rib	
6.19	Comparison of the lateral variation of Nu for different rib and confinement combinations at $Re=5000$	170
6.20	Comparison of the lateral variation of Nu for different rib and confinement combinations at $Re=10000$	171
6.21	Comparison of the lateral variation of Nu for different rib and confinement combinations at $Re=15000$	172
6.22	Comparison of the lateral variation of Nu for different rib and confinement combinations at $Re=20000$	173

LIST OF TABLES

Table No.	Title	Page No.
4.1	Enhancement in the average heat transfer coefficient with 6mm rib at $Re = 2500$ and with 4 mm rib at $Re = 10000$	122
5.1	Variation of Nu with the confinement (%) at $Z/D_h = 6.0$	132
5.2	Variation of Nu with the confinement (%) at $Z/D_h = 0.25$	135
5.3	Variation of Nu with the confinement (%) at $Z/D_h = 0.5$	137
5.4	Variation of Nu with the confinement (%) at $Z/D_h = 1.0$	138
5.5	Variation of Nu with the confinement (%) at $Z/D_h = 2.0$	139
5.6	Variation of Nu with the confinement (%) at $Z/D_h = 4.0$	140
5.7	Variation of Nu with the confinement (%) at $Z/D_h = 6.0$	141
5.8	Variation of Nu with the confinement (%) at $Z/D_h = 8.0$	142
6.1	Values of c_1 to be used in equation (6.1)	174
6.2	Values of c_1 to be used in equation (6.2)	174

NOMENCLATURE

<i>A</i>	area of the smooth surface	(m^2)
<i>a₁</i>	Ares of the venturi meter pipe	(m^2)
<i>a₂</i>	Ares of the venturi meter throat	(m^2)
<i>b</i>	slot width	(m)
<i>D_h</i>	hydraulic diameter of jet = $(4 * \text{Area of the jet}) / \text{perimeter of the jet}$	(m)
<i>d</i>	diameter of a circular jet	(m)
<i>g</i>	Acceleration due to gravity	(m/sec^2)
<i>H</i>	height of the nozzle/jet	(m)
<i>h or HTC</i>	Heat transfer coefficient	(W/m^2k)
<i>I</i>	current supplied	$(amperes)$
<i>V</i>	Voltage supplied	$(volts)$
<i>J2P</i>	Jet to plate	
<i>k</i>	thermal conductivity	(W/mK)
<i>C_p</i>	wall static pressure coefficient $\left(\frac{P - P_{\infty}}{0.5 \rho \bar{V}^2} \right)$	
<i>SP</i>	stagnation point	
<i>c_{WSP}</i>	coefficient of wall static pressure	
<i>SPWSP</i>	stagnation point wall static pressure	
<i>C_{p0}</i>	Coefficient of pressure at the stagnation point	
<i>l</i>	nozzle length	(m)
<i>Nu</i>	Nusselt number based on hydraulic diameter of the slot jet	
<i>Nu₀</i>	stagnation point Nusselt number(SP <i>Nu</i>)	
<i>P</i>	absolute wall static pressure	(Pa)
<i>P_o</i>	absolute wall static pressure at the stagnation point	(Pa)
<i>P_∞</i>	Atmospheric pressure	(Pa)
Δp	wall static pressure at any distance from stagnation point	(Pa)
Δp_o	wall static pressure at stagnation point	(Pa)
<i>PCR</i>	Potential core region	
<i>q_c</i>	heat flux transferred to the jet	(W/m^2)
<i>q_j</i>	heat flux imposed to the target plate, (VI / A)	(W/m^2)

q_l	Loss of heat flux, from target plate	(W/m^2)
$q_{r(f)}$	Radiation losses of heat at the front side of the target plate	(W/m^2)
$q_{r(b)}$	heat lost by radiation at the back side of the target plate	(W/m^2)
q_n	heat lost by natural convection at the back side of target plate	(W/m^2)
Re_{jet}	Reynolds number based on hydraulic diameter $\left(\frac{\rho U_o D_h}{\mu} \right)$	
U_0	Average jet velocity,	m/min
r	Radial distance from the stagnation point	(m)
T_{jet}	jet air temperature	(K)
T_x	Temperature of the Target plate at given stream wise location	(K)
V	Potential difference between the taps on the target surface	(v)
x	stream wise distance from the “stagnation point”	(m)
Z	jet-to-plate (Nozzle to plate) distance	(m)

Greek Symbols:

ε_b	emissivity of target surface facing the infrared camera	
ε_f	emissivity of target surface facing the jet	
κ	kinematic momentum flux of jet $(0.153\pi d^2 \overline{V^2})$	m^4/s^2
μ	coefficient of dynamic viscosity	$Pa \cdot s$
ν	kinematic viscosity of jet fluid	m^2 / s
ρ	density of air at supply pressure	kg/m^3

CHAPTER 1

1.1 Introduction:

Impinging jets have received considerable research attention due to their inherent characteristics of high rates of heat transfer. Such impinging flow devices allow for short flow paths on the surface with relatively high heat transfer rates. The jet impingement heat transfer is one of the well-established high-performance techniques for heating, cooling and drying of a surface. Applications of the impinging jets include drying of textiles and film; cooling of gas turbine components and the outer wall of combustors; and cooling of electronic equipment. Interest and research in this topic continue unabated and may have even accelerated in recent years because of its high potential of local heat transfer enhancements. Besides the above applications, impinging jets are also used in paper industry to enhance drying of paper processes, annealing of metals, tempering of glass and cooling of moving metal strip. Details of the few of the jet impingement applications are given below.

1.1.1 Cooling of gas turbine blades:

The objectives of High-Performance Turbine Engine Technology (HPTET) are to achieve higher engine thrust to weight ratio along with a significant improvement in fuel economy. These engines will use a variety of new technologies. Fifty percent of the improvement will result from advancements in appropriate materials. Even the advanced alloys will extend the current metal temperature limitations slightly but required levels of turbine entry temperature for HPTET show the need to improve turbine blade cooling. Figure 1.1 shows that turbine entry temperatures in advanced gas turbines are far higher than the melting point of the blade material; hence, the turbine blades need to be cooled (Han *et al.*, 2000).

Higher engine compression ratios can increase turbine entry temperature and improve thermal efficiency; greatly reducing fuel consumption. Turbine entry temperatures required for increased performance will cause higher thermal fatigue and higher stress problems for the designer. A reduction of blade metal temperature of 40°C can improve blade life 10-fold (Van Treuren, 1994). Increasing cooling air to lower the blade metal temperature reduces the amount of air available to produce thrust and consequently the cycle efficiency decreases. The use of film cooling on the external surfaces of the turbine blade also decreases the aerodynamic efficiency of the turbine blades.

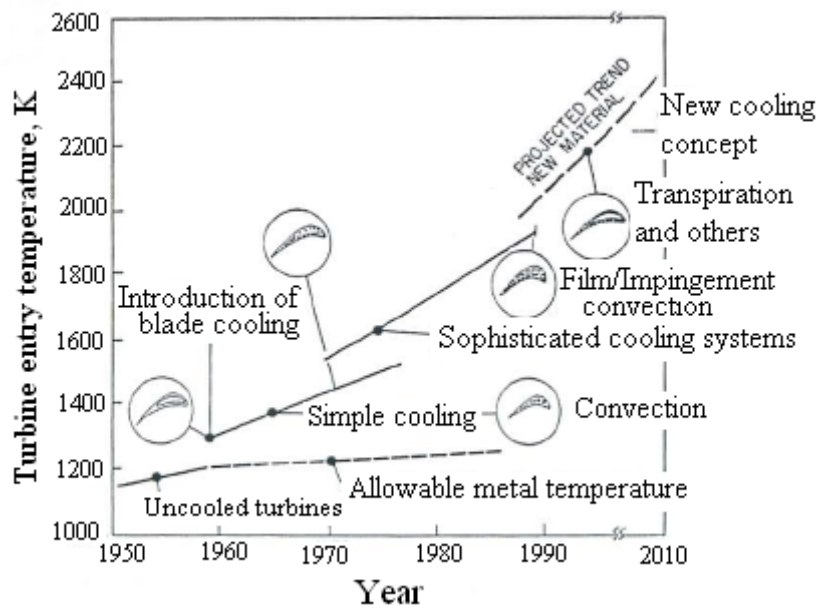


Fig. 1.1 “Variation of turbine entry temperature over recent years (Han *et al.*, 2000)”

The improvements in the performance of the gas turbine engines may be viewed first from the material aspect. Monolithic ceramics have a good high temperature strength in the 1900 K range but, are difficult to fabricate. Another promising material is the carbon/carbon composite which can operate at the 2480 K environment but are subject to oxidation as well as fabrication problems. The new nickel super-alloys are promising material having increased allowable blade temperatures. However, even with these alloys there is still a need to employ turbine cooling using the relatively cool air bled from the compressor for improvement in the performance. There are four basic methods of utilizing cooling air in a turbine which are discussed below and illustrated in Fig. 1.2.

Passage convection cooling- Air flows through internal passages machined or cast into the turbine blade. Convection is often enhanced with ribs or pedestals cast into the passage to increase turbulence, wetted surface area and hence, heat transfer.

Impingement cooling - Air flows through small holes in a blade insert. These form impinging jets on the inside surface of a turbine blade to reduce local blade surface temperature.

Film-cooling – Air flows through holes to the blade external surface to provide a layer of cooler air between the combustor exit gases and the blade surface.

Transpiration cooling – A porous material allows air to seep through and provide protection for the blade. There are considerable problems associated with structure and deposition.

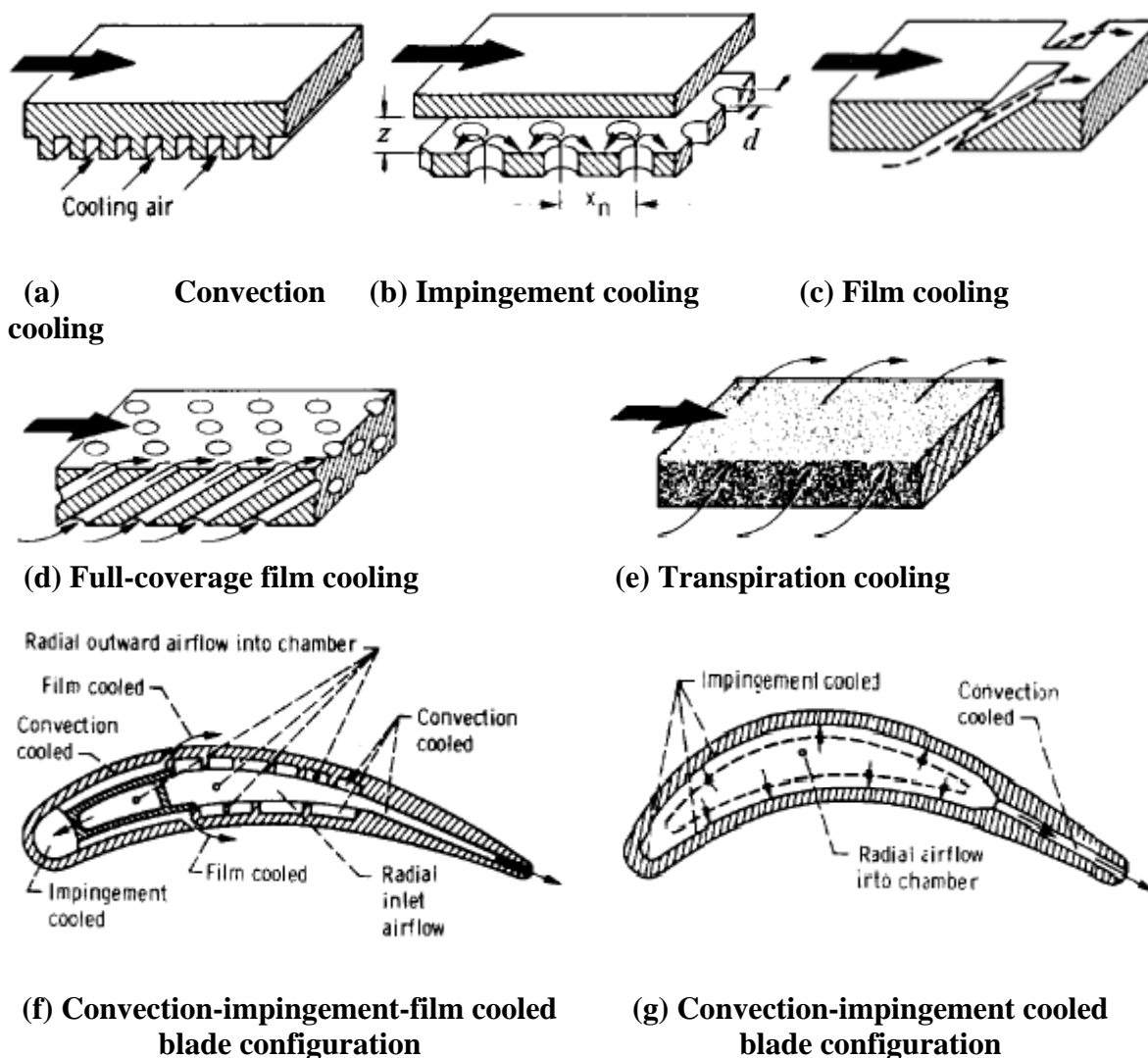


Fig. 1.2 Some methods of turbine blade cooling (Colladay, 1975)

Turbine cooling effectiveness (ϕ) is defined as:

$$\phi = \frac{T_G - T_M}{T_G - T_C} \quad (1.1)$$

Where T_M , T_G and T_C are the temperatures of the metal, gas and coolant. Figure 1.3 shows the effectiveness of various cooling combinations (Van Treuren, 1994). Film cooling in combination with crossflow impingement is extremely effective. Increasing the amount of cooling airflow also improves cooling effectiveness for all cooling methods and combinations. The challenge facing the turbine blade designer is to choose the cooling methods to produce a blade that achieves the required permissible turbine entry temperature and that uses the minimum amount of cooling air.

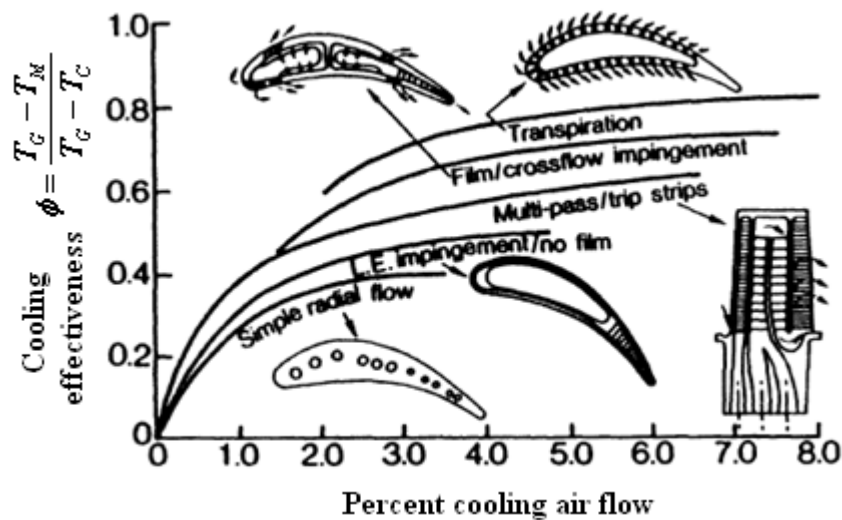


Fig. 1.3 Turbine cooling effectiveness (Van Treuren, 1994)

1.1.2 Combustion chamber wall cooling:

The jet impingement cooling techniques are applied in cooling the combustor wall. Back wall impingement cooling and end wall back cooling are shown in Fig 1.4 schematically for a combustion chamber.

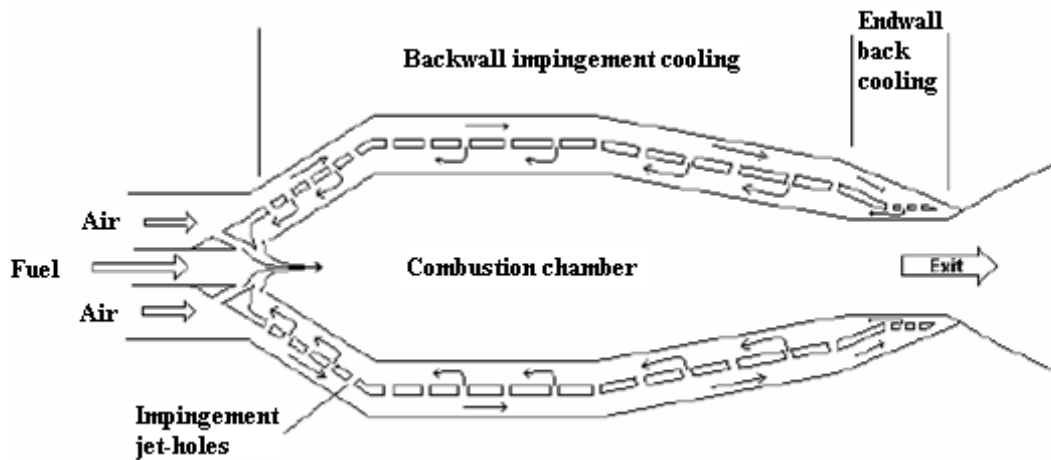


Fig. 1.4 Combustion chamber wall cooling (Gao, 2001)

The modern Dry Low Emission (DLE) combustor is required to produce a low NO_x emission, especially for on-ground use in power generation plant, more complete burn for the fuel is required. Previously in the combustor, the film cooling is being deployed. The spent coolant keeps entering the combustion chamber from film cooling holes on the chamber wall along with combusting fuel/air mixture moving forward, which lowers the inside peak combustion temperature. Hence, impingement cooling is introduced in the newer designs so that the spent coolant after carrying the heat enters the chamber together with the fuel. This may remove the need for film cooling.

1.1.3 Cooling of electronic components:

The electronic components are becoming more and more powerful day by day. This causes more ohmic power consumption and thus more heat dissipation. It is expected that the power dissipation of the future microprocessors will reach about 50-100 W/cm² (Beitelmal *et al.*, 2000 and Karwa *et al.*, 2007) or even more and electronic industry is thus seeking more effective ways to overcome the localized heat loads. The use of cooling system is dependent on two main requirements; the total heat to be removed and allowable temperature rise above the local ambient conditions. If the heat flux is 0.05 W/cm² and allowable temperature rise is 60°, then radiation and natural convection are usually sufficient means of heat dissipation. Forced convection can be employed for 1-2 W/cm². However, for higher heat flux removal impinging jets are the better option. Impinging jets that are normal to the target surface may have space and size limitations. Under such situations, inclined jets are mostly preferred.

1.2 Classification of impinging submerged jets:

The flow of fluid with the tangential separation surfaces is known as a jet. A jet is called submerged jet if the fluid of jet and the surrounding medium is the same. The jets are classified as axis-symmetric jet, two-dimensional jet and three-dimensional jet based on the geometry of the nozzle. An axis-symmetric jet is a jet, which emerges from a circular nozzle or an orifice. Rectangular jets with large length/width ratios (aspect ratio) are two-dimensional jets and rectangular jets with small length/width ratios (aspect ratio) are referred to as three-dimensional jets (Suresh *et al.*, 2008). Two-dimensional jets are mostly referred to as slot jet.

Classification of the jets based on the Reynolds number (based on either diameter or slot width) is as follows (Viskanta, 1993).

- a) The dissipated laminar jet, $Re < 300$
- b) A fully laminar jet, $300 < Re < 1000$
- c) A transition or semi turbulent jet, $1000 < Re < 3000$
- d) A fully turbulent jet, $Re > 3000$

1.2.1 Structure of free jet:

The structure of free jet is as shown in the Fig. 1.5a. The three zones of the free jet are

- a) Potential core zone
- b) Developing zone

c) Developed zone

The jet immediately leaving the nozzle encounters surrounding stagnant air. The free shearing between moving jet and stagnant air causes the mixing due to which fluid particles of the surrounding air are carried with the jet, which causes the sharing of the momentum of the jet and formation of the shear layer. Within the shear layer there exists a flow of jet which is still unaffected by mixing and its velocity is same as the nozzle exit velocity. This zone is potential core of the jet.

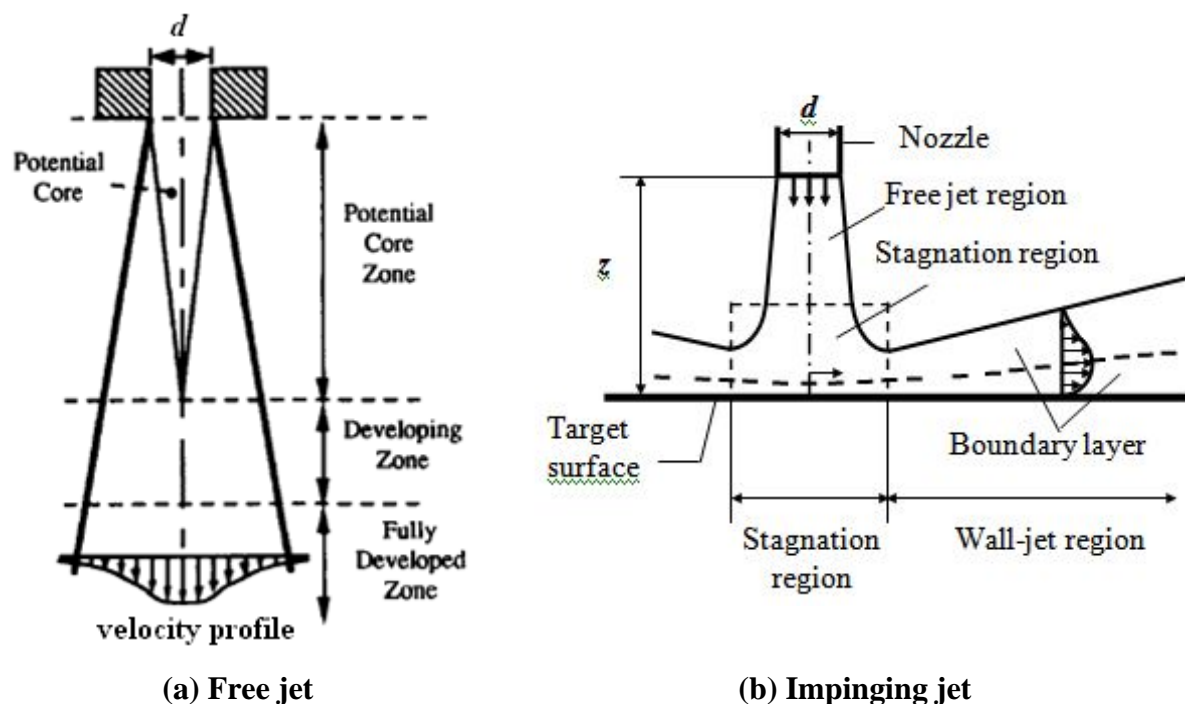


Fig. 1.5 Structure of submerged jet (Viskanta, 1993)

In the potential core zone, the centerline velocity of the jet remains constant and is equal to the nozzle exit velocity. The end of the potential core is defined as the axial distance from the nozzle exit up to the point where the jet velocity is 0.95 times the nozzle exit velocity (Jambunathan *et al.*, 1992). Typical length of the potential core is found to be 6-7 times the nozzle diameter for the axis-symmetric jet and 4.7-7.7 times the slot width for two dimensional jets (Viskanta, 1993). However, this length depends on nozzle geometry and turbulent intensity in the nozzle exit and initial velocity profile. In the developing zone, due to large shear stresses at the jet boundary, axial velocity profile decays. In the developed zone the velocity profile is fully developed and the jet broadens linearly along with linear decay of axial velocity.

1.2.2 Structure of impinging jet:

Unconfined jet impingement system is one in which jet after impingement on a surface is exited without confinement. Figure 1.5b shows the flow field of an impinging jet on to an orthogonal plate. The flow structures of impinging axi-symmetric jet can be subdivided into three characteristic regions.

1. The free jet region
2. The stagnation flow region
3. The wall jet region.

The impinging jets travel from the nozzle exit as a free jet to within a distance approximately 1.2 nozzle diameters from the Target plate surface (Jambunathan *et al.*, 1992). Here, deceleration of flow starts and static pressure increases due to conversion of kinetic energy of the jet. Boundary layer of constant thickness is formed at the stagnation region having a radius of ~ 1.1 nozzle diameters (Gardon and Akfirat, 1966). In the stagnation flow region, the axial velocity component decelerates and converts to an accelerated tangential one. The relative boundary layer thickness varies inversely proportional to exit Reynolds Number. Due to the exchange of momentum with stagnant surroundings and wall friction, the accelerated tangential flow transforms to a decelerated wall jet flow. The velocity fluctuations of free jet are carried along the wall jet region also (Gardon and Akfirat, 1966). However, increase of turbulence in the wall jet region depends on turbulence in the jet prior to impingement. The heat transfer rate in the region of wall jet is found to be higher than stream wise flow over the plate. Following are some of the parameters influencing local distribution of heat transfer and fluid flow on a surface due to impinging jets. They are Reynolds number, jet-to-plate distance, radial distance from the stagnation point, confinement of jets, nozzle geometry, turbulence intensity, surface roughness, jet-to-jet distance, curvature of target surface, etc.

1.3 Scope of the present work:

The high heat transfer rates associated with impinging air jet is well recognized for many years. Direct impingement of turbulent jets onto a surface leads to high heat transfer rates. However, the local distribution of heat transfer coefficients can be highly non-uniform. The jet impingement heat transfer is the focus of the present study to determine both the peak and Local heat transfer distribution for various configurations of jets and surfaces.

This report presents the experimental investigations of local heat transfer characteristics and fluid flow distribution due to impinging slot jet on flat surface. Hence, the objectives of the present work are:

- Experimental investigation of local heat transfer and fluid flow characteristics due to impingement of a single unconfined slot jet is carried out. Analysis of local distribution of Nusselt numbers based on available flow characteristics due to slot jet impingement is carried out.
- Experimental investigation is carried out to study the local heat transfer distribution from a flat surface with detached ribs due to normal impingement of a single slot air jet. Investigation is aimed at performing a parametric study of the size of the detached ribs and suggesting a better configuration producing higher heat transfer augmentation.
- To study the influence of confinement of the slot jet on the distribution of the wall static pressure and local heat transfer coefficients on a smooth flat plate.
- To study the influence of confinement of the slot jet on the distribution of the wall static pressure and local heat transfer coefficients on a rough (with detached rib) flat plate.
- To study the combined effect of confinement of the slot jet and the roughness of the flat surface on the distribution of wall static pressure and local heat transfer coefficients

Single jet finds its application mostly where highly localized heating or cooling is necessary. However, when large surface areas require cooling or heating, multiple jet impingements are desirable. A promising method for cooling turbine blades is to impinge cool air on the internal surfaces of the blades so that the gas turbine cycle may be operated with higher inlet gas temperatures for higher efficiencies. Two critical regions identified in the gas turbine blade which needs to be cooled are the mid-chord region and the leading edge. The impingement cooling of the mid-chord region may be identical to cooling of flat surface due to a two-dimensional array of jets with spent air exiting in one/two/all directions. The internal passage at the leading edge can be considered to have a semicircular concave surface and this region may be convectively cooled by a span-wise row of impinging jets.

1.4 Report organization:

Chapter 1 deals with importance of heat transfer enhancements due to impingement of jets and the scope of present work. The layout of the report has been included in this chapter. Chapter 2 provides the literature review about the flow and heat transfer behavior of single normal impinging jets on a smooth flat plate, ribbed flat plate, confined smooth flat surface and finally confined and ribbed flat plate in separate topics. The conclusions drawn from the literature review and the objectives of the present study are also detailed in this chapter. Chapter 3 deals with the introduction, literature review, experimental investigation and discussion on the fluid flow and heat transfer characteristics of a single unconfined slot jet impinging on a smooth flat surface. Chapter 4 delineates the experimental investigations and analysis of the local heat transfer and fluid flow distribution between rough flat surface and impinging unconfined slot air jet. A detailed parametric study to obtain a better configuration of detached rib is discussed in this chapter. Chapter 5 delineates the experimental investigations and analysis of the local heat transfer and fluid flow distribution between smooth flat surface and impinging confined slot air jet. Chapter 6 portrays the experimental investigations on heat transfer enhancement from a flat surface with detached rib by normal impingement of a confined slot air jet. Simplified correlations are also presented. Chapter 7 summarizes the conclusions of the present study of experimental investigations of local heat transfer characteristics and fluid flow distribution due to an impinging slot air jet on smooth, rough, confined smooth and confined rough flat surface. Scope for future work is also suggested in this chapter.

CHAPTER 2

Literature review on heat transfer and fluid flow distribution of impinging air jets

Impinging jets have received considerable research attention due to their inherent characteristics of high rates of heat transfer. Such impinging flow devices allow for short flow paths on the surface with relatively high heat transfer rates. The jet impingement heat transfer is one of the well-established high-performance techniques for heating, cooling and drying of a surface. Applications of the impinging jets include drying of textiles and film; cooling of gas turbine components and the outer wall of combustors; and cooling of electronic equipment. Interest and research in this topic continue unabated and may have even accelerated in recent years because of its high potential of local heat transfer enhancements. In addition to above, the impinging jets are also used in paper industry to enhance drying of paper processes, annealing of metals, tempering of glass and cooling of moving metal strip.

In the present context, the literature review is organized first with the discussion on heat transfer and fluid flow characteristics of smooth flat surface due to single jet impingement. This is followed by the literature on heat transfer and fluid flow distributions on flat surface with surface rougheners due to a single jet impingement. In addition, the literature on the influence of confinement on heat transfer and fluid flow characteristics of a flat surface due to impinging jets is reviewed. Finally, the literature on the combined effect of confinement and surface roughness (rib) on heat transfer and fluid flow characteristics of a flat surface due to impinging jets is reviewed.

2.1 Heat transfer and fluid flow distribution on smooth flat plate impinged by an unconfined single jet:

Many earlier studies are available on circular jet impinging over flat and smooth surface. Review of the experimental work on heat transfer to impinging circular jets are reported by Livingood and Hrycak [1970], Martin [1977], Jambunathan *et al.* [1992], Viskanta [1993]. Gardon and Cobonpue [1962] and Katti and Prabhu [2008] reported the local heat transfer distribution between circular jet and flat plate.

Similarly, some experimental work is reported on slot jet impinging onto a smooth flat plate. Gardon and Akfirat [1965] studied the effect of free stream turbulence on the local

heat transfer distribution between two-dimensional jet and a constant wall temperature flat plate using a specially designed heat flux gauge. They reported the non-monotonic variation in the heat transfer along the stream-wise direction. This non-monotonic trend is marked in the regions where the mixing induced turbulence is not yet fully developed. They also reported that the stagnation point Nusselt number is highest when jet impinges the plate near the end of its potential core region.

Gardon and Akfirat [1965] studied the heat transfer characteristics by a rectangular jet impinging on a smooth flat plate. They concluded that, for lower Reynolds numbers up to 2750 and jet-to-plate spacing (z/b) less than 5, the stagnation point Nusselt number is fairly independent of nozzle width and jet-to-plate spacing. However, for higher jet-to-plate spaces (z/b), the stagnation point Nusselt number varies with z/b . Nozzle width affects the Nu_0 only for lower jet-to-plate spaces (z/b up to 10) at Reynolds number than 2750. They reported that a secondary peak is observed in the Nusselt number distribution along the stream-wise direction for jet-to-plate spacing less than $9b$. Two secondary peaks are observed at a jet-to-plate spacing of 0.5. The formation of secondary peak in the stagnation region is because of the increasing velocities in the gap between the nozzle exit and plate.

Gardon and Akfirat (1966) conducted series of experiments on the heat transfer characteristics of a 2-dimensional jet and a flat plate and proposed a correlation for stagnation point heat transfer coefficient. Figure 2.1 shows the results plotted for $Nu_0 v/s$ jet to plate distance for various widths of the jet at different Reynolds numbers.

The correlation given by them for the heat transfer coefficient at the stagnation point is,

$$Nu_0 = h_0 * B/k \quad (2.1)$$

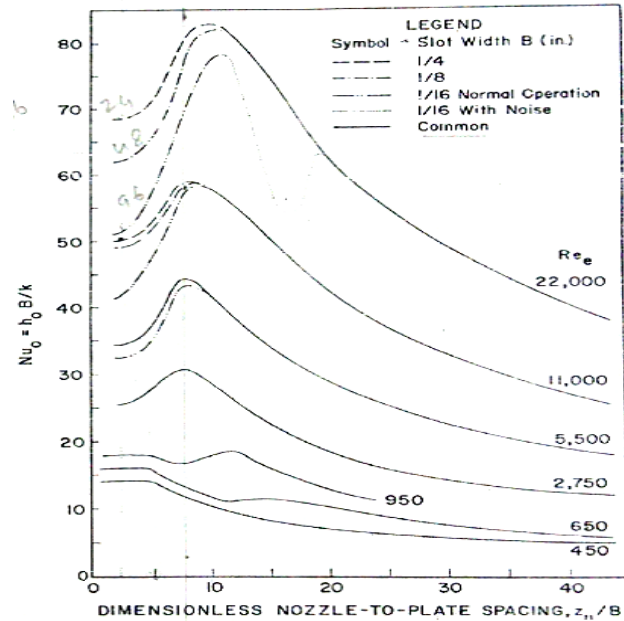
They observed that Nu_0 depends only on Reynolds number for $Re < 2000$ and at larger nozzle to plate spaces the Nu_0 monotonically decreases with the increase in the jet to plate distance.

The variation of local heat transfer rates across the slot, with lateral distance from the stagnation point is shown in figures below. The heat transfer coefficient has a bell shape for the nozzle to plate distances (Z_n/B) above 14 slot widths (fig 2.2) and for (Z_n/B) between 8 to 14 the bell shape abruptly changes its slope around $x/B = 4$. They reported secondary peaks in the heat transfer rates at (Z_n/B) = 5 and 6. These peaks are attribute to the jet transition from laminar to turbulent boundary layers

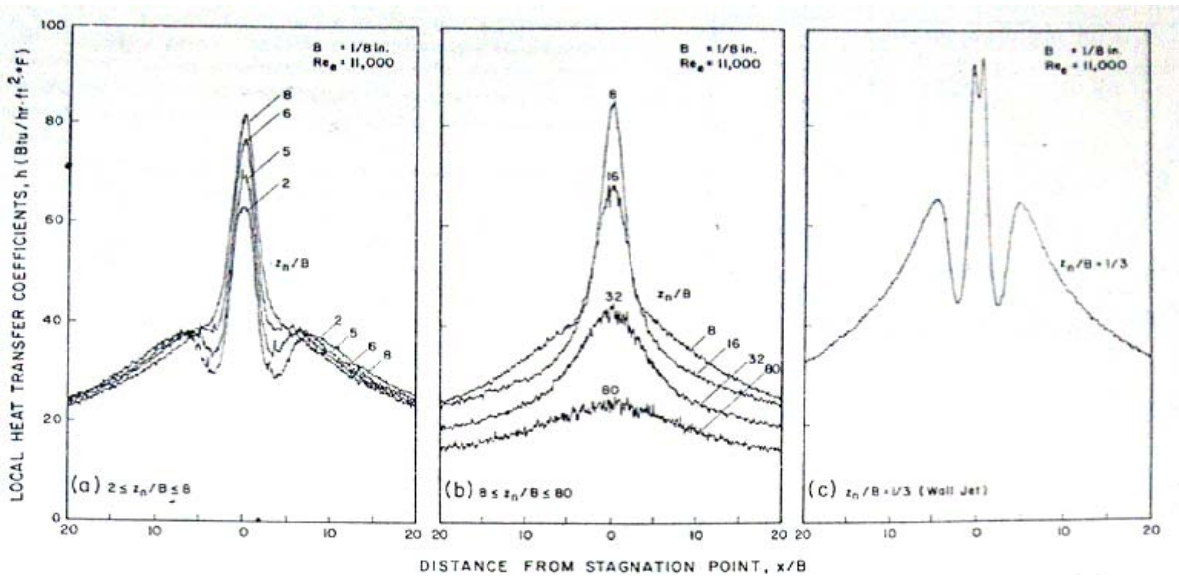
Brahma [1992] worked on impinging slot jet and predicted the Nu_0 on a flat surface.

They analyzed fluid flow and heat transfer for a slot jet impinging on a flat plate for

different nozzle-to-plate spacing, the available potential flow solution has been used to solve the boundary layer and energy equations by using the Blasius-Frossling series solution method. The friction factor and Nusselt number have been evaluated as a function of the dimensionless distance from the stagnation point. Correlation for the Stanton number at



“Fig 2.1 Correlation of heat transfer coefficients at stagnation point” (Gardon, Akfirat 1966)



“Fig. 2.2 Lateral variation of local heat transfer coefficients between a plate and an impinging 2-dimensional jet” (Gardon, Akfirat 1966)

the Stagnation point is obtained in terms of velocity gradient at the stagnation point and Reynolds number.

Ichimiya and Hosaka [1994] conducted experimental study of heat transfer characteristics due to confined impinging two-dimensional jets. Experimental results are presented for characteristics of impingement heat transfer caused by three slot jets for the dimensionless distance $H = 0.5-3$, dimensionless pitch $P = 6-16$, and Reynolds number $Re = 500 - 8000$. For laminar impinging flow, these were compared with numerical results. For turbulent impinging flow, two peaks of the local Nusselt number were observed behind the second nozzle. It is reported that the position of the second peak approached the nozzle as the space between nozzle and impinged surface decreased. The average Nusselt number between the central and second nozzles was determined from the ratio P/H and the Reynolds number based on the pitch of the nozzles.

Slayzak *et al.* [1994] studied the effects of interaction between adjacent free surface planar jets on local heat transfer from the impingement surface. Experiments were conducted to obtain single-phase, local convection heat transfer coefficient distributions along a constant heat flux surface experiencing impingement by two, planar, free surface jets of water. Nozzle widths and nozzle-to-heater separation distances were fixed at 5.1 and 89.7mm, respectively, while two nozzle-to-nozzles pitches (81 and 51 mm) were considered. The ratio of impingement velocities for the two nozzles, V^* , was varied from 0.47 to 1.0. Interacting wall jets created by the impinging jets yielded a strong upwelling of spent flow (an interaction fountain), beneath which convection coefficients were comparable to those associated with the jet impingement regions. With decreasing V^* , impingement heat transfer coefficients beneath the weaker jet were reduced by the effects of cross flow imposed by the stronger jet.

Lytle and Webb (1994) examined experimentally the impact of air impingement heat transfer at low nozzle-plate spacing. The local heat transfer characteristics of air jet impingement at nozzle-plate spacing of less than one nozzle diameter have been examined experimentally using an infrared thermal imaging technique. Fully-developed nozzles were used in the study. The flow structure was investigated using laser-Doppler velocimetry and wall pressure measurements. The stagnation Nusselt number was correlated for nozzle-plate spacing of less than one diameter. The customary Nusselt number dependence on $Re^{1/2}$ for impinging jet transport was observed. A power-law relationship between Nusselt number and nozzle-plate spacing of the form $Nu_o \sim (z/d)^{-0.288}$ observed experimentally is explored from theoretical considerations. The effects of accelerating fluid between the nozzle-plate gap as well as a significant increase in local turbulence leads to substantially increased local heat transfer

with decreased nozzle-plate spacing. A stagnation point minimum surrounded by an inner and outer peak in the local heat transfer was observed for nozzle-plate spacing less than $z/d = 0.25$. These primary and secondary maxima are explained by accelerated radial flow at the exit of the jet tube and an observed local maximum in the turbulence, respectively. These conclusions are drawn from observations made relative to the turbulent flow structure and wall pressure measurements. The outer peak in local Nusselt number was found to move radially outward for larger nozzle-plate spacing and higher jet Reynolds numbers.

Tu and Wood (1996) determined the pressure and shear stress on a surface. Their experiment was with slot-jets having a width 0.97mm & 6.4mm at a slot width-based Re_b , in the range of 3040 to 11000. The jet and plate spacing (Z/D_h) was varied up to 20. They identified that the Gaussian profile describes the pressure distribution on the surface. The experimental results which lead to the conclusions of Tu and Wood are represented in figure 2.4 below.

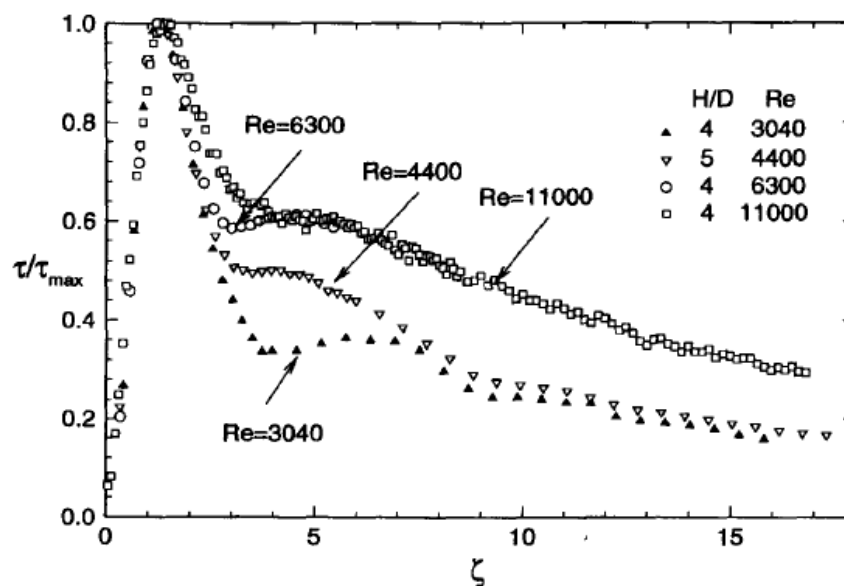


Fig. 2.3 Dependence of wall shear stress on Reynolds number for H/D close to 4.0. Actual H/D and Re given in figure.

Gao and Sunden [2003], Experimentally investigated the heat transfer characteristics of confined impinging slot jets and a flat surface. Single and multiple jets with cross flow effect were considered in the study. They observed that at low nozzle-to-plate spaces such as $H/B = 4$ and 8, the multiple-slot array shows no obvious difference from that of the single-slot jet. However, as H/B increases to 16, the jets of the multiple-slot array start to interact with each other, and at $H/B = 24$ this interaction is strong enough to reduce the stagnation-point Nusselt number of the multiple-slot array by about 15% compared to the

single jet. On the other hand, the heat transfer at the locations of the exhaust port shows a flatter distribution. It was found that the narrower slot gives a larger average heat transfer coefficient for a given value of X/B at the same jet exit velocity. The heat transfer is proved to be enhanced by exhausting the spent air through symmetric exhaust ports, compared to those with cross-flow effects.

Narayanan *et al.* [2004] studied the flow field, surface pressure and heat transfer rates of slot jet impinging on the smooth flat surface. They experimentally studied the heat transfer distribution as the jet impinges on the flat plate within potential core region ($z/D_h = 0.5$) and transition region ($z/D_h = 3.0$) for jet exit Reynolds number (based on hydraulic diameter) of 23000. They reported that, the generation of turbulence near the surface prior to impingement and the presence of span-wise vortices in the stagnation region with an increase in near wall turbulence is responsible for the enhancement in the heat transfer for the transitional jet impingement. They observed that there is a good correlation between the secondary peak in heat transfer and the peak near wall stream-wise turbulence.

Figs. 2.5 presents dimensionless plots of local heat transfer coefficient, Nu_{loc} , for $Y_n/D_h = 3.50$ and 0.50 , respectively, as a function of stream-wise distance from the impingement line. For $Y_n/D_h = 3:5$, the heat transfer coefficient decreased monotonically with increasing distance from the jet centerline, with a change (reduction) in negative gradient at $x/D_h = 1.5$. For spaces of $Y_n/D_h < 2.5$, a non-monotonic decay in Nu_{loc} distribution was observed with a primary peak at the impingement line, followed by a secondary peak that occurred closer to the nozzle centerline with reduced nozzle-to surface spacing. In particular, for the $Y_n/D_h = 0.5$ slot jet impingement, a region of low heat transfer was observed at $x/D_h = 1.6$, followed by a secondary peak region further downstream at $x/D_h = 3.2$. They observed the turbulence generated close to the surface earlier to the jet impact and the formation of vortices in the stagnation region and the increased turbulence promotes the rise in the heat transfer for the transitional jet. A good correlation between the secondary peak in heat transfer and near-wall stream-wise turbulence was identified by them.

Sahoo and Sharif [2004] attempted numerical modeling of slot-jet impingement cooling of a constant heat flux surface confined by a parallel wall with an objective of studying the associated heat transfer process in the mixed convection regime. It is observed that for a given domain aspect ratio and Richardson number, the average Nusselt number at the heat flux surface increases with increasing jet exit Reynolds number. On the other hand, for a given aspect ratio and Reynolds number the average Nusselt number does not

change significantly with Richardson number indicating that the buoyancy effects are not very significant on the overall heat transfer process for the range of jet Reynolds number considered in the study.

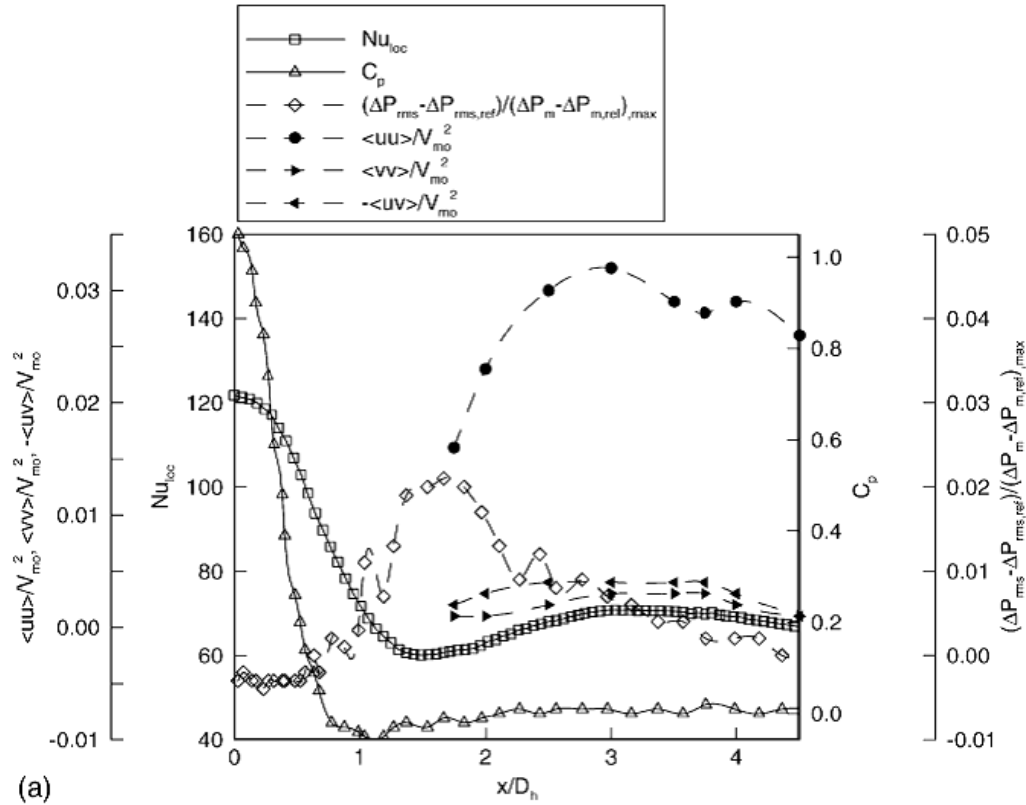


Fig. 2.4 Combined plot of heat transfer coefficient, mean and RMS pressure, and near-wall fluctuating velocity variance distributions on impingement surface for the $Y_n = D_h \frac{1}{4}$ 0:5 slot jet nozzle along the minor axis of the nozzle, at centerline, $z/D_h = 0:00$.

Beitelmal *et al.* [2006] analyzed two-dimensional impinging jets and correlated the heat transfer coefficient in the stagnation region and wall jet region with approximate solutions developed using simplified flow assumptions. They studied for the jet-to-plate spacing ranging from $4b$ to $12b$ with the Reynolds numbers ranging from 4000 to 12000. They measured the heat transfer for x/b ranging from 1.5 to 7.5 along the streamwise direction. They observed that the stagnation region Nusselt number is constant and explained it based on potential theory with constant thermal boundary layer thickness.

Haydar and Celik [2006] conducted experiments to determine the effects of some parameters that were crucial in the cooling of a heated flat plate by an obliquely impinging slot jet. The inclination of the jet relative to the surface was varied from 90° to 30° (90° , 60° , 45° and 30°). For Reynolds number of 5860, 8879, and 11606, the variation of local temperatures with respect to dimensionless length (z/L), were investigated. They developed new correlations for local temperatures in terms of

Reynolds number, dimensionless distance (z/L) and oblique angle ($\sin\phi$). Results of experiments indicated that for a given position this displacement of the position of maximum heat transfer with reference to the geometrical stagnation position, increases with increase in the inclination, and the displacement is towards the compression side of plate.

Zhou and Lee [2007] investigated experimentally the fluid flow and heat transfer characteristics of a rectangular air jet impinging on a heated flat plate. They reported that the jet Reynolds number, the nozzle-to-plate spacing and the turbulence intensity have an important influence on the heat transfer of impinging rectangular jets, especially on the impingement region. They analyzed the heat transfer mechanics in terms of turbulence intensity and proposed correlations for both local and average N_u with free stream turbulence intensity.

Suresh *et al.* [2007] studied experimentally the influence of transition regime of Reynolds number (250–6250) on the evolution of a plane air jet issuing from a slit. They observed that the spread rate of a slit jet is significantly lower than contoured nozzle jets. Based on the axial evolution of turbulence intensities, normalized spectral quantities, and PDFs, it is concluded that the two-dimensional slot jet becomes self-preserving at about 80 slot widths downstream of nozzle exit. Their work also reveals that Reynolds number substantially affects mixing, spread rate, and centerline decay during transition.

Gulati *et al.* [2009] experimental investigated the effects of the shape of the nozzle, J2P spacing and Reynolds number on the local heat transfer distribution to normally impinging submerged air jet on smooth and flat surface with three different nozzle cross-sections, *viz.* circular, square, and rectangular, each with an equivalent diameter of around 20 mm. They reported that: Average Nusselt numbers are found to be insensitive to the shape of the nozzle. The effect of Reynolds number on the performance of noncircular jets is similar to that for the circular jet; with increase of Reynolds number, the heat transfer rate increases.

The heat transfer characteristics of square and circular jets show much similarity. There is a distinct difference between distribution of Nusselt numbers along the major and minor axis for rectangular jet. Up to z/d of 6, the Nusselt number distribution along the horizontal axis for rectangular jet is higher in the stagnation region than those of circular and square jets. The average Nusselt number around the stagnation point is almost same for all the nozzle configurations tested, and Pressure loss coefficient is lowest for the circular jet and highest for rectangular jet.

Choo and Kim [2010] compared the thermal characteristics of confined and unconfined impinging jets for air and water. They observed that the thermal performance of the confined jet was similar to that of the unconfined jet under a fixed pumping power condition, while the thermal performance of the confined jet was 20–30% lower than that of the unconfined jet under a fixed flow rate condition. They also presented generalized correlations for the stagnation and average Nusselt numbers of both the confined and unconfined impinging jets as a function of the dimensionless pumping power and the Prandtl number.

Nirmalkumar, *et al.* [2011] conducted an experimental investigation of local heat transfer distribution and fluid flow characteristics on a smooth flat plate impinged by a normal slot jet. Reynolds number based on slot width is varied from 4200 to 12,000 and jet-to-plate spacing (z/b) is varied from 0.5 to 12. They identified three regimes on the target surface *viz.* stagnation region (laminar boundary layer associated with favorable pressure gradient), transition region (associated with increase in turbulence intensities and heat transfer) and turbulent wall jet region. Semi-empirical correlations for the Nusselt number in the stagnation region and the wall jet region are proposed.

Shariff [2013] numerically modeled and studied using ANSYS Fluent CFD code, the effect of inclination of twin slot jets impingement on an isothermally heated flat surface, with confined flow domain. The flow and geometric parameters are the jet exit Reynolds number, distance between jet exit and the impingement surface and the inclination of the jet with the impingement surface. He reported that for an impingement angle around 45° yielding a peak local Nusselt number of about 5, but the overall heat transfer is reduced by about 36%. For impingement angles between 60° to 90° , while the overall heat transfer (average Nusselt number) remains fairly constant (3.2 to 2.8), the localized cooling is mainly concentrated around the impingement locations on the hot surface with a peak local Nusselt number of about 10.

Alnak, *et al.* (2018) numerically analyzed the forced convection drying behavior of moist surfaces of various geometries impinged by a slot air jet. They considered a 2-D laminar slot jet and obtained the heat and mass transfer distributions for different jet velocities keeping the jet to object distance, diameter of the object, and initial jet height as constant.

Calculations were performed for four different Reynolds numbers, namely, $Re = 100, 200, 300, \text{ and } 400$ using finite volume method for energy and momentum equations.

The geometry of straight semi-circular moist object had better performance of heat and mass transfer than that of the reverse moist object geometry. Increasing Reynolds number

had a positive effect on heat and mass transfer. Jet drying was most effective near the stagnation point on the leading side of the objects.

Rathore *et al.* (2019) computationally investigated and modeled the slot jet impinging on a hot plate at lower Reynolds number. They considered a jet Reynolds number of 9900 and H/w of 7.5 in their study. They analyzed the variations of axial velocity along the centerline, maximum axial centerline velocity, distribution of local Nusselt number along the confinement wall and the impingement wall. But in this study the analysis is limited to low Reynolds number model and practically the turbulent jets with higher Reynolds number may be applicable. Hence experimental investigations on the turbulent slot jet at various Reynolds number is essential.

Zhua *et al.*, (2021) analysed the heat transfer characteristics of multi-slot nozzles air jets with velocity difference between the adjacent jets. They studied the influence of thermal uniformity and heat transfer capacity owing to the existence of adjacent jets. It is observed that, the heat transfer uniformity of multi-slot nozzles jet heat transfer was improved compared with that of a single-nozzle jet heat transfer. It is also noted that the closer the Reynolds number of the adjacent jets, the better the heat transfer uniformity. The existence of adjacent jets would relatively inhibit the heat transfer capacity. They proposed an empirical formula for heat transfer characteristics of a single- nozzle jet using the experiment data.

From the preliminary literature studies, it is found that prior research on impinging “Slot jet” is limited to the average HTC on smooth surfaces. The flow structure of a jet at the exit is found to be very much influential on the rates of “heat transfer”. Correlation for WSP distribution with “heat transfer” for smooth surface is not available. Earlier researchers report no exhaustive work on the influence of fluid flow characteristics on the local HTC.

Hence, it is proposed to study the local *HTC* and fluid flow behavior of impinging slot air jets on flat smooth and flat rough surfaces. In addition, it is intended to propose necessary “heat transfer” correlations for the various configurations studied.

1. Conclusion from literature and objectives of the current work:

It is felt from the preliminary literature studies that prior research on impinging slot jets is limited to the average heat transfer characteristics on smooth surfaces. The heat transfer rate on the impingement surface has a close relationship with flow structure at the nozzle exit. Very little work reported the fluid flow and heat transfer rate of impinging slot jets.

Correlation of wall static pressure distribution with heat transfer from smooth surfaces is not available. Use of surface rougheners on the target surface for heat transfer enhancements is not widely attempted. No exhaustive work on the influence of fluid flow characteristics on the local distribution of the heat transfer is reported by earlier researchers.

Hence, it is proposed to study the local heat transfer and fluid flow characteristics of impinging slot air jets on flat smooth and rough surfaces. Further, the study will be extended with inclined impingement of slot jet. Influence of confinement will also be investigated experimentally. Finally, it is intended to propose necessary heat transfer correlations for the various configurations studied.

2.2 Heat transfer and fluid flow distribution on rough flat plate impinged by an unconfined single jet:

Jet impingement, itself, is a high-rate heat transfer technique but to further enhance the heat transfer rates of the impinging jets, the surfaces may be roughened. The surface roughness creates flow disturbances, which affects the turbulence characteristics of the flow and thereby increases the heat transfer. It is found from the published literature that the heat transfer from a smooth flat surface to a jet is influenced by the parameters like Reynolds number, J2P distance and the distance to a major extent. But in most of the real-life industrial applications the target surface may not be necessarily a flat and smooth surface and the flow behavior on that case will be naturally different which will definitely influence the heat transfer characteristics between the jet and the surface. So, it becomes necessary to study the influence of the surface roughness in the form of ribs, dimples, projections or protrusions on the surface on both the fluid flow and heat transfer characteristics. The work done by the various researchers in the past regarding the roughness effect has been highlighted in the paragraphs below.

Most of the work done by earlier researchers is on the circular air jet impinging over flat and smooth surface. Livingood and Hrycak (1970), Martin (1977), Jambunathan *et al.* (1992) and Viskanta (1993). Gardon and Cobonpue (1962) have experimented and reported the heat transfer distribution between the circular jet and a flat plate for the nozzle plate spacing greater than two times the diameter of the jet, with single jet and array of jets. Gardon and Akfirat (1965) studied the effect of turbulence on the heat transfer between the two-dimensional jet and flat plate.

The fig. 2.5 below shows the axial variation of the velocity and turbulence along the

center line of the jet. Immediately on leaving the nozzle, the air in the jet begins to entrain the surrounding still air. The width of the mixing region increases continuously, and at some distance from the nozzle it is wide enough to have penetrated to the centerline of the jet. up to this point the centerline velocity remains practically unaffected by mixing and substantially equal to the nozzle exit velocity. Beyond the potential core region ($z/D > 5$) the centerline velocity also diminishes as the jet shares its momentum with more and more entrained fluid. It can be observed that the centerline turbulence is very minimum close to the jet and as the z/D increase above 1.0, the turbulence gradually increases and reaches maximum around $z/D = 15$.

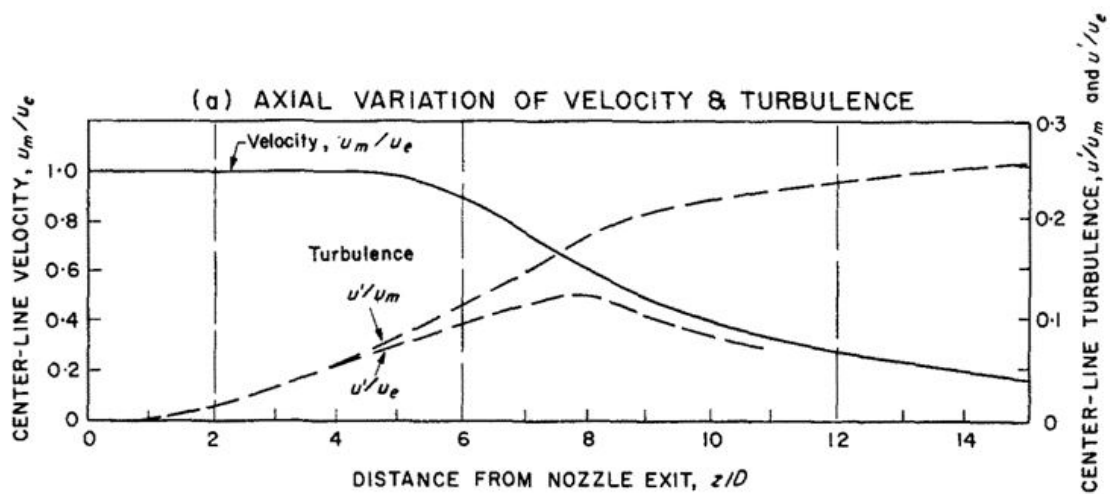


Fig. 2.5 Variation of velocity and turbulence along the center line of a 2-D jet

They also studied the heat transfer distribution due to impingement of multiple two-dimensional jets. Gardon and Akfirat (1965), Baughn and Shimizu (1989) and Hrycak (1983) have conducted experiments of heat transfer to round jet from flat plate employing different methods of surface temperature measurement.

Lytle and Webb (1994) studied the local distribution of heat transfer coefficients of air jet impingement at jet-to-plate distances of less than one nozzle diameter in the Reynolds number range $3600 < Re < 27600$ using thin foil heater and an infrared thermal imaging technique. Fully developed nozzles were used in their study. Measurements of wall static pressures are made. Radial mean velocities and RMS fluctuations are measured using Laser Doppler velocimetry. Figure 2.6 shows the variation of mean radial velocity and RMS fluctuating velocity at two different jet-to-plate distances for $Re = 11000$. Flow structure measurements show significant increases in both mean velocity and RMS turbulence fluctuations as the nozzle-plate spacing is decreased.

Figure 2.7 illustrates the variation in local Nusselt number for z/d ranging from 0.1 to 6.0 for Reynolds numbers of 23000. As the nozzle-to-plate spacing is reduced from $6d$ to $0.5d$, the Nusselt number distribution depends more on the radial flow characteristics. For z/d of 0.5, the Nusselt number decreases monotonically for some distance and then increases reaching peak in the vicinity of r/d of 1.75 before decreasing monotonically for larger radial distances.

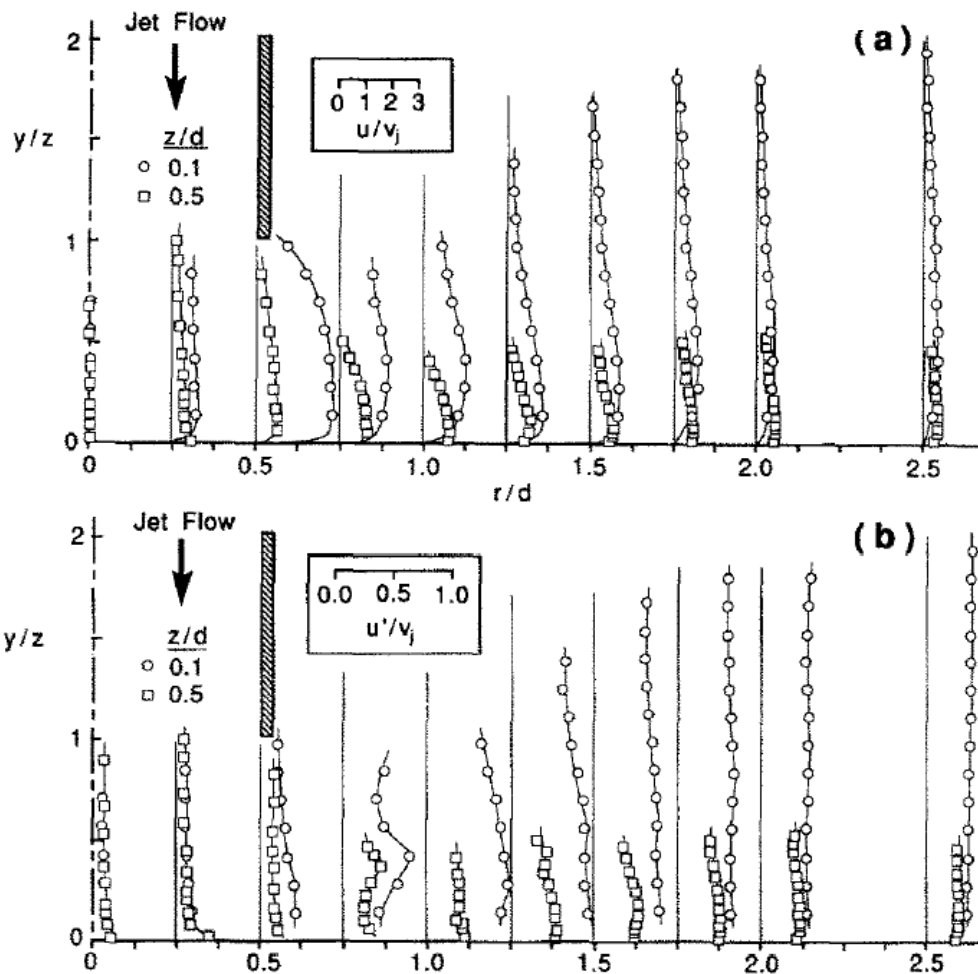


Fig. 2.6 Distributions of mean velocity and RMS velocity fluctuations for $Re = 11000$ (Lytle and Webb, 1994)

The rise in the Nusselt number in the vicinity of r/d of 1.75 is called secondary maxima and is due to the transition from the laminar to turbulent flow. Further decrease in the z/d from 0.5 to 0.25 shows slightly prominent secondary maxima, which is shifted, toward the stagnation point as compared to that for z/d of 0.5. The decrease in the nozzle plate spacing increases the velocity of the flow in the gap. This higher velocity in the gap is responsible for shifting the zone of the transition from laminar to turbulent flow towards the stagnation point. Also, the higher velocity in the gap causes more entrainment of the surrounding air resulting in higher turbulence intensity and causes prominent secondary

maxima. The location of the outer peak is found to coincide with a local maximum in turbulence fluctuations, suggesting considerably higher turbulent transport there.

The measured data of stagnation Nusselt number was correlated for nozzle plate distances of less than one diameter using least-square regression fit. The suggested correlation is given in Equation (2.2).

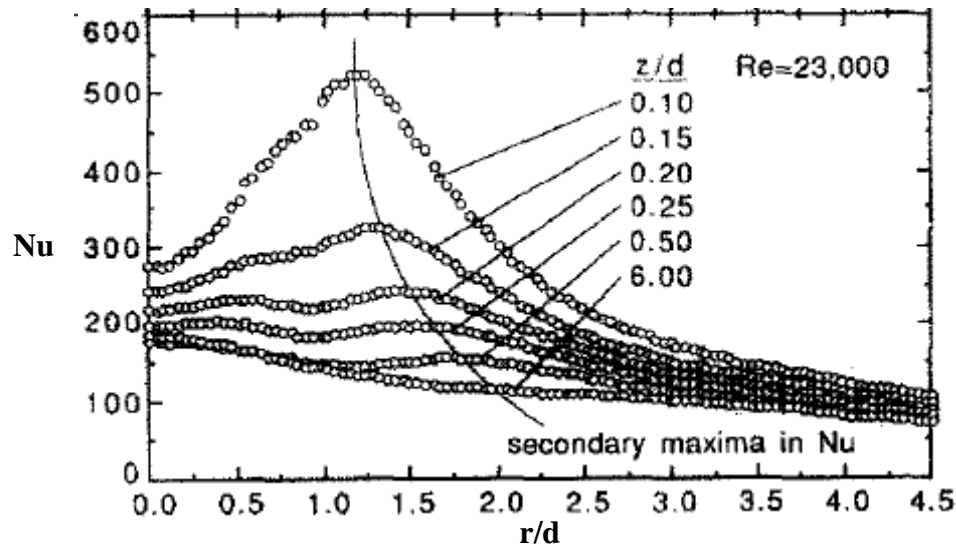


Fig. 2.7 Radial variations of the Nusselt number (Lytle and Webb, 1994)

$$Nu_o = 0.726 Re^{0.53} \left(\frac{z}{d} \right)^{-0.191} \quad (2.2)$$

Lee *et al.* (2004) studied the effect of nozzle diameter on heat transfer characteristics for the jet impinging on a flat plate. Jet Reynolds number of 23000, nozzle diameters of 1.36, 2.16 and 4.40 cm. and nozzle to Target plate spaces from 2 to 14 are considered in this study. The results are as shown in the Fig 2.8. Larger nozzle diameters for a given Reynolds number lead to increase in mass flow rate, jet momentum and turbulence intensity. Hence, it can be seen that stagnation Nusselt number increase with diameters of nozzle for a given Reynolds number. However, in the wall jet region increase in nozzle diameter has no influence on Nusselt number because redevelopment of boundary layer after the jet impingement for different nozzle diameter is same. In addition, it is observed that stagnation Nusselt numbers are higher when nozzle to Target plate distance is around 7, which is as expected because turbulence intensity of a jet reaches maximum at this distance. They reported that local Nusselt numbers in the region of $0 \leq r/d \leq 0.5$ increase with larger nozzle diameters.

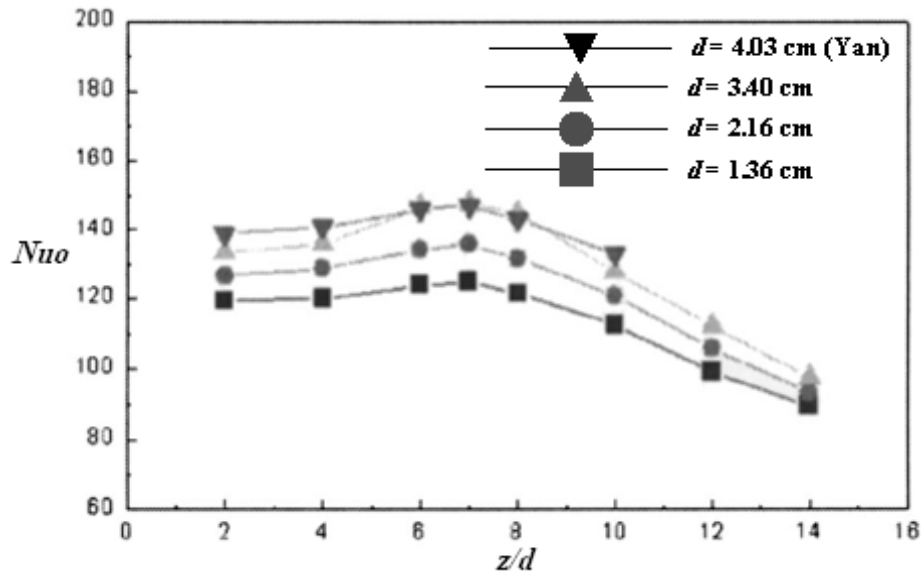


Fig. 2.8 Effect of nozzle diameter on stagnation point Nusselt number(Lee *et al.*, 2004)

Katti and Prabhu (2008) reported experimental investigations and analysis of local heat transfer distribution on a flat surface due to jet impingement from a long pipe nozzle. They identified on the target surface three regions namely stagnation region, transition region, and wall jet region based on heat transfer distribution and have developed Semi-empirical correlations for local Nusselt numbers separately for each region. Han *et al.* (1978) experimentally investigated the effects of rib shape, the angle of attack and pitch to height ratio on the friction and heat-transfer for parallel plate geometry. They developed a general correlation for friction factor and heat transfer considering rib shape, spacing, and angle of attack. They opined that Ribs at a 45° angle of attack have superior heat transfer performance at a given friction power in comparison with ribs at a 90° angle of attack or sand-grain roughness.

Some work is also reported on the slot jet impingement on rough surfaces for internal flows but exhaustive work is not attempted with roughened surfaces particularly with detached ribs on the surface with external flow, normal and oblique impingement. Gau and Lee (1984) experimented on flow structure of “slot jets” and “heat transfer” along the walls with ribs as roughners. They observed that, due to the rib protrusions the air bubbles are formed which encloses the cavity and stops the jet from interacting with the wall and thus reduces the “heat transfer”. But a turbulent flow penetrates the air bubble, interacts with the surface, re-circulates in the cavity formed, and appreciably increases the “heat transfer” rates.

Hansen and Webb (1993) have conducted heat transfer experiments with six different rough surfaces to study the effect of different roughness patterns; one smooth surface is also studied for the comparison. The roughness elements are in the form of cubes of 1.59 mm size, square prisms with 1.59 mm side and 3.18 mm and 4.76 mm height, pyramid of 1.59 mm height with square base of 3.18 mm side, three concentric rings of 1.59 mm wide and 1.59 mm height with 1.59 mm spacing and annular ring with width of 3.18 mm and height of 6.35 mm as shown in Fig. 2.9. Two different nozzles with diameters of 6.91 and 13.3 mm are used. Reynolds number is varied from 4700 to 24000 for the small nozzle and from 8100 to 33000 for large nozzle with z/d of 5. z/d is also varied from 0.25 to 14 for both the nozzles. The average Nusselt number and absolute heat transfer are obtained for all the test surfaces. The temperature is measured with thermocouples, velocity and turbulence intensity are measured by LDV technique.

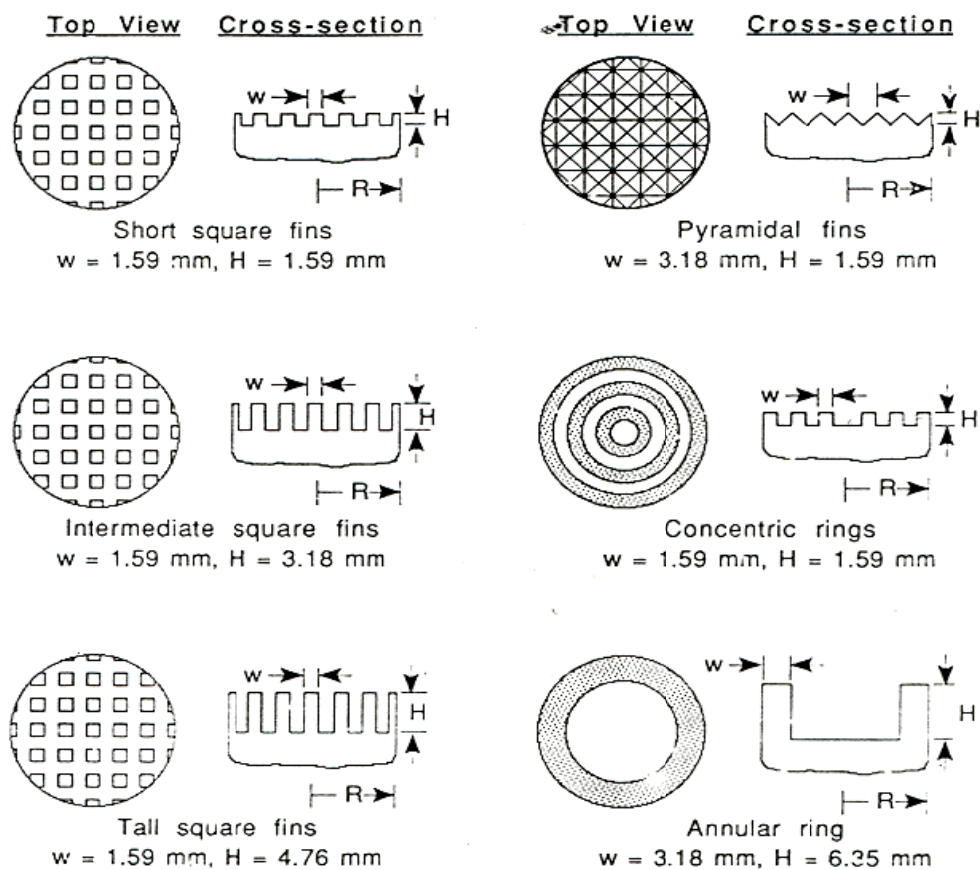
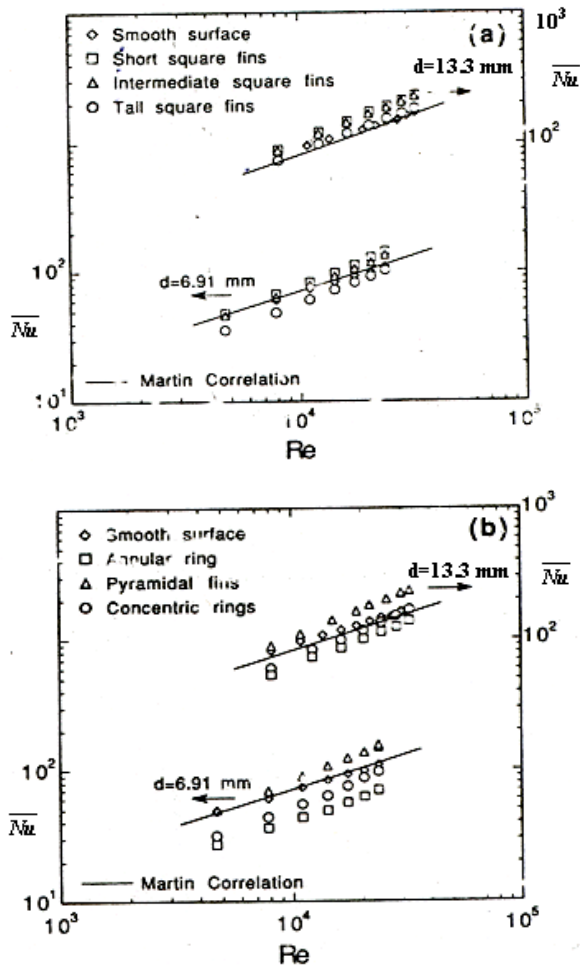


Fig. 2.9 Schematic of rough surfaces (Hansen and Webb, 1993)



“Fig. 2.10 Variation in average Nusselt number with Reynolds number for rough surfaces” (Hansen and Webb, 1993)

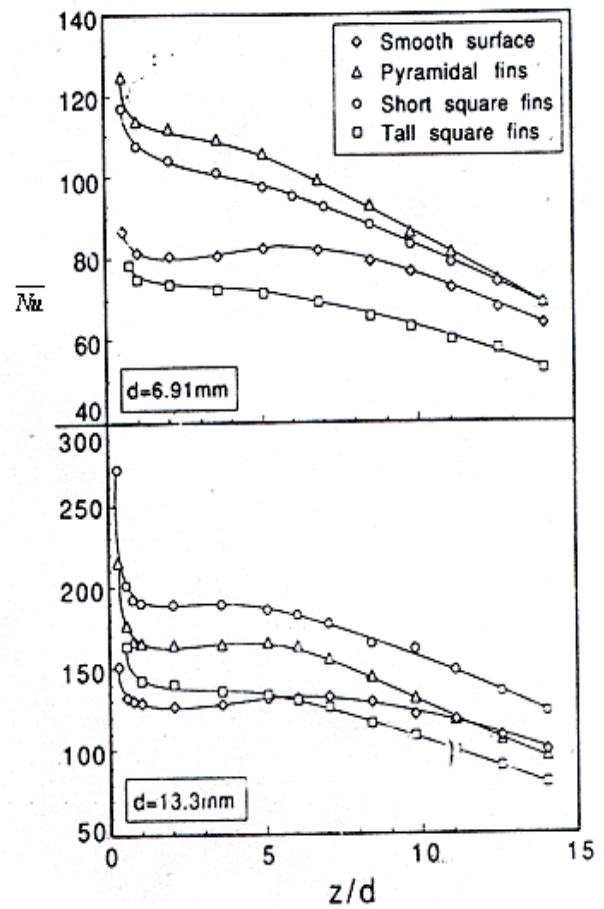


Fig. 2.11 Variation in \overline{Nu} as a function of z/d (Hansen and Webb, 1993)

The variation in the smooth surface \overline{Nu} is similar to that seen earlier i.e., increase in \overline{Nu} as the z/d is increased up to the end of the potential core and thereafter decrease in \overline{Nu} with further increase in z/d due to reduction in both, velocity and the turbulence intensity. The acceleration effect of increasing \overline{Nu} in low nozzle plate spacing can also be seen from the figure. Compared to smooth surface, pyramidal fins yield enhanced \overline{Nu} over entire range of z/d for both nozzle diameters except at large z/d for larger nozzle diameter. The short square fins enhance \overline{Nu} in all the conditions. The tall square fins enhance \overline{Nu} with large nozzle diameter at small z/d and reduce \overline{Nu} for all other test conditions.

Miyake *et al.* (1994) studied heat transfer characteristics of an axisymmetric jet from a converging circular nozzle impinging on a wall with eleven concentric attached square ribs as roughness elements ($0 < r/d < 5.0$). Each rib is separated and heated individually so as to form isothermal surface. Thus, radial distribution of segment averaged heat transfer coefficients is presented for Reynolds numbers ranging from 24000-72000 for jet to plate

distances (z/d) of 3.0-8.0. Rib parameters considered are rib height to nozzle diameter ratio (e/d) of 0.1 and 0.2, rib width to nozzle diameter ratio (w/d) of 0.1 and 0.2 and pitch to rib height ratio (p/e) of 5.0 and 10. The ribbed surface with $p/e = 5.0$ and $e/d = 0.1$ is reported to have higher heat transfer augmentation than other. At lower z/d (3.0), Nusselt numbers in the stagnation region are lower than the corresponding case of smooth surface and it was attributed to the formation of dam in the stagnation region by the first axi-symmetric rib. In the downstream, Nusselt number increase by about 30% at an $r/d = 1.0$ and decrease further monotonically. But, at $z/d = 8.0$ Nusselt numbers with the ribbed surface are reported higher than smooth surface case at all radial locations. Fourth order polynomial curve fit correlations for radial Nusselt number distribution are reported for each configuration.

Liou and Wang (1995) studied the temperature distribution in a rectangular duct having an abruptly contracting inlet and mounted with array of square ribs employing Laser holographic interferometer. They noted a better “heat transfer” in the detached-ribbed duct in comparison with the attached ribbed duct.

Chakroun *et al.* (1998) have conducted experiments with jets impinging on rough surface and the results are compared with those of flat smooth case to study the effect of roughness on the heat transfer characteristics of jets impinging on a flat plate. The roughness is in the form of cubes of size 1 mm distributed 5 mm apart on a square plate of 0.3 m side made up of brass as shown in Fig. 2.12 (Chakroun *et al.*, 1998). Reynolds number is varied from 6500 to 19000. The z/d is varied between 0.05 to 15 for smooth surface and 0.1 to 15 for rough surface. Surface temperatures are measured by 37 thermocouples evenly spaced along the centerline of the plate.

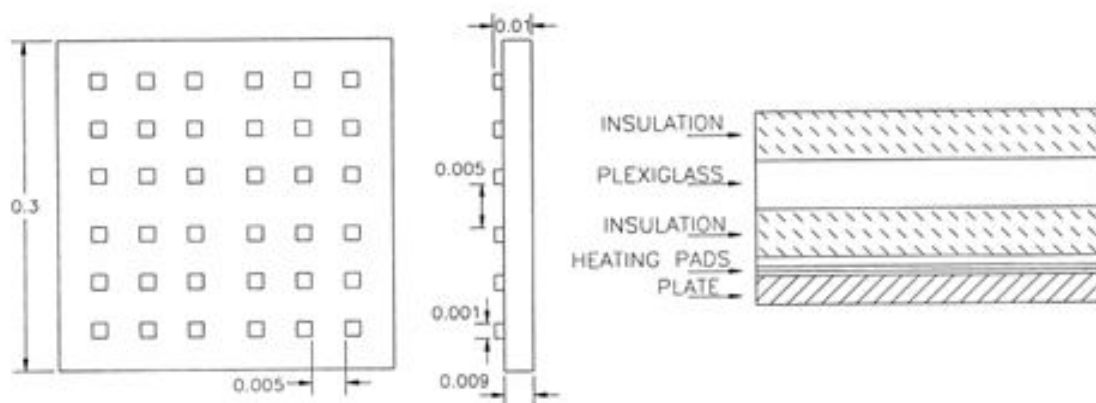


Fig. 2.12 Schematic diagram of the rough surface and plate with its heating pad (Chakroun *et al.*, 1998)

Figure 2.13(a) and 2.13(b) show the variation of Nusselt number with the lateral distance for different z/d for smooth and rough surfaces respectively, at a Reynolds number of 6500. Maximum Nu , for both the cases, occurs at the stagnation point for all the nozzle plate spaces studied and decreases monotonically in the radial direction. The maximum Nu_0 is found at z/d of 8 in both the cases. Comparison of these figures shows that the rough surfaces exhibit higher heat transfer than smooth flat plate case. The increase in local Nu with roughness elements ranges from 8.3% at z/d of 4 to 10% at z/d of 0.1.

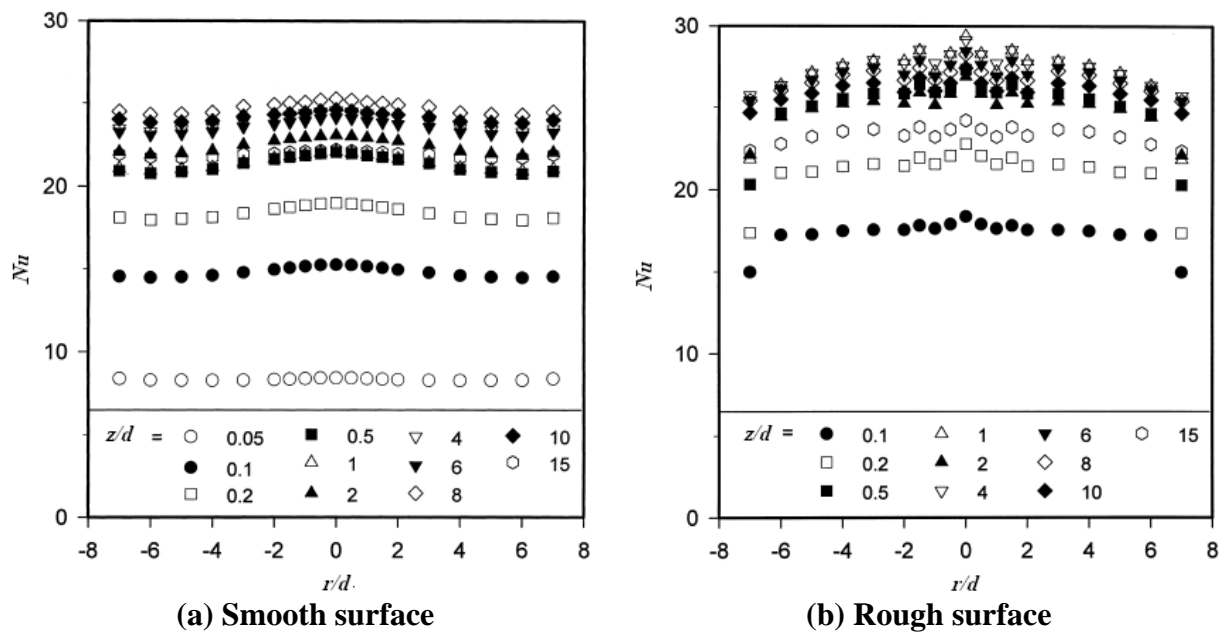


Fig. 2.13 Distribution of local Nusselt number for $Re = 6500$ (Chakroun *et al.*, 1998)

Similar variations are seen for higher Reynolds number. The increase in heat transfer is 12 to 15.5 % for Reynolds number of 11500, 18 to 25 % for Reynolds number of 15200 and 21 to 28% for the Reynolds number of 19000. In this study, no secondary peaks in the heat transfer at the nozzle-plate spacing within the potential core are observed. Similarly, no acceleration effect for very low nozzle-plate spaces is observed. This may be due to the large Target plate thickness, which causes lateral conduction and thus, gives error in calculation of local values of heat transfer coefficients.

Liou and Chen (1998), conducted experiments on spatial distribution of the periodic turbulent “heat transfer” and friction in a rectangular channel having an aspect ratio 4:1 and mounted with rectangular detached ribs on one wall. They used holographic interferometer, pressure probes, flow visualization with smoke, and laser-Doppler velocimetry techniques in their study. ‘They reported that with the attached type ribs the thermal performance non-variably decreases at constant pumping power when the rib height is increased but the detached rib type with moderate height of the rib($H/De =$

0.106) perforations performs better ($\overline{Nu}_p / \overline{Nu}_s$) at lower Re range and ($\overline{Nu}_p / \overline{Nu}_s$) is independent of H/De for the higher Re range. The detached solid-type ribs were noted to be having better “heat transfer” characteristics over the perforated-type detached ribs. Gau and Lee (2000) experimented on triangular rib-roughened walls impinged by slot air jet to study the influence of protrusions and “rib pitch-to-height” ratios on the flow and “heat transfer” characteristics along the wall. Flow visualization was made and local HTC were measured along the wall with ribs. Triangular rib geometry is found to be highly active in re-bouncing the wall jet than the rectangular ribs which leads to a noticeable reduction in the “heat transfer”. Yan *et al.* (2005) examined in detail the HTC distributions on a ribbed surface impinged by an array of jets both in-line and staggered cases. They adopted liquid crystal thermographs for temperature measurements. It was noted that the “heat transfer” over a ribbed surface is periodic-type variation in nature for Nu distributions. The “heat transfer” was best with a surface having 45° angled ribs. Katti and Prabhu (2008) analyzed the “heat transfer” between a circular jet and a flat surface modified with axis-symmetric detached ribs. “A single jet issued from a nozzle of length-to-diameter ratio (l/d) of 83 is used in their study. A consistent increase in the *HTC* from the stagnation point along the stagnation region was observed for the ribbed surface, which is well attributed to the flow behavior in this region”. The $(Nu_{ribbed} + Nu_{smooth})/2.0$ ratio is found to be a function of *Re* and increasing with *Re*

Shukla and Dewan (2018) carried out a computational study using various RANS based turbulence models for slot jet impinging on flat and ribbed surfaces and compared the results with the reported experimental data. Two cases of jet impingement were considered, i.e., on a flat surface and ribbed surface. For the ribbed surface, the jet was impinged directly at the centerline of cavity between ribs. They considered *Re* (based on the slot width) of 5500, 11000, and 20000 and H/B values of 4, 8, 9.2, and 12. For the ribbed surface, two values of the non-dimensional rib pitch (p/e) = 4 and 5 were considered, where e (= 3 mm) is the rib thickness. A non-dimensional parameter, namely, B/e (= 2 and 3) was used to study the effects of slot width on the local heat transfer distribution. They observed that none of the turbulence models considered predicted the heat transfer data accurately. However, some models predicted the experimental data with good trends, e.g., secondary peak and several spikes in Nusselt number for ribbed surface, with a precise computation of the stagnation point Nusselt number. Further, the effects of slot width, rib pitch and jet to ribbed surface spacing were investigated for jet

impingement on a ribbed surface. It was observed that the local Nusselt number increased with slot width and rib to plate spacing. It was also observed that increasing Reynolds number had a positive effect on the local heat transfer. With increasing rib pitch the local Nusselt number increased near the stagnation zone but decreased downstream.

Alenezi *et al.* (2018) studied numerically, the flow structure and heat transfer due to jet impingement on a rib-roughened flat plate. Circular ribs of square cross section placed at different radii around the stagnation point and the effect of the rougheners was simulated. An enhancement of 15.6 % in normalized averaged Nusselt number was found at the rib radial location $R/D = 2$. They observed that the maximum average Nusselt number for each location was achieved when the rib height was close to the corresponding boundary layer thickness of the smooth surface at the same rib position.

Brakmann *et al.* (2019) investigated both experimentally and numerically, the heat transfer behavior of an array of jets impinging on a flat plate with detached ribs. They studied the effect of the distance between the jets and the plate ($H/D = 3.0 - 5.0$) in the jet Reynolds numbers (15000 – 35000) with rib clearances of $0.3D$ and $.008D$. The heat transfer was investigated using TLC (Transient Liquid Crystal) method. ANSYS CFX with RANS and SST turbulence model was used for numerical simulation. They reported that the detached ribs provided a 4% increase in the global Nusselt number with adiabatic ribs. The detached ribs reduce the relative discharge coefficients by 11% compared to a smooth target surface.

Farzad & Yagoobi (2020) worked on the Drying of moist cookie dough with innovative slot jet reattachment (SJR) nozzle as the SJR nozzles overcome the high flow rate requirement associated with the traditional slot jet. An IR camera was used to capture the surface temperature distribution during the drying process. They reported 57% reduction in the drying time at 2% dry basis in comparison to a slot jet nozzle. The moist cookie surface can be considered as a surface with minor surface roughness and the results can be tallied with the slot jet impinging on a rough flat surface rather than slot jet and a smooth flat surface.

Chen *et al.* (2020) conducted experimental and numerical investigation of the heat transfer behavior of a staggered array of jets impinging on a flat plate with detached ribs. They studied the effect of the distance between the jets and the plate ($H/D = 3.0 - 5.0$) in the jet Reynolds numbers (15000 – 35000). The heat transfer was investigated using TLC (Transient thermo chromic Liquid Crystal) method. ANSYS CFX with a steady state RANS method and SST turbulence model was used for numerical simulation. They

reported that the performance of the detached ribs in staggered arrangement is comparable with inline arrangement results of their earlier work with a 4% increase in the global Nusselt number with adiabatic ribs. The detached ribs reduce the relative discharge coefficients compared to a smooth target surface.

Few studies have reported turbulent impinging jet heat transfer over ribbed surfaces. Two types of arrangements are possible for a rib fitted impingement plate, e.g., ribs may be fixed on the impingement surface (i.e., attached ribs) or these may be detached with a small gap from the impingement surface (detached rib). Jet impingement over a rib fitted target surface interrupts the wall jet. Accordingly, turbulence level raises locally and, therefore, the rate of heat transfer increases with the ribbed surface. Very few studies related to slot jet impingement on a ribbed surface have been reported in the literature. Hence there is an ample scope for the study on the fluid flow and heat transfer behavior of a single slot air jet normally impinging on a rib roughened flat surface. It is possible to suggest a best configuration for industrial cooling/heating applications by proper study of the behavior of the jet with rough surface.

2.3 Heat transfer and fluid flow distribution on smooth flat plate impinged by a confined single jet:

Most of the cases like cooling of a combustion chamber wall, turbine blade, cooling of electronic gadgets, cooling of the surfaces happens in an enclosed environment rather than an open impingement cooling or heating. So, the study of the fluid flow and heat transfer behavior of these cases and other similar applications may be entirely different from open impingement on a smooth surface discussed already.

Hence it becomes essential to study the behavior of the jet when confined, to know a better configuration for design a highly efficient heating or cooling device or system for actual industrial applications.

In this regard the the studies made by the earlier researches with reference to the influence of confinement is reviewed in the following paragraphs

Gardon and Akfirat (1965) studied the effect of turbulence on the heat transfer coefficient maximum in a variation of stagnation point heat transfer coefficient with secondary characteristics of submerged impinging jets. On heat transfer characteristics is notable that nozzle to plate spacing distribution in the radial direction of local heat transfer coefficients this phenomenon specifically to slot jets

Gaunter *et al.* (1970) surveyed flow characteristics of single turbulent jet impinging on a flat plate. The flow field is divided into four distinct regions. Methods for predicting velocities and pressures in various regions agree reasonably well with experimental data. Determine the influence of flow Reynolds number on core length and the large discrepancy between the theoretical and experimental velocity gradients near the wall. The axial velocity for a free jet is constant and equal to the nozzle exit velocity over a distance equal to the potential core length. For a slot jet, the axial velocity downstream of the potential core is inversely proportional to the root square distance from the jet nozzle in slot widths.

Vader *et al.* (1991) examined on a technique for unfaltering of measuring on local heat exchange of an impinging fluid stream and found as local convection coefficients for heat exchange to an impinging fluid jet. It is noted that the 5.1mm on opposite side of heater took intervals to find the heat flux distribution and temperature .

Jambunathan *et al.* (1992), surveyed on a Single Circular jet of Heat Transfer information that turbulent jets with spout way out of Reynolds number 5000-124000 and Nusselt number at radii more noteworthy than of six nozzle diameters from stagnation point. Jets issuing from square edged orifices openings give higher Jets exchange contrasted from elliptical and streams to circular jets and noticed that the surrounding temperature is not equivalent to air temperature at the nozzle exit .

R.K. Brahma (1992) studied the slot jet impinging on a flat surface and predicted fluid flow and heat transfer characteristics at the stagnation point. A correlation was proposed for stagnation point heat transfer considering different nozzle to jet placings and Reynolds number. Results obtained in terms of velocity gradient at stagnation point were compared with velocity profile at nozzle outlet of a two-dimensional jet.

Ichimiya and Hosaka (1992) observed heat transfer characteristics of confined two-dimensional jets on a flat surface. For Experiment, they used three slot jets and keeping a distance of $H= 0.5$ to 3, dimensional less pitch $p=6$ to 16 and Reynolds number 500-8000 for comparing with the unconfined jet. They observed that for laminar flow the heat transfer increases locally due to the second jet. The values are estimated numerically for all the jets.

Cooper *et al.* [1993] worked on flow field characteristics of a turbulent jet impinging orthogonally on a large surface at two Reynolds numbers of 23000 and 70000. Turbulence energy of Re 23000 is high rates compared with stream free fluid.

Lin, *et al.* [1997] supervised the heat transfer behavior of a confined slot jet impingement on a flat surface considering various Reynolds number and jet to plate spaces. They found that the stagnation point, average and local Nusselt number are influenced by Reynolds number and depends insignificantly on a jet to plate spaces. A concept of effective cooling length was introduced for evaluating the numerical average heat transfer performance.

Baydar [1999] studied confinement effects air impinging jet at Reynolds number is to be lower. Experimented on a single jet with Reynolds number of 500-10000 and double jet with Reynolds number of 300-10000 at varying z/d in the range of 0.5-4. for greater Reynolds number of about 2700, the subatmospheric pressure occurred for up to nozzle to plate spacing of 2.0. It is observed that there is a link between the peak in heat transfer coefficient and subatmospheric region to some extent.

Carlo Carcasci [1999] experimented on air impinging jets using visualization methods for air impinging jets. Heat transfer coefficient distribution is found to follow for a row of jets the flow pattern with subsonic velocity impinges on a flat plate.

Narayanan *et al.* [2004] experimentally studied on submerged slot jets on a flat plate. With hydraulic diameters of 0.5 and 3.5 which correspond to potential – core region and transitional region respectively. It is observed that heat transfer coefficient of impingement region is peaked at that level and decreases monotonically towards the wall jet region.

Baydar and Ozmen [2005] conducted experiments on the effect of higher Reynolds number for confined air impinging jets on a flat plate and numerical investigated experimental values. They chose Reynolds number of 30000 and 50000 z/d in the range of 0.2-6.0. Deceleration of the jet occurs due to the presence of impingement plate. At z/d up to 2, the subatmospheric region is observed. As the nozzle exit to plate distance increasing the subatmospheric pressure moves radially outward from stagnation point. Concluded that there is a strong relation between heat transfer coefficient, turbulence intensity, and sub-atmospheric region.

Danielle *et al.* [2005] analyzed the behavior of a near to wall impinging jet. For turbulent impinging jet considered single nozzle to plate spacing that of semi-confined is 2.0 and Reynolds number of 35000 and measured the longitudinal turbulence profile. The mean temperature is measured using thermocouples. They observed that the minimum temperature profile occurs away from the wall.

Lupton *et al.* [2008] supervised the effect of variation in confinement levels of miniature air jets on heat transfer and concluded that confinement effects are more significant on miniature diameter jets than for larger diameter jets. For miniature jets at large Reynolds number ($Re = 12,700$), the local heat transfer decreases with increasing confinement over both stagnation and wall jet regions and differences as high as 69% in the stagnation region were seen whilst contrasting the two extreme levels of confinement tested.

Choo and Kim [2010] concentrated on the thermal conductivity of two impinging jets confined and unconfined with dimensionless pumping force of reach 1.35×10^{10} — 4×10^{13} and nozzle to plate dividing is not as much as single nozzle diameter measurement of $z/d = 0.125$ - 1.0 . and result happened as under altered pumping power condition the thermal execution of confined jet is same as that of the unconfined jet while under fixed flow rate stream condition for the confined jet is 20%-30% lower than an unconfined jet.

Nirmalkumar *et al.* [2011] experimented on the “heat transfer behavior of a slot jet in the stagnation region ($0 \leq x/b \leq 2$), transition region ($2 \leq x/b \leq 5$) and wall jet region ($x/b \geq 5$). For a given z/b , heat transfer Coefficient increases with the increase in the Reynolds number in the streamwise direction. In a slot jet, secondary peak is not evident at lower Reynolds numbers and larger z/b s. and is strongly evident at maximum Reynolds number of 12,000” and for the $z/b \leq 1$.

Lee *et al.* [2012] “experimented on an isothermal flat plate with laminar heat Transfer Characteristics are determined subject to a miliscale confined impinging slot jet having an aspect ratio (y/b) of 50.” They found from visualization of slot jet flow of overall structure with jet columns in lateral distortions of at vortex structures, it is found to be Nusselt numbers sensitive to the laminar boundary layer, and laminar space jet close divider temperature gradients will come about consistent surface temperature on thermal boundary conditions. Cooling is focused close to the impingement area on the surface just for a solitary ordinary impinging jet.

Patil *et al.* [2014] experimented on confined impinging circular air jet and measured the wall static pressure at Re 18000-40000 at the nozzle outlet & J2P spacing in the range of 0.25-4. It is found that the maximum pressure occurs at the stagnation point. Maximum pressure decreases with a nozzle to plate spacing and with the increase in r/d . The subatmospheric region also increases with the Reynolds number.

Katti *et al.* [2014] Experimentally Investigated the local distribution of wall static pressure coefficient due to impinging slot air jet on the smooth and rough surface. Co-efficient of wall static pressure is seen to be independent of Reynolds number in the range

of 5000-20000 for a given jet to plate distance in case of a smooth surface. Wall Static pressure Coefficient decreases with increases in a jet to plate distances due to entrainment of surrounding quiescent air and loses effect of impact on the target plate. Wall static pressure coefficient is maximum at the stagnation point for all the configuration studied and decreases along the streamwise direction which may be attributed to increase in the velocity along the plate. It is observed that wall jet region starts around x/D_h of 1.5.

Qiu et al. (2019) studied numerically the effects of surface curvature, jet to target spacing and jet Reynolds number effects on the heat transfer and fluid flow characteristics of a slot jet impinging on a confined concave target surface at constant jet to target spacing. Jet to target spacing, H/B is varied from 1.0 to 2.2, B is the slot width. The jet Reynolds number, Re_j , varied from 8,000 to 40,000, and the surface curvature, R_2/B , varied from 4 to 20. They reported that an obvious backflow occurs near the upper wall and the local and averaged Nusselt numbers considered in the defined region respond positively to the Re_j . They recorded that the surface curvature plays a positive role in increasing the averaged Nusselt number for smaller surface curvature (4-15) but affects little as the surface curvature is large enough (> 15). They concluded that the thermal performance is larger for smaller surface curvature and changes little as the surface curvature is larger than 15. Also, the jet to target spacing shows a negative effect in heat transfer enhancement and thermal performance.

2.4 Heat transfer and fluid flow distribution on a rough (ribbed) flat plate impinged by a confined single jet:

From the studies and experiments it is already confirmed that the roughness on a surface improves the heat transfer characteristics between a jet and the surface in comparison with a smooth surface heat transfer particularly in open impingement cases analyzed. The confinement is also proved advantageous in improving the thermal behavior of the jet in comparison with unconfined smooth as well as unconfined rough surfaces. This advantage of roughness and confinement may be applicable in some special case where the actual environment is truly a rough and confined one. So our study is extended to explore the combined influence of confinement and roughness on the flow and heat transfer characteristics of a single slot jet impinging on a confined ribbed surface.

The confined and rough surfaces are very common in most of the applications like electronic packaging, food industry etc.

The work done by the researchers in the past is summarized as below.

Gardon and Akfirat [1965] analyzed the influence of velocity and turbulence on “heat transfer” characteristics of impinging 2-D jets by varying “Reynolds number” from 450 to 22000 and a slot width of 1.58, 3.175 and 6.35 mm. the observed nonmonotonic variation of “heat transfer” along “streamwise direction”. $SP Nu$ is to be constant for the J2P spacing less than the potential core length. They reported a non-monotonic variation of $SP Nu$ with J2P spacing is due to the effect of centerline velocity, arrival velocity, turbulence and the ratio of arrival velocity to jet width. The occurrence of secondary peaks in heat transfer due to the transition from laminar to turbulent triggered by the disappearance of the pressure gradient. They also observed heat transfer of the laminar boundary layer with a positive pressure gradient is more than the turbulent boundary layer is observed at a pressure gradient. They reported that $SP Nu$ is higher at the point of jet impact on “Target plate” at the end of the potential core region.

Beitelmal *et al* [2000] explored the influence of surface roughness on “average heat transfer” at on impinging air jet. The temperature was measured for “Reynolds numbers” from 9600 to 38500 and J2P spacing (z/d) of 1 to 10. They observed an enhancement of about 6% in the “average Nusselt number” with the roughness on the surface. “The roughness disturbs the boundary layer and hence promotes the turbulence of wall jet in turn increasing the rate of heat transfer from the surface. A correlation was proposed for average Nusselt number considering the Reynolds number and J2P spacing as the variables”.

Gau and Lee [2000] studied fluid flow and “heat transfer” between a triangular rib roughened wall and a slot air jet with reference to the effect of rib heights. They varied: the “Reynolds number” between 2500 and 11000, the ratio of slot width to rib height from 1.17 to 6.67 and J2P spacing from 2 to 16. “They observed that widely opened cavity between neighboring ribs makes more intensive exchange of momentum between the wall jet and the cavity flow that leading to a higher heat transfer rate and in the region of laminar wall jet that leads to a reduction in heat transfer”. The correlation of stagnation “Nusselt number” was proposed.

Chirac and Ortega [2002] adopted the numerical FDM to determine the effect of steady flow and unsteady flow on “heat transfer” between a “slot jet” and an isothermally heated plate. The jet “Reynolds number” ranging from 250 to 750 of “Prandtl number” 0.7 and J2P spacing (H/W) of 5 is studied. They reported that at “Reynolds number” 585-610 the flow become unsteady. In the steady regime stagnation, the Nu is directly proportional to

the Re and distribution of HTC in the wall jet region was influenced by re-entrainment of the flow.

Gao and Sunden [2003] determined the “heat transfer” character of a confined single “slot jet” and multiple “slot jet” experimentally. The liquid thermograph technique was used to tap the distribution behavior of temperature over the surface. The effects of the J2P spacing, “Reynolds number” and width of jet and presence of the exhaust port on the local Nu and average Nu is studied. Comparing the single and multiple jets at two J2P spacing (H/B) 8 and 24, all the local Nu distribution shows the same behavior for all “Reynolds number” from 1150-7550, leading to an opinion that increase in the slot-to-slot distance in multiple jets prevents the jets interacting with each other. The effects of the J2P spacing on $SP Nu$ of central jet of the three-slot system and single “slot jet” at varying Re observed and $SP Nu$ is maximum at $H/B=8$ and both jets have same value up to $H/B=8$, increasing in H/B leads to decrease in Nu_0 values of multiple jets. The effect of slot width shows that higher width has a higher local “Nusselt number” and lower width has a higher “average Nusselt number”, it occurs due to a rise in the intensity of the turbulence with the increase in slot width.

Narayan *et al* [2004] experimented on the WSP and heat transfer between a turbulent slot jet. Two J2P spacing of $3.5D_h$ (transitional jet) and $0.5D_h$ (potential core jets) are considered for exit Reynolds number at 23000. They reported a high heat transfer rate in the transitional jet impingement and non-monotonic decay in the HTC. For potential core jet impingement and generation of turbulence near the surface prior to impingement and pressure at span-wise vertices in the stagnation region with an increase in near-wall responsible for increasing heat transfer in transition jet impingement.

Baydar and Ozmen [2005] experimentally and numerically investigated the impinging air jet at Re ranging from 30000 to 50000. The mean velocity, turbulence and pressure distribution, were obtained for given Re and a J2P spacing ranging between 0.2-6. They observed pressure distribution on the “Target plate” was independent of the “Reynolds number”. Negative pressure region appears on the target surface for the J2P spacing up to 2 and it becomes more prominent with decrease in the J2P spacing. They reported maximum turbulence intensity and a secondary “Nusselt number” peak was observed in the negative pressure region.

Lou *et al* [2005] numerical studied the role of nozzle geometry, nozzle width, “Reynolds number” and roughness of target surface with confined jet “heat transfer”. The nozzle size is varied from 0.6 to 2mm. J2P spacing ranges from 0.5 to 10mm and “Reynolds number”

varied from 26.8 to 1000. Pressure drop for different H/W is plotted. They observed that “heat transfer” depends on all geometric parameters HTC and the Nu increases with decreasing of nozzle width and J2P spacing. The surface roughness may cause an increase in “heat transfer” due to deterioration of laminar impinging jet.

Gao and Ewing [2006] studied the effect of confinement on “heat transfer” characters circular jet exiting from a long pipe. The Re varied from 17000 to 28000. They observed that confinement hardly influences on the “heat transfer” for nozzle to placing (H/D) more than 1 and it reduces “heat transfer” by 50% in the “streamwise direction” of nozzle to placing (H/D) less than 0.5 due to turbulent fluctuation in “heat transfer” region reduced and converted more slowly in this region and they also reported a decrease in “heat transfer” in confined jet shifting outward with increase in the J2P distance.

Zhou and Lee [2007] worked on the “heat transfer” and flow behavior of a rectangular jet interacting with a heated plate. They experimentally determined the effect of Re and J2P distance on the local and average Nu . They observed that higher the “Reynolds number” larger is the turbulence intensity and mean velocity. The mean velocity decreases rapidly at $X/B = 0.4$ to 0.6 due to vena contract in orifice jets (“Reynolds number” varied from 2715 to 25005 and J2P spacing was varied up to 30). They also observed that J2P distance significantly affects the “heat transfer”. A correlation was proposed relating local and average “Nusselt number” and the turbulence of the free-stream.

Katti and Prabhu [2008] “studied the enhancement of heat transfer on a flat plate surface using axis symmetrical ribs by normal impingement of circular jet. Effect of ribs width (w) ribs height (e) pitch between the ribs (p) location of the first rib from stagnation point and clearance under the rib (c) on local heat transfer distribution is studied J2P distance varying from 0.5 to 0.6. They observed an enhancement in heat transfer due to the acceleration of fluid in that region created by clearance under the rib and Nusselt number of stagnation point increases by shifting rib nearer to the stagnation. With increasing in width of rib major flow impinges on the top surface of rib and may not reach to target surface it may lead to decrease in heat transfer and increasing rib height flow velocity along the target surface decaying at a faster rate. They also observed the wall static pressure gradient of stagnation point is higher for a surface with detached ribs than a smooth surface”.

Akansu *et al* [2008] experimented to determine the effect of inclination on the fluid pressure and heat transfer characters of a slot jet and a flat surface. The effect of angle of inclination, J2P spacing and Re were studied. They observed that the angle of inclination

influences significantly on the Maximum heat transfer. As the angle of inclination increases, the point of maximum heat transfer shifts in the direction of the ascending side of the plate. At the lower J2P spacing, the value of heat transfer coefficient increases with inclination.

Gulati *et al* [2009] studied the effects of the nozzle geometry, J2P spacing and Re on impinging air jet. “Reynolds number” varied from 5000 to 15000 and J2P spacing from 0.5 to 12 times the diameter of the nozzle. A suitable l/d ratio of 50 is used to get a developed flow. The local “heat transfer” was determined using IR thermal imaging technique. They observed that rectangular nozzles show high “heat transfer” rate due to high turbulence intensity at nozzle exit and it requires more pumping power due to larger pressure losses. The drop in the pressure drop across the nozzle is measured and the coefficient of pressure loss is determined for all the configurations of the nozzle.

Chao and Kim [2010] compared the thermal behavior of a confined and an unconfined impinging jet. The effect of pumping power and flow rate is studied by varying Reynolds number from 3600 to 17300 and two J2P spacing of 0.125 and 0.25. They observed the thermal characteristics of the confined jet is similar to an unconfined jet of fixed pumping power condition while the thermal performance of confined is 20% to 30% lower than unconfined jet under fixed flow condition. The correlation for stagnation and average Nusselt number for both confined and unconfined impinging jet presented.

Ozmen [2011] carried out the experiment to study the fluid flow behavior of confined twin air jets at Reynolds number of 30000 to 50000, J2P spacing of 0.5 to 4 and jet to jet spacing varying from 0.5 to 2 were studied. The flow is visualized by smoke wire method at $Re=4800$. They observed that sub atmosphere pressure is observed on both target surface and the confinement plate for J2P spacing up to 1.0 for all Reynolds number and jets to jet spacing. They also observed that surface pressure distribution on the target surface and the confinement plate is independent of Reynolds number .

Nirmalkumar *et al* [2011] experimented on the local “heat transfer” distribution and flow properties on a smooth plate and an impinging slot air jet. Slot width based Re is varied from 0.5 to 12. They recognized 03 regimes on the flat surface viz. stagnation region ($0 \leq x \leq 2$), transition region ($2 \leq x/b \leq 5$) and wall jet region ($x/b \geq 5$). The semi-empirical equations were proposed for the Nu in the stagnation region and for the Nu values in the wall jet region.

Katti, *et al* [2014] experimentally studied the local WSP distribution over a flat smooth surface and a flat rough surface interacting with a “circular jet”. They observed that WSP

is sovereign of “Reynolds number” and its strength diminishes as the J2P spacing increases, they also observed an enhancement in “heat transfer” rate at the rough surface using detached ribs compare to smooth surface.

Nevin Celik (2020), studied the effect of style of roughness, the jet geometry, effects of jet-to-surface distance (H) and radial distance (r) on the heat transfer from target surface for a constant jet Reynolds number 20,000 adopting the Design of Experiment (DoE) and Analysis of Variance (ANOVA). The highest effect on Nusselt number is observed to be the radial distance (88%), while surface roughness has the effect in percentage of 8%. The contribution of jet geometry and jet-to-surface distance is much lower, as being 3% and 1%, respectively.

From the review of published and available literature it is identified that there is an ample scope to explore the local distribution of WSP and HTC on a rough surface with confinement under the interaction of “slot jet”.

2.5 CONCLUSIONS FROM LITERATURE REVIEW

The gas turbine engine performance may be improved by providing higher gas temperatures at turbine entry which in turn require active cooling of the turbine blade.

Literature review suggests that heat transfer enhancement by jet impingement has significant potential to increase the local heat transfer coefficient. Impingements from arrays of jets are one of the methodswidely used to reduce the blade temperature on the mid-chord and leading-edge regions. Hence, many researchers have shown keen interest in the topic. The available literature studies reveal that there are still unaddressed issues like the thermal issue of uniformity of distribution of heat transfer. This issue may be dealt adequately if local heat transfer characteristics under the influence of various geometric and flow parameters of the impingement system are investigated. Hence, in the following section a brief discussion on the major studies missing in the literature in different aspects of jet impingement cooling is highlighted which has led to the scope of present work.

2.5.1 The conclusions from literature review on single jet impinging on smooth flat surface:

Many prior studies are carried out on the heat transfer and fluid flow characteristics due to single jet impinging normally over a flat smooth surface. Gardon and Cobonpue (1962) reported the local heat transfer distribution between a circular jet and flat plate using a specially designed heat flux gage. Hrycak (1983) conducted experiments of heat transfer

to round jet from flat plate to study stagnation and average heat transfer characteristics. Lytle and Webb (1994) studied the effect of very low nozzle-to-plate spacing ($z/d < 1$) on the local heat transfer distribution on a flat plate impinged by a circular air jet issued by long pipe nozzle. The correlations for stagnation point heat transfer are reported for low jet-to-plate distances ($z/d \leq 1.0$). Lee *et al.* (2004) studied the effect of nozzle diameter on impinging jet local heat transfer and fluid flow at a Reynolds number of 23000.

Most of the correlations proposed are for average heat transfer coefficients between circular jets and Target plate and a few correlations for stagnation point Nusselt numbers available are based on regression analysis from experimental data. It is understood from the published available literature that there is a need to obtain local distribution of heat transfer coefficients and generalized correlations for local heat transfer coefficients based on the flow characteristics on the Target plate due to a slot jet impingement and the available semi-empirical predictions.

2.5.2 The conclusions from literature review on single jet impinging on flat surface with surface roughners:

The influence of surface roughness elements on heat transfer enhancements are reported by a few researchers. Hansen and Webb (1993) and Chakroun *et al.* (1998) have studied heat transfer characteristics from an impinging circular jet on the flat “Target plate” with different surface roughness elements on it. However, their data reflects the average Nusselt number variation rather than local data because of the large thickness of the target plate. Miyake *et al.* (1994) and Gau and Lee (1992, 2000) have reported the heat transfer augmentation to jet impinging on target surface with attached ribs of thermally active materials. Thus, the augmentations reported may be due to combined effect of two factors, namely (a) the enhanced turbulence mixing by distorting the flow fields caused by the presence of ribs and (b) the extension in heat transfer surfaces *i.e.*, the fin effect caused by the ribs. Few studies are reported on the heat transfer characteristics due to detached ribs in the internal flow situation. The work on the influence of roughness on the fluid flow and heat transfer characteristics of slot jet impingement is not much attempted by the earlier researchers. In view of the above observation, an attempt is required to extend the benefits of heat transfer augmentation due to detached ribs seen in internal flows to impinging jet flows. There is no sufficient information available in the literature on the heat transfer distribution on the flat plate with detached ribs due to slot

jet impingement. It is felt that the present study has to focus on the detailed parametric investigation and identify a configuration which gives higher heat transfer enhancements relative to corresponding smooth surface case.

2.5.3 The conclusions from literature review on single jet impinging on flat surface with confined slot jet

The influence of confinement on the thermal behavior was studied by Chao and Kim [2010] and reported that the thermal performance of confined is 20% to 30% lower than unconfined jet under fixed flow condition. The correlations proposed are limited to the stagnation and average Nusselt number for both confined and unconfined impinging jet presented. Ozmen [2011] carried out the experiment to study the fluid flow behavior of confined twin air jets at and observed that sub atmosphere pressure is observed on both target surface and the confinement plate for J2P spacing up to 1.0 for all “Reynolds number” and jets to jet spacing. They also observed that “surface pressure distribution” on the target surface and the confinement plate is independent of “Reynolds number”. The detailed investigation on the local distribution of C_p and Nu is not available and needs to be focused as part of our experimental studies.

2.5.4 The conclusions from literature review on single jet impinging on flat rough surface impinged by a confined slot jet

Even though a noticeable work is done by the various researchers on circular jets, non-circular jets and two-dimensional jets interacting with smooth surface, ribbed surface, finned surface, etc. and many correlations are also available on various individual cases of impingement heat transfer situations, In particular to the combined influence of surface roughness and confinement of the jet on the fluid flow and heat transfer characteristics of slot air jet is not found in the published literature. There is a lot of scope as this type of situation is very common in most of the industrial cooling/ heating applications and needs to be addressed in detail.

2.6 OBJECTIVES OF THE PRESENT WORK:

There are many unaddressed thermal issues of gas turbine heat transfer. The effective active cooling of the turbine blades using compressor bleed air is required for higher efficiency of the gas turbine engines. The jet impingement cooling technique has significant potential to increase the local heat transfer coefficient. Arrays of impinging jets are one of the methods currently used to reduce the blade temperature on the mid-chord and leading-edge regions.

The primary objective of the present study is to address one of the thermal issues of uniformity of distribution of heat transfer of gas turbine blades. This requires knowledge of local distribution of heat transfer coefficients, particularly for impingement cooling. Based on the review of available literature of impingement cooling, it is felt that the systematic experimental investigations to study the influence of various geometric and flow parameters of the impingement system on the local heat transfer characteristics is essential. Prior to investigating the configurations simulating the impingement cooling of internal passages of typical gas turbine blade, the present study focuses, first, on the local heat transfer distribution due to single jet impingement on flat surface. Thus, the objectives of the present study are explained as in the following paragraphs.

To study the fluid flow and heat transfer characteristics of a single slot jet impinging on:

1) A **smooth flat surface** impinged by a single **unconfined slot air jet** for various J2P spaces and at different Re to assess the best possible combination of flow rate and jet to plate distance for optimum heat transfer attainment as necessitated in open impingement cooling/heating applications.

2) A **rough flat surface** impinged by a single **unconfined slot air jet** for various J2P distances and at different Re to make it possible to enhance the heat exchange between the jet and target in comparison to the smooth open impingement cases. This is highly needed as in real life applications the surfaces are not exactly smooth and bound to have some roughness and irregularities on the surface, may be due to wear and tear, scratches etc. so the knowledge of the jet behavior over the rough surface is very essential to design a suitable cooling/heating device for industrial or real-life applications.

3) A **smooth flat surface** impinged by a single **confined slot air jet** for various J2P distances and at different Reynolds numbers. In many applications it is necessary to provide some cowling or air dams as a feature in working aspects and it becomes similar to a smooth confined surface or confined jet and a smooth surface situation where the heat transfer behavior may be entirely different from an unconfined or open impingement case. To optimize the heat transfer in such situations the information about the flow behavior of the confined jet is very much desirable and hence it forms one of the important objectives of our work.

4) A **rough flat surface** impinged by a single **confined slot air jet** for various J2P distances and at different Reynolds numbers. In some applications the roughness may

be a part of construction of a device to provide strength and stability. This surface is if provided with some flow confinement it needs a special consideration of designing a heating or cooling apparatus to enhance the heat transfer behavior of the system with reference to a smooth, unconfined surface particularly where the high rate of heat transfer is a primary criteria requirement.

5) To propose the correlations for the flow behavior and heat transfer characteristics for the possible configurations

So, our work begins with the smooth surface heat transfer behavior, adds ribs to enhance the local heat transfer and gets confined to match the industry need in an application and finally combines the roughness and confinement to suggest a best possible configuration of jet and the surface parameters to suit any real-life heating/cooling applications.

CHAPTER 003

Local distribution of “heat transfer” on a smooth flat surface due to an impinging slot air jet

3.1 INTRODUCTION:

The impingement cooling is the oldest and popular technique, particularly for applications like the gas turbine blade cooling where heat flux is very high. Impingement cooling is highly appreciated because of its high heat exchange characteristics. This kind of impinging device leads to enhancement of cooling rate for relatively small surface areas. Impinging jets are adopted for the processes requiring heat exchange rate as in: textile industry, papers and films, glass and metal industry, reducing the temperature of combustion chamber wall, turbine blades and electronic equipment, etc. owing to the availability, low cost, and reliability, air may be invariably used as a cooling fluid. Parameters like “Reynolds number” (Re), J2P spacing (Z/D_h), distance from “stagnation point” (x/D_h) along the “streamwise direction”, inclination of target plate, geometry of target surface, nozzle geometry, turbulence level at the jet exit & roughness of the target surface, confinement of the jet influences the heat exchange rates of the impinging jets.

The current study aims on the effect of Re and J2P spacing (Z/D_h) on the Local distribution of CWSP and HTC due to the interaction of slot air jet and the smooth & flat target plate. A fully developed flow is attained for Re varying from 2500 to 20000 with J2P spacing (Z/D_h) varied from 0.25 to 10, using a “slot jet” having $(l/b) = 22$ and an aspect ratio $(h/b) = 11$. The images obtained from the thermal IR camera are used to

determine the heat exchange coefficients at local points. The CWSP are determined for the specified parameters using Differential Pressure Transducer (DPT). The results of the experiment are analyzed in the light of flow physics governing the given situation. The heat exchange characters are related to the flow characteristics for various configurations attempted in the study and are well compared.

Many of the earlier works aimed on interaction between circular jet & flat-smooth surface. Researchers Bietelma *et al.* (2006), Bramha R K (1992), Choo & Kim (2010), Sahoo & Sharif (2004), Gao & Sunden and Gordan & Cobonpue (1962) have worked on the local heat exchange between a flat surface and circular jets.

The work done by Gardon and Akfirat (1965), Gardon and Akfirat (1966), Narayan *et al.* (2004) on the non-circular jets has been discussed already in the chapter 2.0,

Beitelma *et al.* (2006) analyzed the 2-D jets and proposed a correlation for the HTC in the wall jet and stagnation regions with simplified flow assumptions. They considered “Reynolds number” from 4000 to 12000 and J2P spacing from $4b$ to $12b$. They explained the constant stagnation region Nu based on a potential theory and the thickness of the temperature boundary layer.

Zhou and Lee (2007) studied the heat exchange and fluid flow behavior of a rectangular nozzle with sharp edges, for slot width based Re varied from 2715 to 25005 and the J2P spacing was varied up to 30. The outcome of variations in the Re , turbulent intensity, and J2P spacing, was studied and proved the significance of these variables on the “heat transfer” behavior. Also, correlation was proposed relating the $SPNu$ and Nu_{average} and turbulence as variables.

Tu and Wood (1996) determined the pressure and shear stress on a surface. Their experiment was with slot-jets having a width 0.97mm & 6.4mm at a slot width-based Re_b , in the range of 3040 to 11000. The jet and plate spacing (Z/D_h) was varied up to 20. They identified that the Gaussian profile describes the pressure distribution on the surface.

From the preliminary literature studies, it is found that prior research on impinging “Slot jet” is limited to the average HTC on smooth surfaces. The flow structure of a jet at the exit is found to be very much influential on the rates of “heat transfer”. Correlation for WSP distribution with “heat transfer” for smooth surface is not available. Earlier researchers report no exhaustive work on the influence of fluid flow characteristics on the local HTC.

Hence, it is proposed to study the local *HTC* and fluid flow behavior of impinging slot air jets on flat smooth and flat rough surfaces. In addition, it is intended to propose necessary “heat transfer” correlations for the various configurations studied.

3.2 Experimental Setup

The test set-up used to study the local distribution of WSP and local *HTC* on smooth “Target plate” are depicted in Figure 3.1(a) and 1(b) respectively. Air is supplied by a blower and metered using an orifice meter, venturimeter and needle valve to attain the required flow rates. Wire meshes are provided in the plenum chamber to achieve a uniform and completely developed flow at the jet exit. The velocity profile remains uniform because of the diffuser provided upstream of the plenum chamber. An acrylic sheet is used to fabricate the nozzle. The dimensions of the nozzle are $h \times l \times b$ as $45 \times 90 \times 4$ in mm.

The effect of nozzle height is neglected as a high aspect ratio around 22 is maintained for the nozzle. The temperature on the surface are measured using IR thermometry using a ‘FLUKE Ti 55’ IR thermal camera having a good resolution 3.3 pixels/mm can be obtained for the temperature data compared to thermocouple technique. A regulated AC power source is used to heat the target surface. The power supplied is measured to the “Target plate” is metered using a ‘Meco’ digital meters having range of 0 to $400 \pm 0.5\%$ and an accuracy of 0 to $20 \pm 0.5\%$ V respectively. Voltage taps are located at suitable positions on the surface to measure actual voltage supplied. The air jet temperature is measured by a combination of a thermocouple installed at the inlet of the nozzle and a digital milli voltmeter. the “Target plate” is positioned at different J2Pdistances usind 2-D traverse table.

The experiment set up used to measure free jet velocities is shown in the figure 3.2. A pitot tube/ static probe mounted on a 2-D traversing table is aligned to the center line of the jet emerging out of the slot nozzle. The pitot tube is connected a digital pressure transmittter and the pressure values are recorded along the center line of the jet at various distances between the nozzle exit and the probe tip. The procedure is repeated at different Reynolds numbers maintaining a steady state flow at the nozzle exit. this study helps in identifying the potential core region for the jet where the centerline velocity of the jet remains almost constant in the region. This helps in identifying an optimal jet to plate distance for better heating or cooling application design for any application.

The thermal IR camera can read the temperature of any object based on the emissivity of the object. Hence the surface emissivity is calibrated as per the procedure explained in Appendix-A1. The emissivity is estimated experimentally at 0.92. The uncertainties in the thermometry are less than $\pm 0.5^\circ\text{C}$. The power loss due to the radiation natural convection is experimentally estimated and the corrections are used in the determination of the local HTC . The experimental procedure of power loss estimation is discussed in Appendix-A2.

The IR camera is positioned at the backside of the “Target plate” cum heater facing the nozzle to capture the thermal images. The thickness of the “Target plate” is only 30 microns and lateral conduction is negligible. So, the local temperature on both sides of the surface is considered equal. The backside of the “Target plate” is painted black with Asian color paint having an emissivity (0.92).

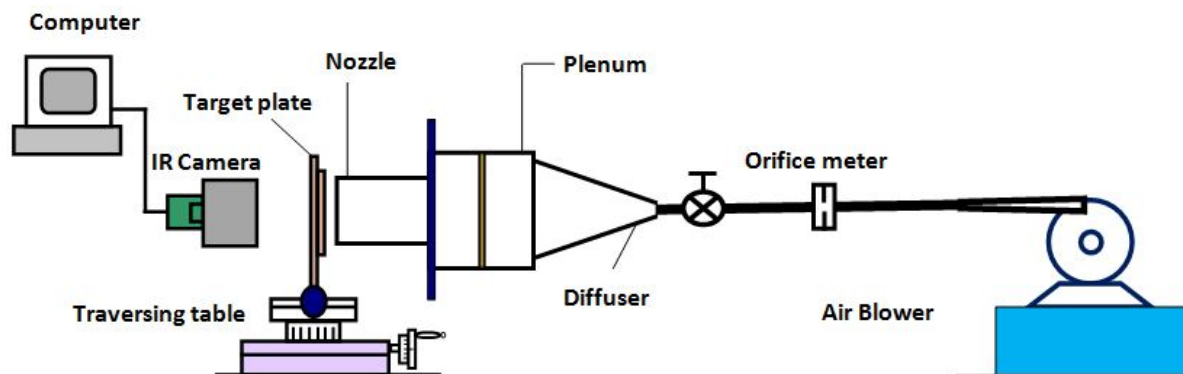


Fig.3.1(a) Experimental setup for measuring the “heat transfer” coefficients

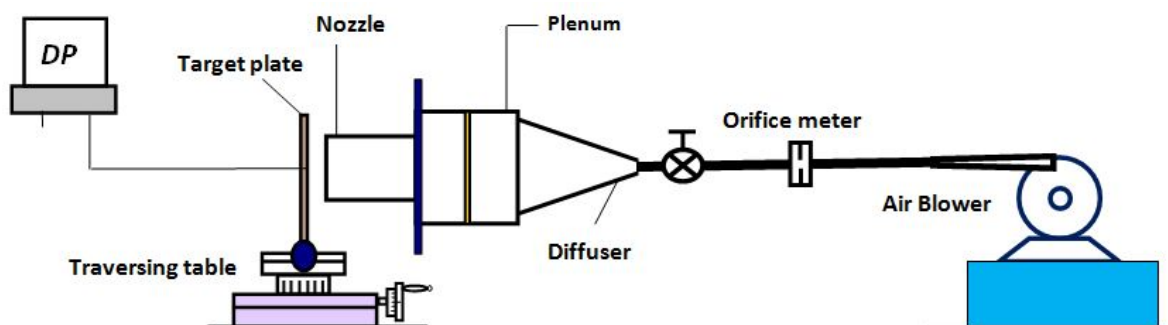


Fig. 3.1(b) Experimental setup for measuring the “wall static pressure”

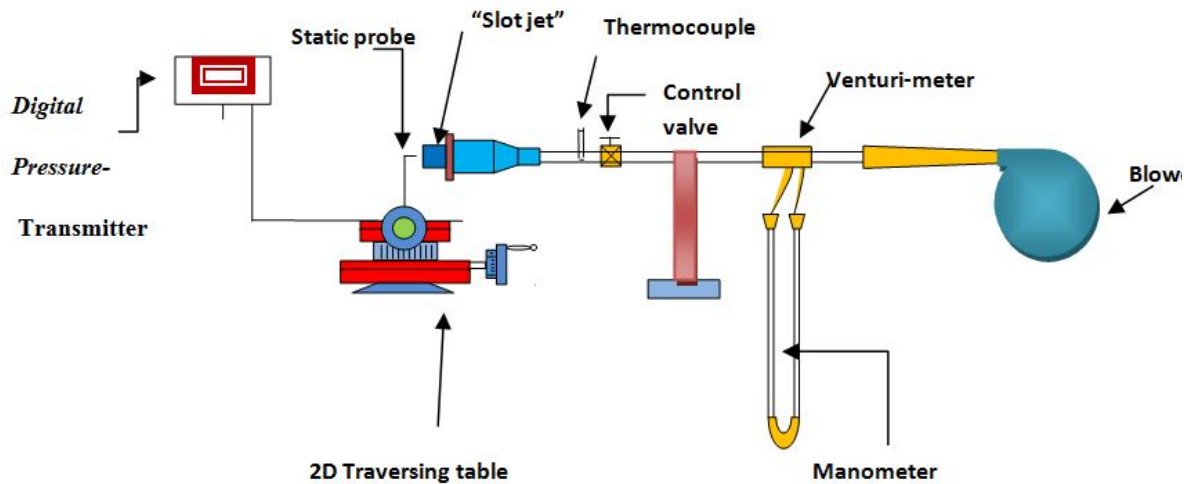
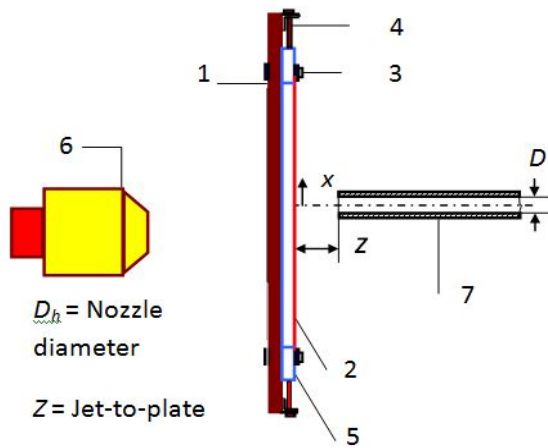


Fig.3.2 Experimental set up for Free jet characteristics study

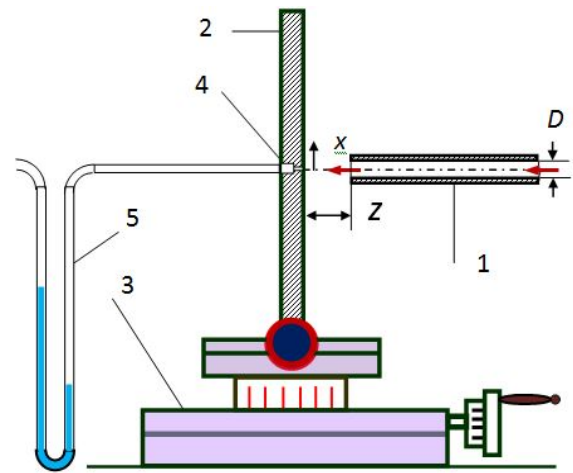
The WSPs are measured by fitting a “Target plate” made of acrylic sheet in place of the SS target plate. The arrangement is shown in Fig. 3.1(b). A static pressure tap having a diameter of 0.5 mm is drilled in a 10 mm thickness acrylic plate up to 3 mm depth from the surface and the remaining depth are counter-bored to 3 mm diameter. The pressure tap is communicating with ‘Furness Control’ digital ‘Differential Pressure Transmitter’ with a range and resolution of $\pm 1.5\text{kPa}$ and $\pm 1.0\text{ Pa}$. The 2-D traverse table is moved along and across the jet axis to record WSP distribution. The details of the positions of the jet, target plate, IR camera and pressure taps are shown in the figures 3.3(a) and 3.3(b).

Fluid flow studies are conducted to relate the HTC distribution characteristics with the WSP distribution over the target surface. It is found that the heat exchange coefficients are larger in the regions where the WSPs are high. Figure (3.4) shows the influence of Re on the WSP coefficient distribution on a flat plate hit by a normal slot-jet. The figure reveals that for the Re ranging from 5000 to 15000 the plots of C_p v/s x/D_h overlaps indicating that the coefficient of WSP is independent of Re but depends on the lateral position from the SP on the impingement plate. The value of C_p is observed sufficiently high at the SP for an entire range of Re investigated. The decrease in the WSP coefficient is very steep up-to J2P spacing of $x/D_h = 1.0$ for the “Reynolds number” 5000 to 15000. The stagnation region extends up to x/D_h of around 1.5 and is a function of Z/D_h .



- 1) Frame. 2) SS foil. 3) Clamp screw
- 4) Stretch screw. 5) Bus bar.
- 6) I.R.Camera. 7) "slot jet" nozzle

Fig. 3.3(a) "Target plate" arrangement for "Heat transfer" experiment



- 1) "slot jet" nozzle 2) Acrylic target plate
- 3) Traversing table 4) Static wall pressure tap
- 5) U-Tube manometer

Fig. 3.3(b) "Target plate" arrangement for "wall static pressure" measurement

Figure (3.5) shows WSP distribution on the "Target plate" for the J2P spacing ($Z/D_h = 0.5$ to 10) studied at $Re = 5000$. The WSP at the "stagnation point" and in the "streamwise direction" decrease with the increase in the J2P spacing as revealed in the figure. The spread of the C_p value varies with Z/D_h and increases with it, whereas the peak value of C_p decreases with an increase in Z/D_h . C_p value drops to zero around x/D_h of 1.0 for $Z/D_h = 0.5$ and around the 3.0 for $Z/D_h = 10$.

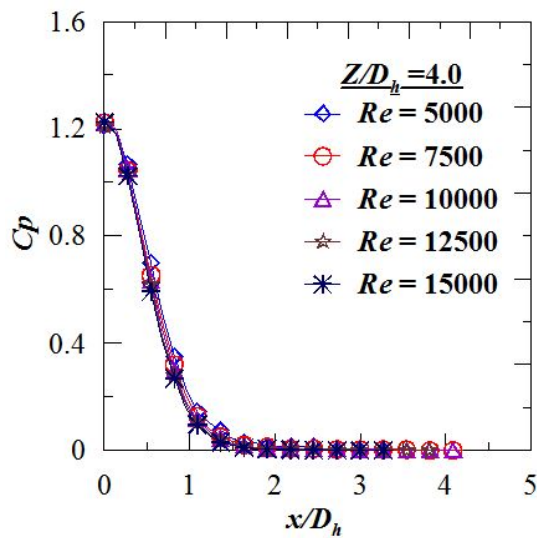


Fig. 3.4 Influence of Re on $C_{p,at}$ various lateral positions from SP for $Z/D_h = 4.0$

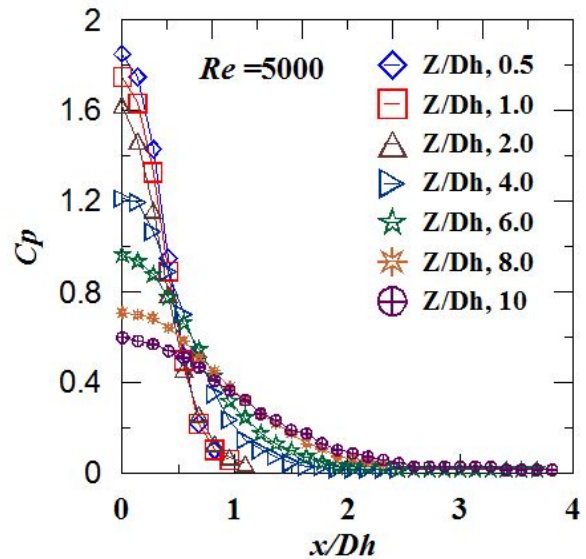


Fig. 3.5 WSP variation along with the plate for the various J2P spacing (Z/D_h) at $Re = 5000$

3.3 Data reduction:

The “Nusselt number” for the surface can be computed using the equation (1) and the “heat transfer” coefficient will be calculated as per equation (2)

$$Nu = \frac{hd}{k} \quad (3.1)$$

$$h = \frac{q_c}{T_r - T_j} \quad (3.2)$$

Heat exchange rate between the “ slot jet” and target plate, q_c , is calculated as given below:

$$q_c = q_j - q_l \quad (3.3)$$

$$q_l = q_{r(f)} + q_{r(b)} + q_n \quad (3.4)$$

$$q_j = \frac{VI}{A} \quad (3.5)$$

$$q_l = q_{r(f)} + q_{r(b)} + q_n = \text{Experimentally estimated} \quad (3.6)$$

Discharge from a calibrated venturi meter is calculated using the equation,

$$Q_{act} = C_d \left[\frac{a_1 \times a_2 \times \sqrt{(2gH)}}{\sqrt{(a_1^2 - a_2^2)}} \right] \quad (3.7)$$

Hydraulic diameter based “Reynolds number” for the jet is obtained from,

$$Re_{jet} = \frac{\rho v_j D_h}{\mu} \quad (3.8)$$

Co-efficient of “wall static pressure” at any point on the “Target plate” is given by the equation,

$$C_p = \frac{2 \Delta p}{\rho_a v_j^2} \quad (3.9)$$

The velocity of the jet at any point can be estimated using the equation:

$$U = \sqrt{2gh} \quad (3.10)$$

The average velocity of the jet leaving the nozzle is given by,

$$U_m = Q/A \quad (3.11)$$

Uncertainties are measured as prescribed by Moffat [24]. The uncertainties of “heat transfer” coefficients are around 4.2 % at “Reynolds number” of 5000 and 2.9 % at “Reynolds number” of 20000. Uncertainty in the C_p measurement is 3.4% at $Re = 5000$ and 2.8% at $Re = 20000$.

3.4 Results and Discussion

3.4.1 Validation of the experiment set up

The experiment setup used in the present study is similar to that of Nirmal *et al.* [16] used in their work.

Figure 3.6(a) shows the variation of normalized pressure along the width on the “Target plate” at a “Reynolds number” 11000 for the J2P spacing 1.0. “The current experimental results are compared with the published work of Nirmal *et al.* [16]”. The results compare well thus the setup is validated for pressure measurements.

Figure 3.6(b) shows the lateral variation of “Nusselt number” (Nu) at slot width based “Reynolds number” 5200 for the J2Pspacing of 2.0. “The results are compared with the experimental results of similar published work from Nirmal *et al.* [16]” and they compare extremely well and hence the set up for “heat transfer” measurements is validated for further work.

3.4.2 Free jet characteristics of unconfined Single “slot jet”: Structure of the free jet issued by a “slot jet”:

The structure of the free jet issued by a fully developed “slot jet” is as shown in Fig. 3.7(a) The three zones identified for the free jet are “a) Potential core zone b) developing zone c) Developed zone. The jet immediately leaving the nozzle comes in contact with surrounding stagnant air. The free shearing between moving jet and stagnant air causes the mixing due to which fluid particles of the surrounding air are carried with the jet, which causes the sharing of the momentum of the jet and formation of the shear layer. Within the shear layer, there exists a flow of jet which is still unaffected by mixing and its velocity is the same as the nozzle exit velocity”. This zone is the potential core of the jet.

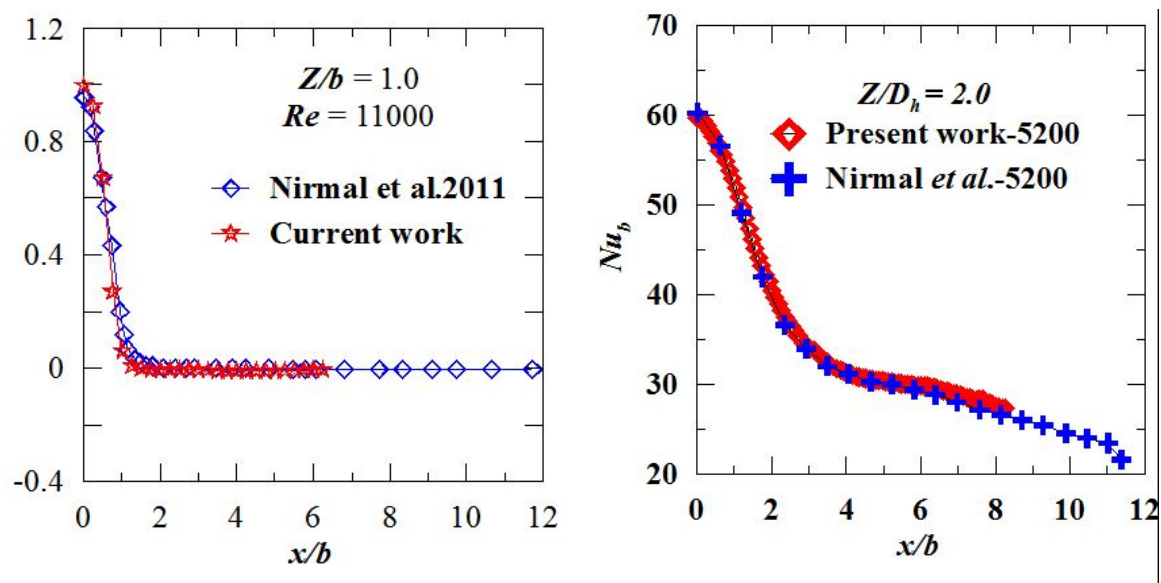


Fig. 3.6 (a) comparison of results with the published work on pressure distribution

Fig. 3.6(b) comparison of results with the published work on “Nusselt number” distribution

In the potential core zone, the centerline velocity of the jet remains constant and is equal to the nozzle exit velocity. The end of the potential core is defined as the axial distance from the nozzle exit up to the point where the jet velocity is 0.95 times the nozzle exit velocity (Jambunathan *et al.*, 1992). The typical length of the potential core is found to be 6-7 times the nozzle diameter for the axis-symmetric jet and 4.7 -7.7 times the slot width for two-dimensional jets (Viskanta, 1993). However, this length depends on nozzle geometry and turbulent intensity in the nozzle exit and initial velocity profile. In the developing zone, due to large shear stresses at the jet boundary, axial velocity profile decays. In the developed zone the velocity profile is fully developed and the jet broadens linearly along with the linear decay of axial velocity.

3.4.3 Structure details of the jet when impinges on a target surface:

Figure 3.7(b) shows the flow regions of a jet normally impinging on a flat plate. The flow structures of an axis-symmetric jet can be divided into three major regions viz. Free-jet region, Stagnation region, and the wall jet regions.

“The impinging jet travels as a free jet from the nozzle approximately for a distance of 1.2 nozzle diameters from the “Target plate” (Jambunathan *et al.*, 1992). The deceleration of flow starts here and the increase in the static pressure happens as the kinetic energy of the jet converts into the static pressure on the target plate. A constant thickness boundary layer with a radius around 1.1 times the diameter of the nozzle is formed at the stagnation region” (Gardon and Akfirat, 1966). “The axial velocity of the flow decreases and the tangential velocity component increases in the stagnation region of the flow. The boundary layer thickness is inversely proportional to jet exit Reynolds number. Due to the loss of momentum with stagnant surroundings and wall friction, the accelerated tangential flow converts into a reduced speed wall jet. The velocity fluctuations of the free jet are carried along the wall jet region also (Gardon and Akfirat, 1966)”. The turbulence in the jet before the impingement influences the turbulence in the wall jet region. The “heat transfer” rate in the region of wall jet is found to be higher than stream-wise flow over the plate. Following is some of the parameters influencing the local distribution of “heat transfer” and fluid flow on a surface due to impinging jets. They are “Reynolds number”, J2P distance, the radial distance from the “stagnation point”, nozzle geometry, turbulence

intensity, surface roughness”, jet-to-jet distance, the curvature of the target surface, confinement of jets, etc.

3.4.4 Centerline velocity profiles of a turbulent “slot jet”

An experiment is conducted to know the influence of “Reynolds number” on flow characteristics of free jet ejected from a slot type nozzle. The centerline velocity profiles of the jet are plotted for different “Reynolds number” 5000 to 15000 from nozzle exit at 0 to 10 Hydraulic diameters of the nozzle, as shown in Figure 3.8. The velocity profiles for the “Reynolds number” studied overlaps on each other, indicating non-dimensional velocity profiles are independent of “Reynolds number”. Maximum Velocity is observed at the nozzle exit for all the “Reynolds number” studied and increase in the J2P distance decreases the velocity.

The velocity remains almost same as at the nozzle exit or within 5% variation up to a nozzle to probe distance of around 2.0 Dh and this region of the flow field can be considered as potential core length for the given “slot jet”. Potential core length is independent of the “Reynolds number”. The results of the Gordon and Akfirat [7] show that the potential core region for a “slot jet” extends up to a distance of around four nozzle widths equivalent to 2 Hydraulic diameters from the slot exit and the results obtained from current work are comparable.

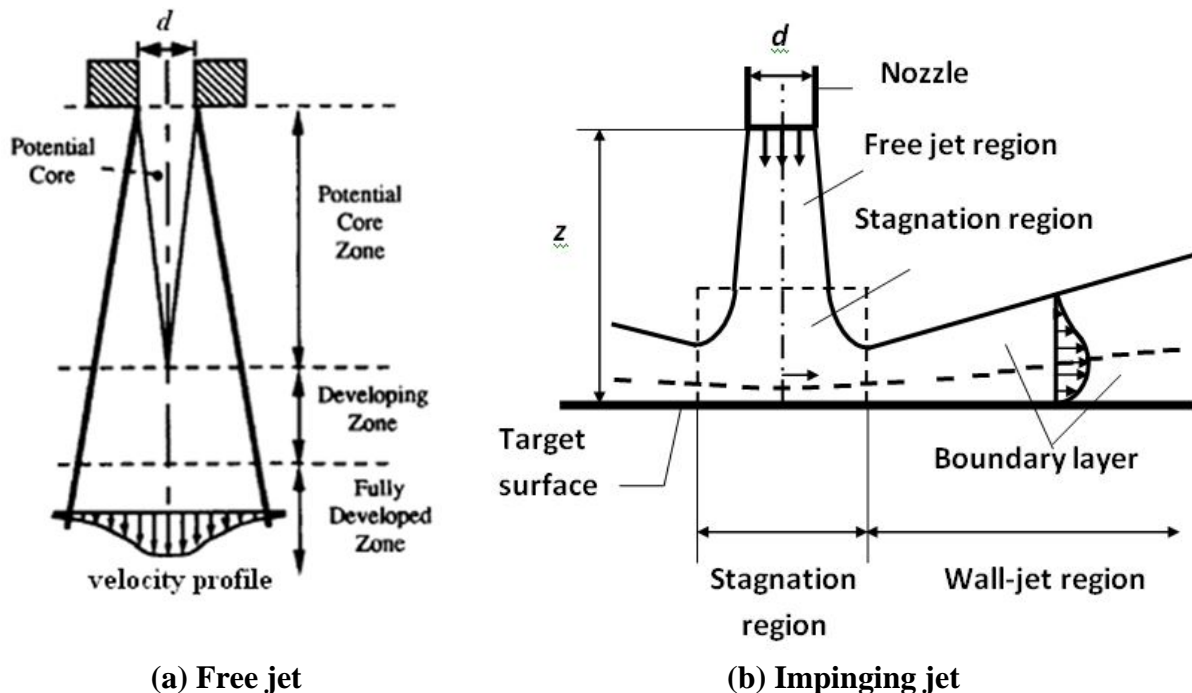


Fig. 3.7 Structure of submerged jet (Viskanta, 1993)

Beyond the PCR, the velocity of the jet decreases rapidly, which may be attributed to the developing jet and entrainment of atmospheric air into the jet. This trend continues up to

Y/D_h of 6.0. Later the velocity of the jet decreases very drastically showing a fully developed region and a diffused jet.

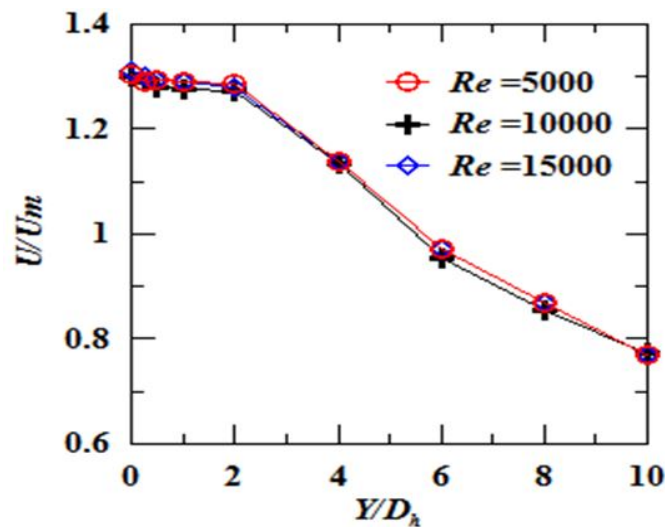


Fig. 3.8 Normalized centerline velocity profiles of a free jet at various “Reynolds number”

Figure.3.9 shows the change in the normalized velocity profiles of the free jet in the “stream wise direction” of the “Target plate” at “Reynolds number” of 10000 for the different nozzle to probe distances(Y/D_h).

For the laminar jet issued from a “slot jet”, the maximum velocity is observed for the lower nozzle to probe spacing and the velocity of the jet centerline decreases as the nozzle to probe distances(Y/D_h) increases.

3.4.5 Local distributions of “wall static pressure” coefficients due to unconfined jet impingement:

Fluid flow studies are done to relate the “heat transfer” distribution characteristics with the distribution of WSP over the target surface. It is found that the HTC values are larger in the regions where the WSP values relatively are high. Figure.3.10 shows the influence of Re on the WSP coefficient on a flat plate interacting with a normal jet. The figure reveals that for a “Reynolds number” range of 5000 to 15000 the plots of C_p v/s x/D_h overlaps indicating that the C_p is independent of Re but depends on the lateral position from the “stagnation point” on the impingement plate. The value of C_p is observed sufficiently high at the “stagnation point” for the whole range of Re investigated. The decrease in the WSP coefficient is very steep up-to J2P spacing of $x/D_h = 1.0$ for the “Reynolds number” 5000 to 15000. The stagnation region extends up to x/D_h of around 1.5 and is a function of Z/D_h .

Figure 3.11 shows WSP distribution on the “Target plate” for the J2P spacing ($Z/D_h = 0.5$ to 10) studied at $Re = 5000$. The WSP at the SP and in the stream wise direction is

inversely proportional to the J2P distance as revealed in the figure. The spread of the C_p value varies with Z/D_h and increases with it, whereas the peak value of C_p decreases with an increase in Z/D_h . C_p value drops to zero around x/D_h of 1.0 for $Z/D_h=0.5$ and around the 3.0 for $Z/D_h=10$.

Figures 3.12(a) and 3.12(b) show the variation of SPWSP coefficient (C_{p0}) on the plate for various “Reynolds number” ranging from 5000 to 15000 and $Z/D_h=0.5$ to 10. For a given Re the C_{p0} value decreases as the J2P distance Z/D_h increases because as the plate moves away from the jet the entrainment of atmospheric air into jet begins and if the target is much beyond the PCR, the jet starts diffusing and spreads wide with reduction in the pressure on the plate. C_{p0} value is found independent of Re for the range investigated.

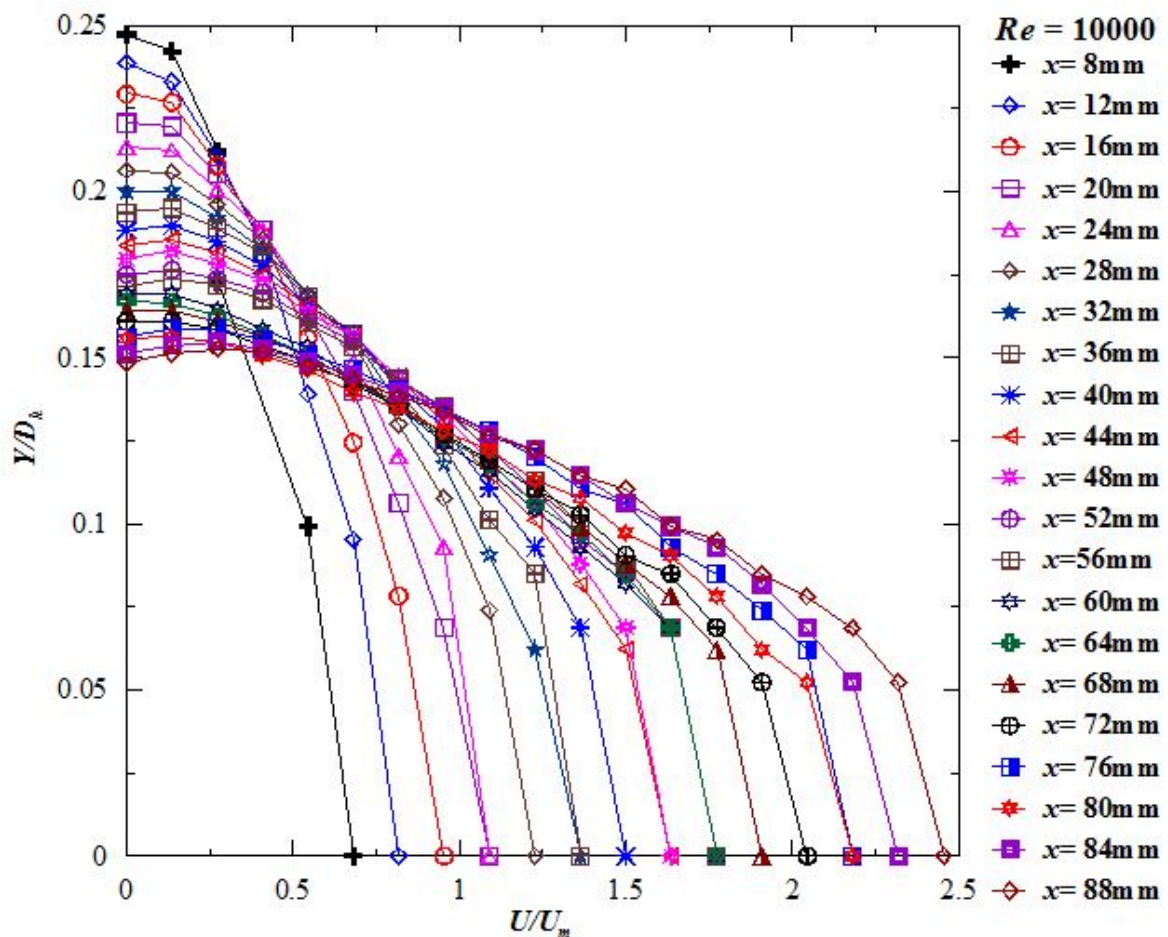


Fig. 3.9 Variation in the velocity profiles of an unconfined single turbulent “slot jet” with a nozzle to probe spacing at $Re=10000$

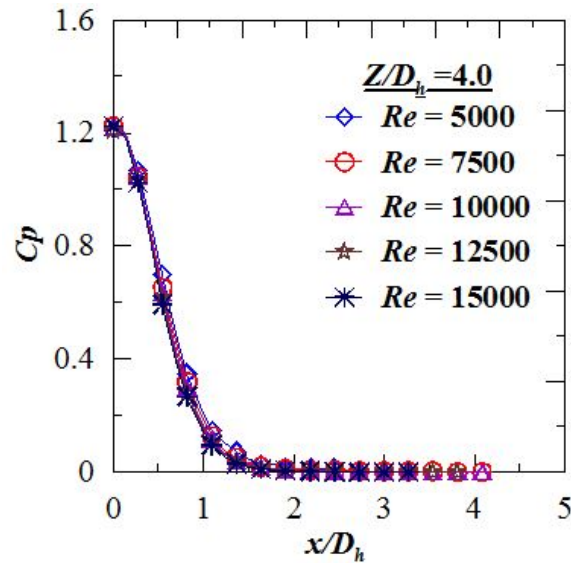


Fig.3.10 Influence of Re on C_{p0} at various lateral positions from “stagnation point” for $Z/D_h = 4.0$

It is observed that the stagnation pressures are almost the same for the Re 7500 to 15000 showing the completely developed turbulent jet hitting the plate. There is a little drop in pressure from Z/D_h , 0.5 to 2.0 which can be attributed to the velocity of the jet which will remain almost constant in the potential core region which extends up to two hydraulic diameters from the nozzle exit as confirmed by the free jet analysis for the jet used in the experiment. The C_{p0} value decreases monotonically for the remaining J2P distances studied which may be due to the reduction in the velocity of the jet in this region.

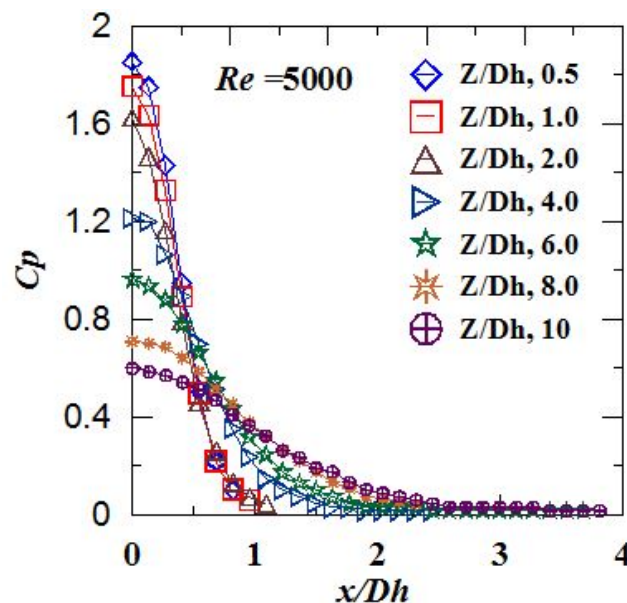


Fig. 3.11 “wall static pressure” distribution along the width of the plate for the various J2P spacing (Z/D_h) at $Re=5000$

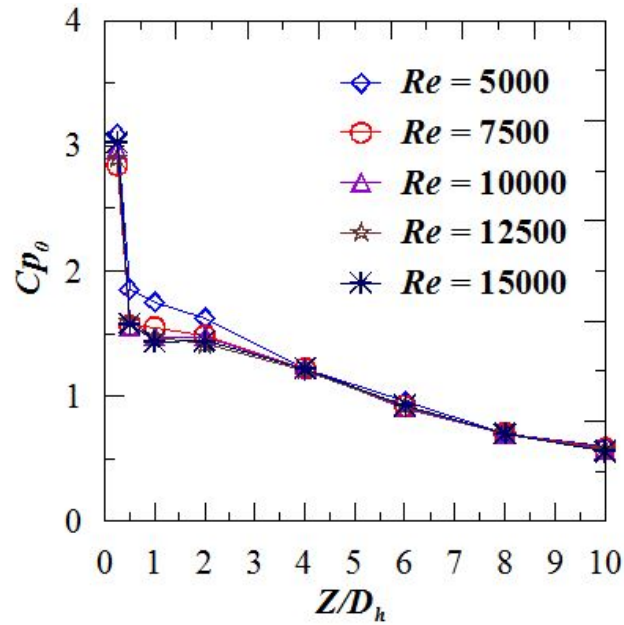


Fig. 3.12(a) Influence of Re on Cp_0 at the various J2P spacing distances

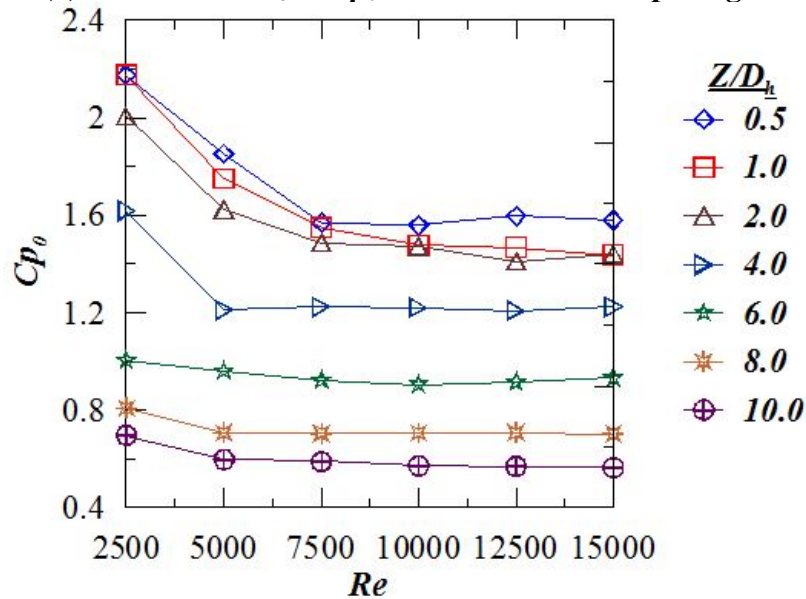


Fig. 3.12(b) Influence of Z/D_h on Cp_0 at the various J2P spacing distances

3.4.6 “Heat transfer” characteristics of an unconfined single “slot jet” orthogonally impinging over a smooth flat surface:

The experiment is conducted to know the local distribution of HTC along the “stream wise direction” of the plate. Figure 3.13 reveals the influence of the Re on the Nu for a given $Z/D_h = 0.5$. Nu is a function of and directly proportional to Re as revealed by figure 3.13. The reason may be the increasing mass flow with the Re , reduction in the thickness of the thermal boundary layer, wall jet and increase in the velocity of the jet air with the “Reynolds number”. A secondary peak is observed at Re above 7500 and the peak

increases with the Re which may be attributed to the strong recirculation of the jet leading to a conversion of laminar flow to turbulent flow gradually in the transition region beyond the stagnation region on the “Target plate” at higher Re .

Figures 3.14 and 3.16 show the distribution of the Normalized Nu in the stagnation region for $Z/D_h=0.5$ and $Z/D_h=1.0$ respectively at different “Reynolds number”. In the stagnation region which extends up to one x/D_h around the SP, the normalized Nu is independent of the Re . The variation in the normalized “Nusselt number” (Nu/Nu_0) value is parabolic in nature. The reason for this may be the laminar nature of the jet as it slowly and gradually picks up the speed in this region before it translates into the wall jet where it is turbulent in nature.

A correlation is developed for the Normalized Nu as a function of x/D_h , in the stagnation region for Z/D_h below 2.0 (potential core region) independent of Re . The values of the Nu/Nu_0 obtained from the experiment and the data from the correlation are plotted against x/D_h at various “Reynolds number” as shown in Figures 3.15 and 3.17. The data compares well and fits in the acceptable range of 2% deviation.

The Normalized value of Nu can be estimated using the equation given below.

$$Nu/Nu_0 = 1 - 0.36 \cdot (x/D_h)^2$$

This correlation holds good for any J2P distance in the PCR of the jet irrespective of the “Reynolds number”.

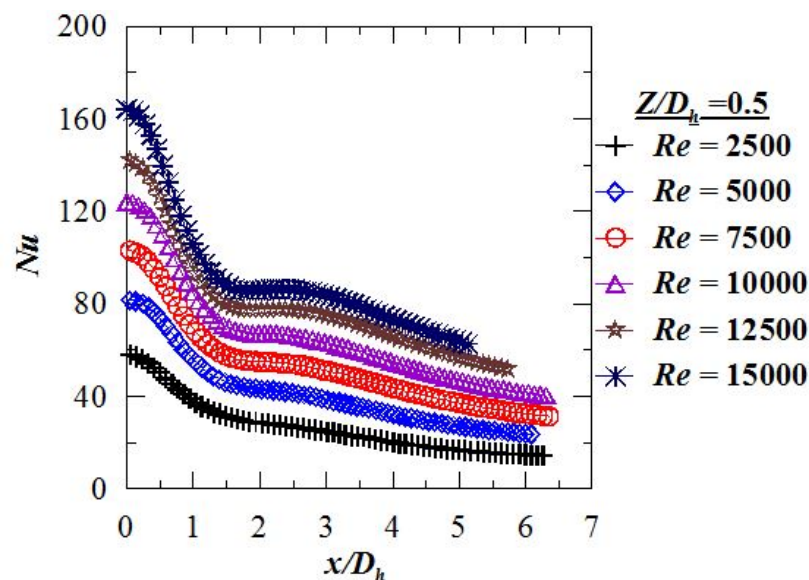


Fig. 3.13 lateral Variation of the Nu for $Z/D_h=0.5$ at various “Reynolds number”

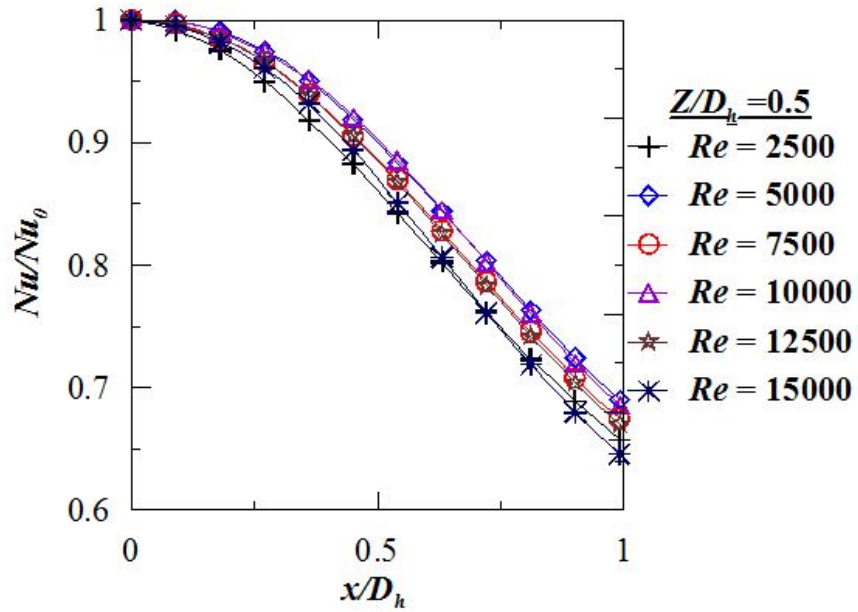


Fig. 3.14 Distribution of Normalized Nu in the stagnation region for $Z/D_h = 0.5$ at different Re

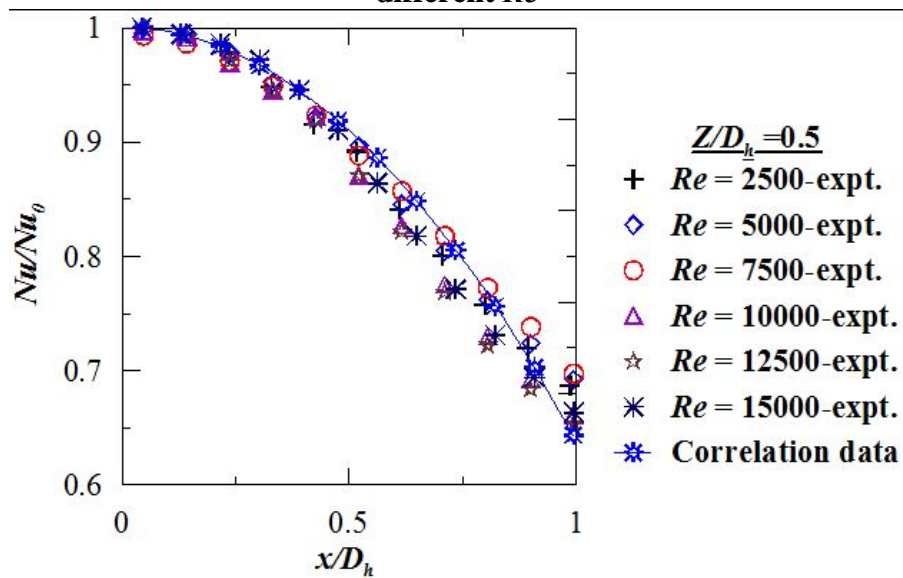


Fig. 3.15 Comparison of the Normalized "Nusselt number" data from the expt. and from the correlation developed

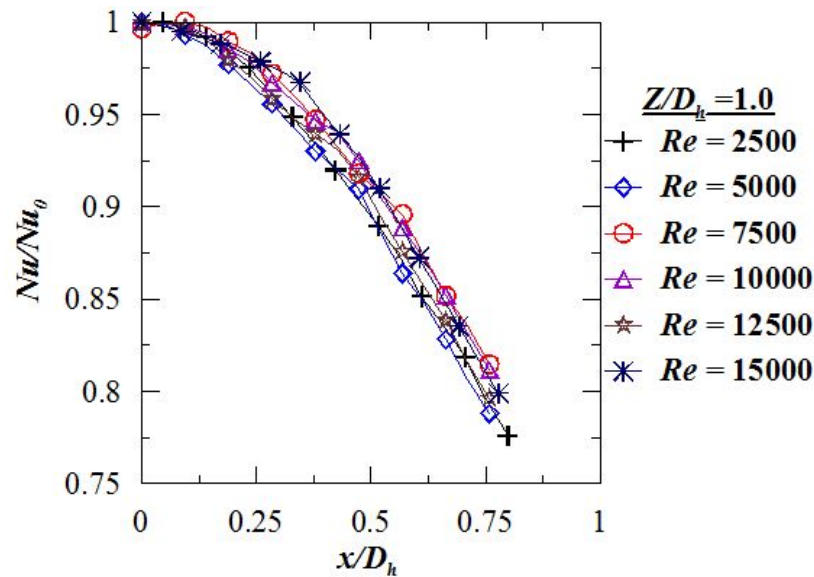


Fig. 3.16 Distribution of Normalized “Nusselt number” (Nu/Nu_0) in the “stagnation region” for $Z/D_h=1.0$ at different Re

3.5 Conclusions:

The distribution of HTC between a slot air jet interacting with a flat smooth surface are studied experimentally. A Re based on the D_h (hydraulic diameter of the jet) is altered between 2500 and 15000 and the J2P spacing Z/D_h is varied between 0.25 and 10. The WSP are measured and distribution behaviour on the target surface is studied from the SP to ax/D_h up to 10.

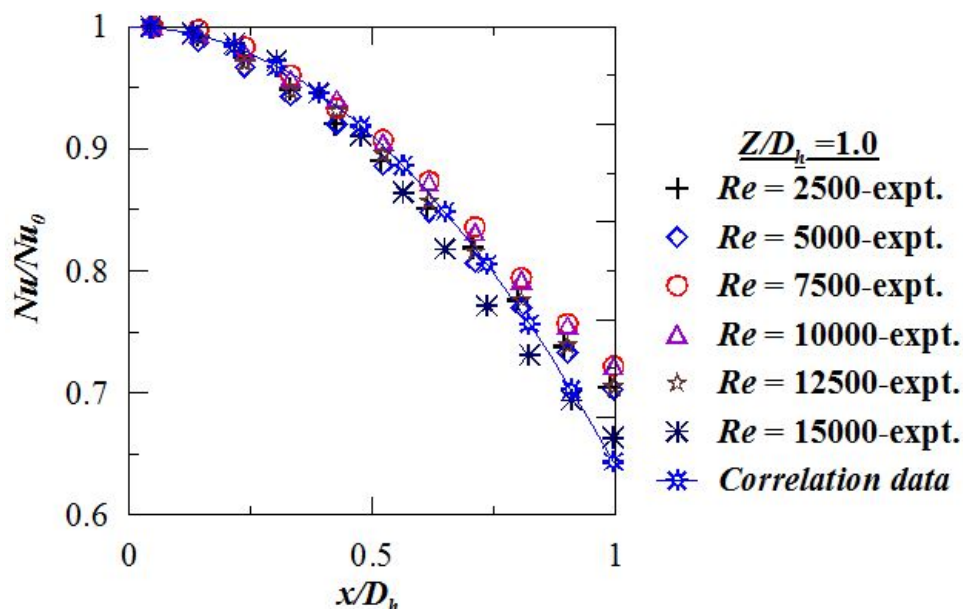


Fig. 3.17 Comparison of the Normalized “Nusselt number” (Nu/Nu_0) from the expt. and the from the correlation developed for $Z/D_h=1.0$

The conclusions derived from the study can be summarized as below:

- *HTC* are highest at the SP for all J2P distances and “Reynolds numbers” considered.
- At smaller J2P distances and higher *Re*, the secondary *HTC* peaks are noted. The fluid changing from laminar to turbulent on the surface may be a reason for the appearance of the secondary peaks in the *HTC*. The secondary peaks are not prominent at lower *Re*.
- *WSP* coefficients are observed behaving independent of “Reynolds numbers” between 5000 and 15000 for any J2P distance. This may indicate the self-similar behavior of the turbulent submerged jet.
- The subatmospheric pressure region is identified for the Z/D_h of 0.25 for all the “Reynolds numbers” investigated. However, the Subatmospheric pressure region vanishes at a higher J2P distance.
- The correlation for estimation of normalized value of *Nu* for stagnation region is:

$$Nu/Nu_0 = 1 - 0.36 * (x/D_h)^2$$

The correlation is independent of the *Re* and holds good for any J2P distance in the potential core region.

CHAPTER 004

Local distribution of “wall static pressure” and “heat transfer” on a rough surface interacting with an orthogonally impinging slot air jet

4.0 Introduction

Jet impingement is popular for cooling applications and considered highly efficient due to its basic nature of high “heat transfer” rates. Also, this kind of impinging jet flows provides shorter flow paths of cooling from the relatively small surface areas comparatively. Impinging jets are invariably used in various applications like: drying food products, films, paper, textiles, processing of several metals and glass. The gas turbine blades, electronic components, and combustion chamber walls etc. are also cooled using the air jets of various configurations. The use of air for cooling applications will be continued due to availability, low cost, and reliability in future also.

Most of the work done by earlier researchers is on the circular air jet impinging over flat

and smooth surface. “Livingood and Hrycak (1970), Martin (1977), Jambunathan *et al.* (1992) and Viskanta (1993). Gardon and Cobonpue (1962) have experimented and reported the “heat transfer distribution between the circular jet and a flat plate for the nozzle plate spacing greater than two times the diameter of the jet, with single jet and array of jets. Gardon and Akfirat (1965) studied the effect of turbulence on the heat transfer between the two-dimensional jet and flat plate. They also studied the heat transfer distribution due to impingement of multiple two-dimensional jets”. Gardon and Akfirat (1966), “Baughn and Shimizu [1988] and Hrycak (1983) have conducted experiments of heat transfer to round jet from flat plate employing different methods of surface temperature measurement. Lytle and Webb (1994) have studied the effect of very low nozzle-to-plate spacing ($z/d < 1$) on the local heat transfer distribution on a flat plate impinged by a circular air jet issued by long pipe nozzle which allows for fully developed flow at the nozzle exit. They observed that for lower nozzle-to-plate spacing ($z/d < 0.25$), maximum Nusselt number shifts from the stagnation point to the point of the secondary peak and is more pronounced at higher Reynolds number. Lee *et al.* (2004) have studied the influence of nozzle diameter on impinging jet heat transfer and fluid flow. They reported that local Nusselt numbers in the region of $0 \leq r/d \leq 0.5$ increase with larger nozzle diameters. Katti and Prabhu (2008) reported experimental investigations and analysis of local heat transfer distribution on a flat surface due to jet impingement from a long pipe nozzle. They identified on the target surface three regions namely stagnation region, transition region, and wall jet region based on heat transfer distribution and have developed Semi-empirical correlations for local Nusselt numbers separately for each region. Han *et al.* (1978) experimentally investigated the effects of rib shape, the angle of attack and pitch to height ratio on the friction and heat-transfer for parallel plate geometry. They developed a general correlation for friction factor and heat transfer considering rib shape, spacing, and angle of attack. They opined that Ribs at a 45° angle of attack have superior heat transfer performance at a given friction power in comparison with ribs at a 90° angle of attack or sand-grain roughness.”

Some work is also reported on the slot air jet impingement on rough surfaces for internal flows but exhaustive work is not attempted with roughened surfaces particularly with detached ribs on the surface with external flow, normal and oblique impingement. Gau and Lee [14] experimented on flow structure of “slot jets” and “heat transfer” along the walls with ribs as roughners. They observed that, due to the rib protrusions the air bubbles are formed which encloses the cavity and stops the jet from interacting with the wall and

thus reduces the “heat transfer”. But a turbulent flow penetrates the air bubble, interacts with the surface, recirculates in the cavity formed, and appreciably increases the “heat transfer” rates. Hansen and Webb [15] conducted studies on the “heat transfer” between the surface with extended fin like modifications and an orthogonal air jet. They observed that the enhancement of the system effectiveness is significantly affected by the fin-type and the “Reynolds number” whereas, slightly influenced by both z/d and R/d . They also reported that the average Nu decreases non-variably with the increase of z/d for the modified surfaces. Liou and Wang [16] studied the temperature distribution in a rectangular duct having an abruptly contracting inlet and mounted with array of square ribs employing Laser holographic interferometer. They noted a better “heat transfer” in the detached-ribbed duct in comparison with the attached ribbed duct. Chakroun *et al.* (1998) experimentally explored the effect of roughness on both the “heat transfer” and the flow character of a circular air jet focused normally onto a hot square plate. The surface roughness was provided in the form uniformly spaced cubes of 1 mm, over the target surface. They recorded an enhancement of about 8.9% to 28% in the local Nu and average Nu values respectively for the rough plate in comparison to a smooth plate. It was also observed that roughness has a strong effect on the mean velocity and the intensity of turbulence of the flow. Liou and Chen (1998), conducted experiments on spatial distribution of the periodic turbulent “heat transfer” and friction in a rectangular channel having an aspect ratio 4:1 and mounted with rectangular detached ribs on one wall. They used holographic interferometer, pressure probes, flow visualization with smoke, and laser-Doppler velocimetry techniques in their study. ‘They reported that with the attached type ribs the thermal performance non-variably decreases at constant pumping power when the rib height is increased but the detached rib type with moderate height of the rib ($H/De = 0.106$) perforations performs better ($\overline{Nu}_p / \overline{Nu}_s$) at lower Re range and ($\overline{Nu}_p / \overline{Nu}_s$) is independent of H/De for the higher Re range.’ The detached solid-type ribs were noted to be having better “heat transfer” characteristics over the perforated-type detached ribs. Gau & Lee (2000) experimented on triangular rib-roughened walls impinged by slot air jet to study the influence of protrusions and “rib pitch-to-height” ratios on the flow and “heat transfer” characteristics along the wall. Flow visualization was made and local HTC were measured along the wall with ribs. Triangular rib geometry is found to be highly active in re-bouncing the wall jet than the rectangular ribs which leads to a noticeable reduction in the “heat transfer”. Yan *et al.* (2005) examined in detail the HTC

distributions on a ribbed surface impinged by an array of jets both in-line and staggered cases. They adopted liquid crystal thermographs for temperature measurements. It was noted that the “heat transfer” over a ribbed surface is periodic-type variation in nature for Nu distributions. The “heat transfer” was best with a surface having 450 angled ribs. Katti and Prabhu (2008) analyzed the “heat transfer” between a circular jet and a flat surface modified with axis-symmetric detached ribs. “A single jet issued from a nozzle of length-to-diameter ratio (l/d) of 83 is used in their study. A consistent increase in the HTC from the stagnation point along the stagnation region was observed for the ribbed surface, which is well attributed to the flow behavior in this region”. The $(Nu_{ribbed} + Nu_{smooth})/2.0$ ratio is found to be a function of Re and increasing with Re

From the available published literature, it is observed that there is an ample scope to explore the influence of roughness on the local distribution of WSP and HTC over a flat roughened surface interacted with a single fully developed slot air jet. Hence the current work is intended to explore the influence of “Reynolds number” (Re), roughness, and J2P spacing (Z/D_h) on the Local distribution of WSP coefficient and HTC due to the impinging slot air jet. A single “slot jet” with a length to width ratio (l/b) of about 24 is used to achieve a fully developed jet at the nozzle outlet. “The Re based on hydraulic diameter (D_h) of the jet is varied from 2500 to 20,000 and J2P spacing (Z/D_h) is varied for smooth surface from 0.25 to 10 and for rough surface 0.5 to 10.” The local HTC are estimated from the thermal images obtained from an IR Thermal camera. The WSPs are measured for various J2P spaces at “Reynolds number” varying from 2500 to 20,000. The results of the experiment are analyzed in the light of flow physics governing the given situation. The “heat transfer” characters are related to the flow characteristics for various configurations attempted in this study and are well compared.

4.1 Experiment set up and methodology

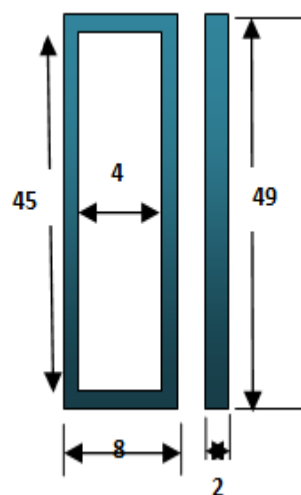
The experimental set-up used for WSP distribution and “heat transfer” studies used for the experimentation on smooth surface is discussed already in the chapter 3.0 is used in this experiment also.

The target surface is modified by mounting the detached ribs to provide the roughness. The influence of the detached ribs on the distribution of local WSP and the HTC is studied. Figure 4.1 reveals the construction of a rectangular rib made of an acrylic sheet of 2mm thickness. The slot width of the rib is 4mm whereas the height is 45 mm and the rim width is 2mm. four different ribs of widths 4, 6, 8 and 12 mm are used in the study. Figure 4.2 shows the rib and the target surface. The center of the rib mounted over the

target surface is aligned with the center of the “slot jet” to assure uniform impingement on the rib. Spacers made of nonconductive material with a thickness of 1mm, width 2mm are provided at the ends to support the rib firmly and to maintain 1 mm uniform gap between the rib and target surface. The same rib is used with the target surface for flow study and the “heat transfer” studies. The measurement of temperature and pressures are made first with the smooth plate with pre-defined parameters and next for the rough surface. All parameters of jet to plate distance, Reynolds numbers etc. are same as used for the smooth surface studies. The results are compared and analyzed to identify the better arrangement for heat exchange enhancement.

4.2 Results and discussions

The results of the investigation to determine the local WSP and HTC distribution of “slot air jet” orthogonally impinging on a flat rough surface at “Reynolds number” range of 2500 to 20000 are discussed here. WSP and HTC distribution are estimated for the J2P spacing (Z/D_h) of 0.5 to 10. Temperatures on the surface are measured using IR thermal imaging camera and the “pressure distribution over the target surface” is measured using Differential Pressure (DP) transducer.



(All dimensions are in mm, not to scale)

Fig. 4.1 Details of the detached rib (representative)

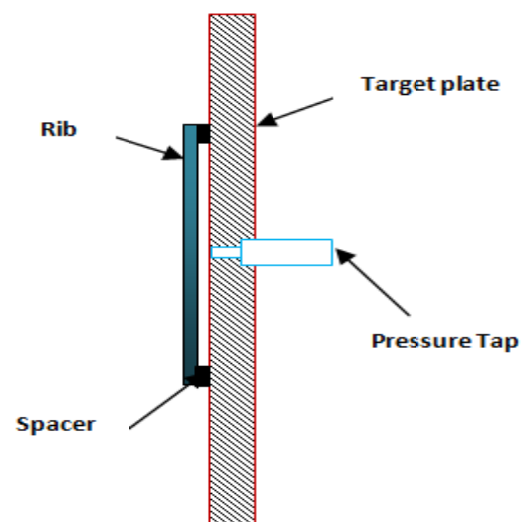


Fig. 4.2 Details of the “Target plate” with detached rib mounted

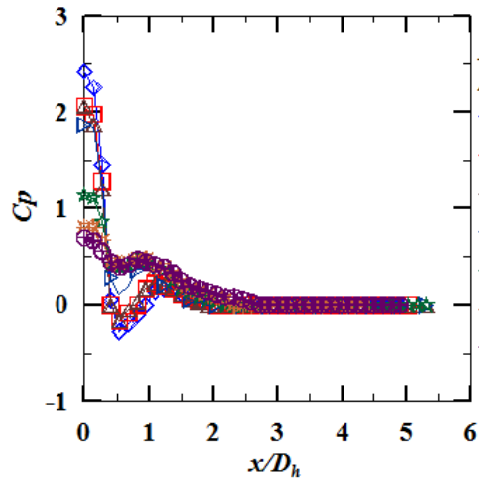
4.2.1 Wall static pressure distribution over the target surface mounted with a 4mm detached rib for J2P spacing (Z/D_h) at $Re=2500$ to 20000.

Fig. 4.3(a) to fig. 4.3(h) shows the distribution of WSP on the “Target plate” for the J2P spacing ($Z/D_h=0.5$ to 10) studied at “Reynolds number” 2500 to 10000 for the rib of 4mm width. The “wall static pressure” (C_p) peaks at the “stagnation point” and decreases in the “streamwise direction” on the target plate. C_p reduces non-variably with an increase in the J2P distance invariably for the various Re studied. Subatmospheric regions are identified for the entire range of “Reynolds number” studied for the J2P spaces 0.5, 1.0 and 2.0 hydraulic diameters. The subatmospheric region is dominant at higher “Reynolds number” which may be accredited to the higher mass flow rate and acceleration of the jet under the rib due to adverse pressure gradients. Secondary peaks can be observed for all the J2P spaces at the position under the rib, in the stream-wise direction, unlike smooth surface. The C_p value drops to zero around x/D_h of 2.0, which may be an indication of the start of the wall jet region where the pressure gradient is zero. Maximum “wall static pressure” is observed at the J2P spacing (Z/D_h) =0.5 at various “Reynolds number” considered in the study.

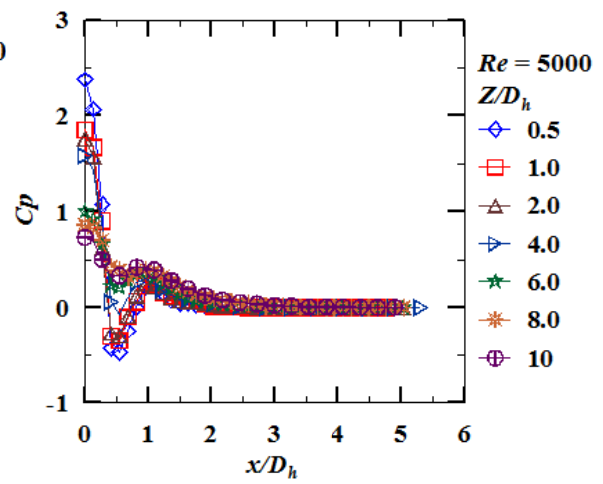
4.2.2 “Wall static pressure distribution over the target surface” mounted with a 6 mm detached rib for J2P spacing (Z/D_h) at $Re=2500$ to 20000.

Figures 4.4 (a) to (h) show the distribution of “wall static pressure” on the “Target plate” for the J2P spacing ($Z/D_h=0.5$ to 10) at “Reynolds number” 2500 to 10000 for rib size of 6mm width. The WSP at the “stagnation point” in the “stream-wise direction” is inversely related to the J2P distance. Sub-atmospheric pressure region is identified for the Z/D_h of 0.25. For all the J2P spacing, the C_p value drops to zero around x/D_h of 1.5 which indicates the start of the wall jet region. At this point the pressure gradient is zero. By observing the fig.4.5 we can identify that there will be a second peak and again they decreases monotonically and reaches atmospheric pressure along the wall of Target plate due to a decrease in the jet impingement effect.

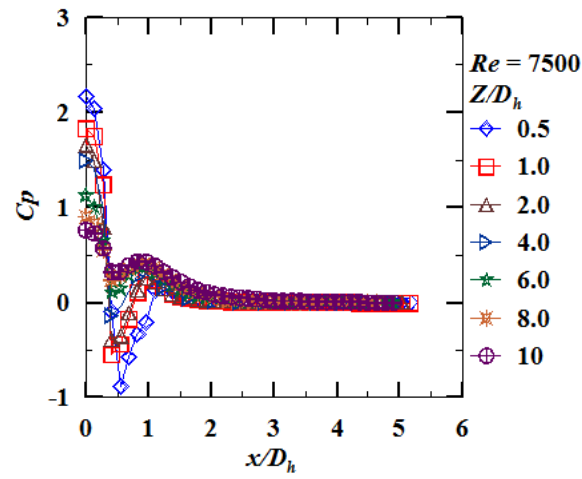
The combined influence of the increase in turbulence intensity and reduction in the centreline velocity of the “slot jet”, instantly after leaving the nozzle the air in the jet begins to include the surrounding atmospheric air. “The width of the mixing region increases continuously and at same time distance from the nozzle exit, it is wide enough to have penetrated o the centreline of the jet. Up to this point, the centreline velocity is practically unaffected by mixing and subsequently equal to the jet velocity.” Beyond the PCR, the centreline velocity also decreases due to mixing of more and more atmospheric air with the jet. Hence along the wall of the plate coefficient of pressure (C_p) decreases gradually and reaches atmospheric pressure.



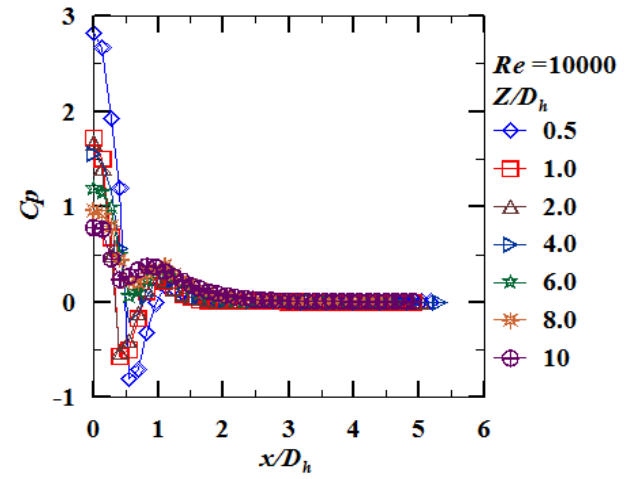
(a)



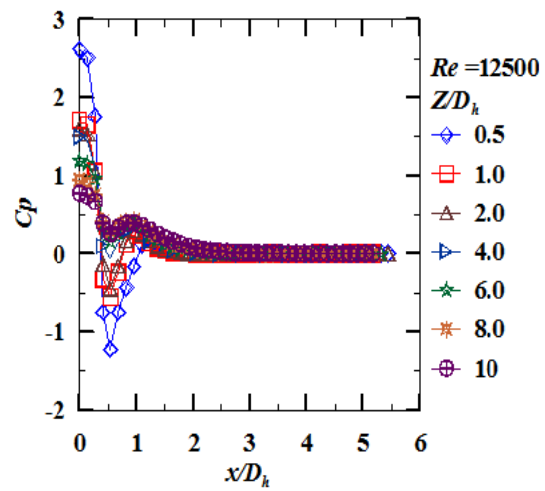
(b)



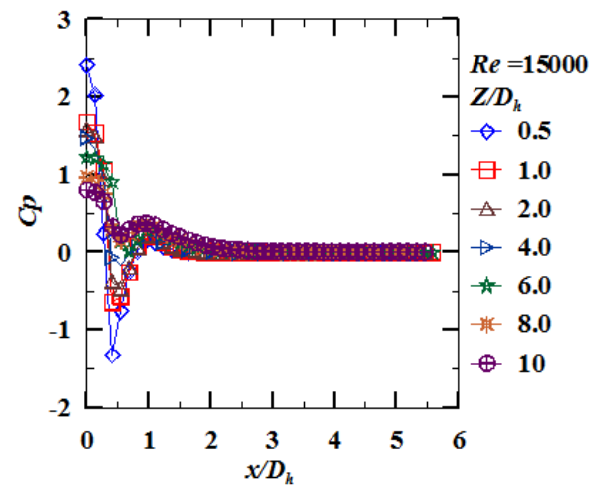
(c)



(d)



(e)



(f)

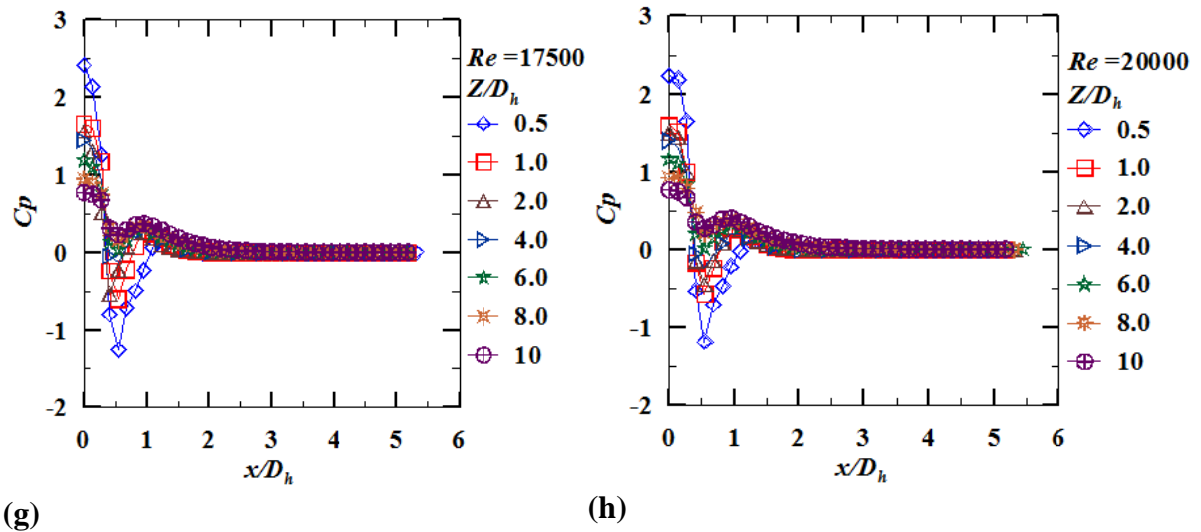
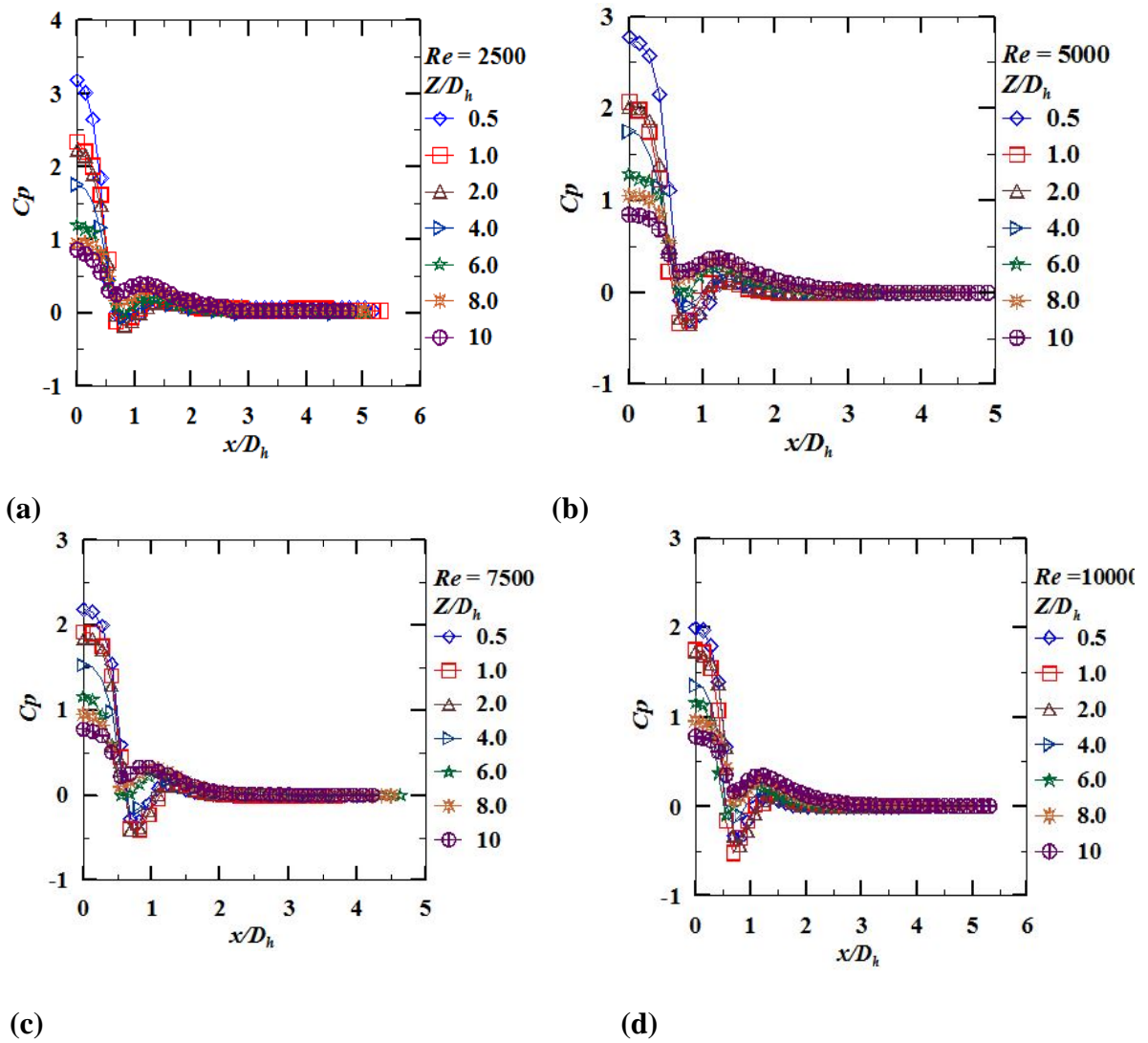


Fig. 4.3 “wall static pressure” variation along the plate for the various J2Pspacing (Z/D_h) at $Re=2500$ to 20000 for Rib size=4mm



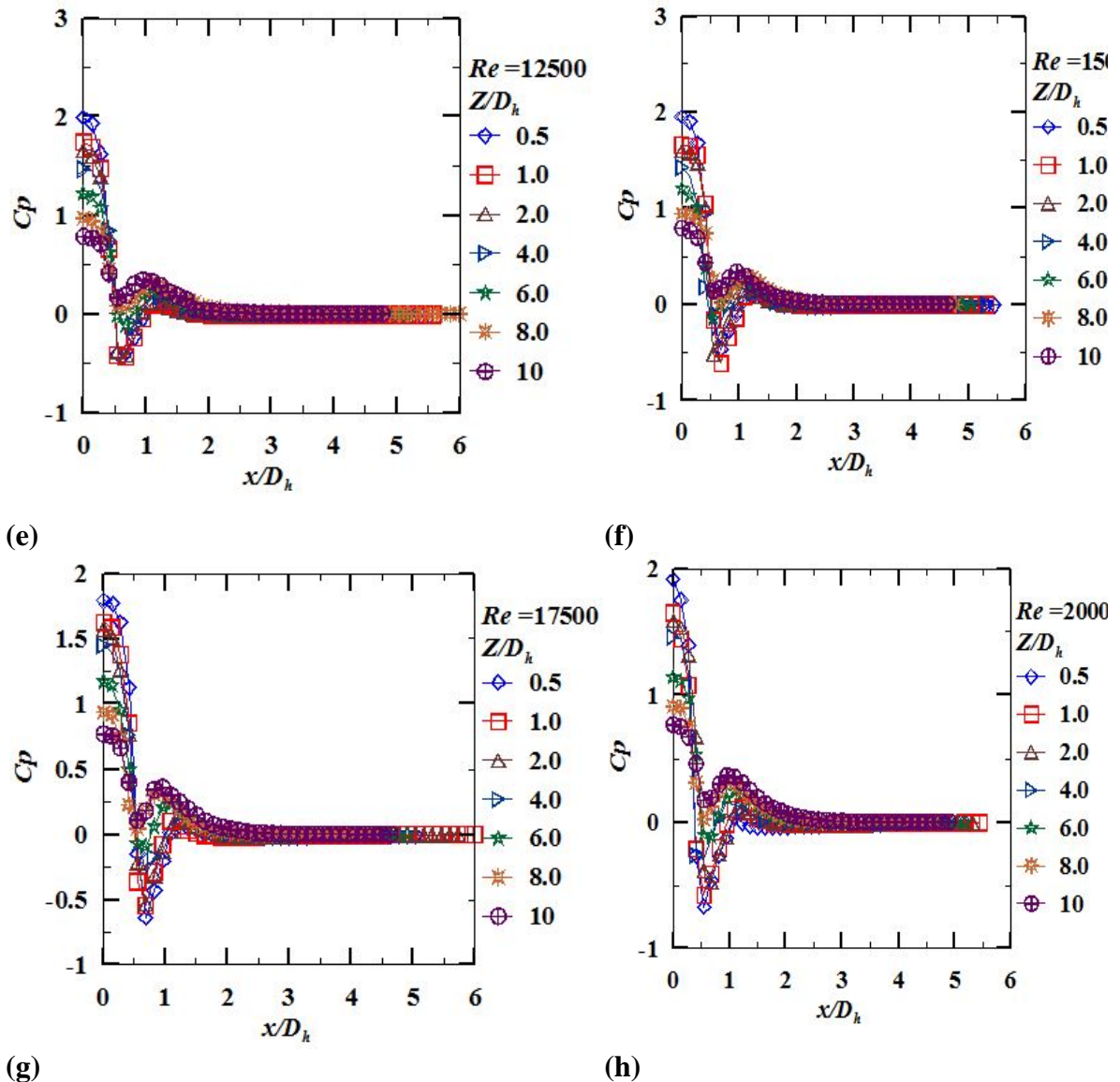
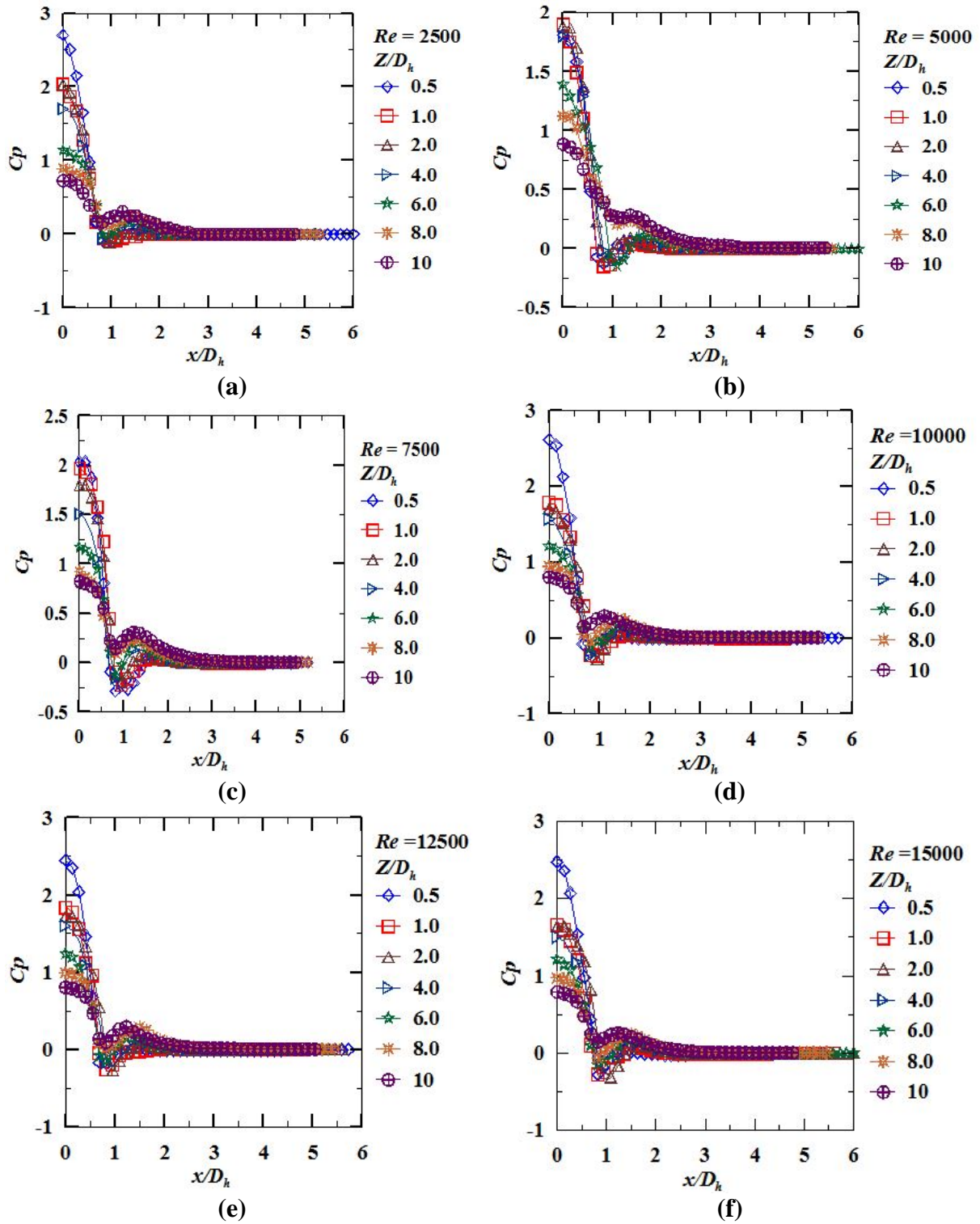


Fig. 4.4 “wall static pressure” variation on the plate at various J2P spacing (Z/D_h) at $Re=2500$ to 20000 for Rib size=6mm

4.2.3 “Wall static pressure” distribution over the target surface mounted with a 8 mm detached rib for J2P spacing (Z/D_h) at $Re=2500$ to 20000.

Figure 4.5(a) to figure 4.5(h) shows the variation of the local “wall static pressure” along the plate for the various J2P spacing (Z/D_h) at “Reynolds number” varying from 2500 to 20000 are studied. The coefficient of “wall static pressure” peaks at the “stagnation point” and diminishes along the wall of the plate and reaches the atmospheric pressure. At the end of the stagnation region, the wall jet region starts in this region and the jet shares some of its momentum to the atmospheric air hence the strength of the jet core decreases. In the wall jet region due to the low velocity of the jet the boundary layer thickness increases, the velocity of the jet decreases hence pressure gradients are converted to zero.

The coefficient of “wall static pressure” is higher for a rough surface in comparison to the smooth surface which can be accredited to the speeding up of fluid under the rib and the viscous effects.



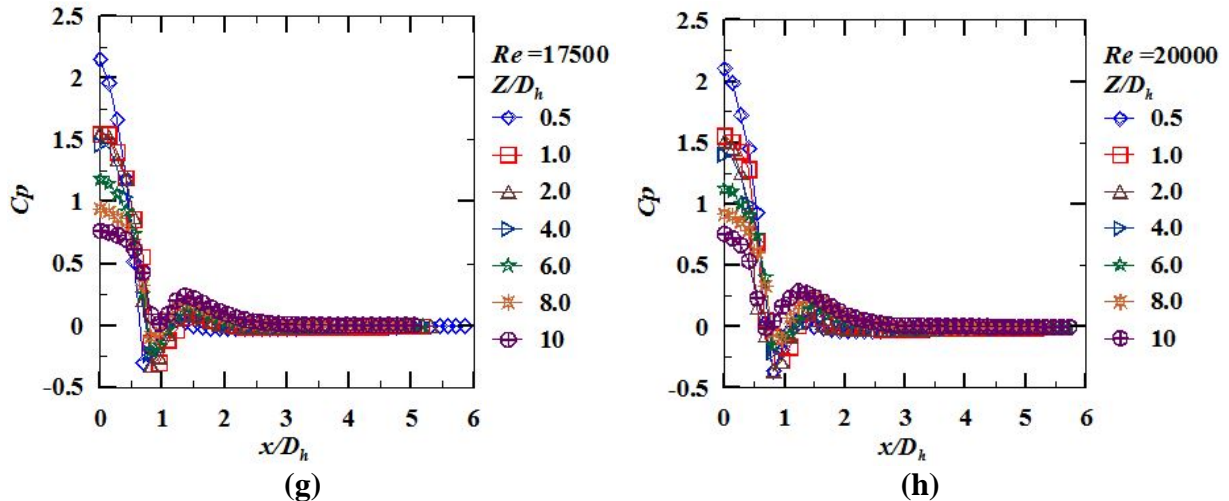
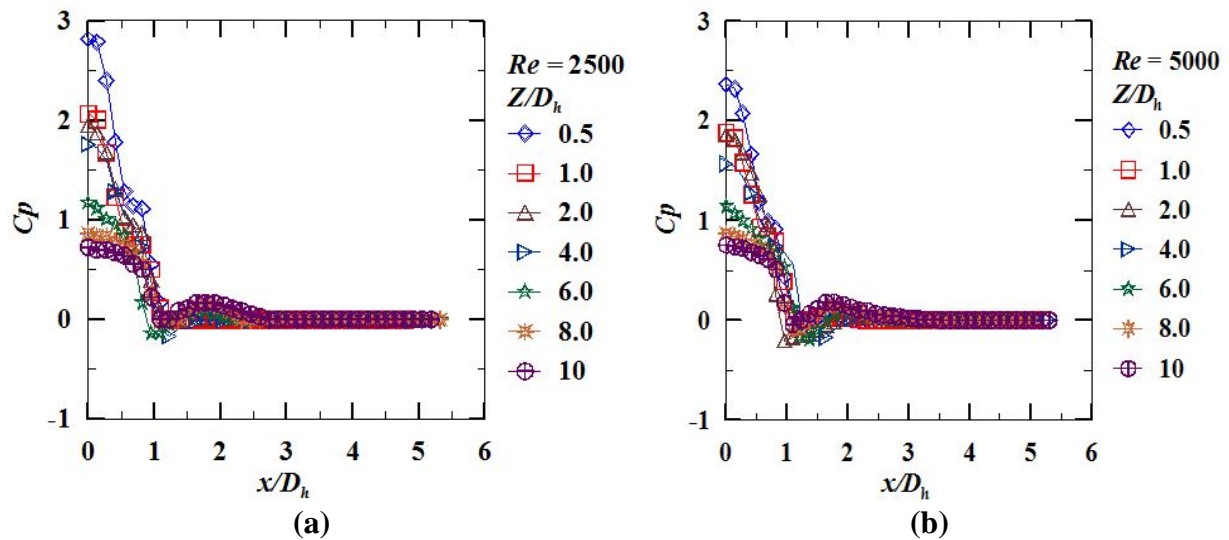


Fig. 4.5 “wall static pressure” variation along the plate for the various J2P spacing (Z/D_h) at $Re=2500$ to 20000 for Rib size=8mm

4.2.4 “Wall static pressure” distribution on the “Target plate” mounted with a 12 mm detached rib for J2P spacing (Z/D_h) at $Re=2500$ to 20000 .

Figure 4.6(a) to figure 4.6(h) shows that local “wall static pressure” variation along the width of the “Target plate” for the various J2P spacing (Z/D_h) at “Reynolds number” varying from 2500 to 20000 are studied. Figures 4.7 reveals that local WSP is a function of the J2P spacing and it is independent of “Reynolds number”. C_p value decreases along the wall of the “Target plate” and equals the atmospheric pressure around x/D_h of 2.5.



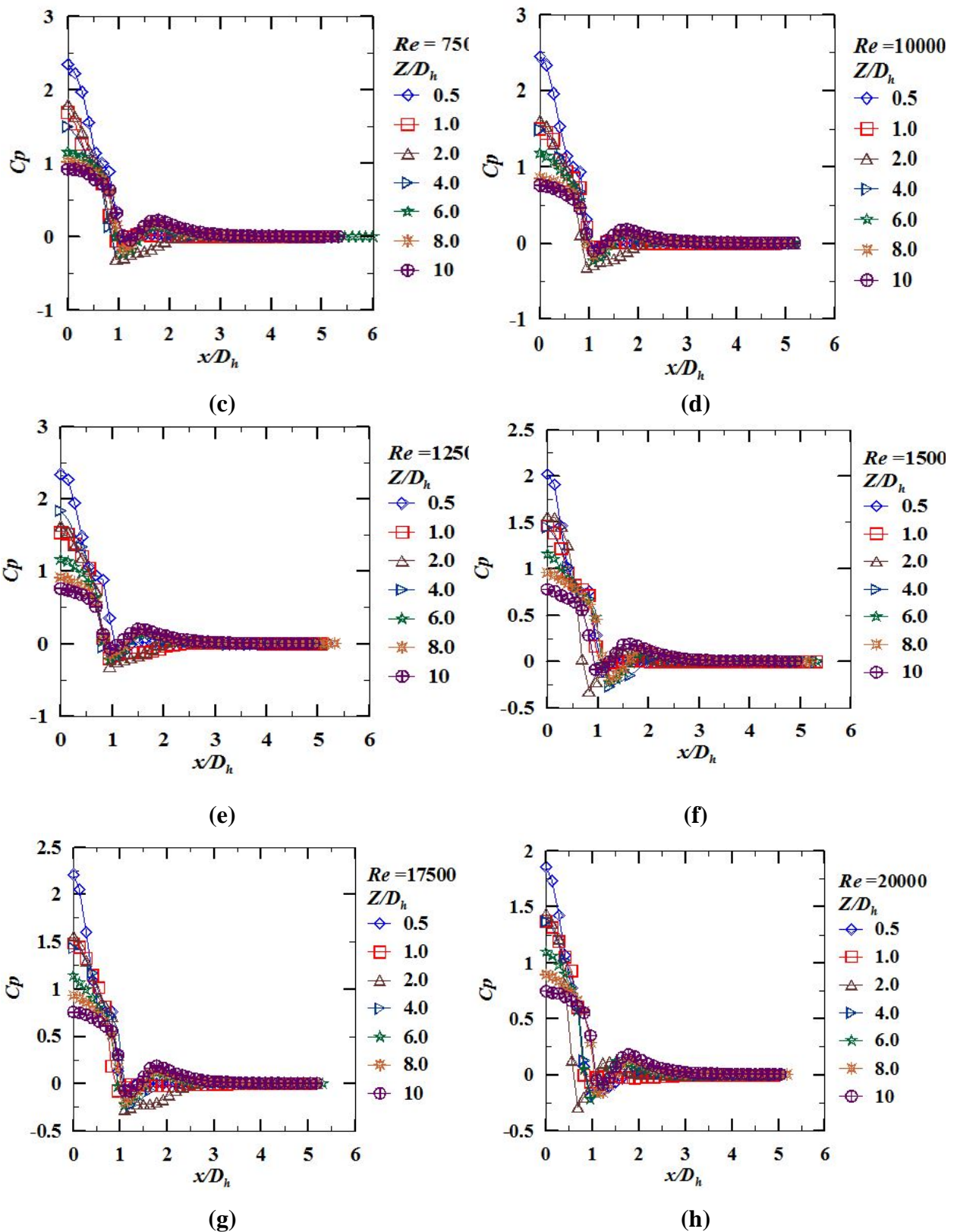
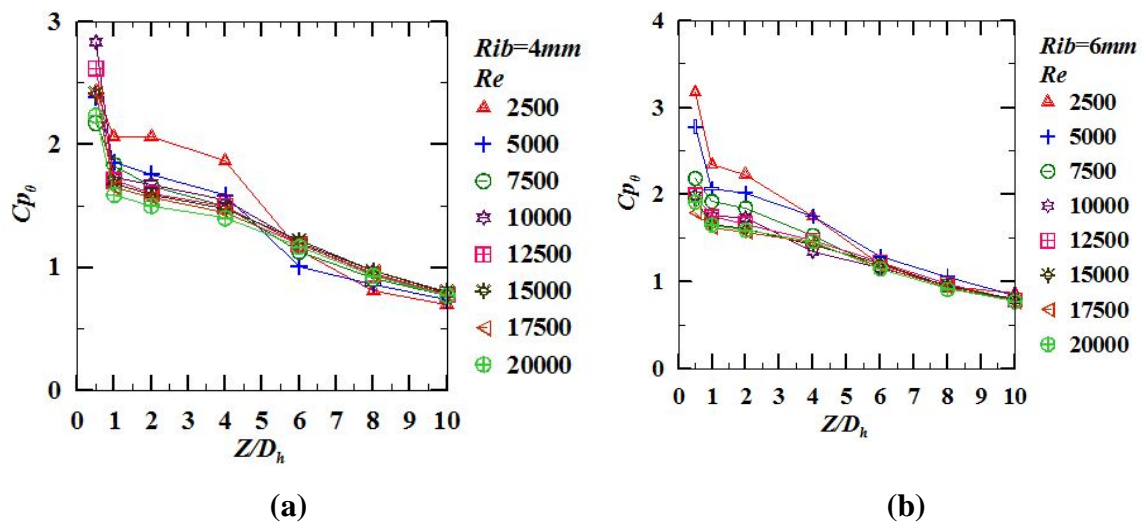


Fig. 4.6 “Wall static pressure” variation along the plate for the various J2Pspacing(Z/D_h) at $Re=2500$ to 20000 for Rib size=12mm

4.2.5 Variation of “stagnation point wall static pressure” distribution on the “Target plate” mounted with detached rib for J2P spacing(Z/D_h) 0.5 to 10, at $Re=2500$ to 20000.

Figures 4.7(a) to (d) shows the variation of “stagnation point” wall static pressure coefficient (C_{p0}) for the J2P distances (Z/D_h , 0.5 to 10) at various “Reynolds numbers” 2500 to 20000 for Rib sizes 4, 6, 8, and 12 mm respectively. It is observed in general, that WSP at the “stagnation point” decreases with an increase in the J2P distance. This trend continues to the $Z/D_h = 6$. There is a drastic drop in the C_{p0} value from $Z/D_h = 0.5$ to $Z/D_h = 1$ and C_{p0} value decreases monotonically for the remaining J2P distances. For all the ribs considered in the study, the C_{p0} value is higher at $Re=2500$, the reason may be the laminar nature of the jet. This domination is maintained up to J2P spacing of 4.0 for all the ribs. Beyond $Z/D_h = 6$, the ribs and also the Re does not influence the C_{p0} significantly.

Figure 4.8(a) to fig 4. 8(g) show the lateral distribution of C_p at $Re = 2500$ for J2P spacing's 0.5, 1.0, 2.0, 4.0, 6.0 and 8.0 respectively. It can be observed that the C_p values are greater for the ribbed surface in comparison to the smooth surface. Light secondary peaks are observed for all Z/D_h . The jet spreads wider as the distance of the jet from the nozzle increases. The reason may be the mixing of atmospheric air with the jet.



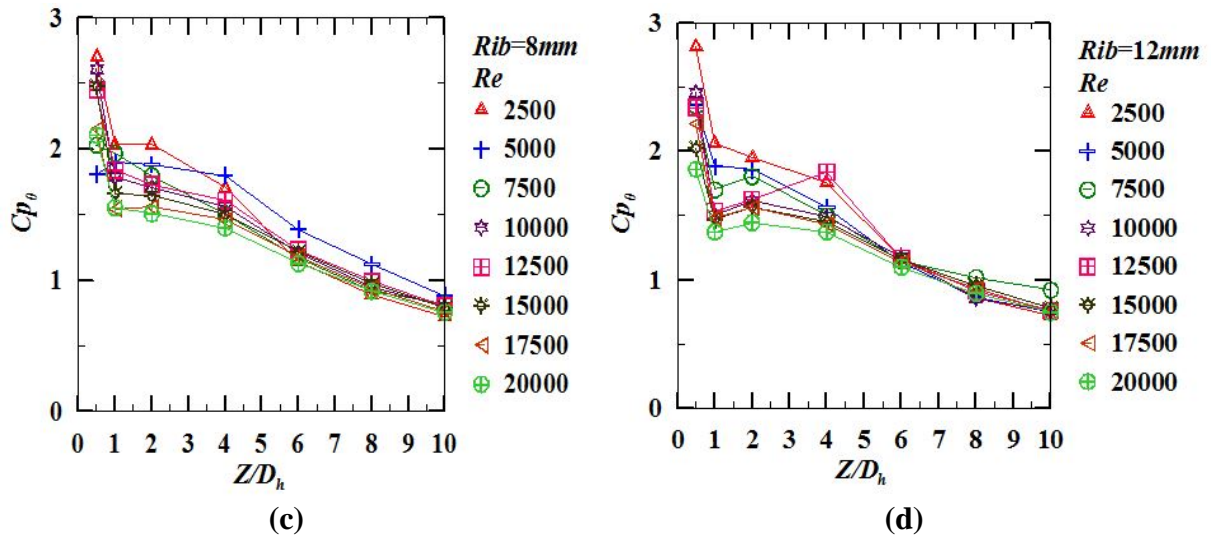
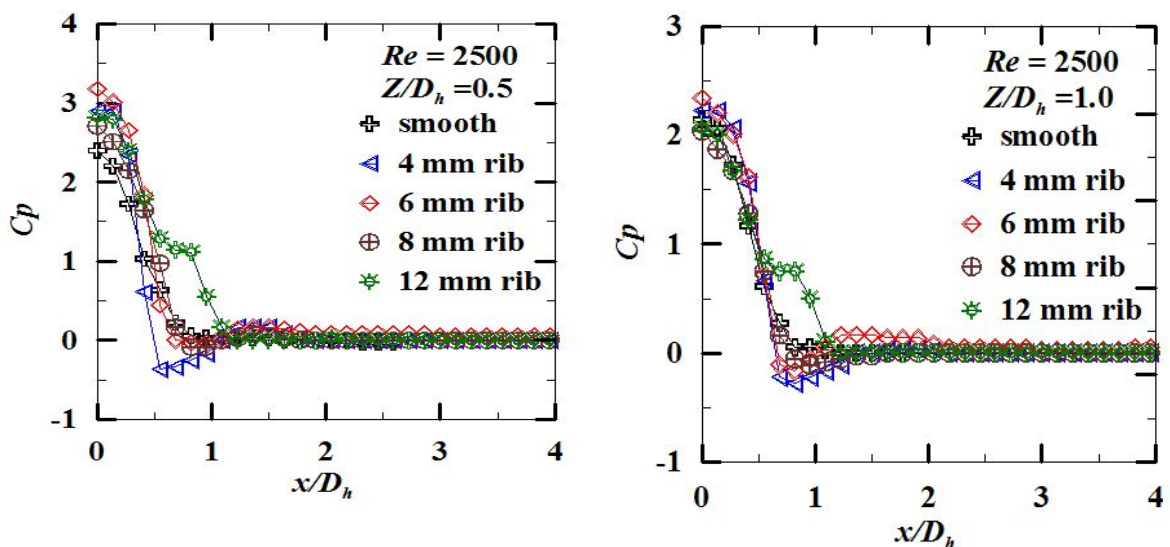
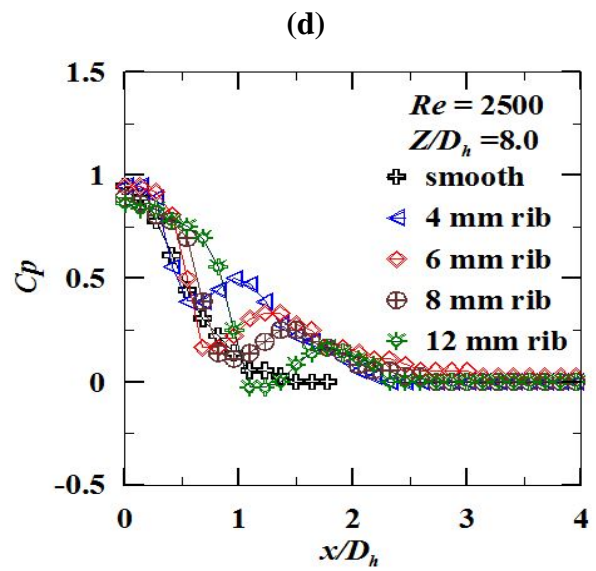
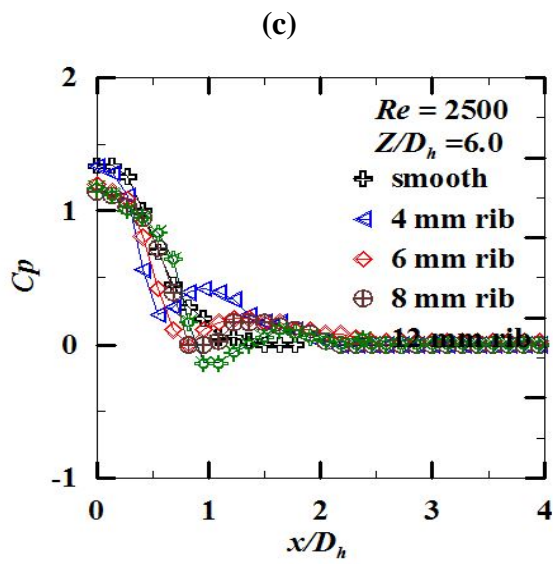
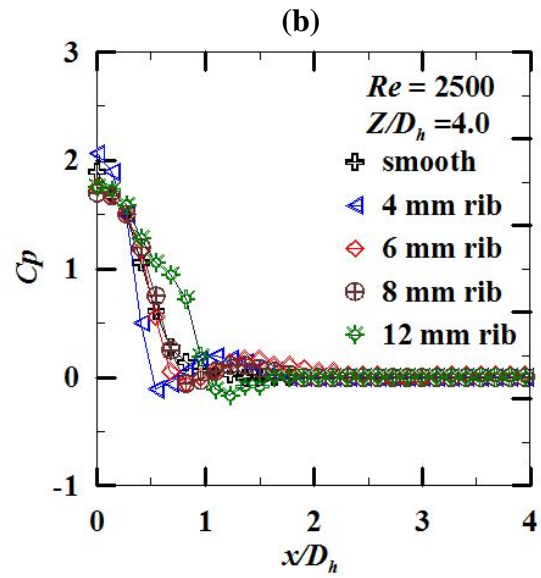
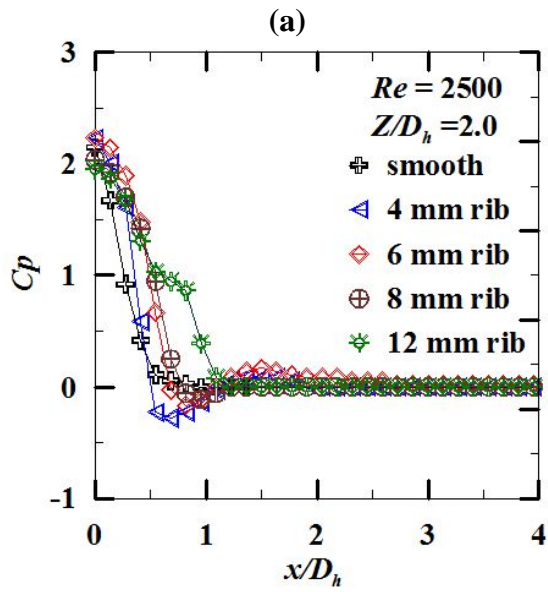


Fig.4.7 Variation of Cp_0 for the different J2P spacing at various Reynolds number for different Rib configuration

Ribs of width 4mm and 6mm give better distribution of pressure on the plate in comparison with other ribs and smooth surfaces as well. Because of the detached rib, the jet accelerates under the rib, creating adverse pressure gradients and helps in the heat exchange enhancement in that region. The decrease in WSP coefficient is very steep up to J2P spacing of $x/D_h = 1.0$ for all the ribs and reaches atmospheric pressure around $x/D_h = 1.6$.

For the whole range of “Reynolds numbers”, all the ribbed configurations are shows maximum WSP than the smooth surface for a given J2P spacing and “Reynolds number”. The coefficient of wall static pressure inversely related to the J2P distance. The trends are shown in figures 4.9 through 4.15 at various “Reynolds numbers” 5000, 7500, 10000, 12500, 15000, 17500 and 20000 respectively





(e)

(f)

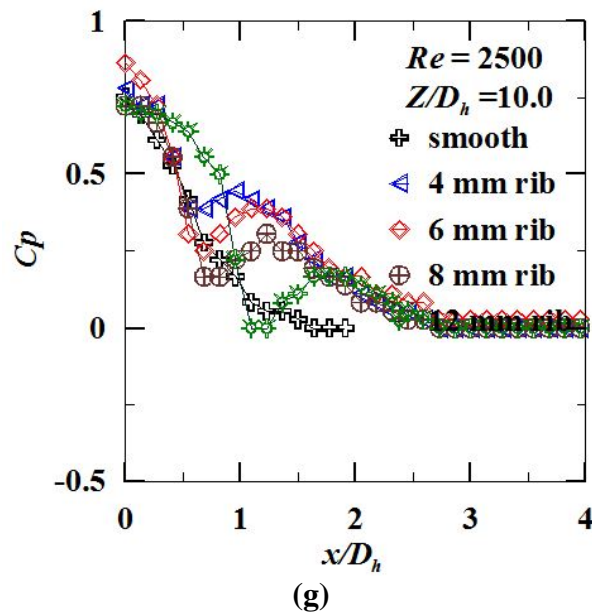
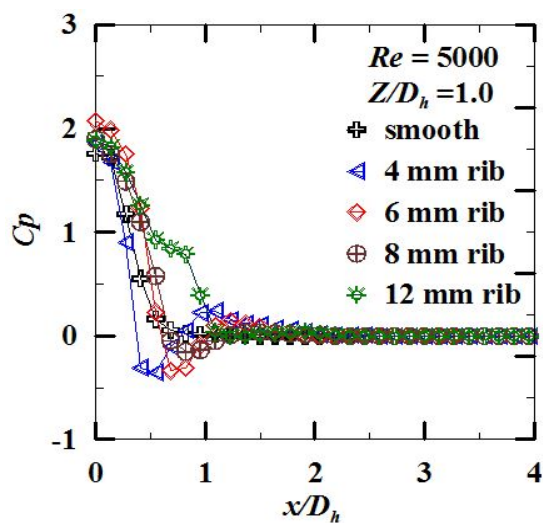
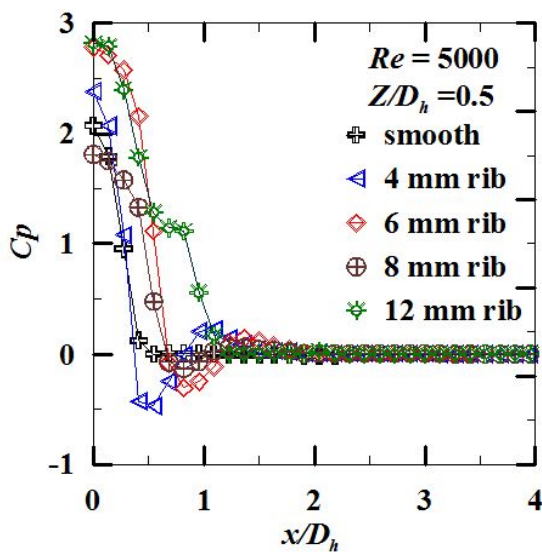
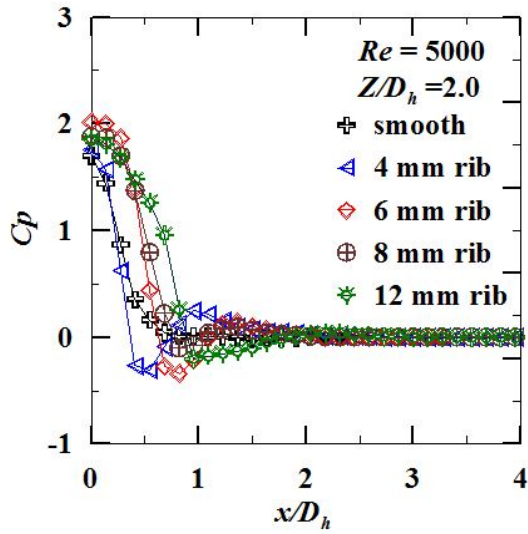


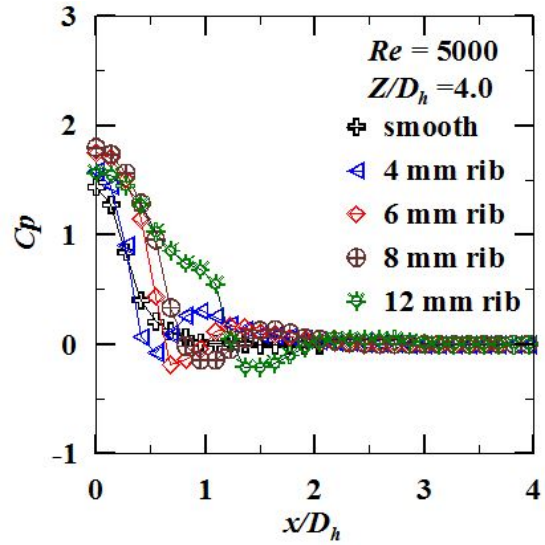
Fig.4.8 “Wall static pressure” variation along the plate for the various J2Pspacing(Z/D_h) at $Re=2500$ for different rib size

A general observation that can be made from the graphs is that for any given J2P distance and the “Reynolds number” the height of the secondary peak decreases gradually with the increase in the width of the rib whereas the spread of the jet before the value of the wall static pressure coefficient reaches zero increases with the width of the rib in all the cases. This trend may be due to the major part of the jet missing to hit the surface for the wider ribs. The overall the value of the wall static pressure coefficients at any point for ribbed surface are higher than the C_p values for the smooth surface. This clearly indicates the change in the fluid flow behavior which may be useful in the “heat transfer” from surface to fluid and can be studied experimentally.

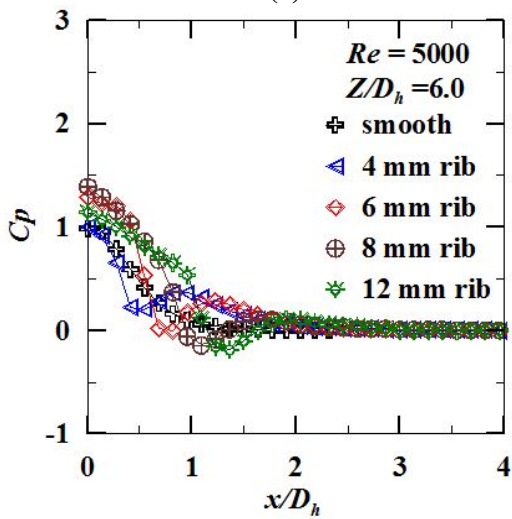




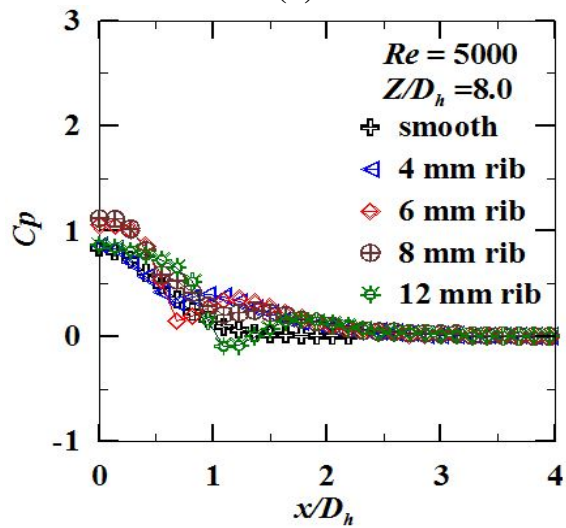
(c)



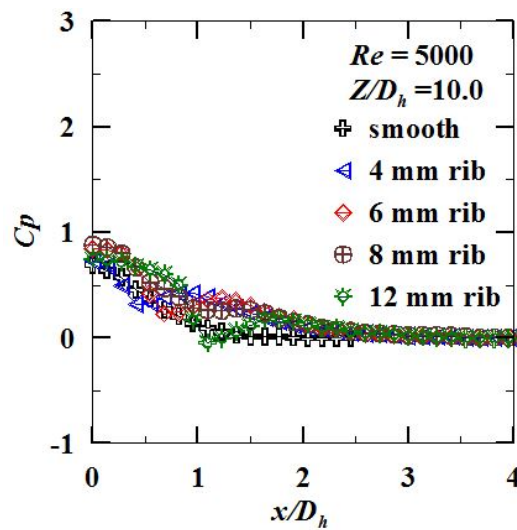
(d)



(e)

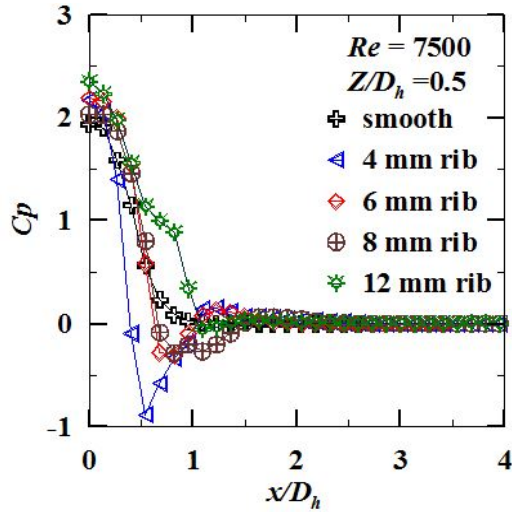


(f)

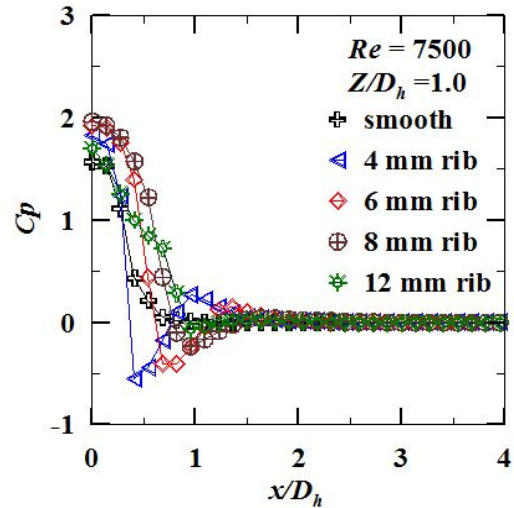


(g)

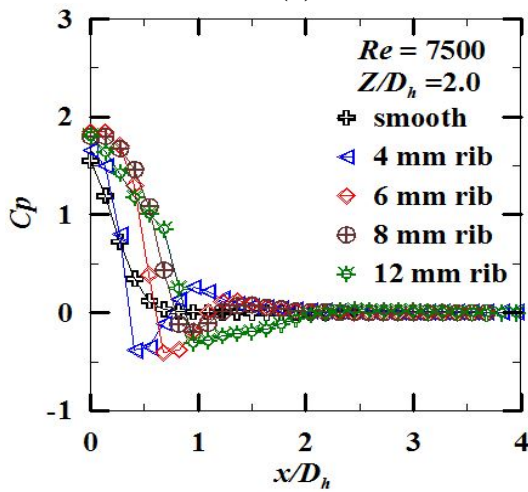
Fig.4.9 “Wall static pressure” variation along the plate for the various J2P spacing (Z/D_h) at $Re=5000$ for different rib size



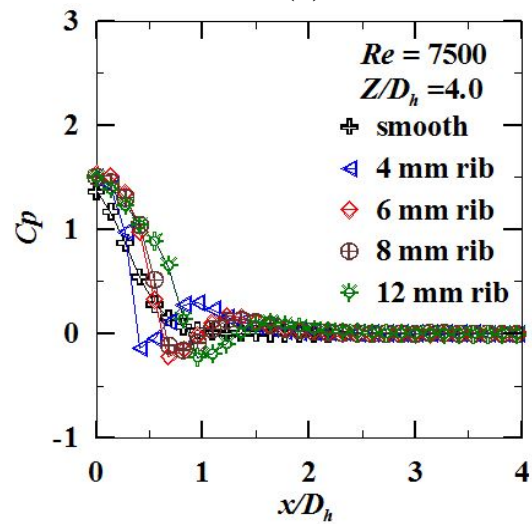
(a)



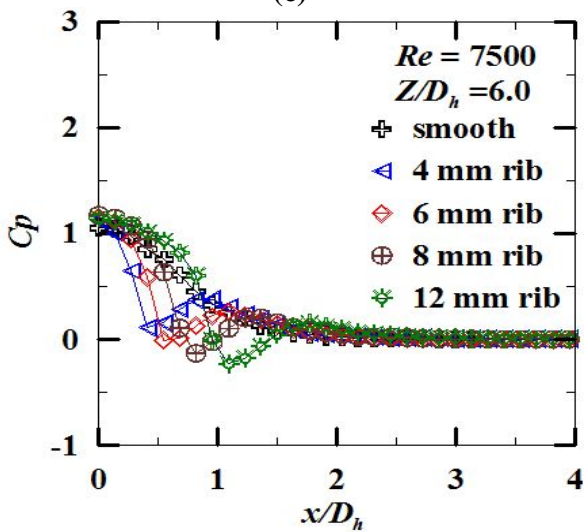
(b)



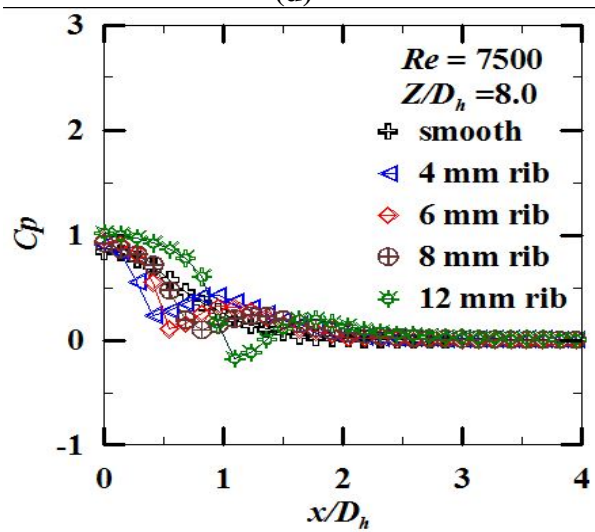
(c)



(d)

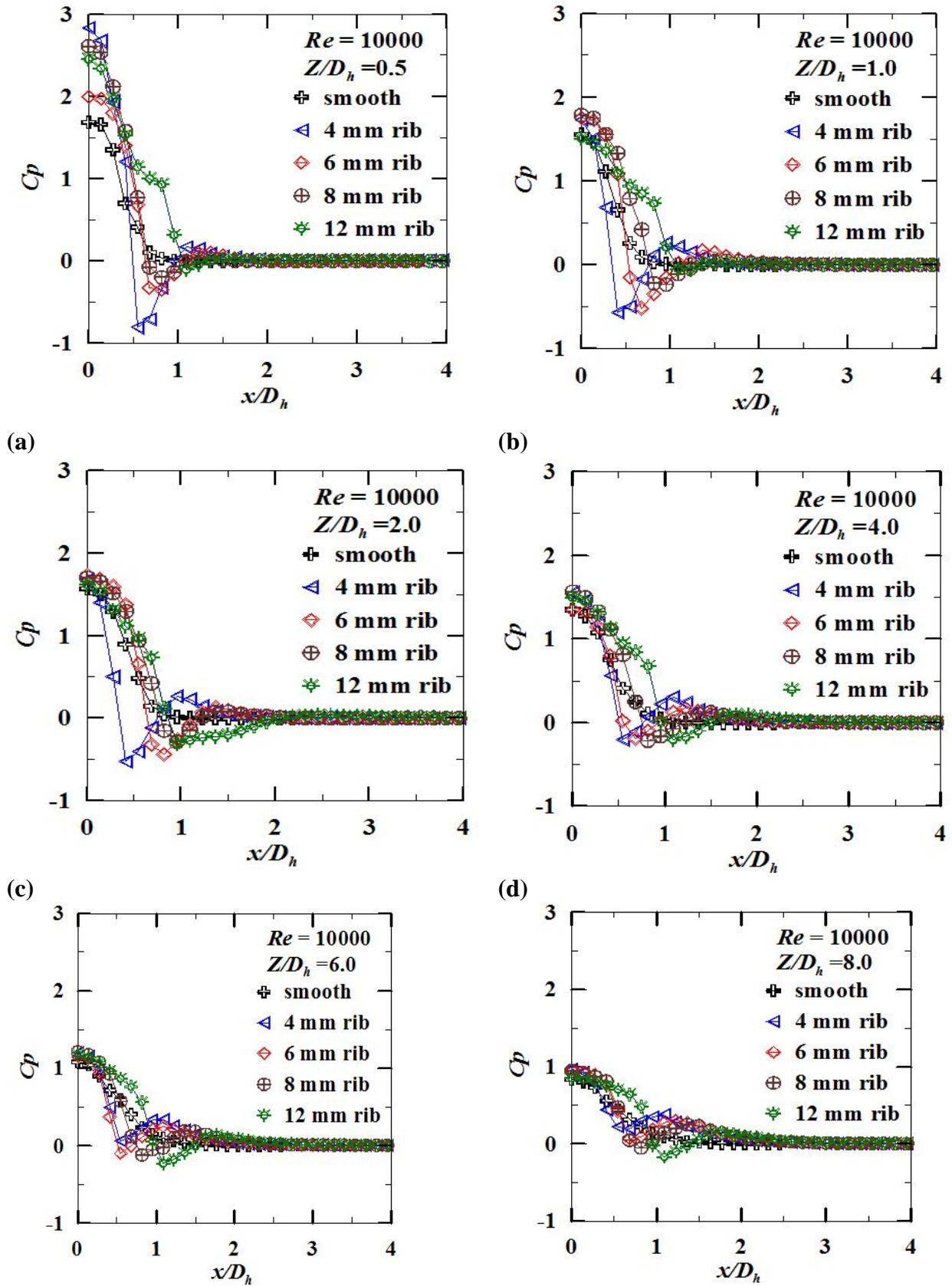


(e)

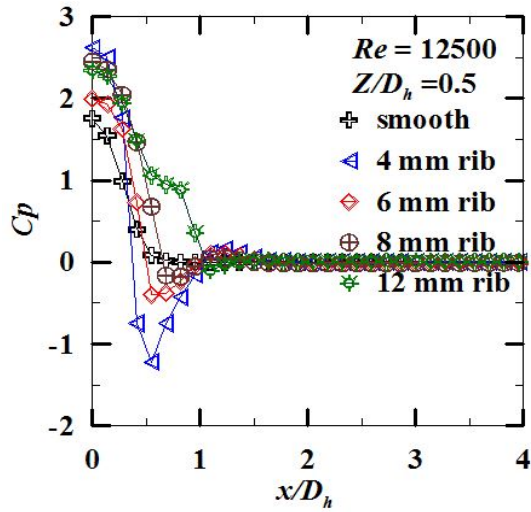


(f)

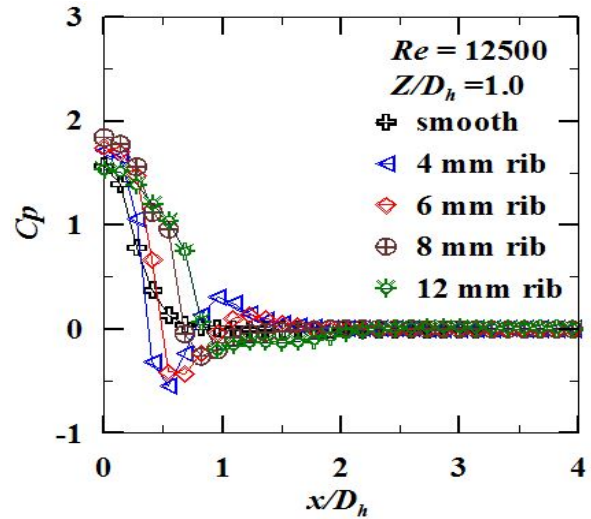
Fig.4.10 “Wall static pressure” variation along the plate for the various J2P spacing (Z/D_h) at $Re=7500$ for different rib size



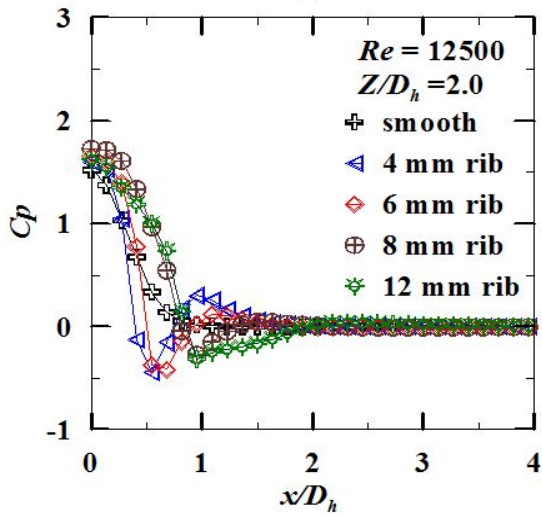
(e) (f)
Fig.4.11 “Wall static pressure” variation along the width of the “Target plate” for the various J2P spacing (Z/D_h) at $Re=10000$ for different rib size



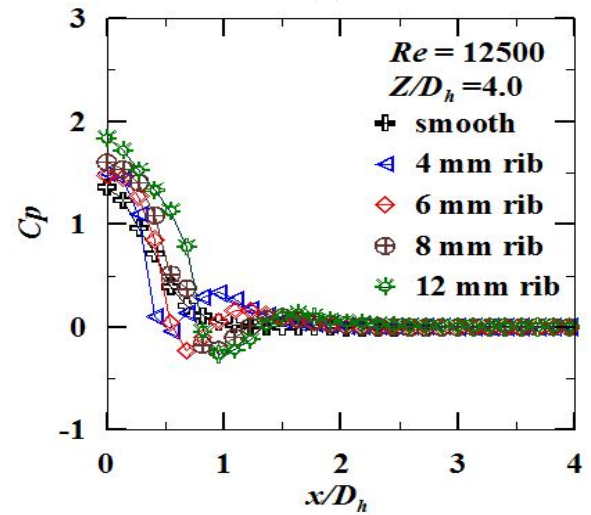
(a)



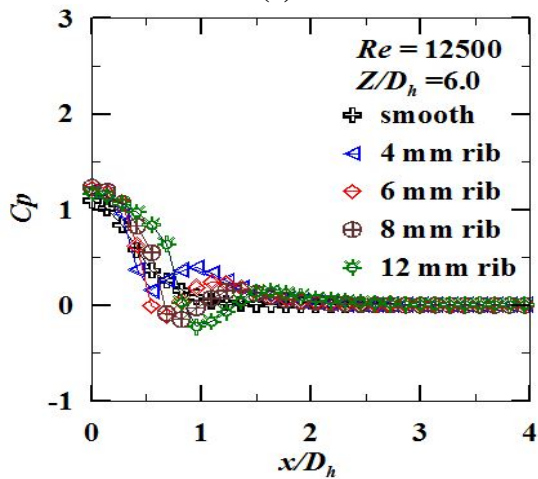
(b)



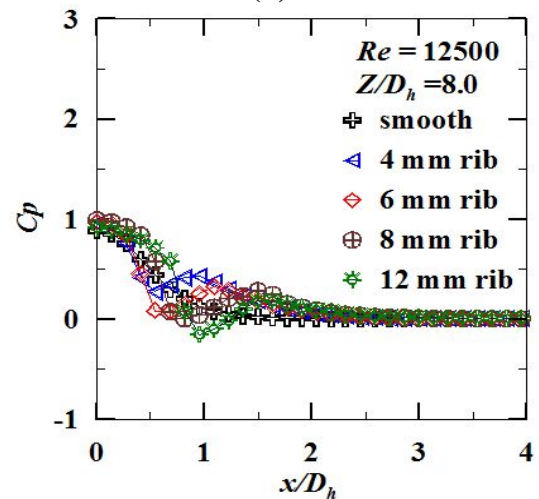
(c)



(d)



(e)



(f)

Fig.4.12 “Wall static pressure” variation along the plate for the various J2P spacing(Z/D_h) at $Re=12500$ for different rib size

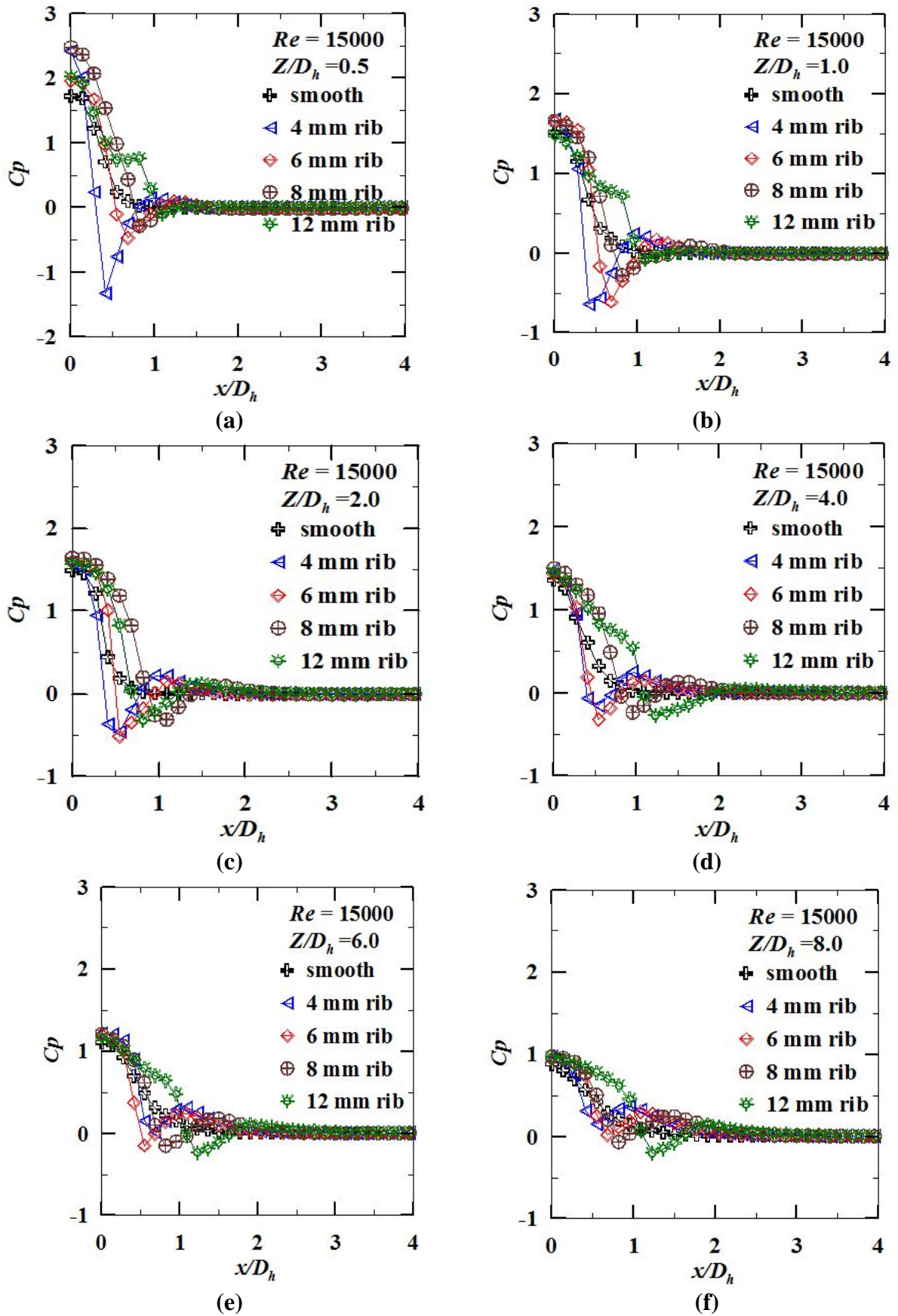


Fig.4.13 “Wall static pressure” variation along the plate for the various J2P spacing (Z/D_h) at $Re=15000$ for different rib size

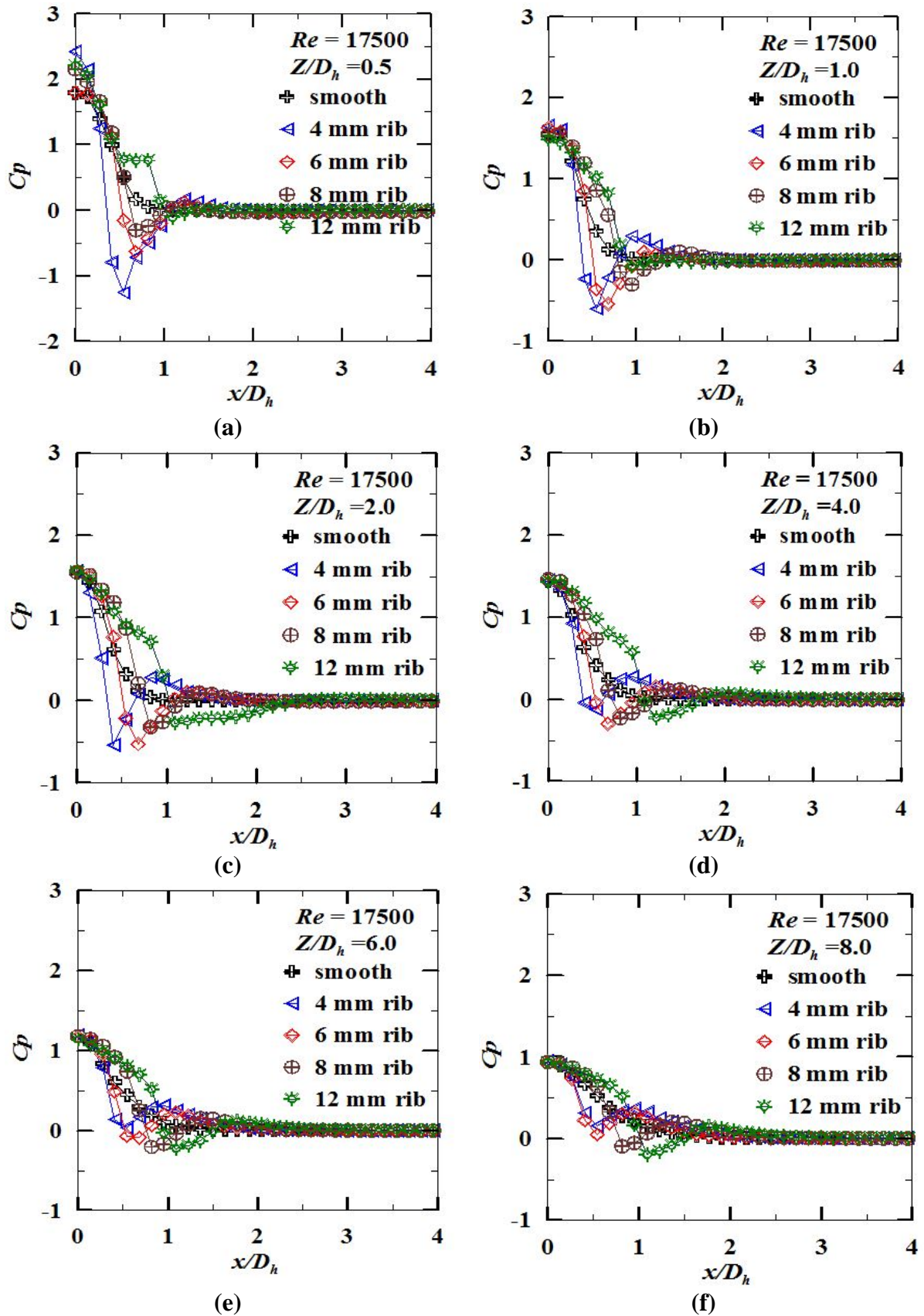


Fig.4.14 “Wall static pressure” variation along width of the plate for the various J2Pspacing(Z/D_h) at $Re=17500$ for different rib size

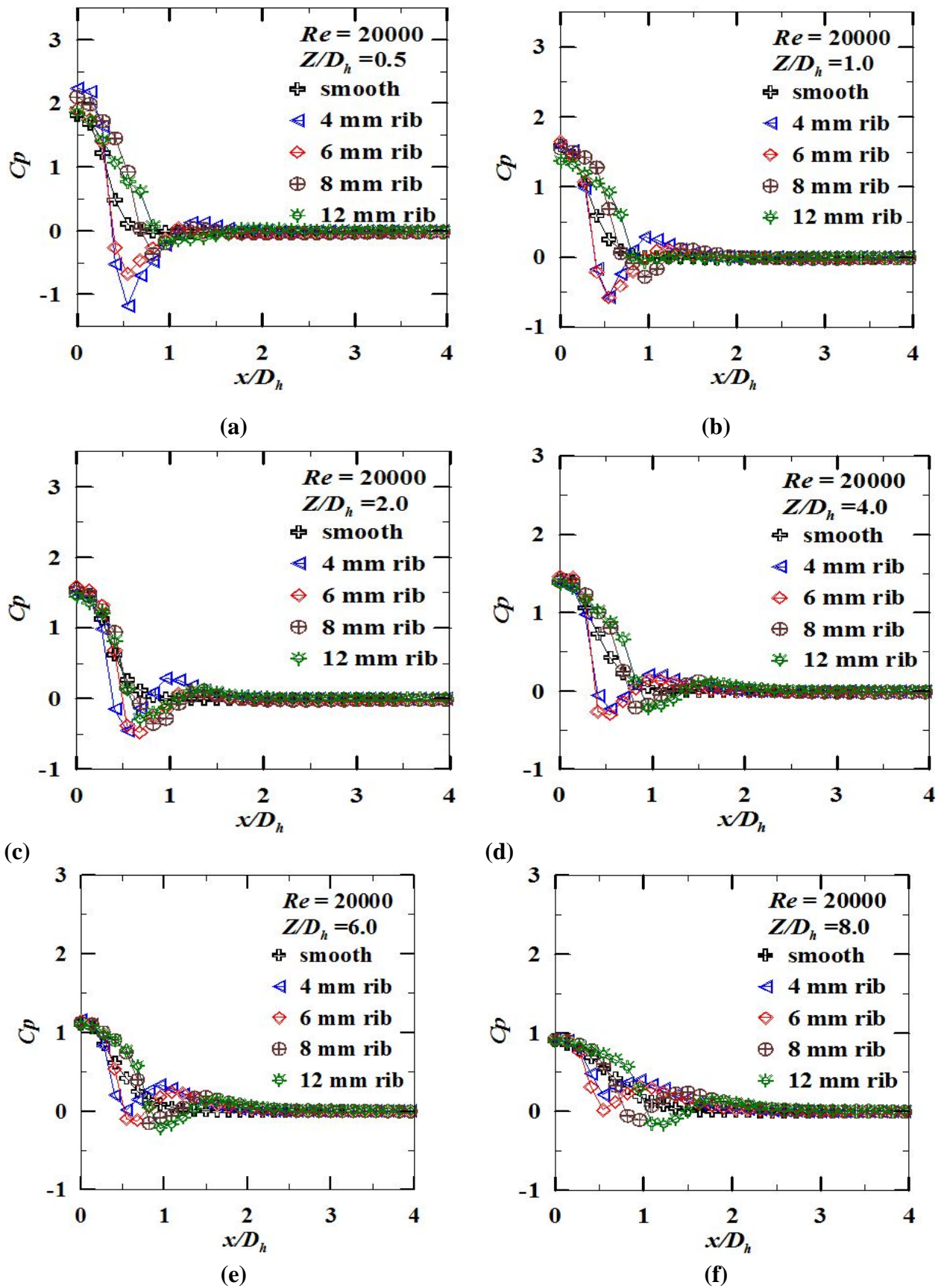
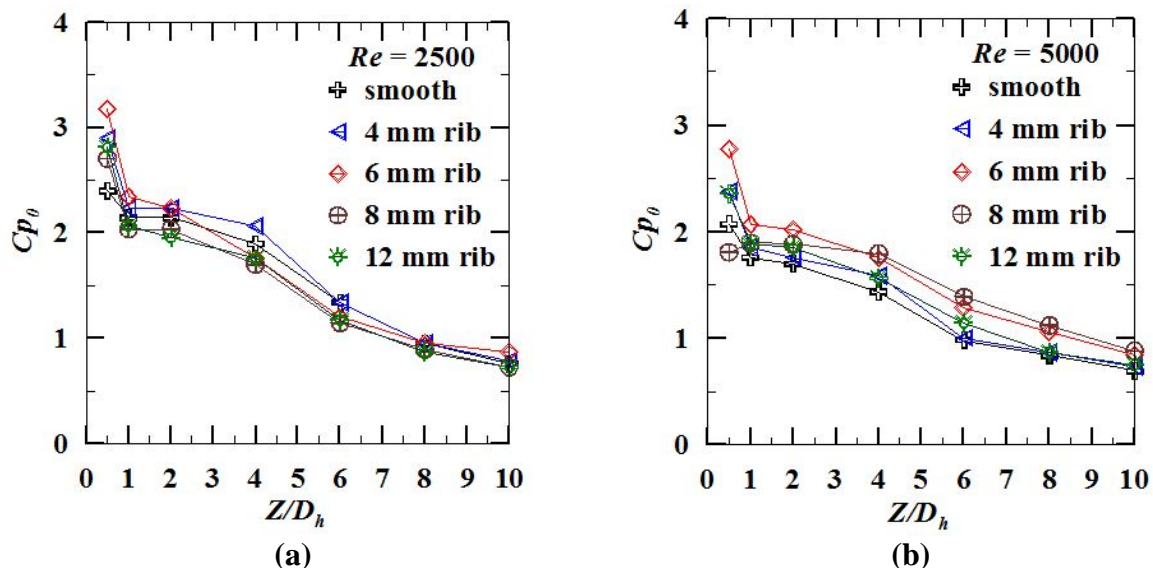


Fig.4.15 “Wall static pressure” variation along the width of the plate for the various J2Pspacing(Z/D_h) at $Re=20000$ for different rib size

A similar trend is observed at the $Re = 10000$ as shown by figures 4.11 (a) to 4.11(f). WSP was found to be higher for the ribbed surface, for the entire range of Re and the Rib sizes investigated.

Fig. 4.16(a) to (h) shows the variation of SPWSP coefficient (C_{p0}) for the various J2P distances (Z/D_h of 0.5 to 10) at various Re from 2500 to 20000 and for different Rib sizes studied. It can be observed that SPWSP decreases as the J2P distance increases. The effect will be observed up to the $Z/D_h = 4$. There is a drastic drop in the SPWSP coefficient from J2P distance $Z/D_h = 0.5$ to $Z/D_h = 1$ at the whole set of “Reynolds numbers”. The C_{p0} values are found decreasing monotonically for the remaining J2P distance. From the figure.4.16 we can conclude that for all the rib sizes “stagnation point” wall static pressure decreases as the distance of the point from the jet increases. The C_p value for any J2P distance remains almost same at varying “Reynolds numbers” and hence C_p is not a dependent of the “Reynolds number”.

The Rib of width 4mm gives the maximum value for SPWSP in comparison with other ribs. The 6mm Rib also shows better pressure distribution, but 8mm and 12mm Ribs are not much effective they show similar behaviour like smooth surface but at the lower J2P distance (Z/D_h) of 0.5 and 1 there is a little influence of the rib.



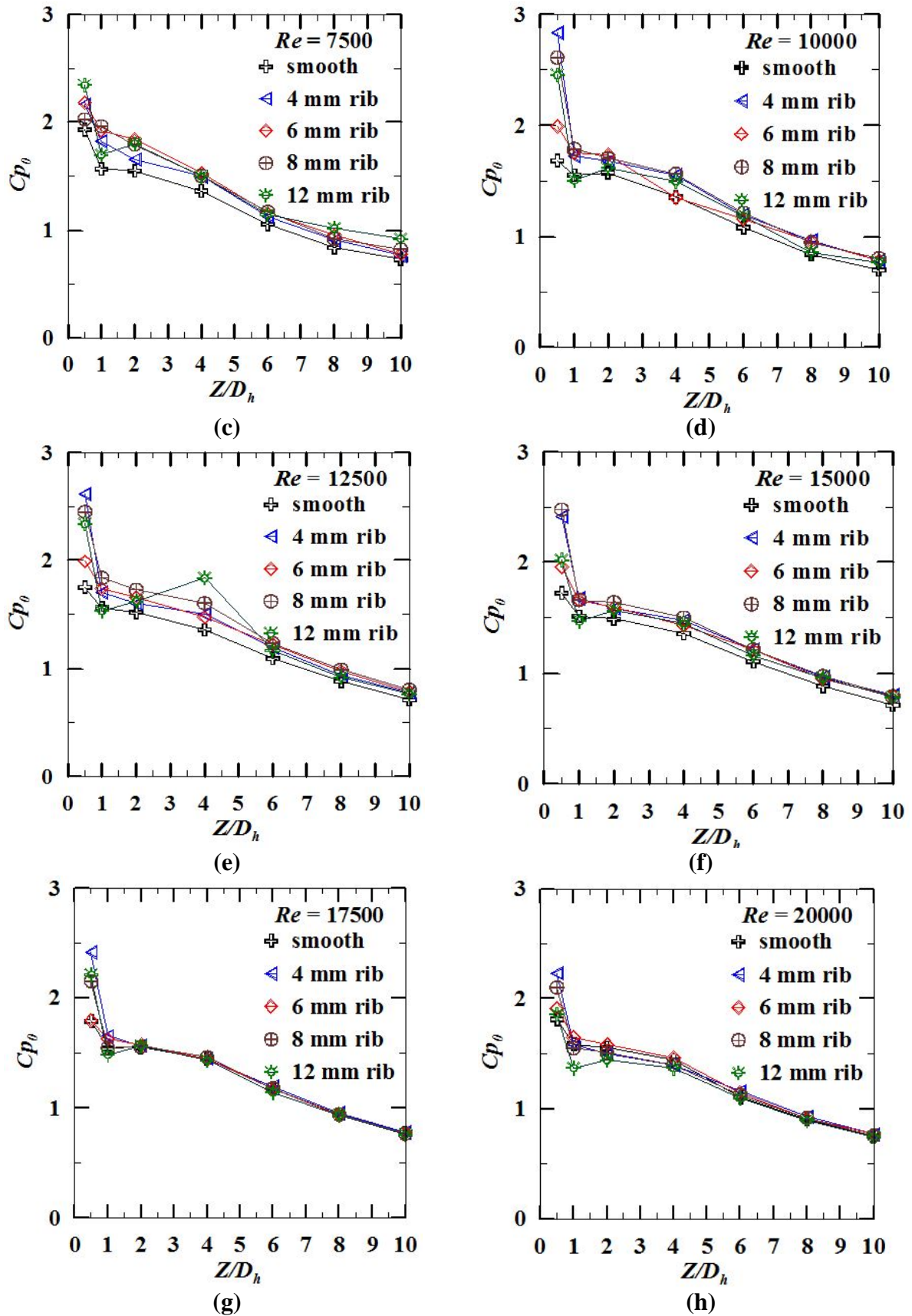


Fig.4.16 Variation of Cp_0 for the different J2P spacing at various “Reynolds number” and different Rib configurations

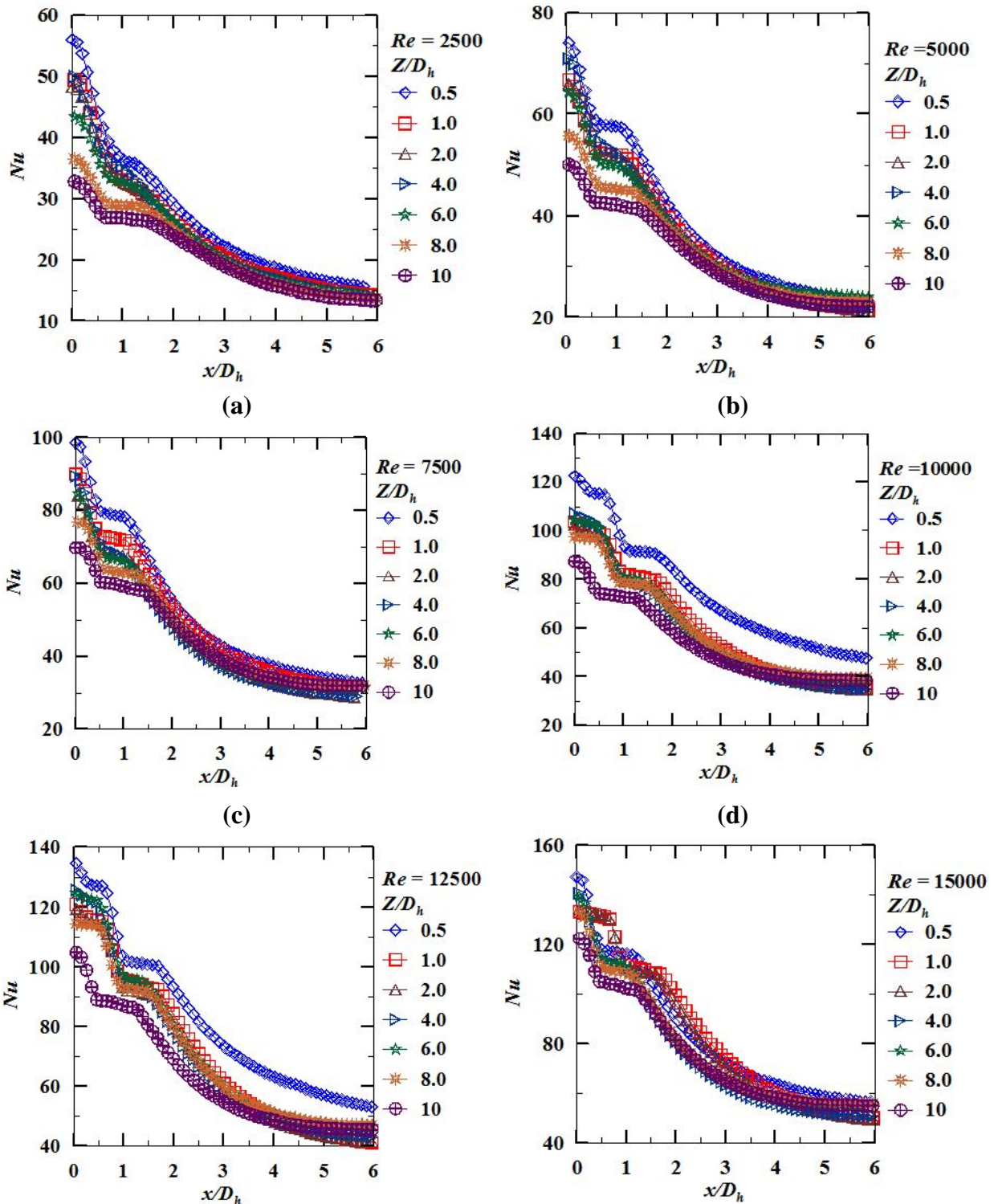
4.3 “heat transfer” between a rough surface and a “slot jet”

“Heat transfer” characteristic of an impinging jet can be understood better if the various regions on the target the plate are identified suitably like stagnation region and wall jet region. The centreline velocity of the impinging jet will be at its peak and suddenly reduces to zero at the “stagnation point” which is nothing but the point of jet impact. The WSP is high at the “stagnation point”. “It leads to a favourable pressure gradient in the direction parallel to the target surface in the stagnation region. Finally, the flow over the target surface forms the wall jet region where the jet adheres to the surface and flows over the plate interacting with the surrounding air. The flow from stagnation to wall jet region occurs through the transition region where the boundary layer changes from laminar to turbulent.

In this study, rectangular detached ribs having a of 45mm height in common and varying slot widths of 4mm, 6mm, 8mm, and 12mm were used. The ribs were made of 2mm thick non thermal conductive flexi-glass sheet. The width of the rib frame is constant at 2mm for all the ribs. The roughness is introduced by mounting the ribs in the flat surface. Roughness strongly influences on the flow characteristics, the mean velocity of the jet and the turbulence intensity of the flow as observed in this study. “The flow over the plate at low Reynolds number will be aerodynamically smooth and the influence of roughness very small and the flow behaves similar to on a smooth wall, whereas at higher Reynolds number the flow changes from laminar to turbulent and the roughness so dominates the momentum transport to the wall that viscous effects are negligible. Roughness increases the swirl (superposition of the tangential velocity component onto axial flow) which can markedly affect the flow and turbulence characteristic of the flow”.

Figure.4.17(a) to (h) indicates the change in the local “Nusselt number” along the length of the plate for the J2P distance (Z/D_h) of 0.5 to 10 for the set of “Reynolds number” studied. By observing fig.4.21 it can be noted that at all the “Reynolds number” the Nu value peaks at the “stagnation point” and diminishes non-variably along the length of the plate. The flow from the stagnation region passes through a transition region before it enters the wall jet region and the flow transits into turbulent from laminar. The transition region is sensitive to J2P spacing. The Nu value increases with the “Reynolds number” and peaks at $Z/D_h=0.5$. For the J2P distance at various “Reynolds number” the stagnation region is identified at x/D_h of around 0.5 after that secondary peak is observed around x/D_h of 1.0.

From the figure.4.17 we can conclude that the local Nu value is maximum for a higher Re and is recorded at $Re = 20000$. It is accredited to the turbulent nature of the fluid flow reducing the thickness of the stagnant thermal margin layer and making the interactions between the surface and the jet more prominent. Roughness increases the swirl; the swirl widens the jet spread, the mixing rate of the quiescent air and jet velocity decays faster and all the favorable situations increases “heat transfer” rates.



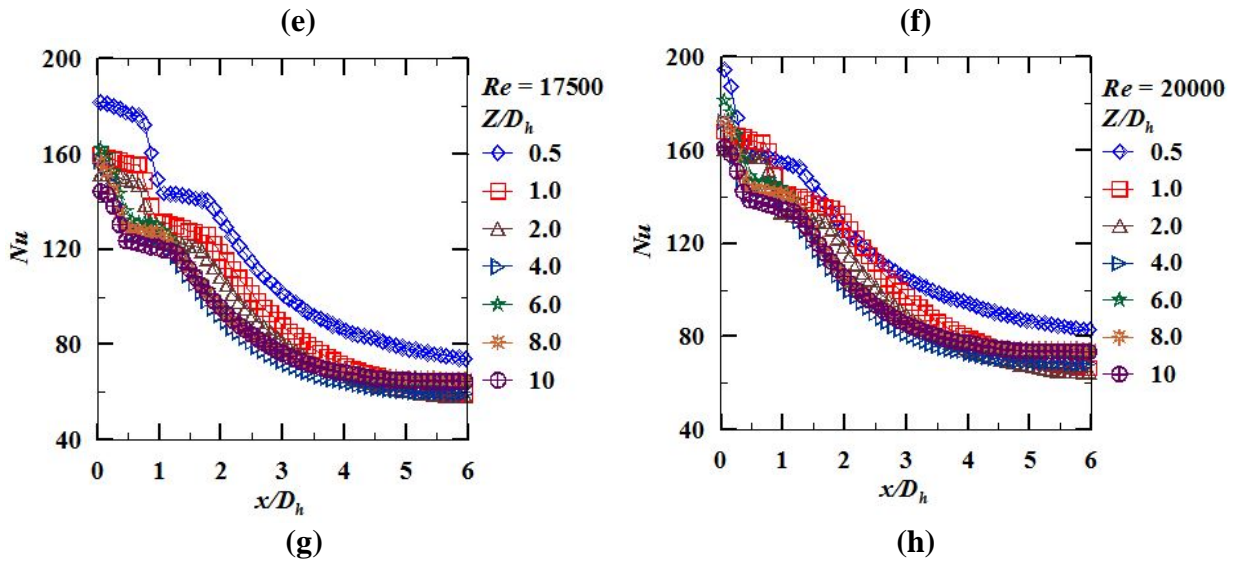
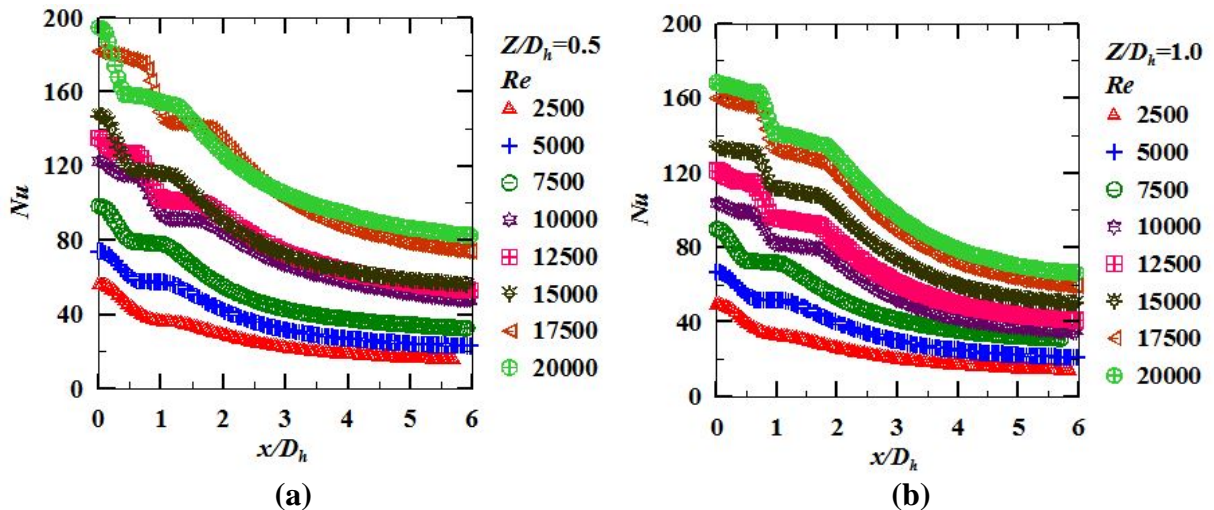


Fig.4.17 Variation of the Nusselt number along the length of the plate for the different J2P spaces (Z/D_h) at $Re = 2500$ to 20000 for Rib size = 4mm

Figure 4.18 (a) to fig.4.18 (f) shows the distribution of the local Nu along with the length of the plate at various “Reynolds number” for the different J2P spacing studied.

By observing figures 4.22 it can be identified that local Nu is maximum at higher Re and lower J2P spacing (Z/D_h) of 0.5. The local Nu decreases as the J2P distance increased due to the reduction in the strength of the jet core and increase in the thickness of the thermal boundary layer. “The thickness of the boundary layer depends on both Z/D_h and x/D_h . Turbulence intensity decreases as we move away from the stagnation point. Roughness causes higher turbulence intensity. The increase in turbulence intensity depends on both Z/D_h and x/D_h . It is observed that for all the J2P spaces local Nusselt number decreases non-variably and equals atmospheric pressure around x/D_h of 2.0.



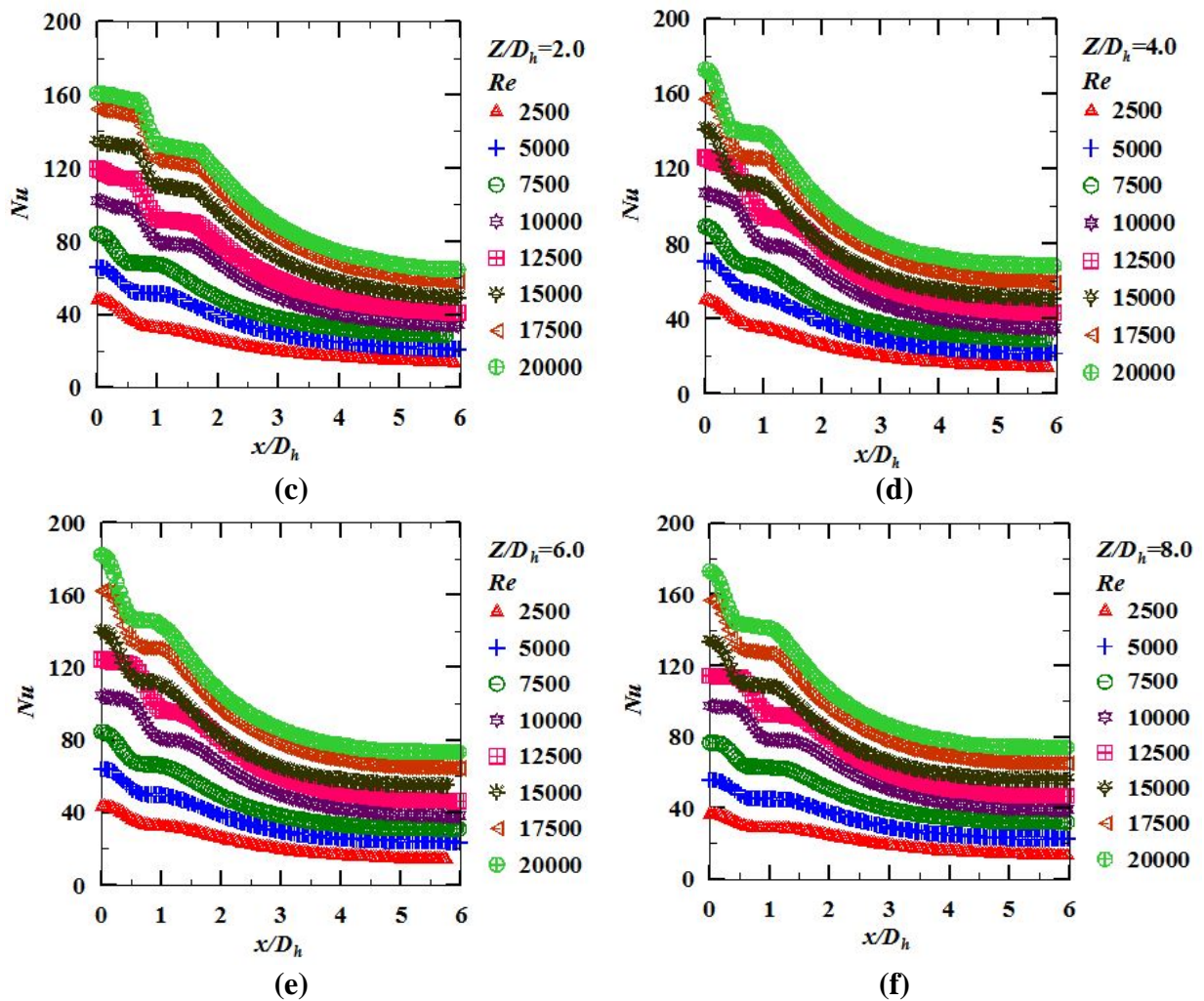
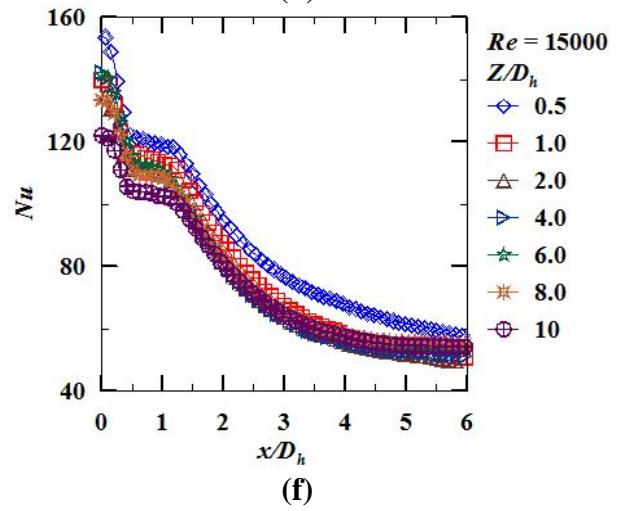
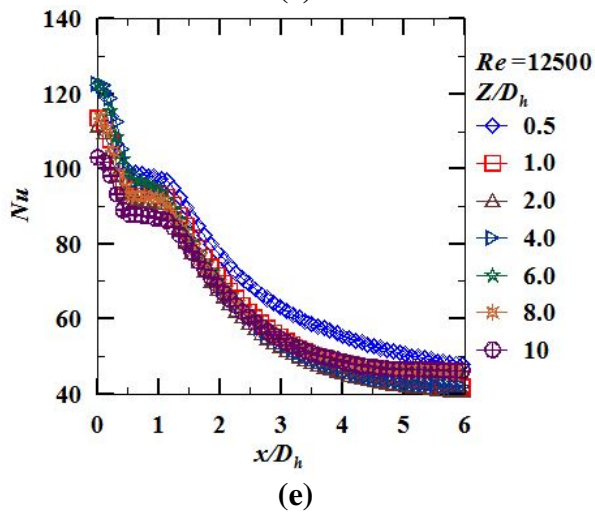
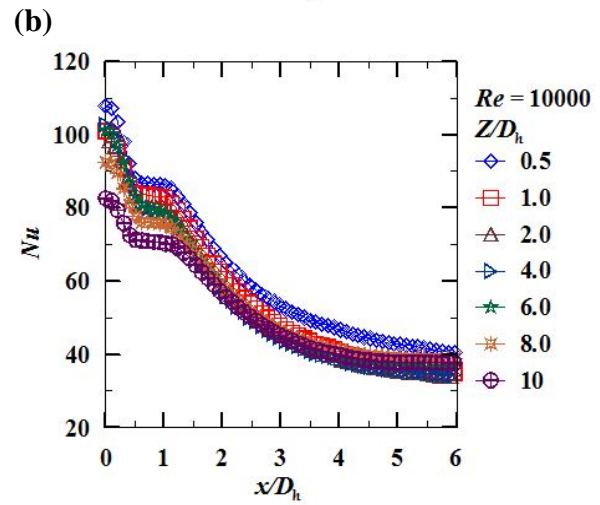
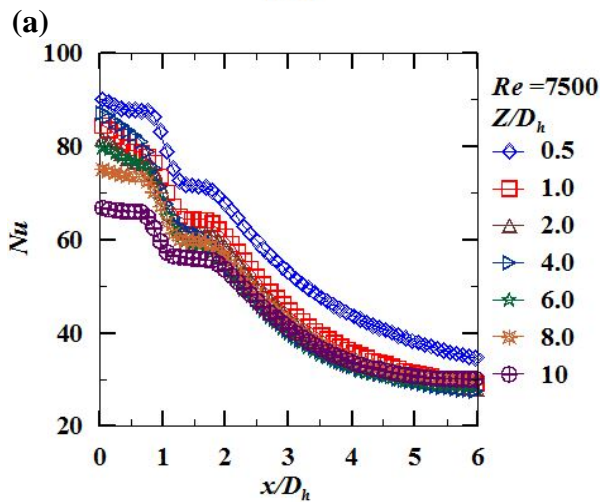
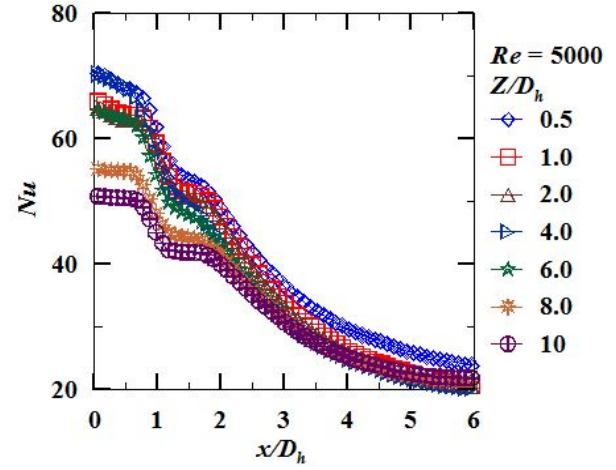
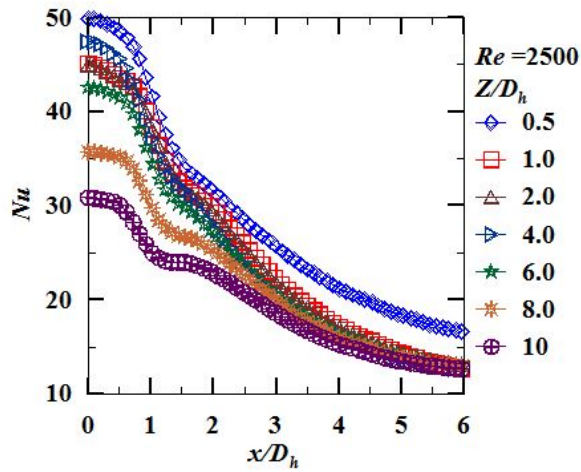


Fig.4.18 Variation of Nu along with the length of the plate at different “Reynolds number” s for $Z/D_h=0.5$ to 10 for Rib size=4mm

Figures 4.19 (a) to fig. 4.19(h) show the variation of the local Nu along the length of the plate for the J2P distance (Z/D_h) of 0.5 to 10 for the “Reynolds number” studied with the rib of width 6 mm. From the fig.4.19 it can be noted that at all the “Reynolds number” s studied the value of the maximum Nu is identified at “stagnation point” and decreases non-variably along plate. The flow from the stagnation region passes through a transition region before it enters the wall jet region and the flow transits into turbulent from laminar. The transition region is sensitive to J2P spacing. The Nu value increases with the rise in the “Reynolds number” and peaks at $Z/D_h=0.5$. For the J2P distance at various “Reynolds number” the stagnation region is identified at x/D_h of around 0.5 after that secondary peak is observed around x/D_h of 1.5.



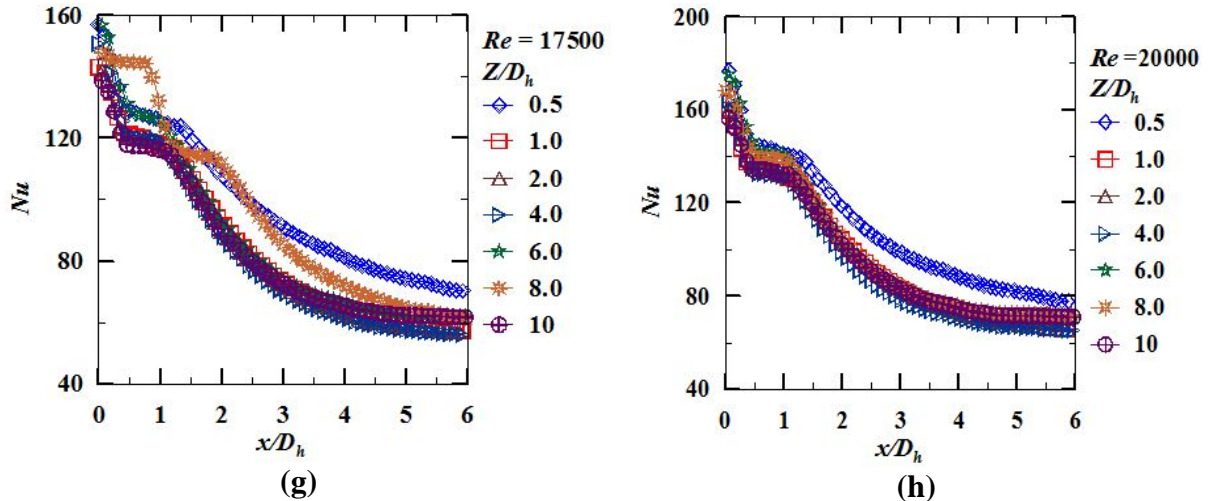
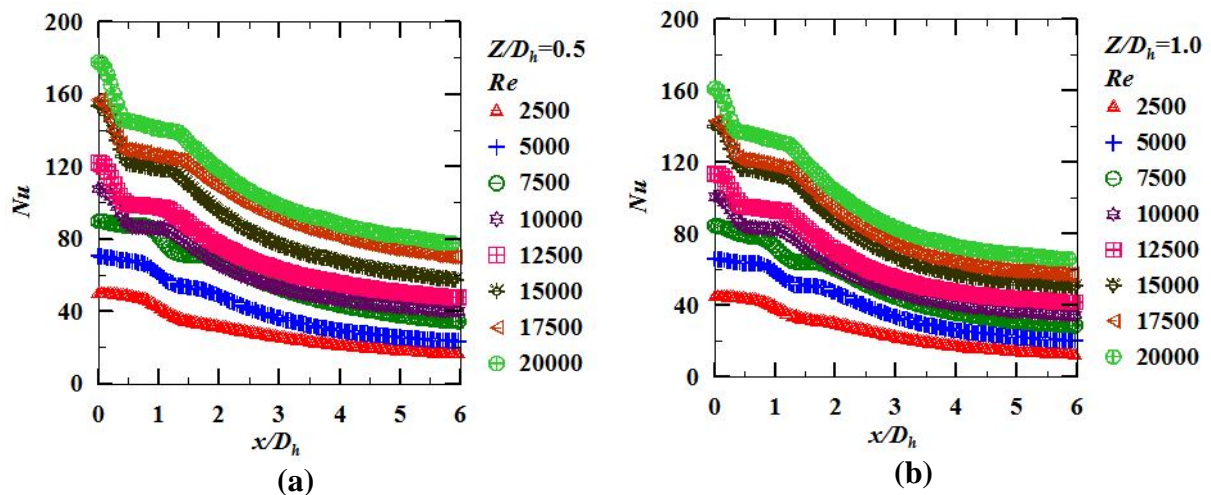


Fig.4.19 “Variation of the Nu along the length of the plate for the different”J2P spacing (Z/D_h)at $Re = 2500$ to 20000 for Rib size=6mm

Figures 4.20 (a) to fig.4.20 (f) represents the variation of the local Nu along with the length of the plate at various “Reynolds number” and J2P spacing studied. It is observed that local Nu is high at “Reynolds number” of 20000 and varies proportionately with the “Reynolds number” and inversely related to the J2P distance. As compared to the rib with 4mm width the rib with 6mm width has a lower value for the Nu at the “stagnation point”. It may be due to larger width of the rib and a major portion of the jet missing to hit in the stagnation region. Nu value is higher for Z/D_h of 0.5 and decreases as the plate moves away from the jet. For remaining J2P spacing, there are no much significant variations in the Nu values.



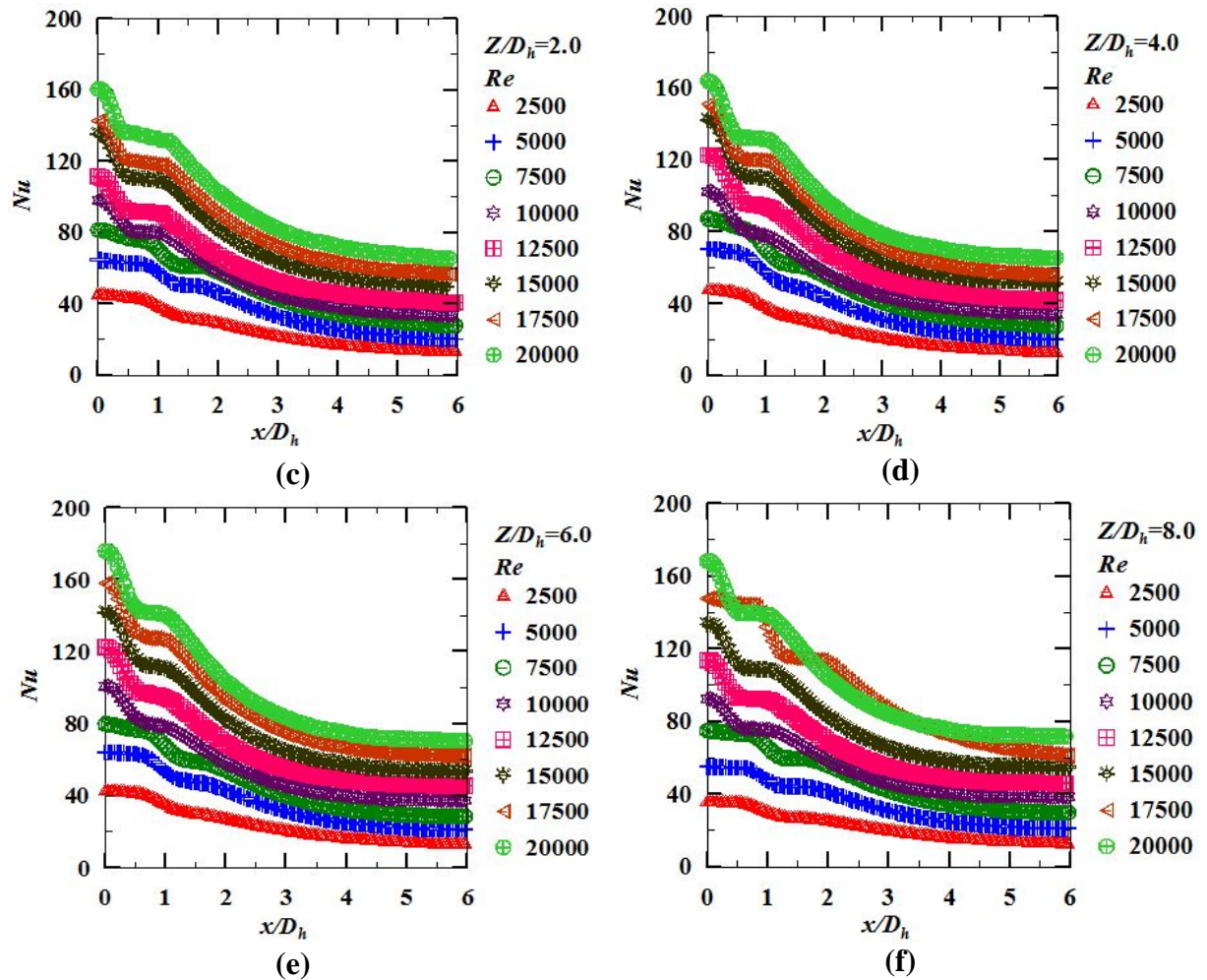
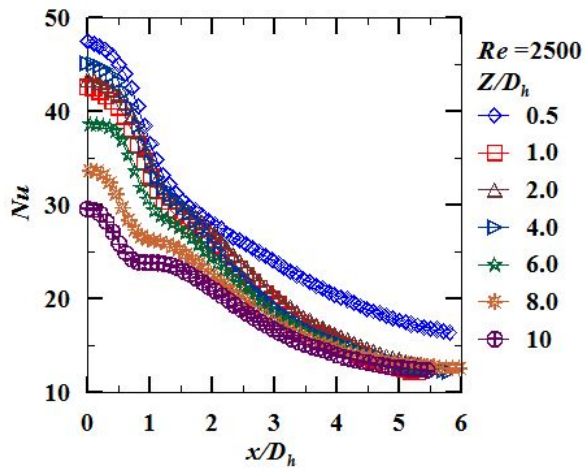
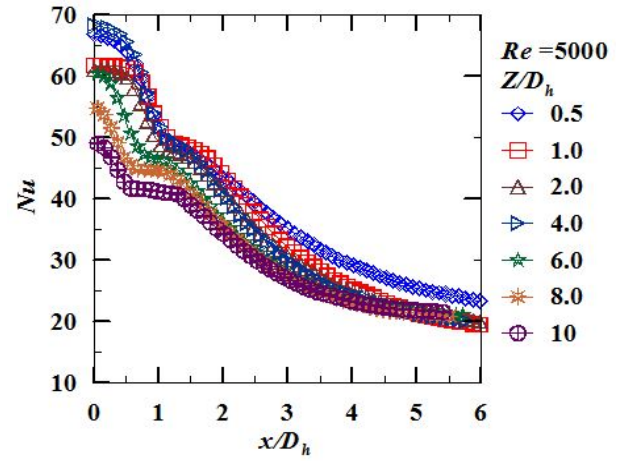


Fig.4.20 Variation of Nusselt number along with the length of the plate at different “Reynolds number” for $Z/D_h=0.5$ to 8.0 for Rib size=6mm

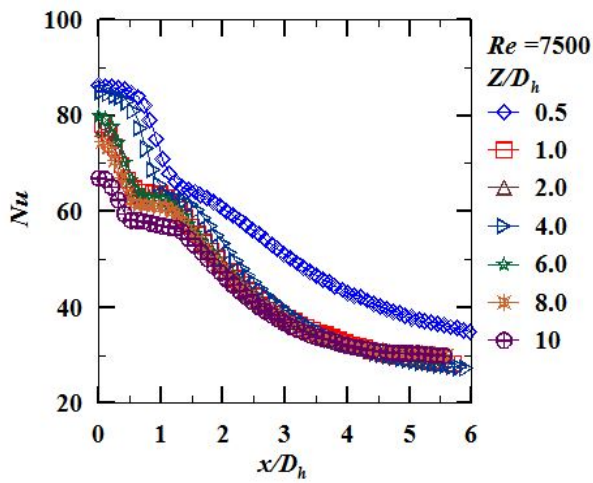
Figures 4.21 (a) to 4.21(h) shows the variation of the “local Nu ” along the length of the plate for the J2P distance (Z/D_h) of 0.5 to 10 for the “Reynolds number” studied for Rib of width 8mm. It can be experiential from figure 4.21 that the local Nu is high at “Reynolds number” of 20000 and varies proportionately with the Re and inversely varies with the J2P distance. As compared to the rib with 4mm width the rib with 8mm width has a lower value for the Nu at the “stagnation point”. It may be due to more width of the rib and a major portion of the jet missing to hit in the stagnation region. Nu value is higher for Z/D_h of 0.5 and decreases as the plate moves away from the jet. Here we can identify that a secondary peak which is much influenced by higher “Reynolds number” due to the turbulent nature of the fluid. At lower “Reynolds number” of 2500 secondary peak is not much prominent. The secondary peak is observed due to the acceleration of the fluid under the rib. At “Reynolds number” 5000 to 20000 the secondary peak is observed at a distance of x/D_h around 1.5 and later there is a sudden decrease in the Nu value and reaches its minimum.



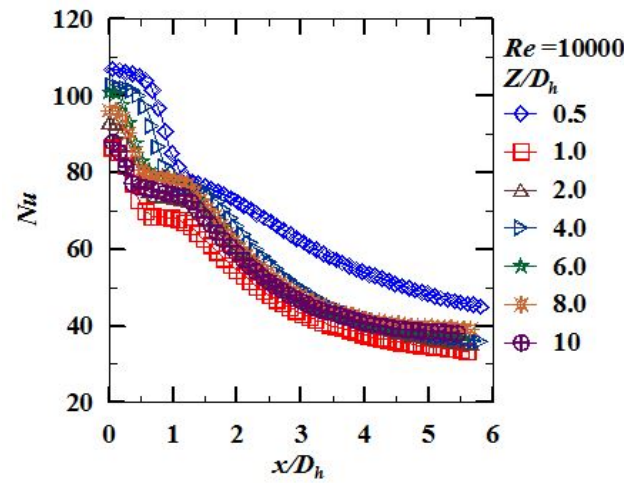
(a)



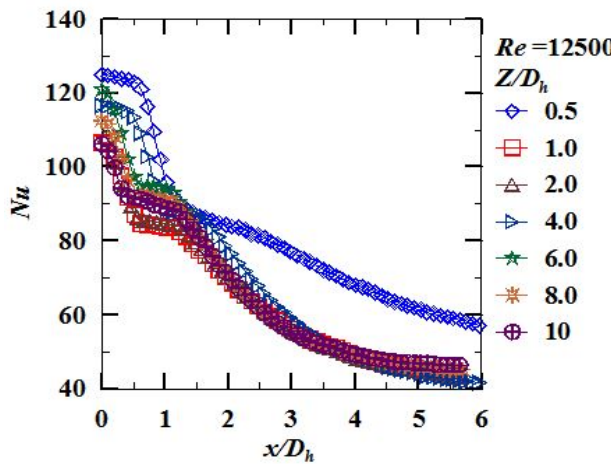
(b)



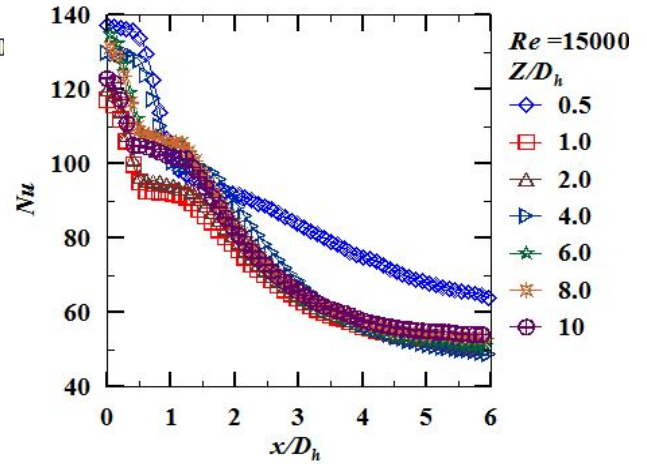
(c)



(d)



(e)



(f)

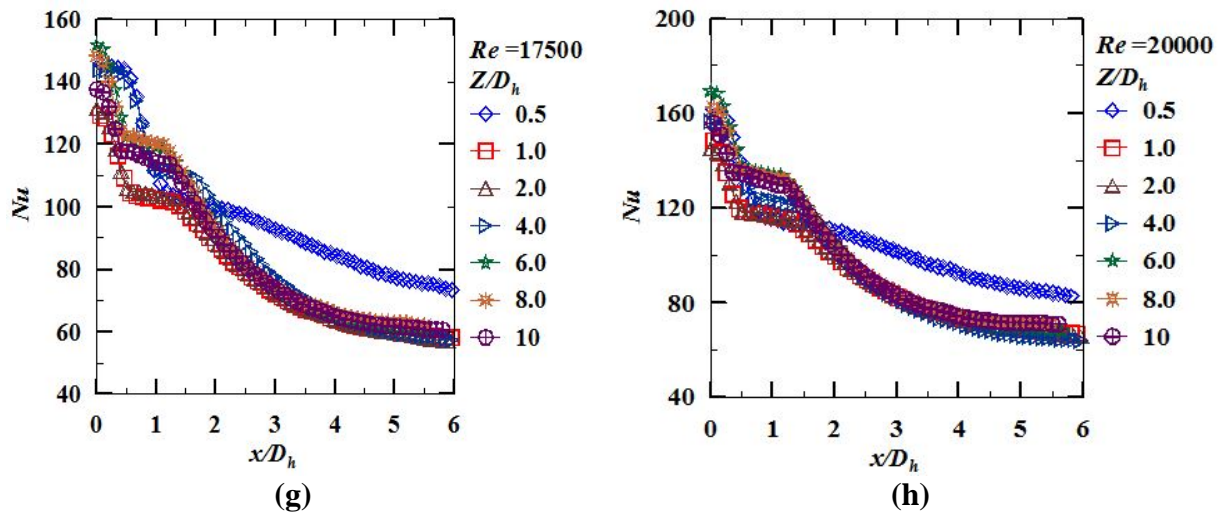
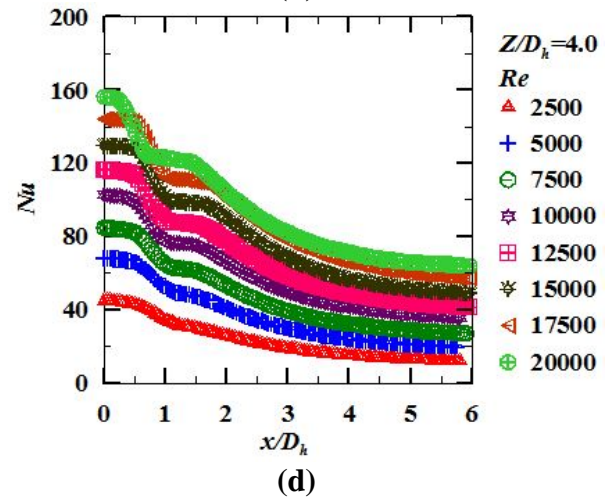
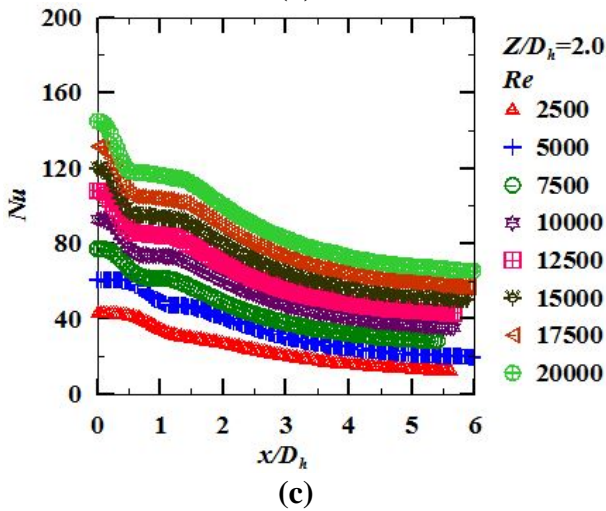
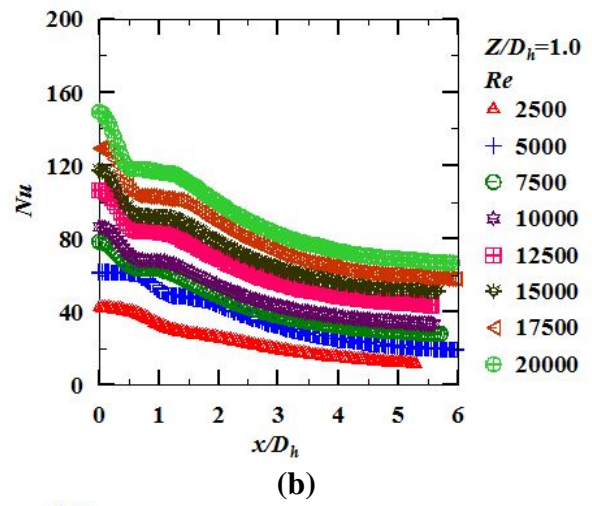
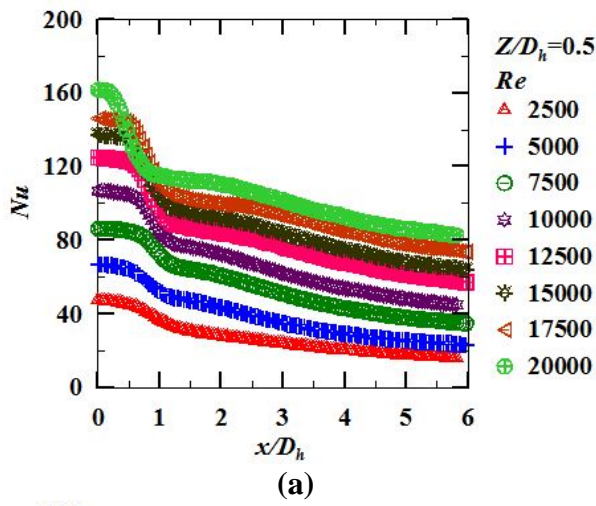
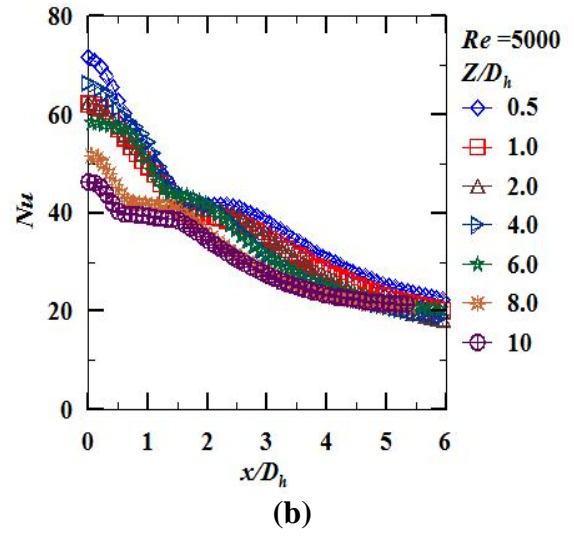
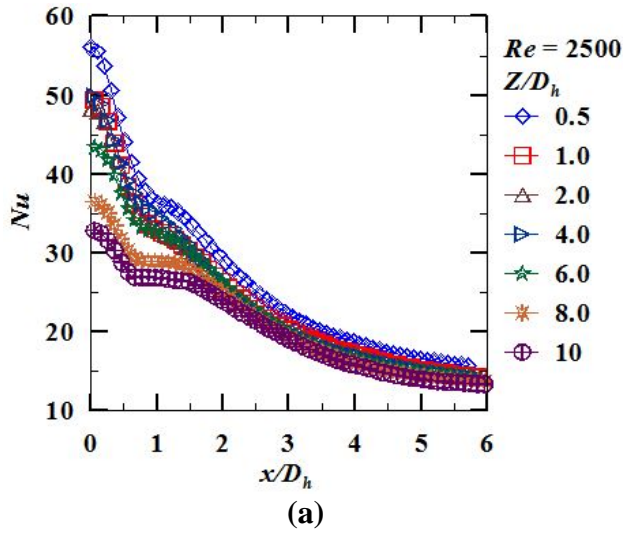


Fig.4.21 “Variation of the Nu along the length of the plate for the different” J2P spacing (Z/D_h) at $Re = 2500$ to 20000 for Rib size = 8mm

From figure.4.22 (a) to (f) shows a variation of the local Nu along with the length of the plate at various “Reynolds number” for the different J2P spacing is studied. We can observe that the local Nu is at its peak at “Reynolds number” 20000 and decreases with lower “Reynolds number” and higher J2P distance. Compared to 4mm and 6mm rib width the 8mm width rib giving the lower value of the local Nu in the “stagnation region”. It decreases monotonically along “stream wise direction” of the plate invariably for all J2P spacing.

Figures 4.23 (a) to 4.23(h) show the variation of “local Nu ” along the length of the plate for the J2P distance (Z/D_h) of 0.5 to 10 for the range of “Reynolds number” is studied for Rib size of 12mm. It can be noted that the local Nu is maximum in the stagnation region at higher “Reynolds number” of 20000. For the higher “Reynolds number” 12500 to 20000, Z/D_h of 6 and 8 shows the maximum value of local Nu compared to Z/D_h of 2 and 4. The secondary peak is observed around an x/D_h of 1.5 at low “Reynolds number” and x/D_h of 2.0 at higher “Reynolds number” of 12500 to 20000.



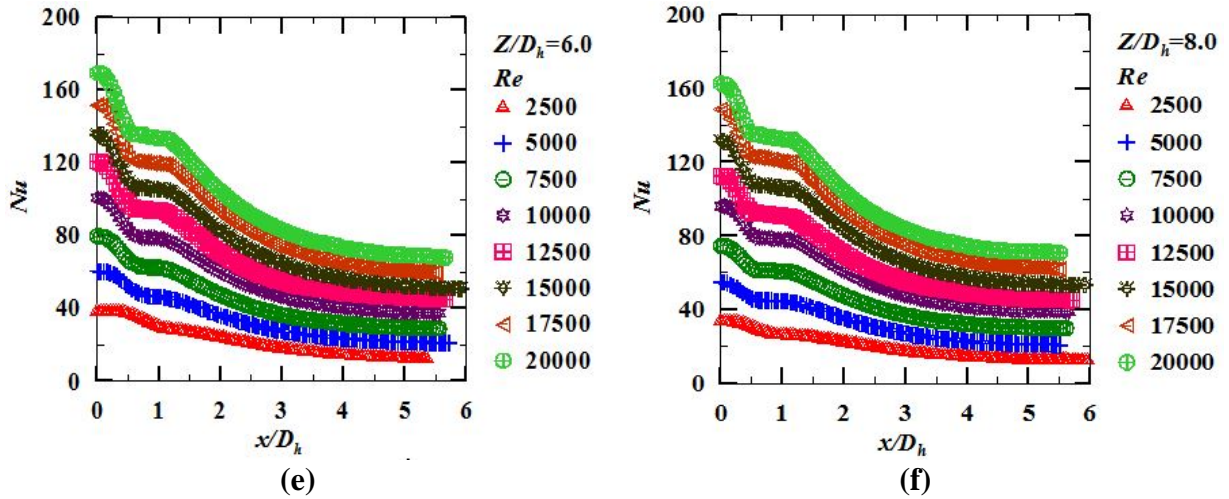
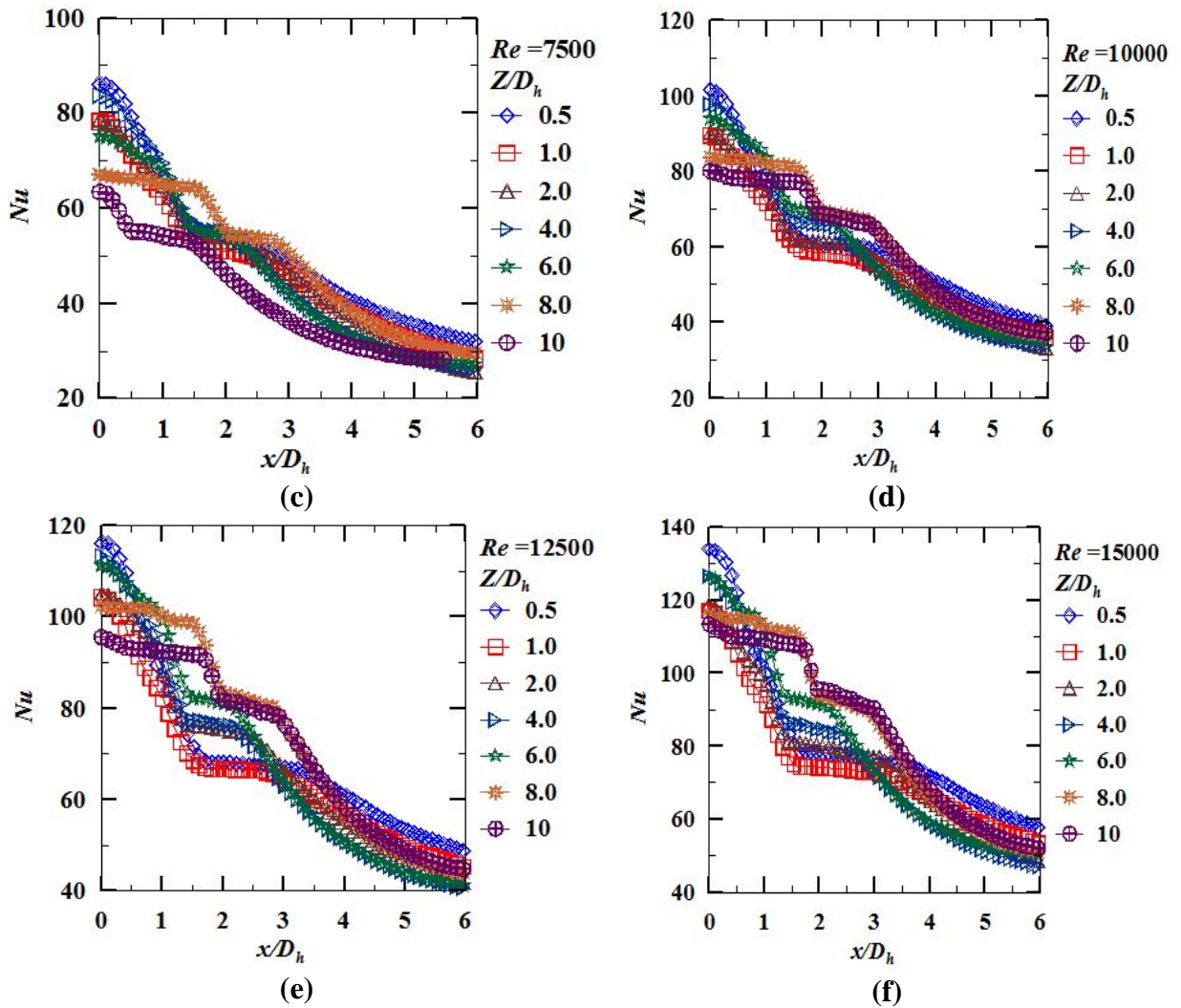


Fig.4.22 Variation of Nu along with the length of the plate at different “Reynolds number” for $Z/D_h=0.5$ to 10 for Rib size=8mm



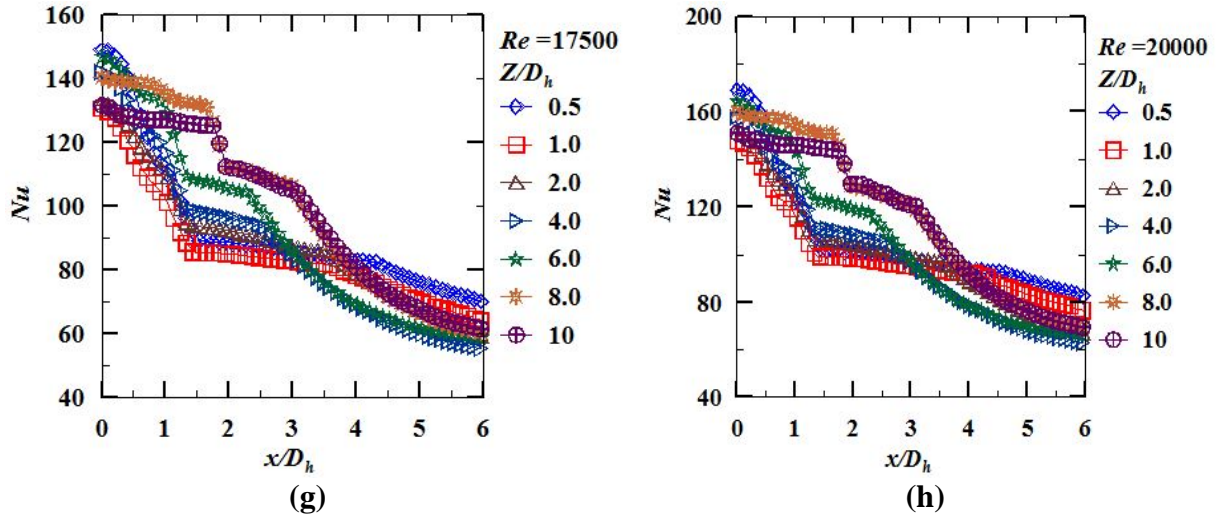
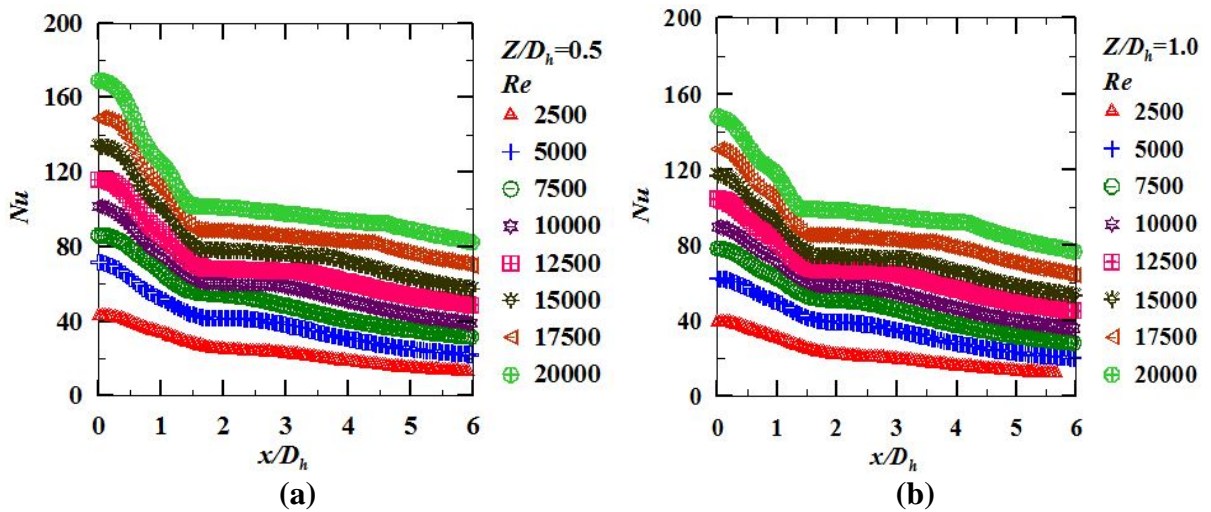


Fig.4.23 “Variation of the Nu along the length of the plate for the different”J2P spacing (Z/D_h)at $Re = 2500$ to 20000 for Rib size=12mm

Figures 4.24 (a) to (f) show a variation of the local Nu along with the length of the plate at various “Reynolds number” for the different J2P spacing for rib size of 12mm. It shows that the local Nu is at its high at the “stagnation point” and non-variably diminishes along the wall up to the end of the stagnation region. The Nu drops monotonically in the “wall jet region” invariably for all Z/D_h . For all Z/D_h considered for the study the Nu distribution curves overlap for in the “wall jet region” for any given “Reynolds number”. The reason for the decrease in the value of Nu can be ascribed to the loss in the fluid velocities over the surface because of a large exchange of momentum between the surrounding atmosphere and the jet.



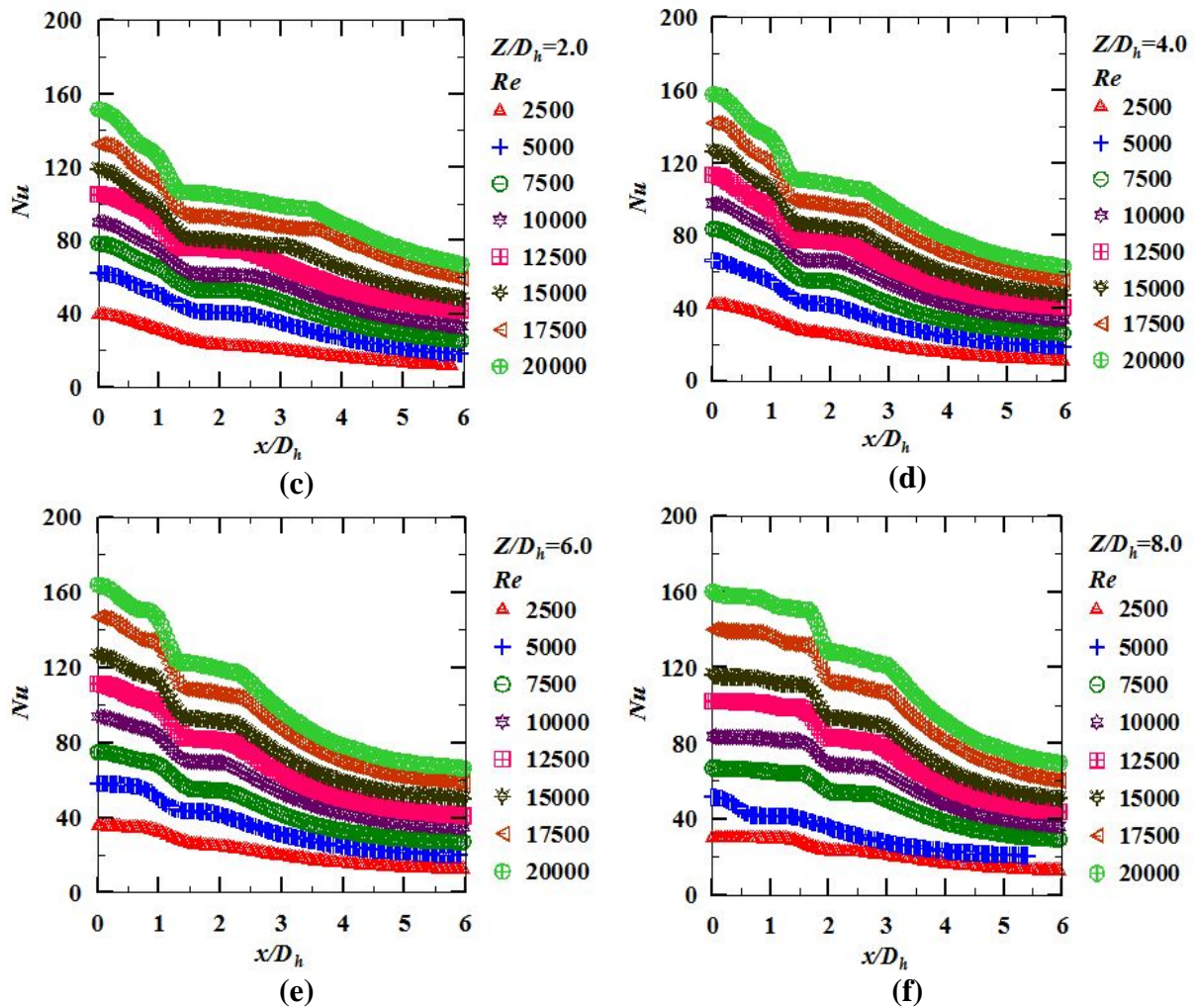


Fig.4.24 Variation of Nusselt number along with the length of the plate at different “Reynolds number” for $Z/D_h=0.5$ to 10 for Rib size=12mm

Figures 4.25(a) to (d) shows the difference of SP Nu i.e. (Nu_0) for J2P distances (Z/D_h of 0.5 to 4), various “Reynolds number” 2500 to 20000 and for various rib sizes investigated. It is observed that SPNU is high for the lower J2P spacing (Z/D_h) of 0.5 and for higher “Reynolds number” of 20000 irrespective of the rib size. Nu_0 gradually decreases in the “streamwise direction” for any Z/D_h and Re and this trend is similar for all the rib sizes studied. The figure shows that 4mm rib outperforms all other ribs with better SPNU and hence better “heat transfer” coefficient.

At a given “Reynolds number” SPNU is maximum for the J2P distance (Z/D_h) of 0.5 decreases suddenly from Z/D_h 0.5 to 1.0. This is maybe attributed to the dispersion of the jet with an increase in the J2P distance, particularly beyond the PCR for the “slot jet” ($Z/D_h \geq 2.0$). It is only when the surface is outside the PCR that strong effects of Z/D_h are observed. The secondary peak in the Nu can be observed at lower Z/D_h and it gets dominated by the increase in the “Reynolds number”.

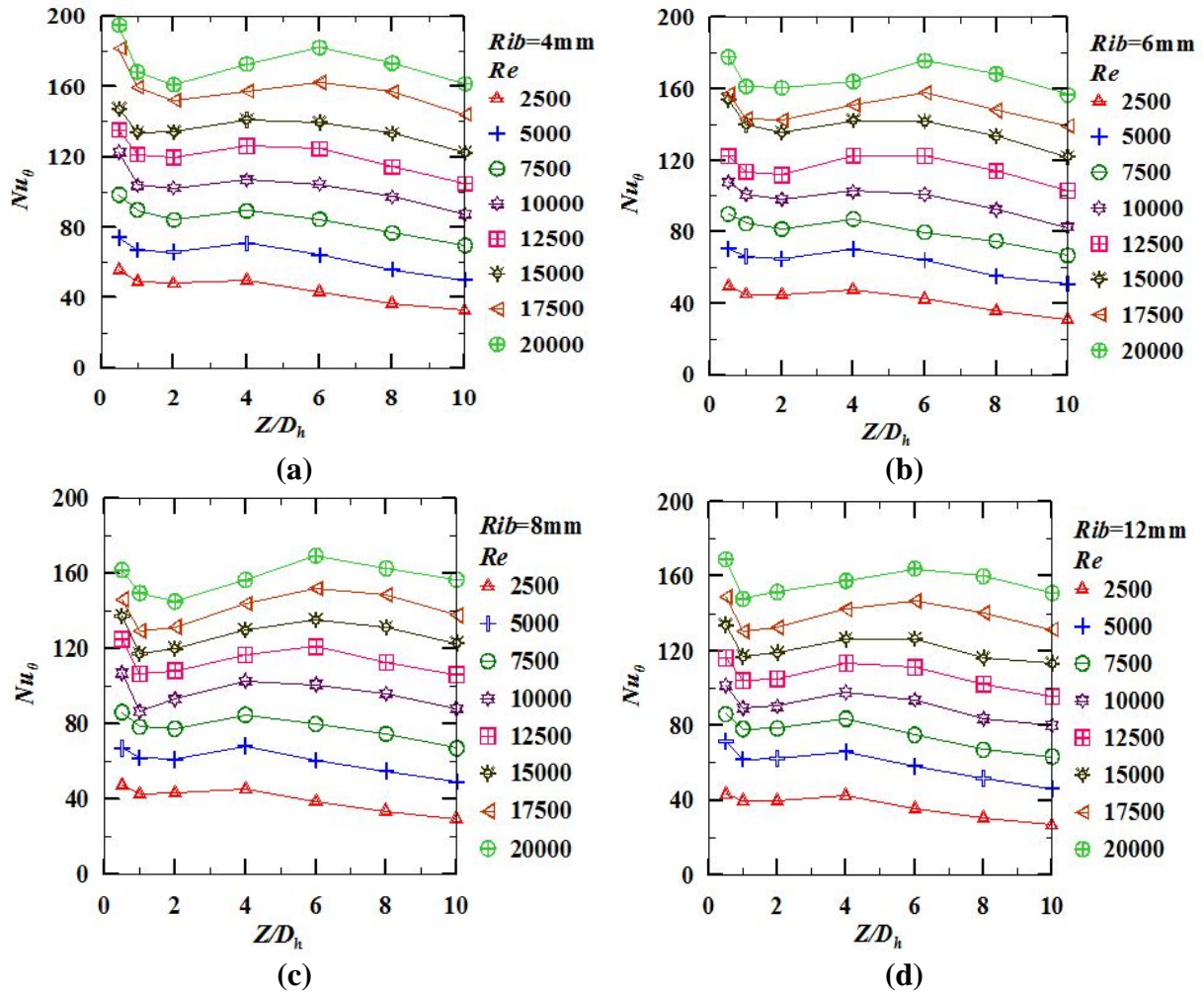


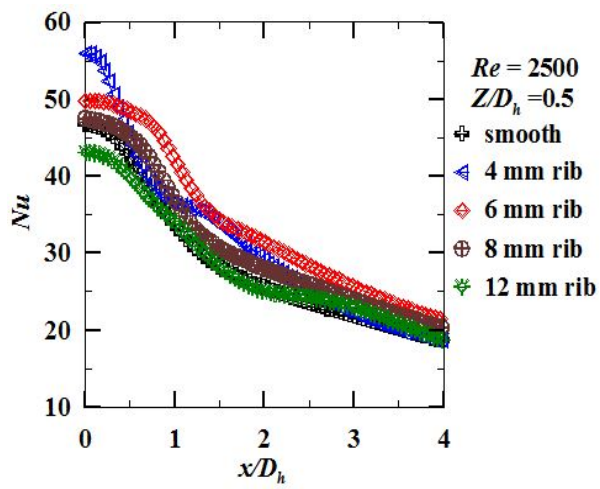
Fig.4.25 Variation of “stagnation point” “Nusselt number” for the different J2Pspacing at various “Reynolds number” for different Rib sizes

4.4 Comparison of “heat transfer” behavior of the jet on smooth and rough surfaces

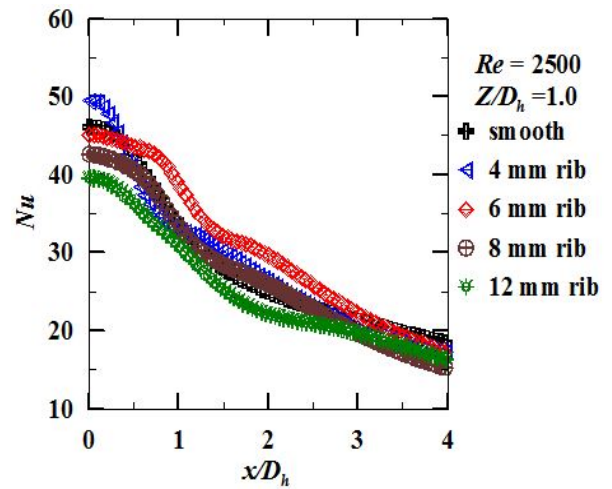
Figures 4.26 (a) to 4.26 (g) show the change in the local Nu along with the wall of the plate compared for the smooth surface and the rough surfaces at $Re = 2500$ for the different J2P spacing studied. It is observed that rough surface gives the maximum local Nu than that of the smooth surface. In the study, we identified that the ribs with a width of 4mm and 6mm provides better values for the HTC in comparison with the smooth surface. Overall performance of the 4mm width rib is better than other ribs and that of a smooth surface.

The flow visualization study of Liou *et al.* reveals the presence of recirculation flow instantly behind the detached rib they observed an asymmetric wake behind the rib because of asymmetric flow area across the rib. The vortex shedding promotes the mixing of the fluid and hence leads to a higher level of heat transfer distribution. This provides

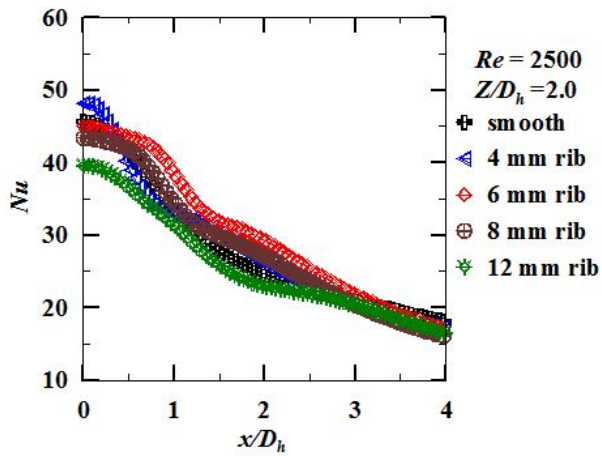
better HT augmentation immediate behind the rib and depends on the clearance under the rib.



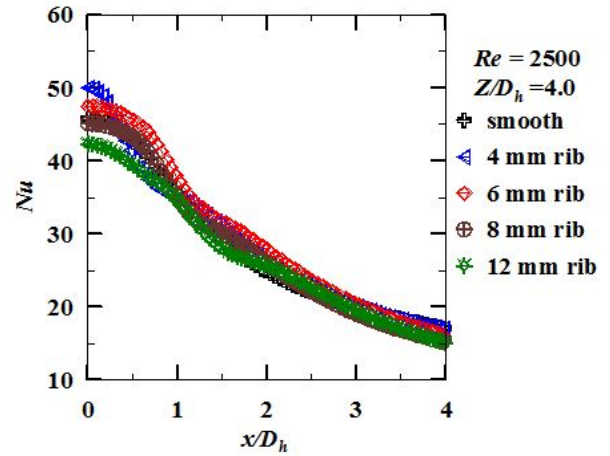
(a)



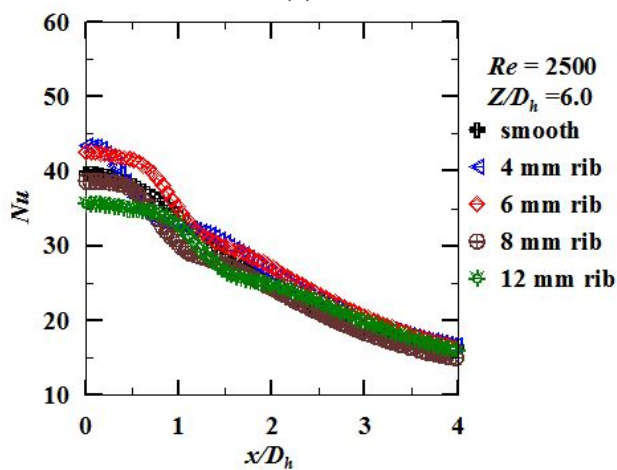
(b)



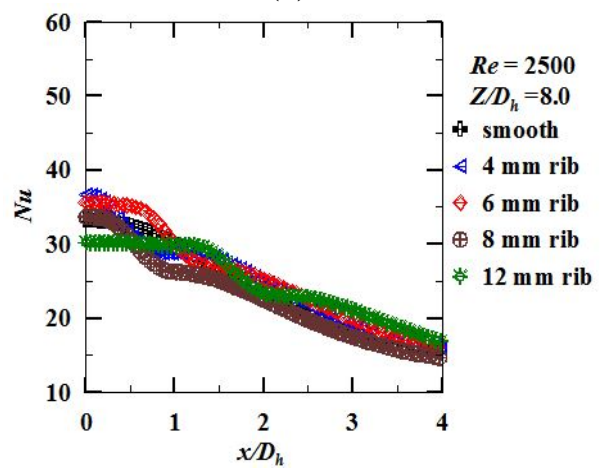
(c)



(d)



(e)



(f)

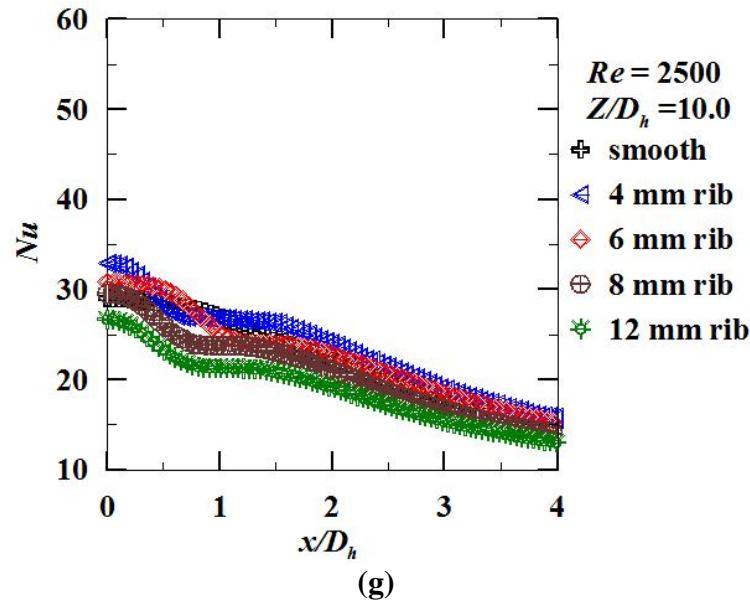
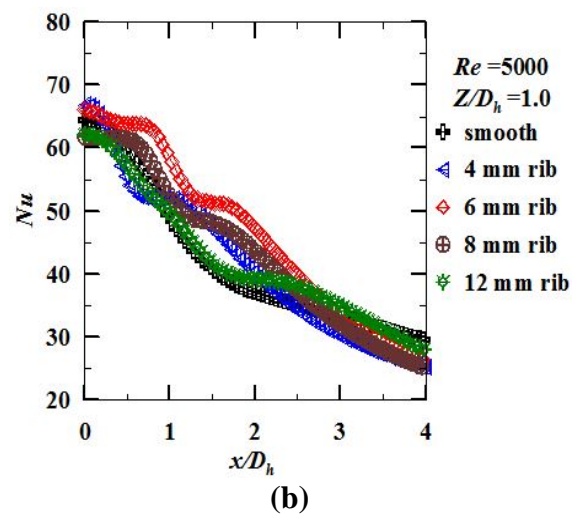
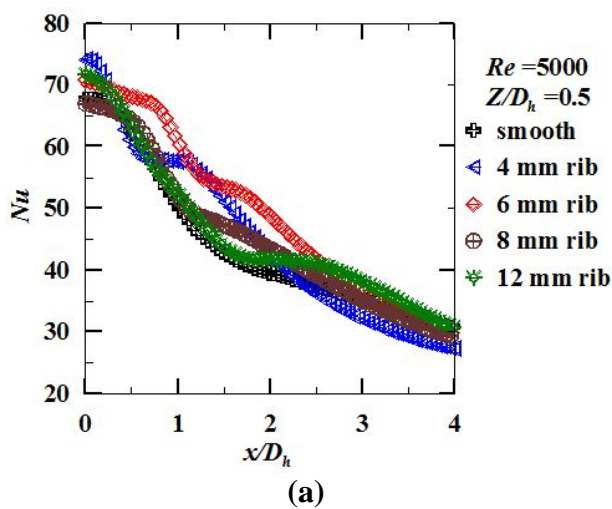


Fig.4.26 Variation of the Nusselt number along with the length of the plate for the different J2P spacing (Z/D_h) at $Re = 2500$ for different sizes

Figures 4.27(a) to 4.27 (g) show the distribution of the local Nu along with the length of the plate, at “Reynolds number” = 5000 for the smooth and rough surfaces. It shows that local Nu is maximum at the “stagnation point” and gradually diminishes along the wall of the plate because of more mixing of the atmospheric air with the jet and weakening the core. From the figures it is identified that the ribs of width 4mm and 6mm shows the peak values for the “Nusselt number” and for other ribs Nu values are almost similar to that of a smooth surface. But compared to smooth surface 4mm rib gives a better effect. It is due to the turbulence intensity of rough surface.



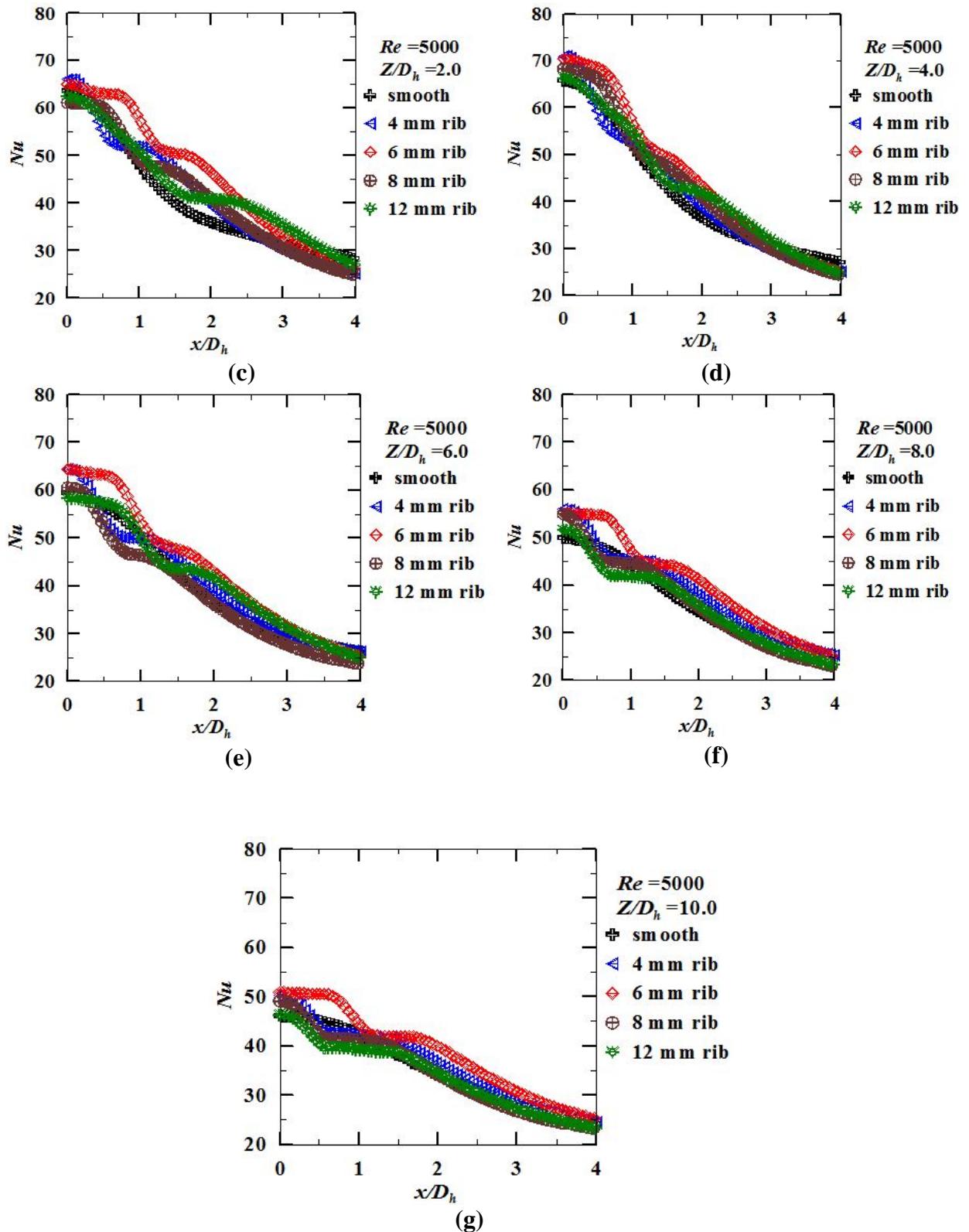
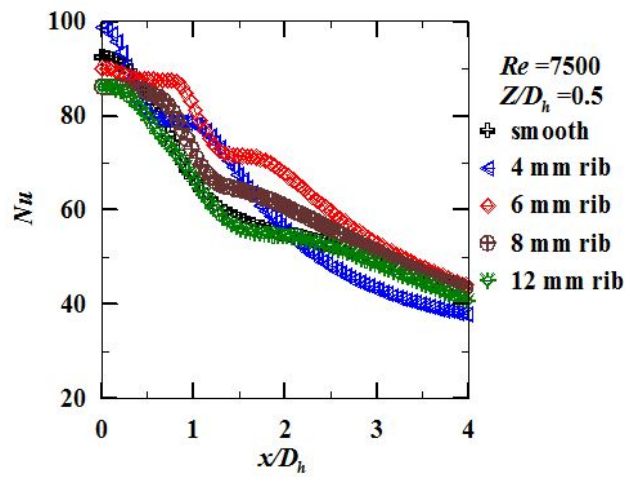


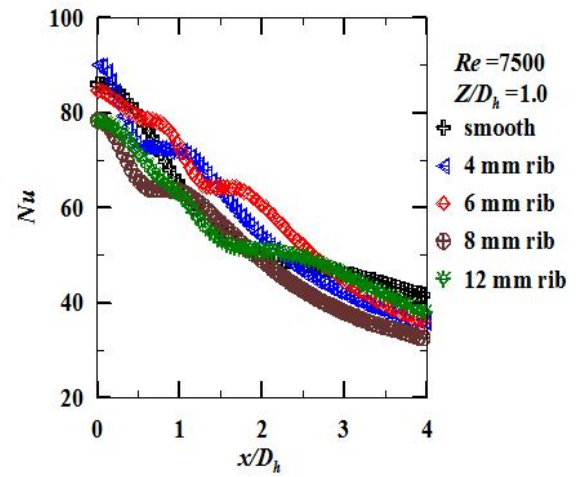
Fig.4.27 “Variation of Nusselt number along the length of the plate for different J2P spacing (Z/D_h) at $Re = 5000$ for different rib sizes

The trends available with figures 4.28, through 4.33 show that the “Nusselt number” is increasing with “Reynolds number” and it is maximum at the lower J2P spacing (Z/D_h) of 0.5. Among all the ribs, the rib of width 4mm is a better configuration and gives better

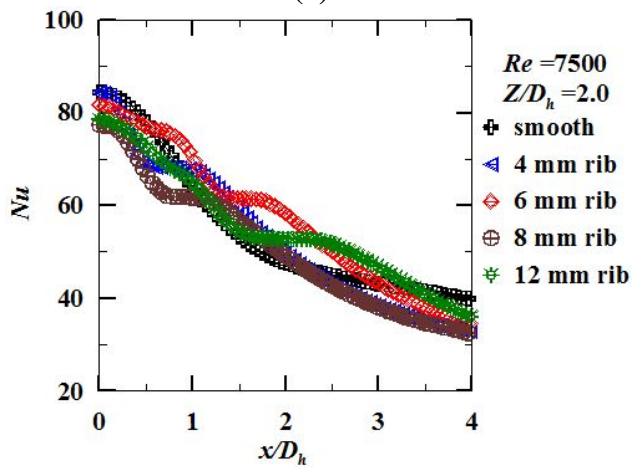
HTC values and higher “local Nusselt number” at all the range of “Reynolds number” considered in the study.



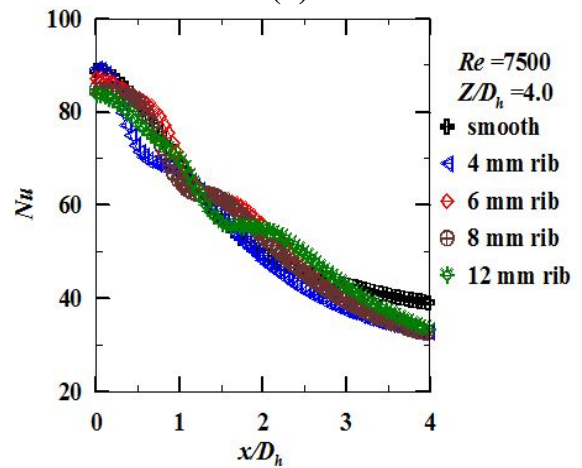
(a)



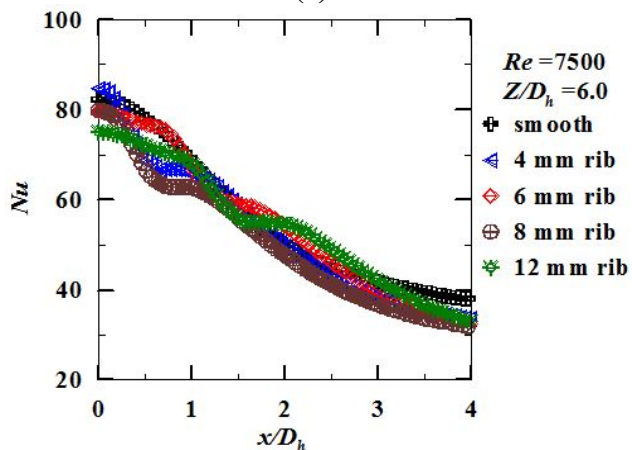
(b)



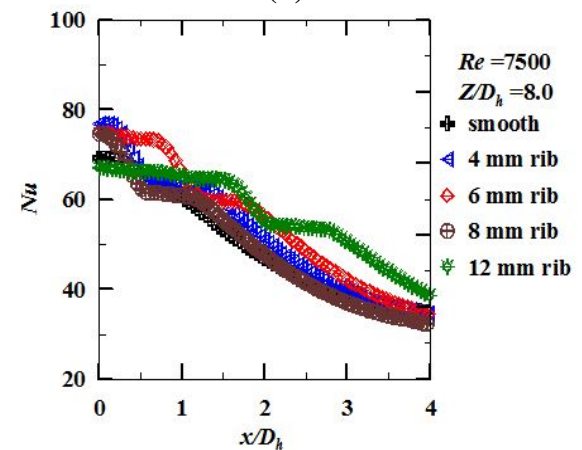
(c)



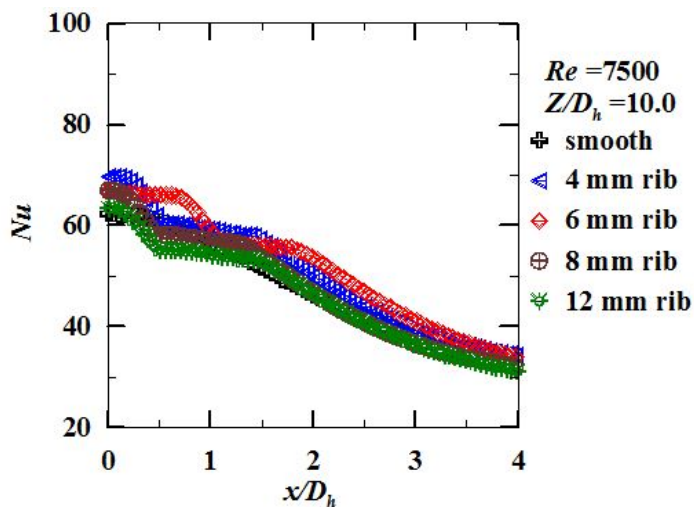
(d)



(e)

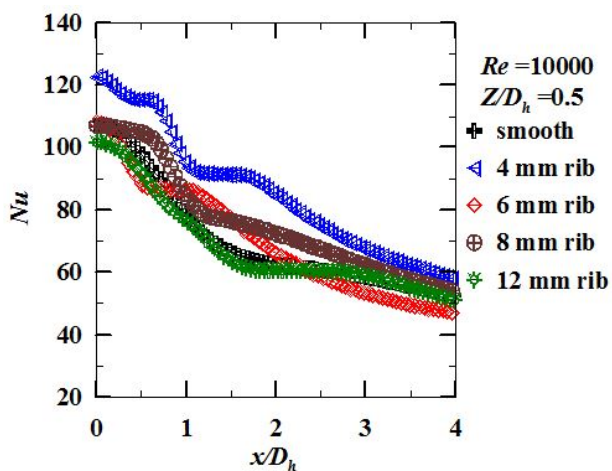


(f)

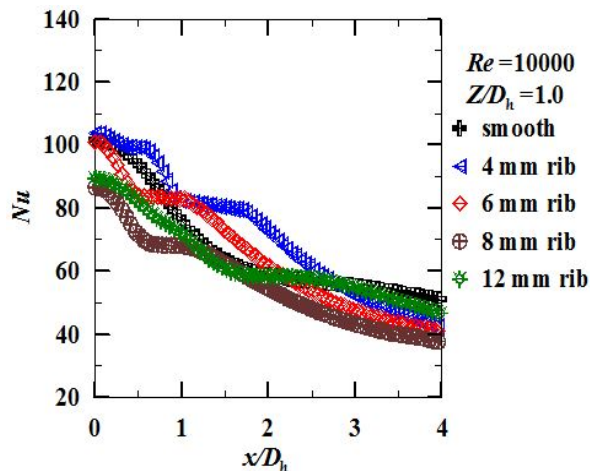


(g)

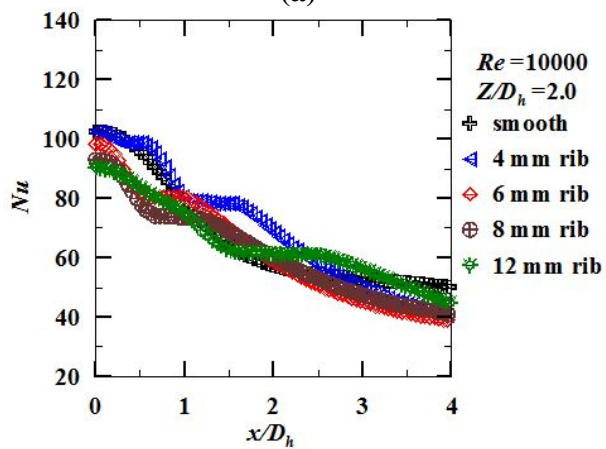
Fig.4.28 “Variation of the Nusselt number along with the length of the plate for the different J2P spacing (Z/D_h) at $Re = 7500$ for different sizes



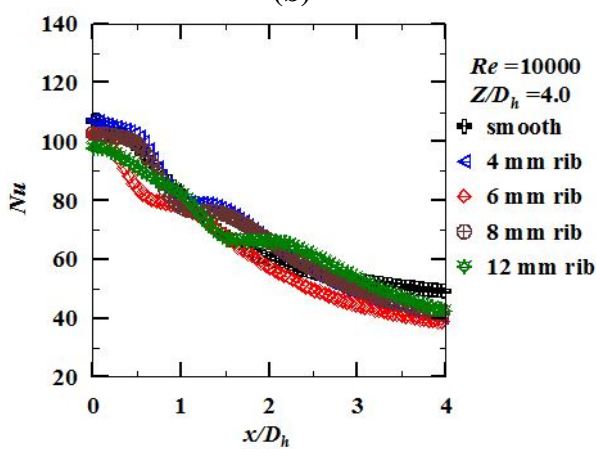
(a)



(b)



(c)



(d)

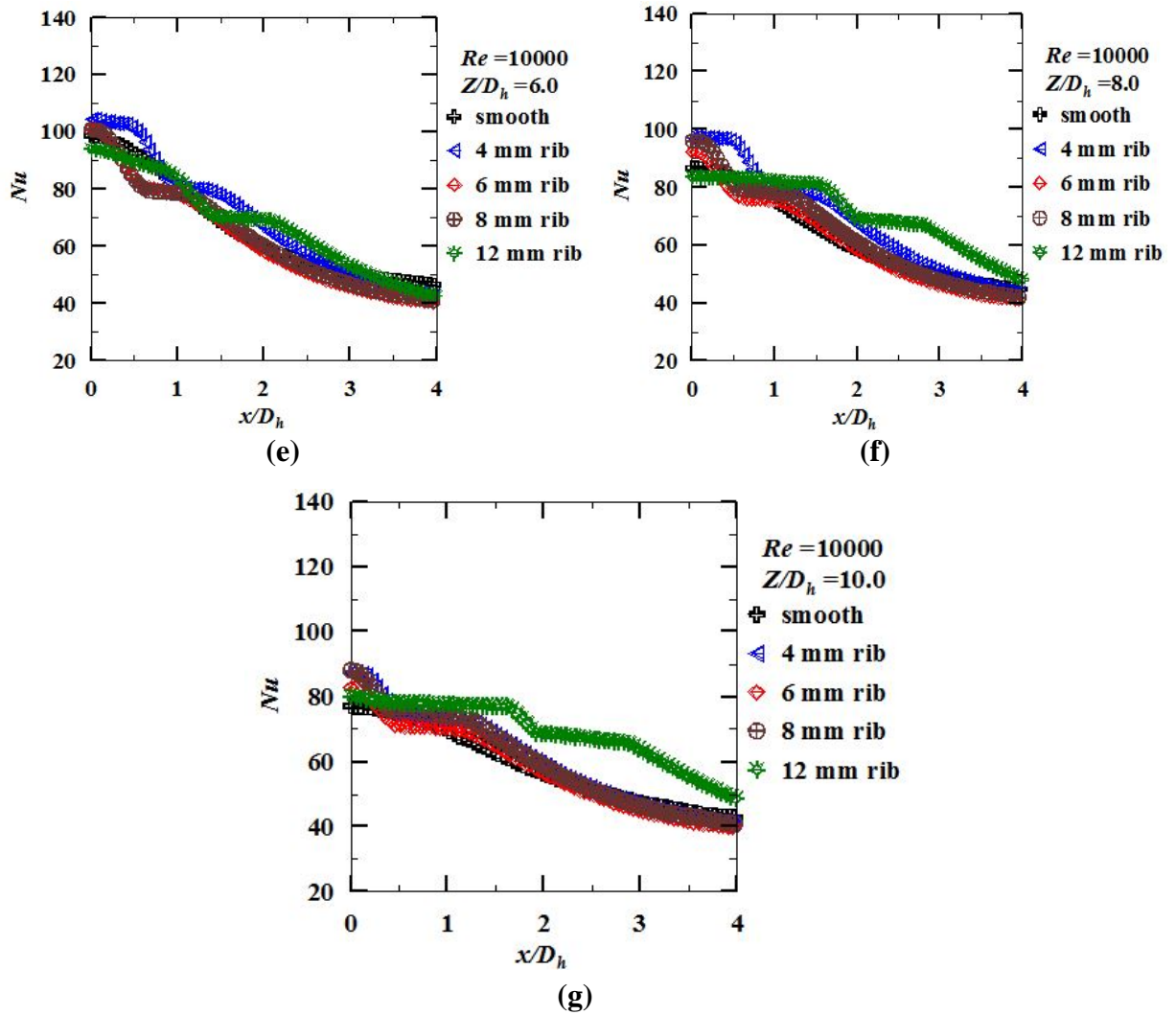
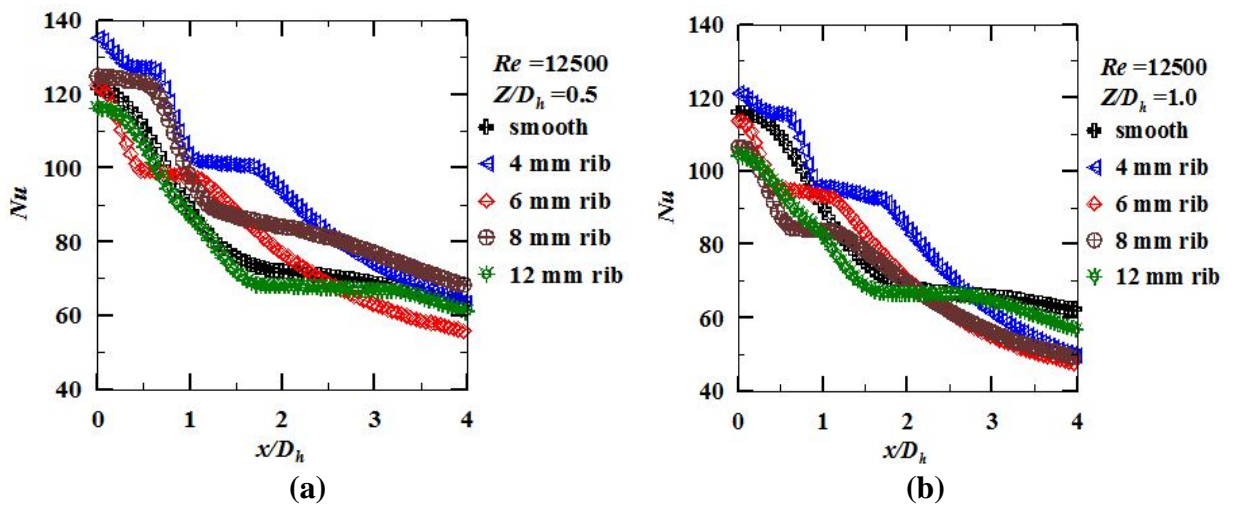


Fig.4.29 Variation of the Nusselt number along length of the plate for different J2P spacing (Z/D_h) at $Re = 10000$ for different Ribs



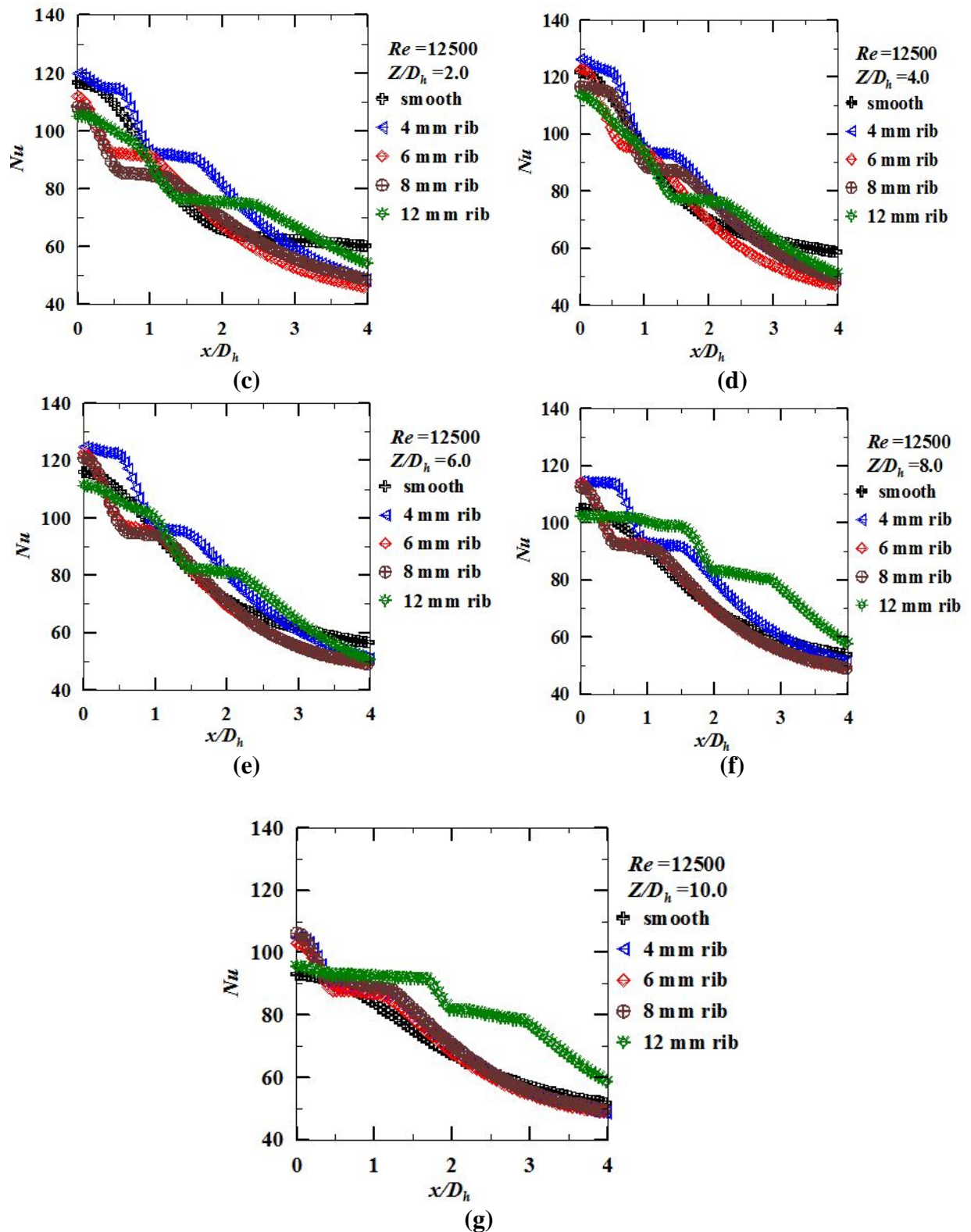
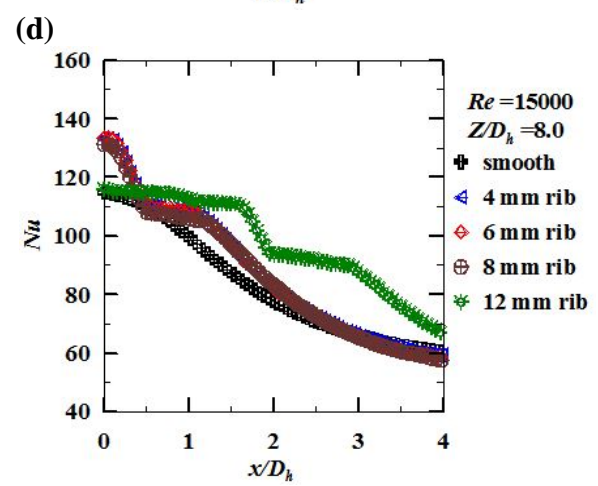
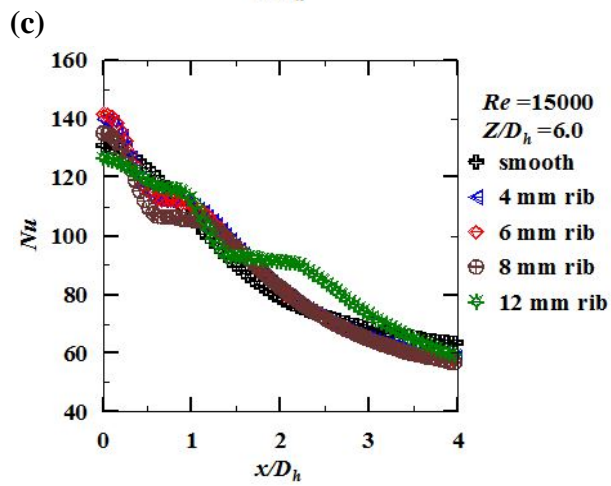
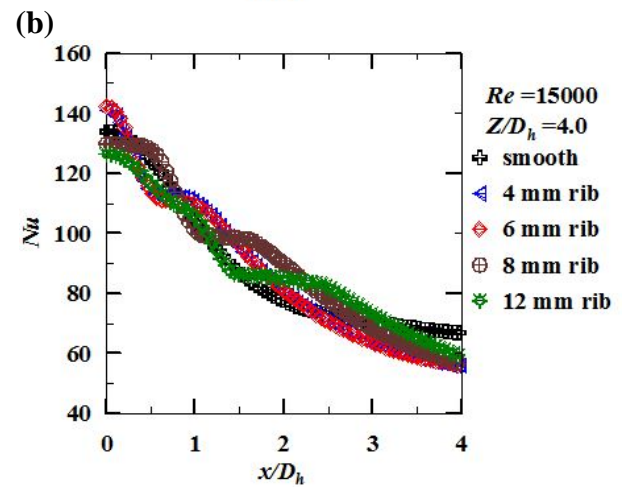
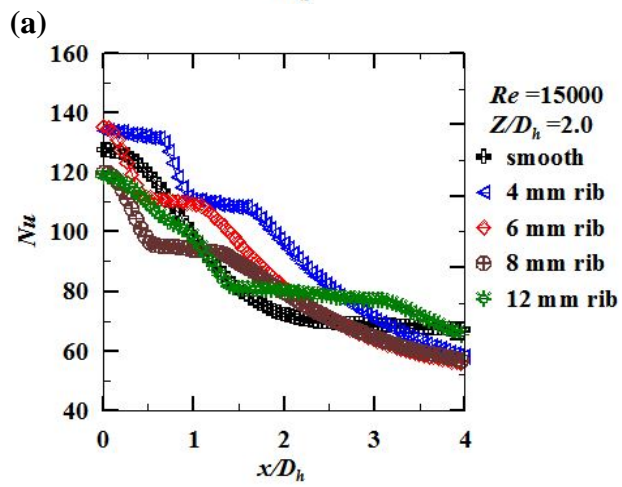
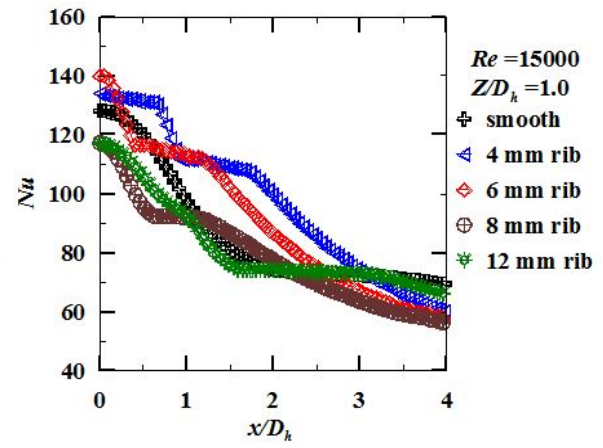
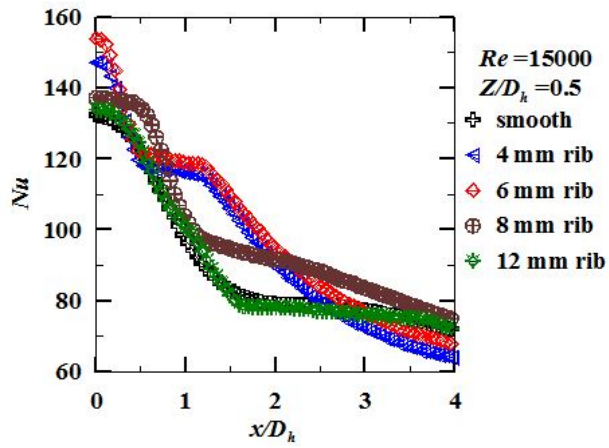
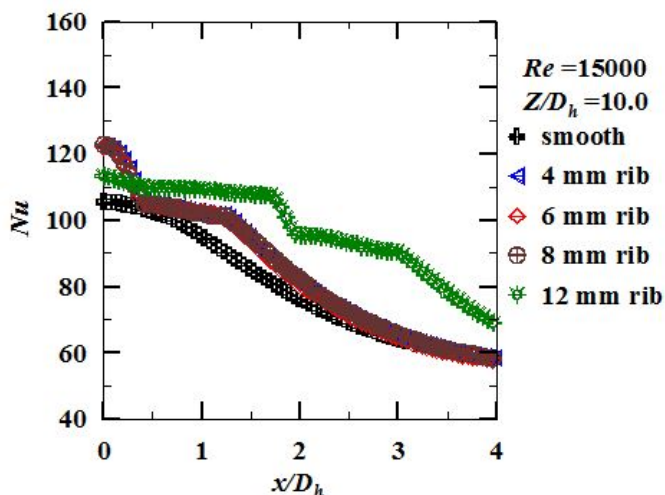


Fig.4.30 “Variation of the Nusselt number along with the length of the plate for the different J2P spacing (Z/D_h) at $Re = 12500$ for different sizes



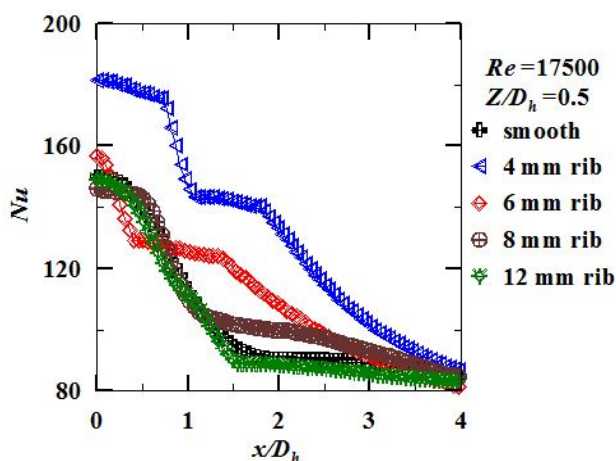
(e)

(f)

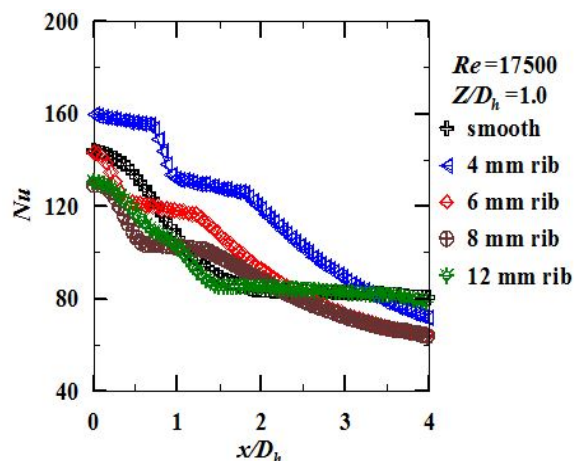


(g)

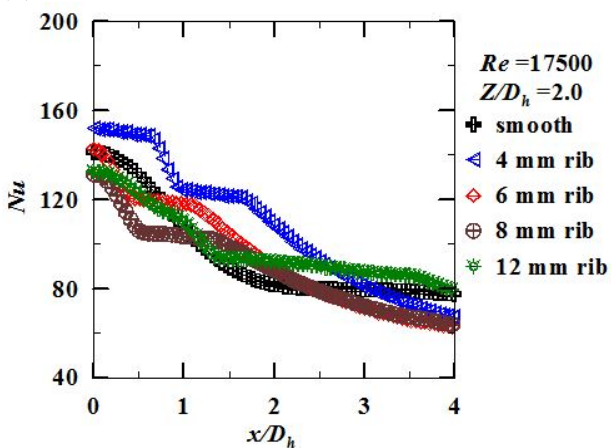
Fig.4.31 Variation of the Nusselt number along with the plate for the different J2Pspacing (Z/D_h) at $Re = 15000$ for different Rib sizes



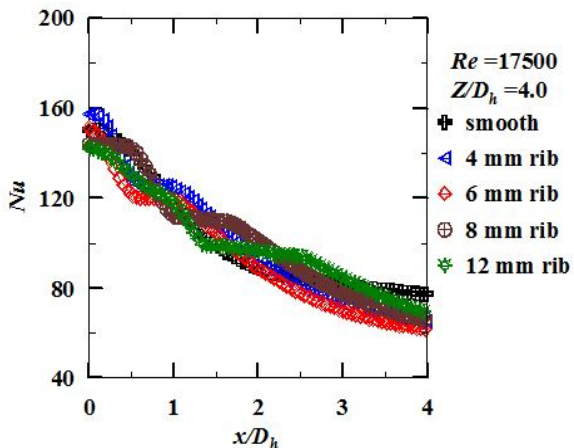
(a)



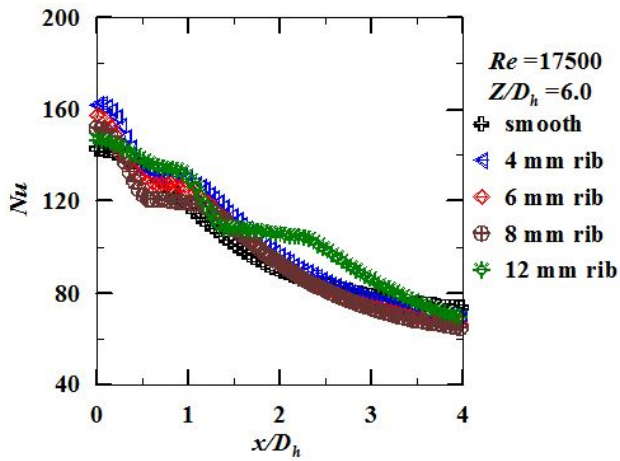
(b)



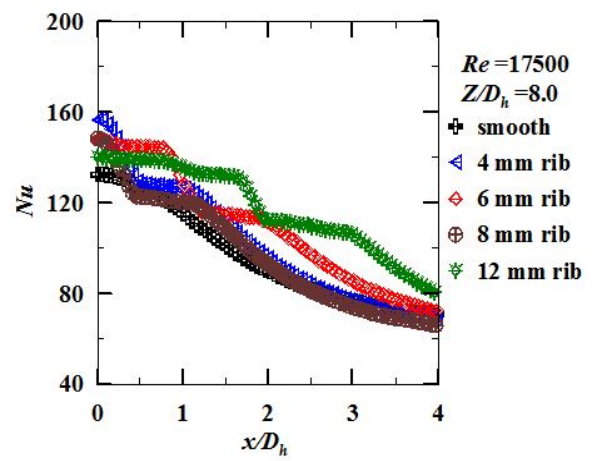
(c)



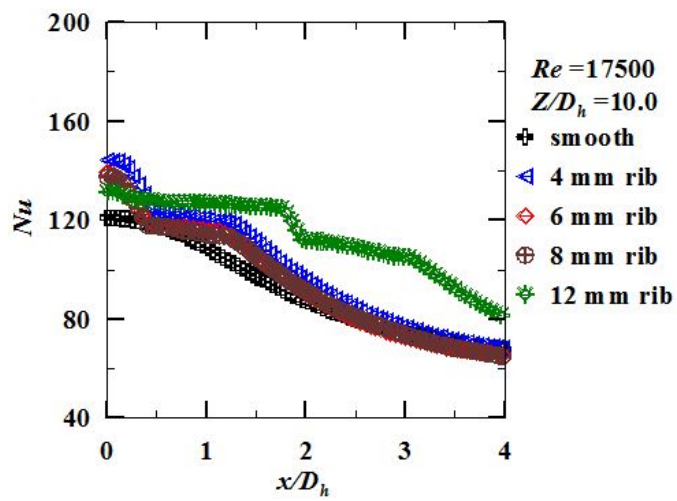
(d)



(e)

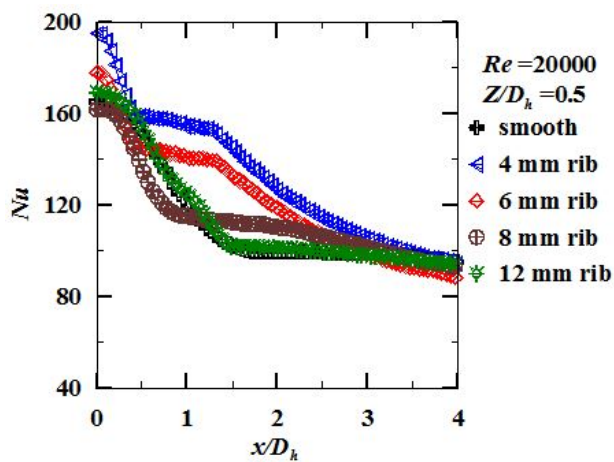


(f)

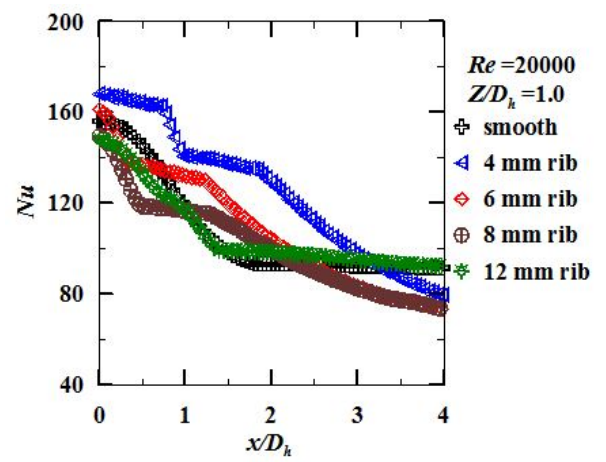


(g)

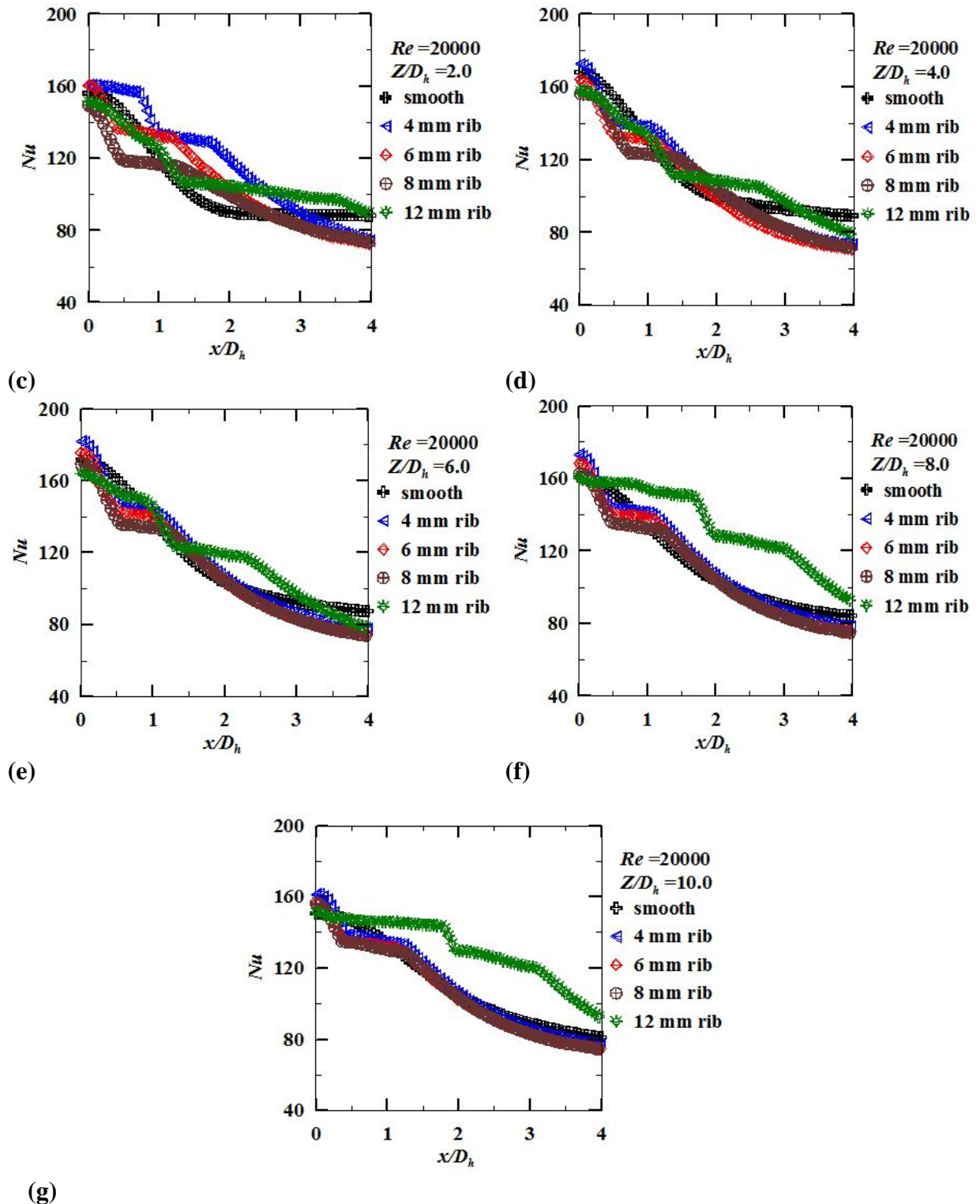
Fig.4.32 Variation of the Nusselt number along the plate for the different J2Pspacing (Z/D_h) at $Re = 17500$ for different Rib sizes



(a)



(b)

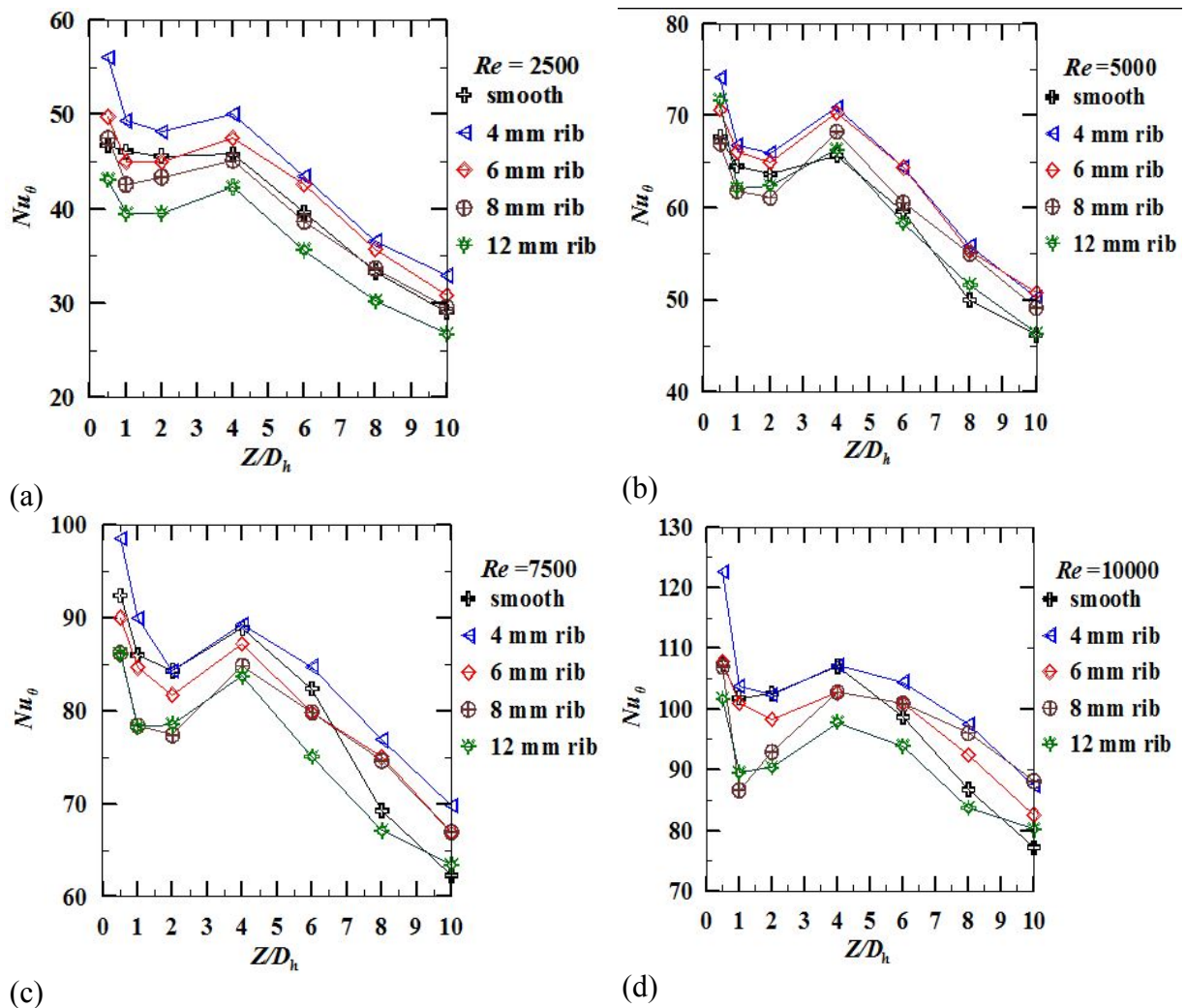


(g)
Fig.4.33 Variation of the Nu along the plate for the different J2P spacing (Z/D_h) at $Re = 20000$ for different Rib sizes

Figures 4.34 (a) to (h) show the change in the $SP Nu$ for the various J2P spacing and various rib sizes at a given Re 2500 to 20000 resp. The figures reveal that the 4mm rib provides the maximum $SP Nu$ at a range of “Reynolds numbers” studied and gives a better cooling effect due to the peak value of $SP Nu$ comparatively with a smooth surface

and other rib sizes. The variation of the $SPHTC$ with $J2P$ spacing is influenced by two factors viz. the centreline velocity of the jet and the turbulence intensity at a small $J2P$ spacing. The “heat transfer” rate of the jet is conquered by the velocity of the jet and the low turbulence intensity. Jet once leaves the nozzle; it starts mixing with the surrounding ambient air. The potential core decreases as the $J2P$ distance and the turbulence intensity increases.

“The variation of the stagnation heat transfer with the $J2P$ spacing is mainly affected by two factors viz. the turbulence intensity and the arrival jet centerline velocity. At a lower $J2P$ spacing the heat transfer rate of an impinging jet is dominated by the jet velocity because of lower turbulence intensity. Once leaving the nozzle exit the jet begins to entrain the surrounding quiescent fluid. Flow visualization measurements showed that the toroid form vortex is formed due to an intrinsic instability in the outer shear layer of the impinging jet(D.W. Zhou (2007). As the $J2P$ spacing increases the potential core width decreases and yet the turbulence intensity increases gradually”.



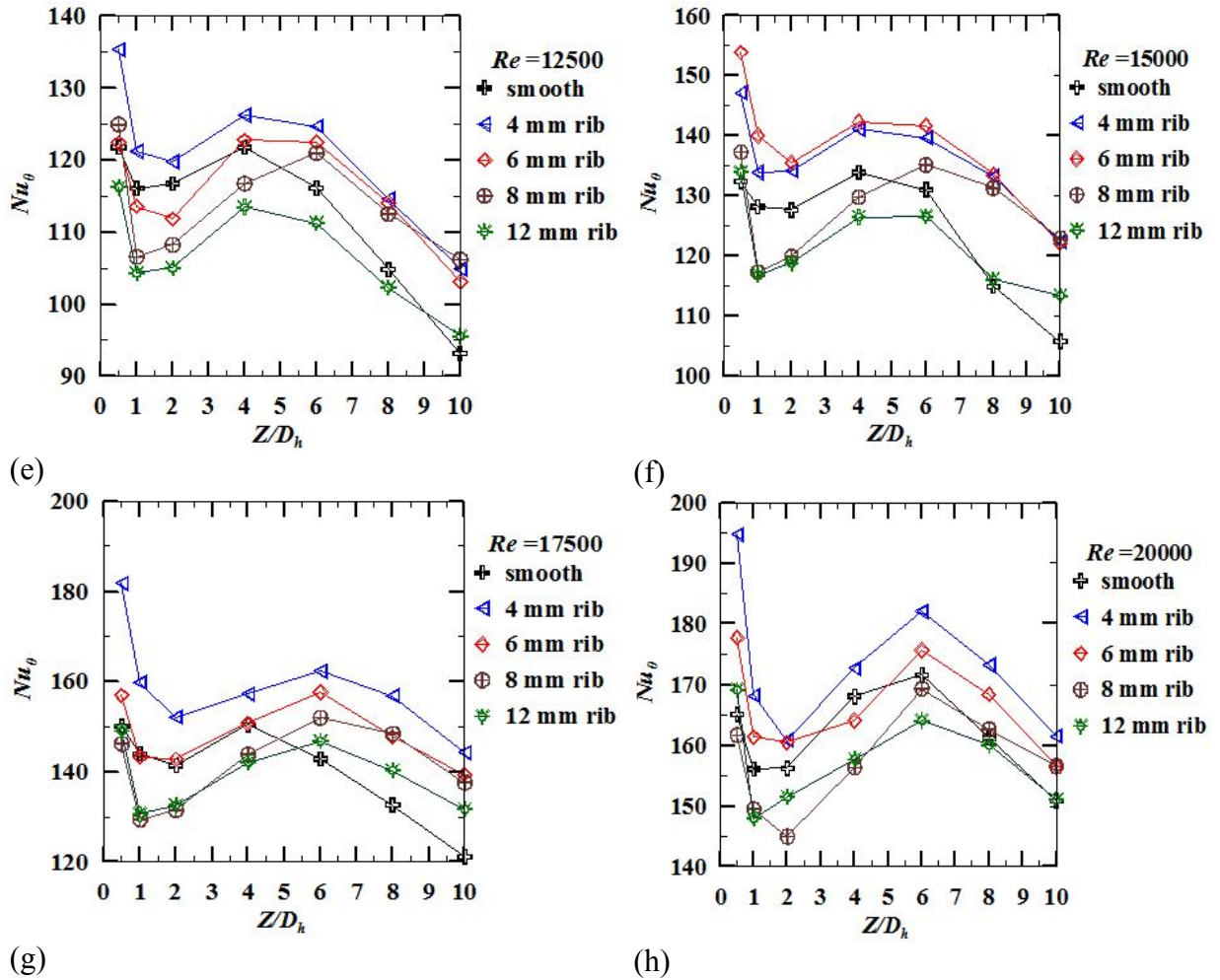


Fig. 4.34 Variation of “stagnation point” “Nusselt number” for the different J2Pspacing at various Rib sizes for particular “Reynolds number”

4.5 Enhancement in the Average “Nusselt number” ($Nu_{2.0}$) with the Ribbed surface.

Figure 4.35 shows the axial distribution of the Nu averaged up to $x/D_h = 2.0$ ($Nu_{2.0}$) for various rib configurations at $Re=2500$. From the figure, it can be observed that the rib with a 6 mm width shows higher values for average $Nu_{2.0}$ comparatively at all the J2P spacing studied. The % of enhancement in the average $Nu_{2.0}$ is given in Table 1. Substantial enhancement of about 15% is observed at lower $Z/D_h=0.5$ and reduces monotonically with an increase in the Z/D_h . No significant heat is observed beyond Z/D_h of 8.

Figure 4.36 shows the axial distribution of the $Nu_{(2.0)}$ for various rib configurations at $Re=10000$. From the figure, it can be observed that the rib with a 4 mm width shows higher values for average $Nu_{2.0}$ comparatively for most of the J2P distances studied. The percentage of enhancement in the average $Nu_{2.0}$ is given in Table 1. The maximum enhancement of around 19% is observed at lower $Z/D_h = 0.5$ and enhancement level

reduces with increase in the Z/D_h up to 4.0 and the minimum enhancement of 3.3% is recorded for Z/D_h of 4.0., Further, the increase in Z/D_h up to 8.0 shows a little improvement in enhancement whereas the levels of enhancement observed at Z/D_h of 1.0 and 6.0 are almost similar. A similar trend is observed for other turbulent flow conditions.

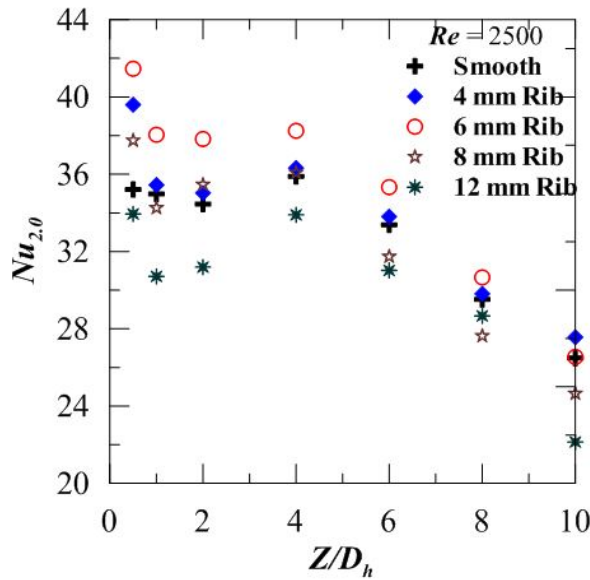


Fig. 4.35 Variation of average $Nu_{2,0}$ with Z/D_h for different ribs at $Re=2500$

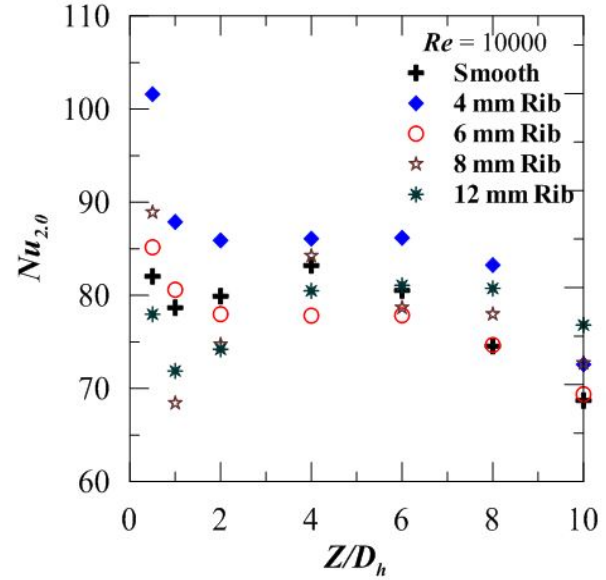


Fig. 4.36 Variation of average $Nu_{2,0}$ with Z/D_h for different ribs at $Re=10000$

Table 4.1 Enhancement in the average heat transfer coefficient with 6mm rib at $Re = 2500$ and with 4 mm rib at $Re = 10000$

Z/D_h	$Nu_{2,0}$ enhancement at $Re=2500$ for 6mm rib (%)	$Nu_{2,0}$ enhancement at $Re=10000$ for 4mm rib (%)
0.5	15.08	19.24
1.0	8.05	10.46
2.0	8.89	6.95
4.0	6.15	3.33
6.0	5.49	6.55
8.0	3.71	10.43
10.0	0.24	5.33

4.6 Conclusions

The local distribution of WSP and HTC between a normally impinging slot air-jet and flat smooth surface and a rough surface is experimentally explored for the influence of defined parameters. The roughness is introduced on the plate by mounting detached rib-rougher. A single fully developed jet issued from a rectangular slot configuration is chosen for the study. “Reynolds number” is varied between 2500 and 20000. Four detached ribs of varying width are used one at a time on the target plate. A sequential parametric study is carried out to investigate the influence of different ribs on the local WSP and local HTC distributions. The J2P distance is varied from 0.5 to 10.

Conclusions drawn from this investigation can be summarized as below:

- Wall static pressure coefficient is observed to be independent of Re in the range of 5000 to 20000 for a given J2P distance in case of smooth surface.
- WSP coefficient is inversely related to the J2P distance. The reason may be the mixing of surrounding quiescent air.
- The ribbed surface gives the maximum coefficient of stagnation point WSP than the smooth surface at all “Reynolds numbers” studied. This can be attributed to the acceleration of the fluid under the rib.
- The Ribs are effective only up to the Z/D_h of 6.0 and later the results are comparable with the smooth surface.
- For any J2P spacing (Z/D_h) considered, an increase in the Re enhances the “heat Transfer coefficient” at all the places in the “streamwise direction” irrespective of smooth or a rough surface.
- Rib with 4mm width provides the maximum heat exchange coefficient in comparison with the other ribs (6mm, 8mm, and 12mm) and also the smooth surface. Larger width for the rib leads to drop in “Nusselt number” in the downstream. The reason may be the major flow of the jet is at the rib’s periphery miss to hit the target surface.
- Enhancement up to 19% in the average $Nu_{2,0}$ can be achieved by a 4 mm rib with turbulent slot air jet in the stagnation region with no additional pumping power.

- Enhancement up to 15% in the average $Nu_{2,0}$ can be achieved by a 6 mm rib with a laminar slot air jet in the stagnation region with no additional pumping power.
- At any “Reynolds number” considered, the Nu_0 increases with an increase in J2P distance (Z/D_h) 1.0 to Z/D_h of 6.0. The reason for this trend can be the increase in turbulence intensities near the wall as the J2P spacing increases.

CHAPTER 05

Influence of confinement on local wall static pressure and heat-transfer distribution

5.1 Introduction

Impinging jets are popular in many Industrial applications to enhance the coefficient for convective cooling, heating, and drying. In addition, the applications include drying of textile, annealing of metal sheets, tempering of the glass plate, cooling of gas turbine blades, engines, Computers and electronic devices. The heat transfer and fluid flow characteristics of impinging jets are influenced by a number of parameters like the nozzle-to-plate spacing (Z/D_h), nozzle geometry and Reynolds number. The impinging jets are classified by their boundary conditions as confined and un-confined jets. In case of confined jets, the radial spread of the jet is restricted by a confinement plate. Confined geometry, has been extensively investigated extensively in the literature due to their industrial applications. The cooling of the gas turbine blade is performed using cold air often bled from the compressor. The effect of confinement on wall static pressure distribution on a flat and smooth surface due to impingement of slot air jet is investigated in the present work. The wall static pressures are measured for different parameters such as size of confinement plates (having a constant height of 80mm and length ranging from 25 mm to 200 mm, with $L_c/D_h=3.0$ to 27.23), nozzle-to-plate spacing Z/D_h , (ranging from 0.5 to 10), x/D_h along streamwise direction and at a Reynolds number 10000. The pressure distribution is found to be independent of the Re and varies with the nozzle-to-plate spacing and size of confinement plate (Katti and Prabhu, 2008) . The maximum pressure is recorded at the stagnation point ($x/D_h=0$) for various nozzle-to-plate spacing studied, and the pressure decreases as x/D_h increases (Baydar and Ozmen, 2005). Sub-atmospheric regions are observed at lower Z/D_h and gradually vanish with an increase in Z/D_h for the given Reynolds number.

5.2 Literature review

The important explorations made by the earlier researchers and their findings about the impinging jets is briefed in the paragraphs below.

Gardon and Akfirat (1965) studied the effect of turbulence on the heat transfer characteristics of submerged impinging jets. On heat transfer characteristics is notable that maximum in a variation of stagnation point heat transfer coefficient with secondary

peaks and nozzle to plate spacing distribution in the radial direction of local heat transfer coefficients this phenomenon specifically to slot jets

Gaunter *et al.* (1970) surveyed flow characteristics of single turbulent jet impinging on a flat plate. The flow field is divided into four distinct regions. Methods for predicting velocities and pressures in various regions agree reasonably well with experimental data. Determine the influence of flow Reynolds number on core length and the large discrepancy between the theoretical and experimental velocity gradients near the wall. The axial velocity for a free jet is constant and equal to the nozzle exit velocity over a distance equal to the potential core length. For a slot jet, the axial velocity downstream of the potential core is inversely proportional to the root square distance from the jet nozzle in slot widths.

Vader, *et al.* (1991) examined on a technique for unfaltering of measuring on local heat exchange of an impinging fluid stream and found as local convection coefficients for heat exchange to an impinging fluid jet. It is noted that the 5.1mm on opposite side of heater took intervals to find the heat flux distribution and temperature

Jambunathan *et al.* (1992), surveyed on a Single Circular jet of Heat Transfer information that turbulent jets with spout way out of Reynolds number 5000-124000 and Nusselt number at radii more noteworthy than of six nozzle diameters from stagnation point. Jets issuing from square edged orifices openings give higher Jet's exchange contrasted from elliptical and streams to circular jets and noticed that the surrounding temperature is not equivalent to air temperature at the nozzle exit.

Brahma (1992) studied the slot jet impinging on a flat surface and predicted fluid flow and heat transfer characteristics at the stagnation point. A correlation was proposed for stagnation point heat transfer considering different nozzle to jet placings and Reynolds number. Results obtained in terms of velocity gradient at stagnation point were compared with velocity profile at nozzle outlet of a two-dimensional jet.

Ichimiya and Hosaka (1992) observed heat transfer characteristics of confined two-dimensional jets on a flat surface. For Experiment, they used three slot jets and keeping a distance of $H= 0.5$ to 3, dimensional less pitch $p=6$ to 16 and Reynolds number 500-8000 for comparing with the unconfined jet. They observed that for laminar flow the heat transfer increases locally due to the second jet. The values are estimated numerically for all the jets.

Cooper *et al.* (1993) worked on flow field characteristics of a turbulent jet impinging orthogonally on a large surface at two Reynolds numbers of 23000 and 70000. Turbulence energy of Re 23000 is high rates compared with stream free fluid.

Lin, *et al.* (1997) supervised the heat transfer behavior of a confined slot jet impingement on a flat surface considering various Reynolds number and jet to plate spaces. They found that the stagnation point, average and local Nusselt number are influenced by Reynolds number and depends insignificantly on a jet to plate spaces. A concept of effective cooling length was introduced for evaluating the numerical average heat transfer performance.

Baydar (1999) studied confinement effects air impinging jet at Reynolds number is to be lower. Experimented on a single jet with Reynolds number of 500-10000 and double jet with Reynolds number of 300-10000 at varying z/d in the range of 0.5-4. for greater Reynolds number of about 2700, the subatmospheric pressure occurred for up to nozzle to plate spacing of 2.0. It is observed that there is a link between the peak in heat transfer coefficient and subatmospheric region to some extent.

Narayanan *et al.* (2004) experimentally studied on submerged slot jets on a flat plate. With hydraulic diameters of 0.5 and 3.5 which correspond to potential – core region and transitional region respectively. It is observed that heat transfer coefficient of impingement region is peaked at that level and decreases monotonically towards the wall jet region.

Baydar & Ozmen (2005) conducted experiments on the effect of higher Reynolds number for confined air impinging jets on a flat plate and numerical investigated experimental values. They chose Reynolds number of 30000 and 50000 z/d in the range of 0.2-6.0. Deceleration of the jet occurs due to the presence of impingement plate. At z/d up to 2, the subatmospheric region is observed. As the nozzle exit to plate distance increasing the subatmospheric pressure moves radially outward from stagnation point. Concluded that link occurred between heat transfer coefficient, turbulence intensity, and sub-atmospheric region.

Guerra *et al.* (2005) analyzed the behavior of a near to wall impinging jet. For turbulent impinging jet considered single nozzle to plate spacing that of semi-confined is 2.0 and Reynolds number of 35000 and measured the longitudinal turbulence profile. The mean temperature is measured using thermocouples. They observed that the minimum temperature profile occurs away from the wall.

Lupton *et al.* (2008) supervised the effect of variation in confinement levels of miniature air jets on heat transfer and concluded that confinement effects are more significant on miniature diameter jets than for larger diameter jets. For miniature jets at large Reynolds number ($Re = 12,700$), the local heat transfer decreases with increasing confinement over both stagnation and wall jet regions and differences as high as 69% in the stagnation region were seen whilst contrasting the two extreme levels of confinement tested.

Choo and Kim (2010) concentrated on the thermal conductivity of two impinging jets confined and unconfined with dimensionless pumping force of reach 1.35×10^{10} — 4×10^{13} and nozzle to plate dividing is not as much as single nozzle diameter measurement of $z/d = 0.125$ - 1.0 . and found that under altered pumping power condition the heat transfer in case of confined jet is same as that of the unconfined jet while under fixed flow rate stream condition for the confined jet is 20%-30% lower than an unconfined jet.

Nirmalkumar *et al.* (2011) experimented on the heat transfer behavior of a slot jet in the stagnation region ($0 \leq x/b \leq 2$), transition region ($2 \leq x/b \leq 5$) and wall jet region ($x/b \geq 5$). For a given z/b , heat transfer Coefficient increases with the increase in the Reynolds number in the streamwise direction. In a slot jet, secondary peak is not evident at lower Reynolds numbers and larger z/b s. and is strongly evident at maximum Reynolds number of 12,000 and for the $z/b \leq 1$.

Lee *et al.* (2012) experimented on an isothermal flat plate with laminar heat Transfer Characteristics are determined subject to a miliscale confined impinging slot jet having an aspect ratio (y/b) of 50. They found from visualization of slot jet flow of overall structure with jet columns in lateral distortions of at vortex structures, it is found to be Nusselt numbers sensitive to the laminar boundary layer, and laminar space jet close divider temperature gradients will come about consistent surface temperature on thermal boundary conditions. Cooling is focused close to the impingement area on the surface just for a solitary ordinary impinging jet.

Patil *et al.* (2014) experimented on confined impinging circular air jet and measured the wall static pressure at Re 18000-40000 at the nozzle outlet and jet to plate spacing in the range of 0.25-4. It is found that the maximum pressure occurs at the stagnation point.

Maximum pressure decreases with a nozzle to plate spacing and with the increase in r/d . The subatmospheric region also increases with the Reynolds number.

Katti *et al.* (2014) Experimentally Investigated the local distribution of wall static pressure coefficient due to impinging slot air jet on the smooth and rough surface. Co-efficient of wall static pressure is seen to be independent of Reynolds number in the range of 5000-

20000 for a given jet to plate distance in case of a smooth surface. Wall Static pressure Coefficient decreases with increases in a jet to plate distances due to entrainment of surrounding quiescent air and loses effect of impact on the target plate. C_p value is maximum at the stagnation point for all the configuration studied and decreases along the streamwise direction which may be attributed to increase in the velocity along the plate. It is observed that wall jet region starts around x/D_h of 1.5.

5.3 Objectives

Form the available published literature, it is noted that no sufficient information is available on the local distribution of wall static pressure and heat transfer coefficients of a slot jet impingement on a flat confined surface. Hence the following objectives and parameters are considered for the current study.

- ✓ To study the Influence of Confinement, on the local distribution of wall static pressure on a Flat Surface.
- ✓ To study the Influence of Confinement on the local distribution of heat transfer coefficient on a Flat Surface.

5.4 Experimental set up and methodology for fluid flow characteristics study

The major experiment set up for the steady of fluid flow behavior and the C_p distribution is explained in chapter 3.0 while discussing the slot jet impingement on a smooth flat surface. The same set up is used here also with some minor modifications to suit the requirement. In this study the slot nozzle is mounted with a confinement plate made of 10 mm thick acrylic sheet at the nozzle exit. The confinement sheets having various widths 50mm, 75mm, 100mm, 125mm, 150mm, 175mm and 200mm with a common height 80 mm are used in turn with the slot nozzle to know the influence of width of confinement plate on the fluid flow and heat transfer characteristics of a slot jet and a smooth surface. The details of the confinement plate are shown in fig. 5.1. Figure 5.2 shows the mounting of the confinement plate at the nozzle exit. The confinement plate is mounted so that the center of the slot nozzle and the center of slot on the confinement plate are coinciding and the surface of the confinement plate is flushed exactly with the nozzle exit surface to avoid the formation of air pockets between the two. The confinement plate should be exactly parallel to the impingement surface for any jet to plate distance considered. The confinement plate will be positioned firmly by using Anabond adhesive and two angle plates (not shown in the figure) made of acrylic sheet material. Different

confinement plates ranging from 50mm width to 200mm width are used in the flow behavior study. The same set of confinement plates are used with the jet during the Heat transfer studies also. The operating parameters *i.e.*, Reynolds numbers, nozzle to plate distances are exactly same as that used in the flow study of an unconfined smooth plate case.

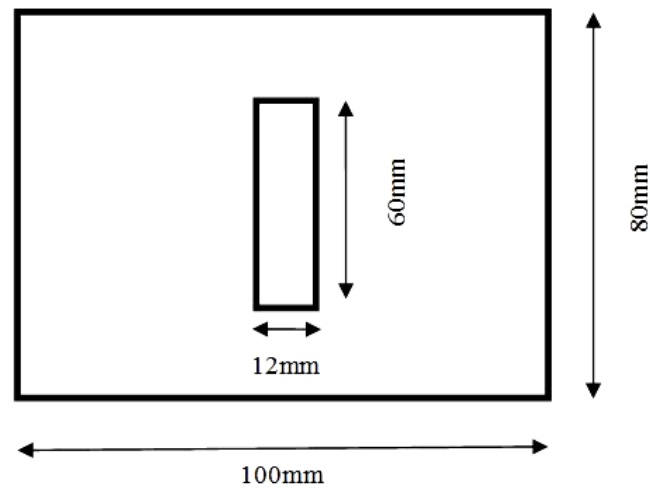


Fig 5.1 Details of the confinement plate(sample)

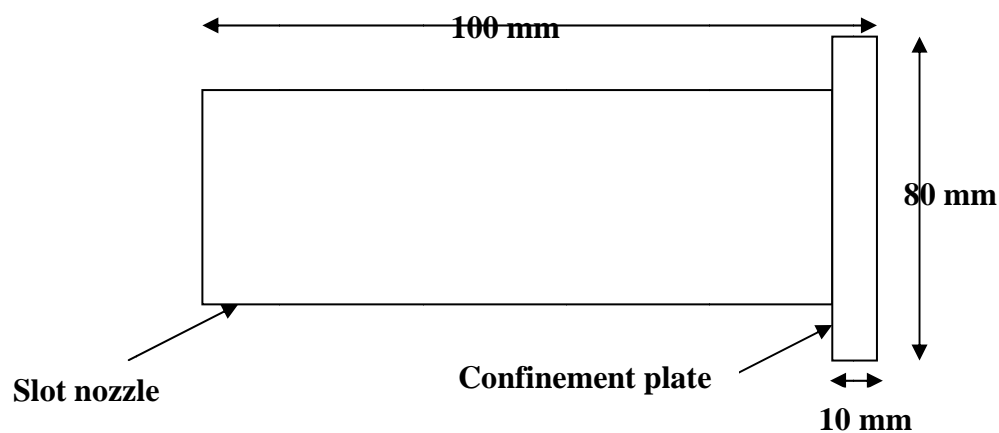


Fig 5.2 Details of mounting the confinement plate at nozzle exit
(Dimensions are not to scale)

Air is supplied by a blower through a calibrated orifice meter. The metered air passes through a flow control valve, diffuser, plenum chamber and a rectangular slot thus creating a jet. The jet is made to impinge on the target plate. Wall static pressure distribution is measured with the help of a sliding pressure tap and an inclined single column manometer. Jet to plate spacing is varied by using a traverse table. Reynolds number based on hydraulic diameter (D_h) is set. Jet-to-plate spacing (in the range of 0.5to

10) and confinement is varied from $L_c/D_h = 6.8.0$ to 27.2 . The variation in coefficient of pressure is plotted in streamwise direction.

5.5 Data Reduction

The notations and the formulae used to determine the major parameters like the velocity of the jet, flow rate, Reynolds numbers and the coefficient of wall static pressure are discussed already in the chapter 03. The same equations and notations are used here also.

5.6 Results and Discussion

The coefficient of wall static pressure (C_p) remains independent of Reynolds number for a circular jet impinging on a flat surface (Baydar [1999]). The relation between the Reynolds number and the wall static pressure coefficient is tested and it is found that for the slot jet also the C_p is independent of Reynolds number. The details follow in the next paragraph.

5.6.1 Independency test

Variation of stagnation point wall static pressure (C_{p0}) with Reynolds number at $Z/D_h = 0.5$ is shown in Fig. 5.3 It may be noted from the plot that the peak pressure coefficient is almost same for all the Reynolds numbers for the given Z/D_h and the value is around 1.5. This indicates that the stagnation point wall static pressure (C_{p0}) is independent of Reynolds number (Re).

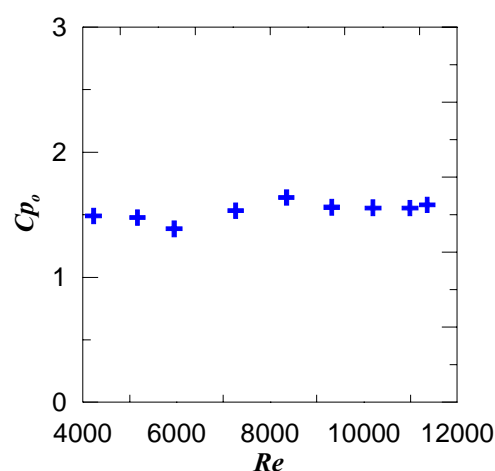


Fig 5.3 Variation of C_{p0} with Reynolds number at $Z/D_h = 0.5$.

5.6.2 Lateral Distribution of Wall Static Pressure on a flat surface impinged by a Slot air Jet.

The experiment is conducted to study the lateral distribution of the wall static pressure over the impingement plate with confinement and without the confinement of the jet. An attempt is made to determine the better confinement ratio, which can improve the flow performance in cooling or heating applications of industrial purpose. The results of unconfined jet and confined jet are discussed in subsequent sections of the report. Slot air jet impinges orthogonally on a flat surface. The influence of confinement is studied by mounting a confinement plate at the nozzle exit. The confinement plate is made of an acrylic plate of 10mm thickness and 80 mm height. Various confinement ratios (Length of the confinement plate/Hydraulic diameter of the slot jet) in the range of $L_c/D_h = 6.8, 10.2, 13.6, 17.0, 20.1, 23.4, \& 27.2$ are used in the present study. Confinement plates have a slot of 12mm×60mm at their center to facilitate the mounting on the slot jet. The sample confinement is shown in fig 5.1.

[a] Fluid flow characteristics of an unconfined Slot Jet impinging on a smooth surface

Fig 5.4 Shows the lateral variation of coefficient of pressure at Reynolds number 10000. The figure reveals that the coefficient of pressure is maximum at the stagnation point i.e., at $x/D_h=0$ for all jet to plate spacing's studied and the value of C_p decreases monotonically with an increase in x/D_h as well as the nozzle to plate spacing. The coefficient of pressure at stagnation point (C_{p0}) is higher for Z/D_h of 0.5 in comparison with another nozzle to plate spaces. For nozzle to plate spacing Z/D_h 0.5-10 the coefficient of pressure at stagnation point is 1.6 and it becomes zero nearly at $x/D_h=0.82$. sub-atmospheric in pressure can be observed for the lower jet to plate spacing 's up to 1.0 and this region vanishes with the increase in the jet to plate spacing. The re-circulation of the jet at lower Z/D_h may be the reason for the formation of the subatmospheric region. The lateral spread of the pressure increases with the jet to plate distance whereas the pressure intensity decreases along the length of the plate as the jet velocity gradually increases in the wall jet region on the plate.

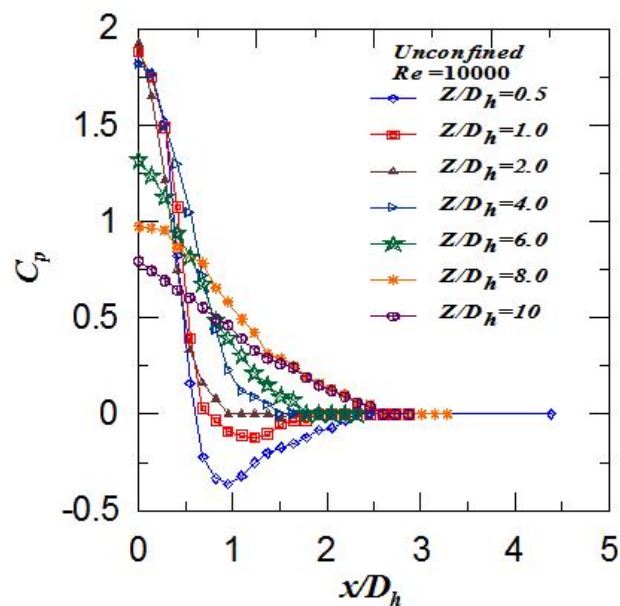


Fig 5.4 Local wall static pressure distribution along the streamwise direction at $Re = 10000$ for the unconfined jet.

[b] Fluid flow characteristics of a Confined Slot Jet impinging on a smooth surface

The Fig 5.5. Shows the lateral variation of coefficient of pressure for $Re = 10000$ at different nozzle to plate spacing's ($Z/D_h = 0.5-10.0$) and confinement ratio $L_c/D_h = 6.8$. The fig clearly reveals that the coefficient pressure is maximum at the stagnation point i.e. at $x/D_h = 0$ and it decreases with increase in x/D_h ratio. The coefficient of pressure was observed to become sub-atmospheric up to $Z/D_h = 0.5-10$ and further, there is no evidence of subatmospheric region for any nozzle to plate spacing. The Cp_0 is maximum (1.81) for $Z/D_h = 0.5$ and monotonically decreases as Z/D_h and minimum is 0.97 recorded for Z/D_h is 8.0.

Fig 5.6 Shows the lateral variation of coefficient of pressure for $Re = 10000$ at the different nozzle to plate spacing's ($Z/D_h = 0.5-10.0$) and confinement ratio $L_c/D_h = 10.2$. The fig clearly reveals that the coefficient of pressure is maximum at the stagnation point i.e. at $x/D_h = 0$ and it decreases with increase in x/D_h ratio. The coefficient of pressure was observed to become sub-atmospheric up to $Z/D_h = 0.5$ to 1.0 and further, there is no evidence of subatmospheric region for any nozzle to plate spaces. is also clear that the coefficient of pressure at the stagnation point is maximum for $Z/D_h = 0.5$ and goes on decreasing as Z/D_h increases. The Cp_0 value also tabulated the Cp_0 value ranges maximum 1.417 at $Z/D_h = 0.5$ and minimum 0.45 recorded for Z/D_h is 8.0.

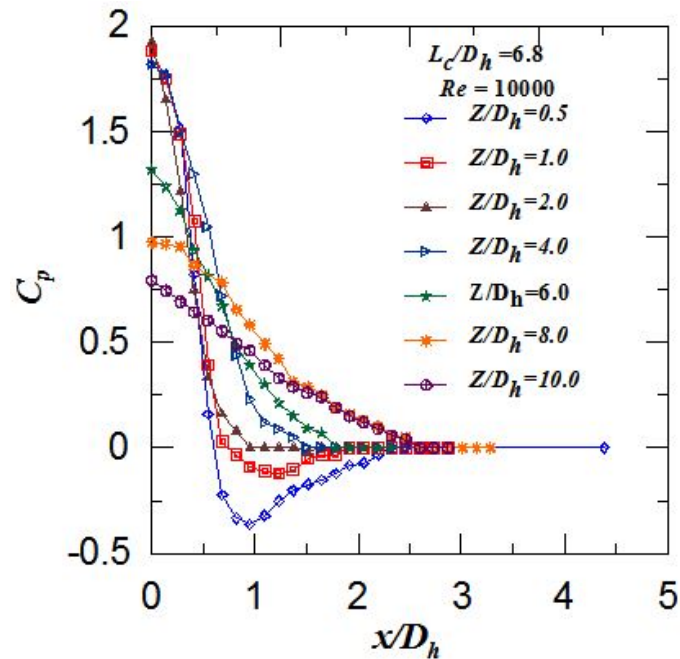


Fig. 5.5. Effect of the Z/D_h on lateral distribution of C_p for confinement ratio $L_c/D_h=6.8$ at $Re=10000$

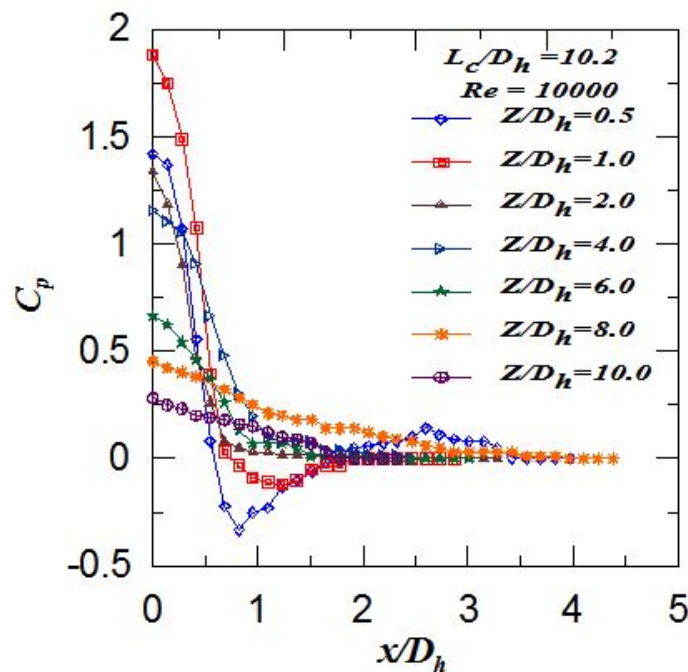


Fig 5.6 Effect of the Z/D_h ratio on pressure distribution for a confinement ratio $L_c/D_h=10.2$.

Fig 5.7 Shows the lateral variation of coefficient of pressure for $Re = 10000$ at the different nozzle to plate spacing's ($Z/D_h = 0.5-10.0$) and confinement ratio $L_c/D_h=13.6$. The coefficient of pressure is maximum at the stagnation point and it decreases with increase in x/D_h . It is also clear that the C_{p0} is maximum for $Z/D_h = 0.5$ and goes decreasing as Z/D_h increases. The C_{p0} value reaches 2.25 at $Z/D_h = 0.5$ and minimum 0.65 recorded for Z/D_h is 8.0.

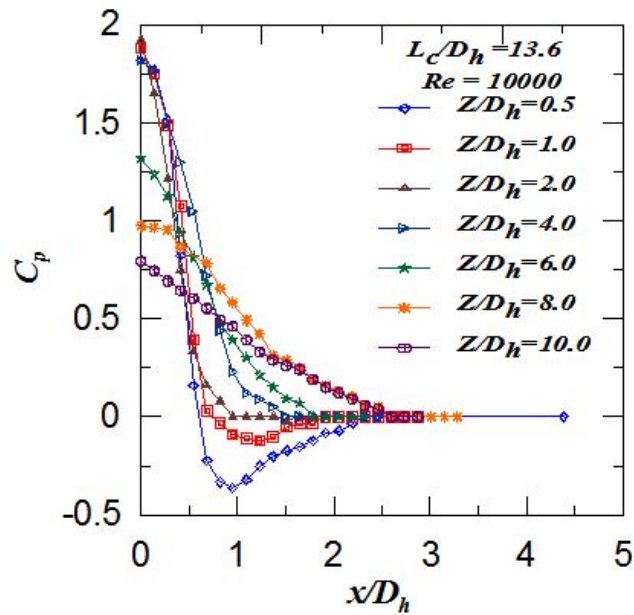


Fig 5.7 Effect of the Z/D_h ratio on pressure distribution for confined jet size $L_c/D_h=13.6$

Fig 5.8 shows the lateral variation of coefficient of pressure for $Re = 10000$ at the different nozzle to plate spacing's ($Z/D_h = 0.5-10.0$) and confinement ratio $L_c/D_h=17.0$. The C_{p_o} value ranges maximum 1.645 at Z/D_h 0.5 and minimum 0.70 recorded for Z/D_h is 8.0.

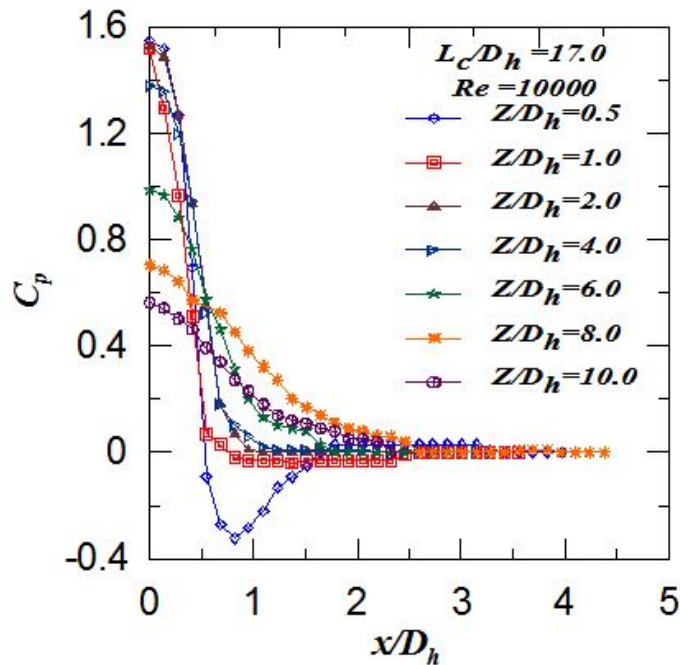


Fig 5.8 Effect of the Z/D_h ratio on pressure distribution for confined jet size $L_c/D_h=17.0$

Fig 5.9 shows the lateral variation of coefficient of pressure for $Re = 10000$ at the different nozzle to plate spacing's ($Z/D_h = 0.5-10.0$) and confinement ratio L_c/D_h .

=23.8. The C_{p_o} value ranges maximum 1.43 at Z/D_h 0.5 and minimum 0.43 recorded for Z/D_h is 8.0.

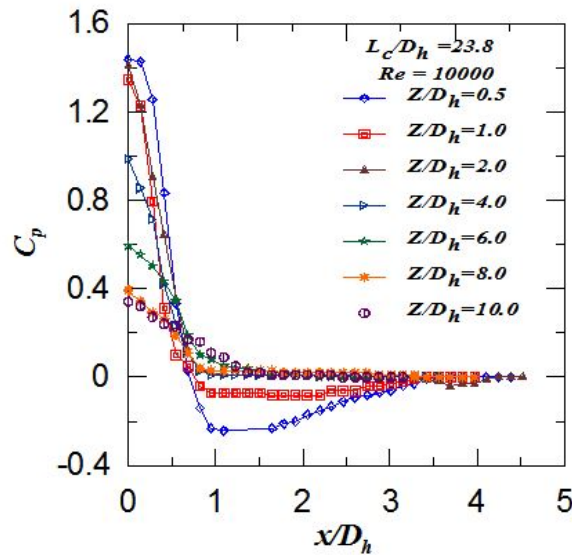


Fig 5.9 Effect of the Z/D_h ratio on pressure distribution of confined jet size $L_c/D_h=23.2$.

Fig 5.10 shows the lateral variation of coefficient of pressure for $Re = 10000$ at different nozzle to plate spacing's ($Z/D_h = 0.5-10.0$) and confinement ratio $L_c/D_h = 27.0$. The coefficient of pressure is least at $x/D_h = 1.8$. The C_{p_o} value ranges maximum 1.56 at Z/D_h 0.5 and minimum 0.57 recorded for Z/D_h is 8.0.

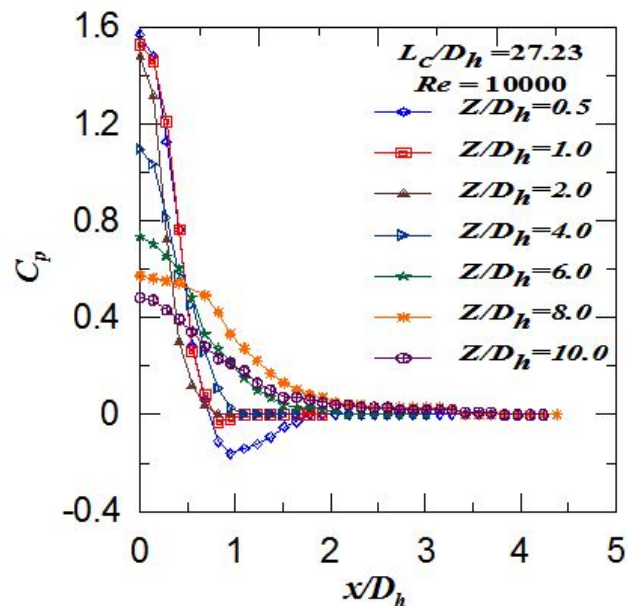


Fig 5.10 Effect of the Z/D_h ratio on pressure distribution of confined jet size $L_c/D_h = 27.0$.

5.6.3 Effect of confinement ratio on the coefficient of pressure

The Fig 5.11 shows the lateral variation of coefficient of pressure at $Z/D_h = 0.5$ for $Re = 10000$. The maximum pressure occurs at the stagnation point ($x/D_h = 0$) for all the confinements considered and for the unconfined jet. The confinement ratio (L_c/D_h) of 10.2 gives the peak value for C_p and is followed by the (L_c/D_h) = 5.8, all other confinements have the C_p value lower than that of the unconfined jet. So at lower J2P spacing of 0.5 the better choice is 10.5-confinement ratio.

The Fig 5.12 shows the lateral variation of coefficient of pressure at $Z/D_h = 1.0$ for $Re = 10000$. At this J2P spacing also the confinement ratio (L_c/D_h) of 10.2 gives the peak value for C_p and is followed by the (L_c/D_h) = 5.8, all other confinements have the C_p value lower than that of the unconfined jet. So at lower J2P spacing of 1.0 also the better choice is 10.2, confinement ratio.

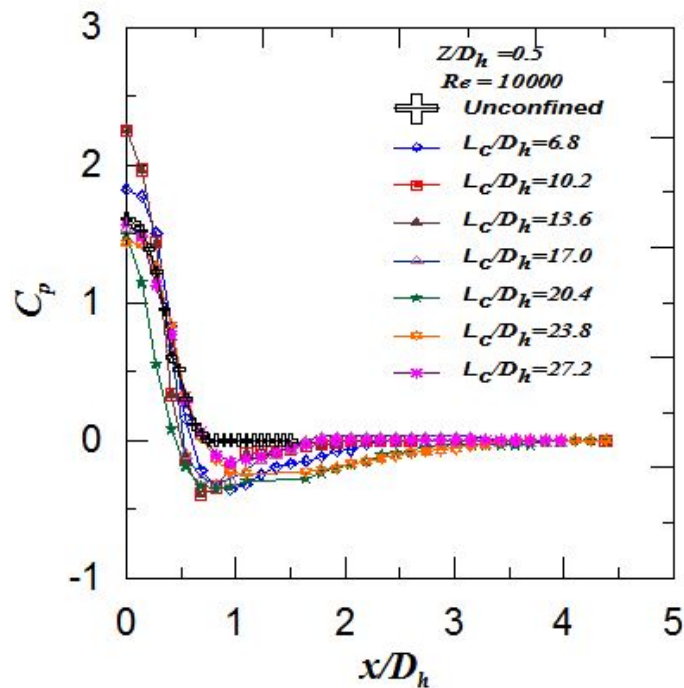


Fig 5.11 Local wall static pressure distribution for $Z/D_h = 0.5$ at $Re = 10000$

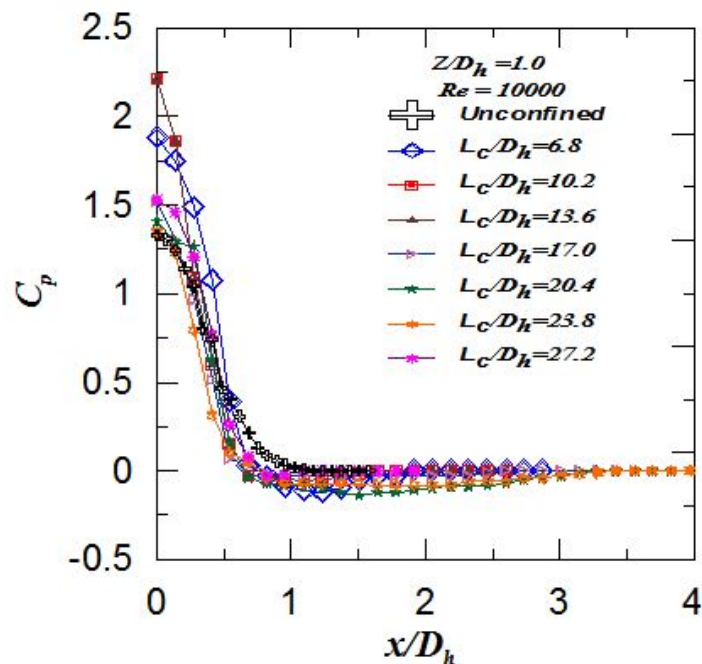


Fig 5.12 Local wall static pressure distribution for $Z/D_h = 1.0$ at $Re = 10000$

The Fig 5.13 shows the lateral variation of coefficient of pressure at $Z/D_h = 2.0$ for $Re = 10000$. The maximum pressure occurs at the stagnation point ($x/D_h = 0$) for all the confinements considered and for the unconfined jet. As x/D_h increases, the coefficient of pressure decreases. There is no subatmospheric region occurs. At this J2P space also the confinement ratio 10.2 outperforms all other ratios, particularly very close to the stagnation point.

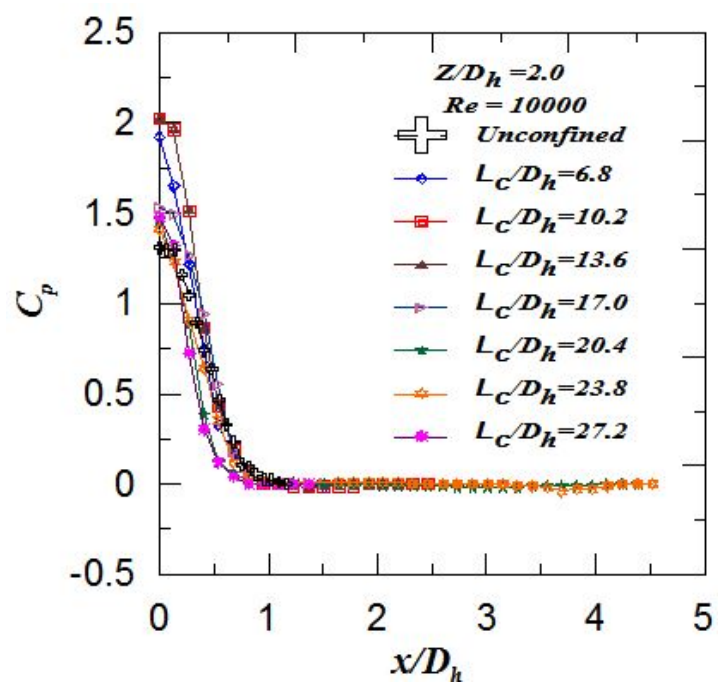


Fig 5.13 Local wall static pressure distribution for $Z/D_h = 2.0$ at $Re = 10000$

The experiment was repeated with the different J2P spaces of 4.0, 6.0, 8.0 and also 10.00 and it is found the same trend of the confinement ratio 10.2 performs better followed by 6.8. To avoid the repetition, the data is not presented here.

The main finding of this study is that the confinement of the slot jet in proper ratio will improve the jet characteristics and will be useful in designing a cooling or heating application.

5.7 Experimental set up and methodology for heat transfer characteristics studies

The setup used in the experiment is same which is used for the smooth surface study discussed in the Chapter 3.0. The only modification made here is during the entire experimental study the confinement plate (The length of the plate is varied from 50mm to 200 mm) is mounted at the end of the slot nozzle to confine the flow of the jet, so that the influence on the heat transfer can be understood. The experiment is conducted for various Reynolds numbers and J2P space combinations. The confinement Ratio is varied between $L_c/D_h = 6.8$ & $L_c/D_h = 27.23$. But the results of the experiment are presented only for The Turbulent Reynolds number 10000. The figures 5.15 and 5.16 show the actual photographs of the experiment setup.

5.7.1 Methodology for heat transfer characteristics study with a confined slot jet impingement

Figures 5.17 and 5.18 shows the sample images taken by IR thermal imaging camera taken at for $Z/D_h = 0.25, L_c/D_h = 6.8$ & for $L_c/D_h = 27.23$ at $Re = 10000$ respectively. The central blue strip in the image shows the impingement area of the jet and minimum temperatures can be seen comparatively at this region. The temperature on the plate seen gradually increasing along the width of the “Target plate” from the center of impingement as visible in the image.



Fig. 5.15 Photograph of the Experimental Set Up for Heat Transfer studies.



Fig 5.16 Photograph of the set up showing the position of Slot Jet, Target Plate, and IR Camera.

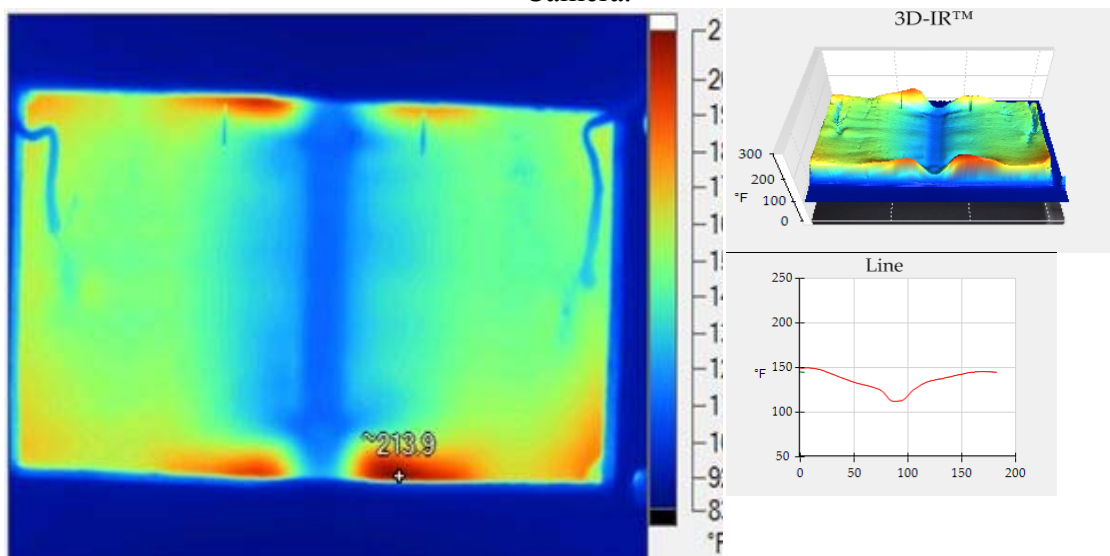


Fig. 5.17 Sample IR image taken at $Z/D_h = 0.25, L_c/D_h = 6.8$ & Re of 10000.

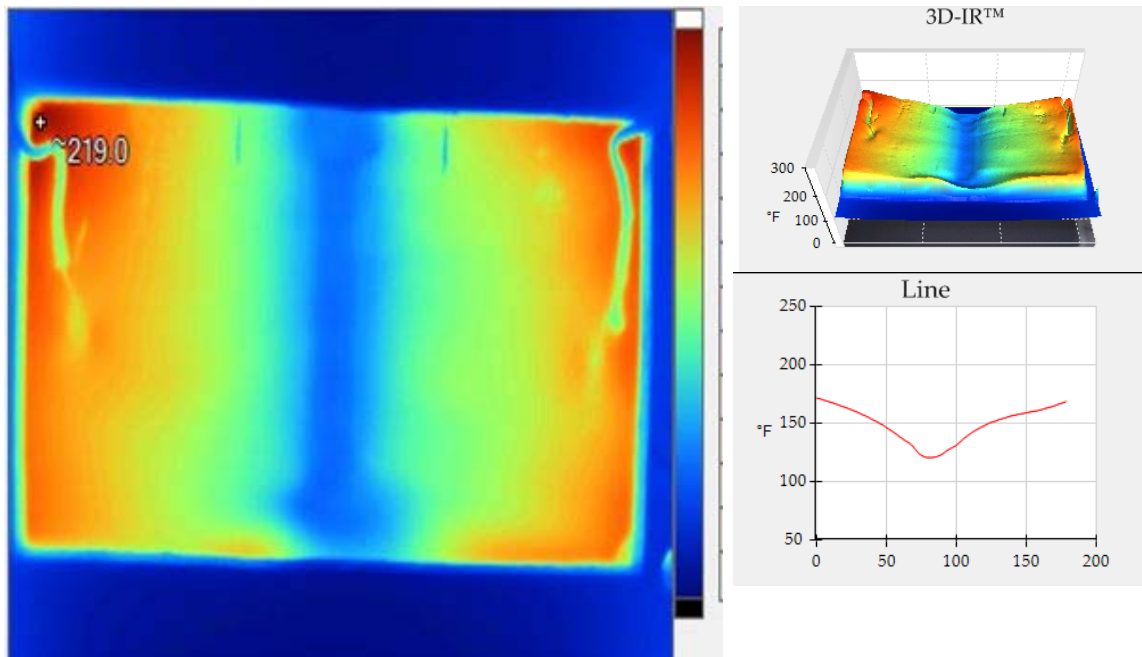


Fig. 5.18 Sample IR image taken at $Dh = 0.25$, $Lc/D_h = 27.23$ & Re of 10000

5.7.2 Data Reduction:

The equations presented in the chapter 03, section 3.3 is applicable for the calculation of fluid flow and heat transfer parameters here also.

5.7.3 Results and Discussion

Impact of confinement ratio and jet to- target distance on the heat transfer coefficient distribution is analyzed. Jet widths extended from 0.6 mm to 2 mm, and jet toTarget plate” dispersing from 0.5 to 10. The plane Reynolds number went from 26.8 to 1000 in the laminar boundary. For the case with the limit condition, for example, $W = 2$ mm, $H = 5$ mm and $Re = 26.8$ laminar boundary layer (Z.Q. Lou *et al.* [2005]). This result gives only 1% better performance for laminar flow keeping this in mind we tried for turbulent flow i.e., Re 10000. This understanding of note to be useful for confined slot air jet for Re 10000.

5.7.3.1 Heat transfer estimation for the target plate

The target surface temperature measurements for each configuration are made under steady state conditions using the thermal images collected by the infra-red camera. The plenum air temperature is used as reference jet fluid temperature for all heat transfer calculations. The local heat transfer coefficients are estimated based on the defining equation,

$$h = \frac{q''}{T_w - T_j} \quad (5.6)$$

Where q'' = Net heat flux imposed on the target plate, after heat loss correction

T_w = Local surface temperature on the target plate

T_j = Reference jet fluid temperature

Nusselt number is computed from Equation (5.6)

$$Nu = \frac{hd}{k} \quad (5.7)$$

Uncertainties in the measurement of different parameters are carried out using the method suggested by Moffat (1988) and are listed in Table 5.1.

Table 5.1 variation of Nu with the confinement (%) at $Z/D_h = 6.0$

Parameter	% Uncertainty	
	$Re = 3000$	$Re = 10000$
Temperature	5.0	
Mass flow rate	3.2	2.92
Reynolds number	3.8	3.54
Nusselt number	6.3	5.6
Wall static pressure	0.5	

5.7.3.2 Heat transfer characteristics of an unconfined slot Jet

The lateral distribution of local heat transfer coefficients for Z/D_h range from 0.25 -8.0 for the unconfined jet at $Re = 10000$ is carried out and the results are presented in Fig. 5.19. At the stagnation point, the local Nusselt number for $Z/D_h = 0.25$ is just about 1.5 times of that for $Z/D_h = 8$. The estimation of Nusselt number basically lies on heat transfer coefficient. Whenever Z/D_h shifts from 8.0 to 0.25 nearby Nusselt number increments significantly in the stagnation point as well as the downstream region. Whenever Z/D_h is greater than 1, the heat transfer coefficient move in the wall jet region is not influenced to a great extent by the lessening of Z . Certainly; a reduction of Z/D_h causes a sharp increase of Nusselt number in the potential core region of the jet.

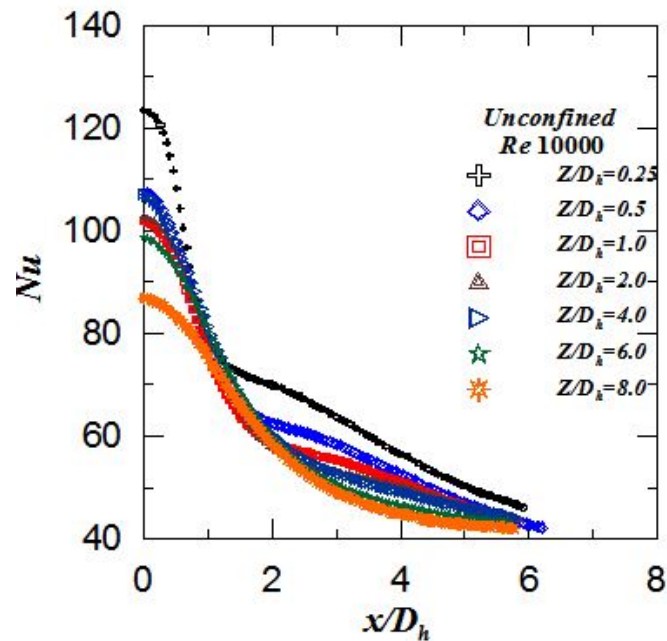
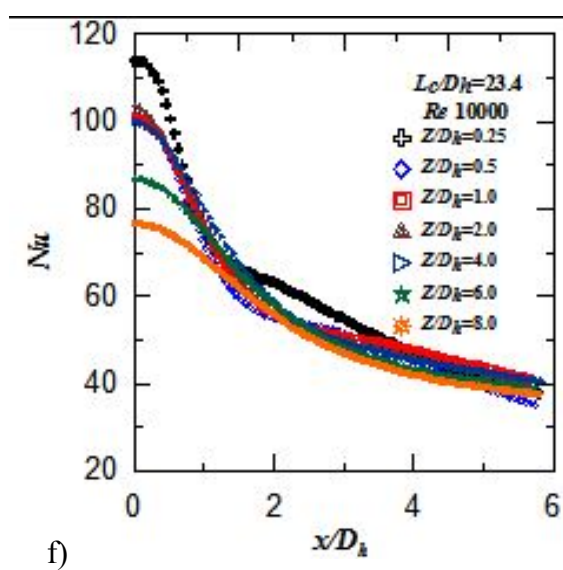
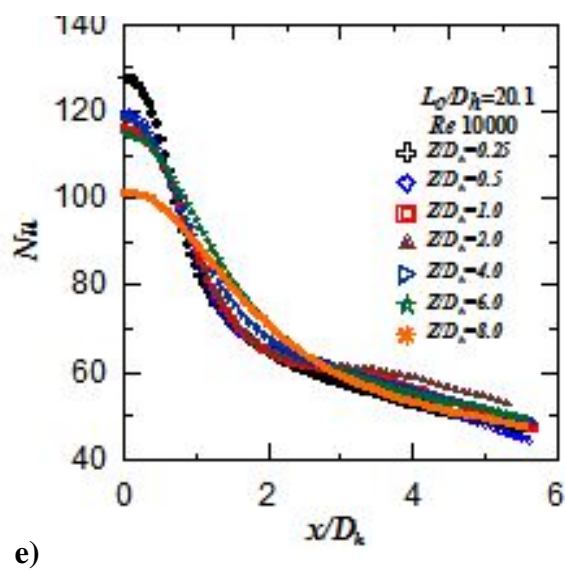
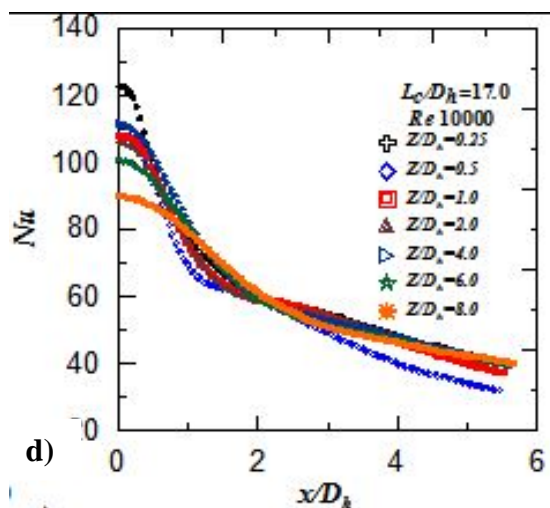
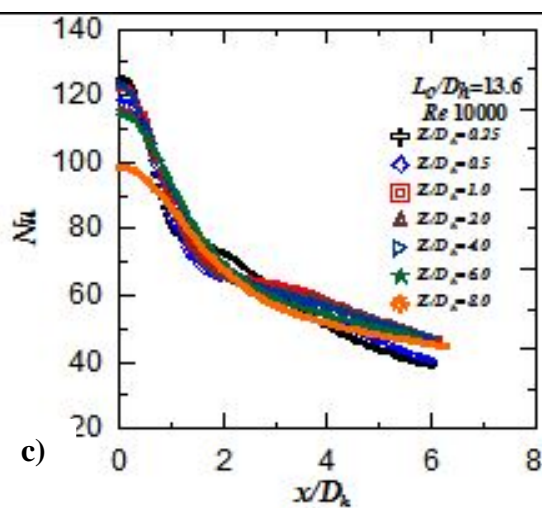
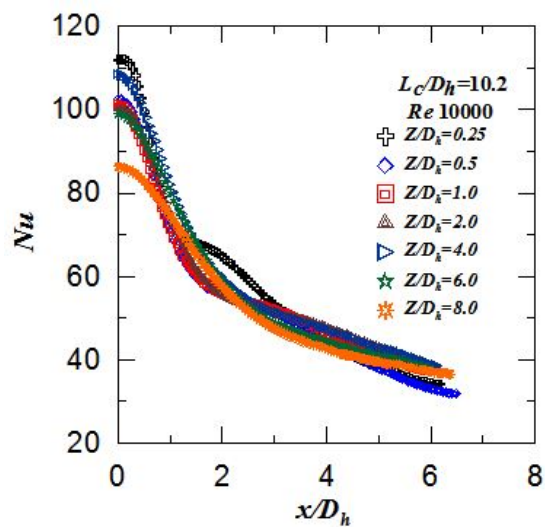
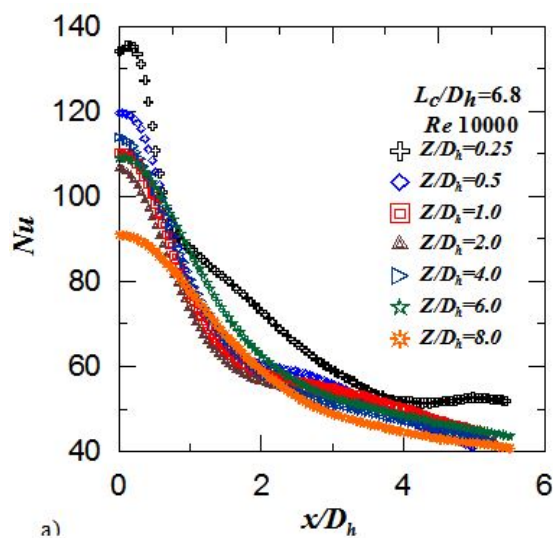


Fig. 5.19 Local heat transfer distribution for $Z/D_h=0.25-8.0$ at $Re=10000$ and $L_c/D_h=0.0$

5.7.3.3 Heat transfer characteristics of a confined slot Jet: Effect of the nozzle to target spacing on Heat transfer distribution

The lateral distribution of local heat transfer coefficients for Z/D_h range from 0.25 -8.0 and with an L_c/D_h range of 6.8 to 27.23 for the confined jet at $Re = 10000$ is studied and the Figures 5.20 (a) to (e) presents the distribution of local Nusselt number along the “Target plate” with a variation of Z/D_h . The general observation is, at the stagnation point, the local Nusselt number for $Z/D_h = 0.25$ is just nearly about 1.5 times of that for $Z/D_h = 8$. The estimation of Nusselt number basically lies on heat transfer coefficient. Whenever Z/D_h shifts from 8.0 to 0.25, the Nusselt number increases significantly at the stagnation point as well as the downstream region. Whenever $Z/D_h > 1$, the heat transfer coefficient moves in the wall jet region and is not influenced to a great extent by the lessening of Z/D_h . Certainly, a reduction of Z/D_h causes a sharp increase of Nusselt number in the potential core region of the jet.



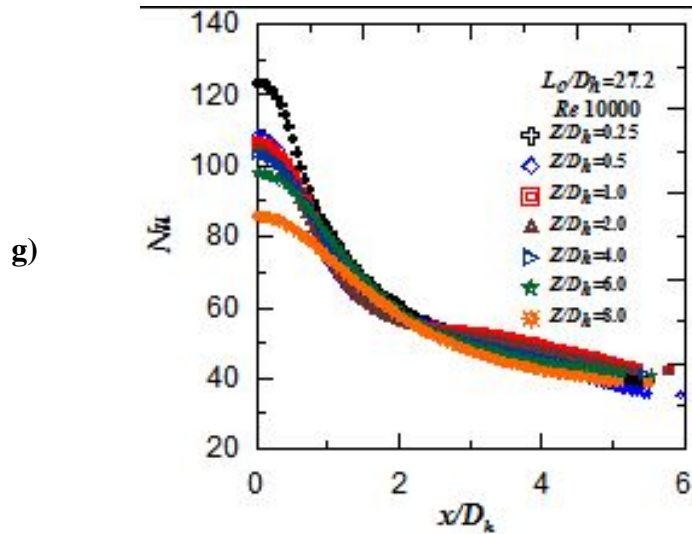


Fig 5.20 Effect of the Z/D_h ratio on Local heat transfer distribution for Confined Slot Jet size $L_c/D_h = 6.8$ to $L_c/D_h = 10.2$ at $Re = 10000$

5.7.3.4 Effect of confinement ratio (L_c/D_h) on Heat transfer distribution

The confinement ratio (L_c/D_h) used in the current study ranges from 6.8 to 27.23 whereas the Reynolds Number (Re) is kept constant at 10000. It is seen from Fig 5.21 that the coefficient of heat transfer for different confinement ratios for particular $Z/D_h = 0.25$. As x/D_h decreases the Nusselt number increases at the stagnation point and higher the $x/D_h = 0$. Nusselt number at wall jet region decreases gradually. For confinement ratio of L_c/D_h of 6.8 the heat transfer coefficient is maximum at the stagnation point for $Z/D_h = 0.25$. From the data available in table 5.2, it can be concluded that for the given $Z/D_h = 0.25$ at $Re = 10000$, confinement ratio L_c/D_h of 6.8 gives +8.76% better thermal distribution, L_c/D_h of 17.0 & 20.6 also are better in comparison with unconfined jet. The Nu value is lower than unconfined jet for the remaining confinement ratios considered.

Table 5.2 variation of Nu with the confinement (%) at $Z/D_h = 0.25$

Unconfined slot air jet $Nu_o = 123.41$		
at $Z/D_h = 0.25$ for $Re = 10000$		
L_c/D_h	Nu_o	% change in Nu_o
6.8	134.22	+ 08.76
10.2	111.89	- 09.33
13.6	122.76	- 00.53
17.0	124.81	+ 01.13
20.6	127.80	+ 03.56
23.8	114.02	- 07.60
27.2	123.37	- 00.03

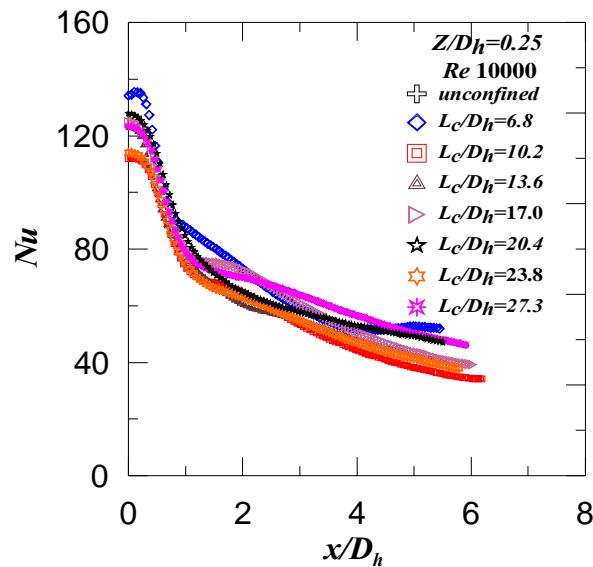


Fig 5.21 Effect of the L_c/D_h ratio on Local heat transfer distribution for Confined Slot air Jet at Re 10000 and Z/D_h at 0.25.

The confinement proposition ranges from 6.8 to 27.23. Other parameters $Re = 10000$ were kept constant. It is seen from Fig 5.22. that the coefficient of heat transfer for different confinement ratio 's for particular $Z/D_h = 0.5$ and as the x/D_h decreases surface at Nusselt number increment at close to the stagnation point and higher the x/D_h Nusselt number at wall jet region decreases. As lower the x/D_h sharper the potential core region. Here for confinement ratio of L_c/D_h of 17.0 & 6.8, heat transfer rate in core region get maximum. Hence the preferred heat transfer rate at $Z/D_h = 0.5$ the $L_c/D_h = 6.8$ gives a better thermal performance. In the wall jet region heat transfer coefficient at unconfined and $L_c/D_h = 17.0$ at $Z/D_h = 0.5$ gives a maximum thermal distribution. By comparing the data from the table 5.3, it can be concluded that for the given $Z/D_h = 0.5$ at $Re = 10000$, confinement ratio L_c/D_h of 20.6 gives +11.47 % better thermal distribution, L_c/D_h of 6.8, 13.6, 17.0 & 27.2 has good preferences but efficiency is less than L_c/D_h of 20.6. L_c/D_h of 13.6 and 27.23 has no influence on Nu_o . L_c/D_h of 10.2 & 23.8 gives a reduction in Nusselt number in comparisons with the unconfined jet and are not preferable.

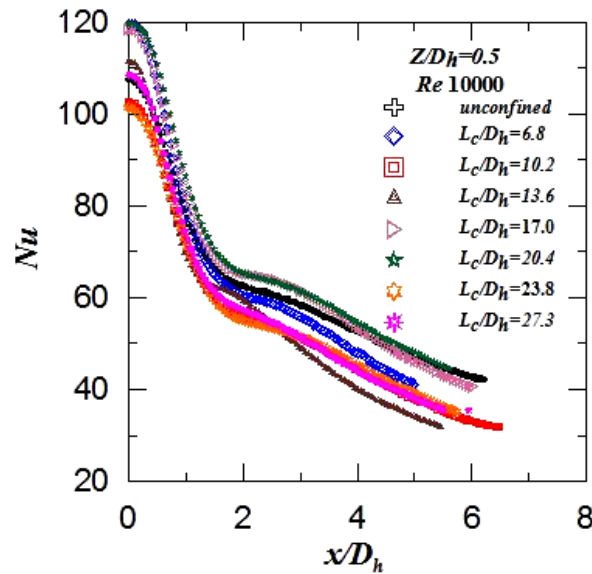


Fig 5.22. Effect of the L_c/D_h ratio on the local heat transfer distribution for Confined Slot air Jet at Re 10000 and Z/D_h at 0.5

Table 5.3 variation of Nu with the confinement (%) at $Z/D_h = 0.5$

Unconfined slot air jet $Nu_o = 107.29$ at $Z/D_h = 0.5$ for $Re = 10000$				
L_c/D_h	Nu_o	% change in Nu_o on Confinement		
6.8	119.57	+	11.43	%
10.2	102.64	-	04.33	%
13.6	111.39	+	03.80	%
17.0	118.41	+	10.36	%
20.6	119.60	+	11.47	%
23.8	101.45	-	05.44	%

The confinement proposition ranges from 6.8 to 27.23. Other parameters $Re = 10000$ were kept constant. It is seen from Fig 5.23 that the coefficient of heat transfer for different confinement ratio 's for particular $Z/D_h = 1.0$ as x/D_h decreases the Nusselt number is builds up in the stagnation region and higher the x/D_h Nusselt number at wall jet region decreases. As lower the x/D_h sharper the potential core region. Here for confinement ratio of L_c/D_h of the 17.0 heat transfer rate in core region get maximum hence its preferred heat transfer rate at $Z/D_h = 1.0$ and $L_c/D_h = 17.0$ gives a better thermal performance. In the region of wall jet, the heat transfer coefficient at $L_c/D_h = 17.0$ gives a maximum thermal performance. By comparing the data from the table 4.03, it can be concluded that for the given $Z/D_h = 1.0$ at $Re = 10000$, confinement ratio L_c/D_h of 17.0 gives +20.12 % better thermal efficiency, L_c/D_h of 6.8, 13.6, 20.6 & 27.2 has good preferences. L_c/D_h of 10.2 & 23.8 gives a reduction in Nusselt number in comparisons with the unconfined jet and are not preferable.

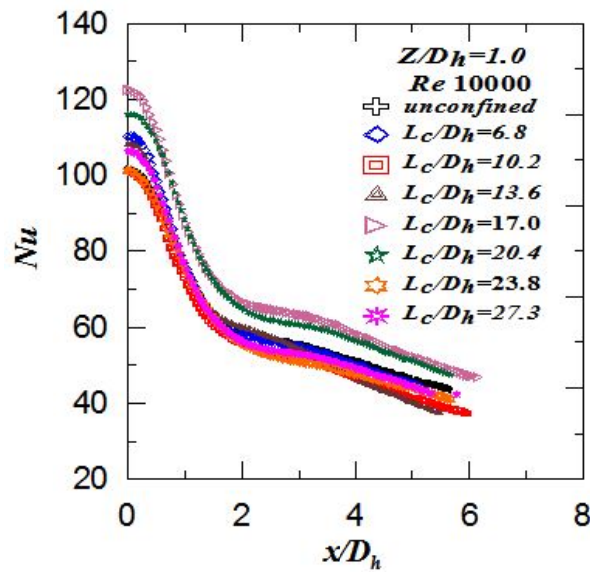


Fig 5.23. Effect of the L_c/D_h ratio on Local heat transfer distribution for Confined Slot air Jet at Re 10000 and Z/D_h at 1.0

Table 5.4 variation of Nu with the confinement (%) at $Z/D_h = 1.0$

Unconfined slot air jet $Nu_o = 101.82$ at $Z/D_h = 1.0$ for $Re = 10000$			
L_c/D_h	Nu_o	% change in Nu_o on Confinement	
6.8	110.19	+	08.22
10.2	101.03	-	00.77
13.6	108.09	+	06.16
17.0	122.31	+	20.12
20.6	116.03	+	13.96
23.8	101.24	-	00.56
27.2	106.41	+	04.50

By observing the data from the table 5.5, it can be concluded that for the given $Z/D_h = 2.0$ at $Re = 10000$, confinement ratio L_c/D_h of 20.6 gives +15.30% better thermal efficiency, L_c/D_h of 6.8, 13.6, 23.8 & 27.2 has good preferences. L_c/D_h of 10.2 gives a reduction in Nusselt number in comparisons with the unconfined jet and is not preferable.

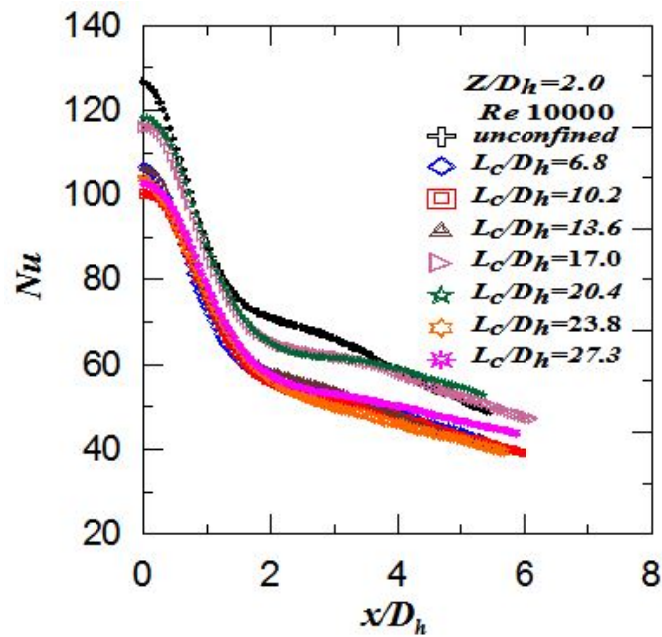


Fig 5.24. Effect of the L_c/D_h ratio on Local heat transfer distribution for Confined Slot air Jet at Re 10000 and Z/D_h at 2.0

Table 5.5 variation of Nu with the confinement (%) at $Z/D_h = 2.0$

Unconfined slot air jet $Nu_o = 102.55$ at $Z/D_h = 2.0$ for $Re = 10000$				
L_c/D_h	Nu_o		Percentage of Nu_o on Confined Slot Air Jet.	
6.8	106.53	+	03.90	%
10.2	100.28	-	02.20	%
13.6	106.11	+	03.40	%
17.0	116.03	+	13.10	%
20.6	118.22	+	15.30	%
23.8	103.72	+	01.14	%
27.2	104.94	+	02.33	%

By comparing the data from the table 5.6, it can be concluded that for the given $Z/D_h = 4.0$ at $Re = 10000$, confinement ratio L_c/D_h of 17.0 gives +15.10% better thermal efficiency, L_c/D_h of 6.8, 10.2, 13.6, & 20.6 has good preferences. L_c/D_h of 23.8 & 27.2 gives a reduction in Nusselt number in comparisons with the unconfined jet and are not preferable.

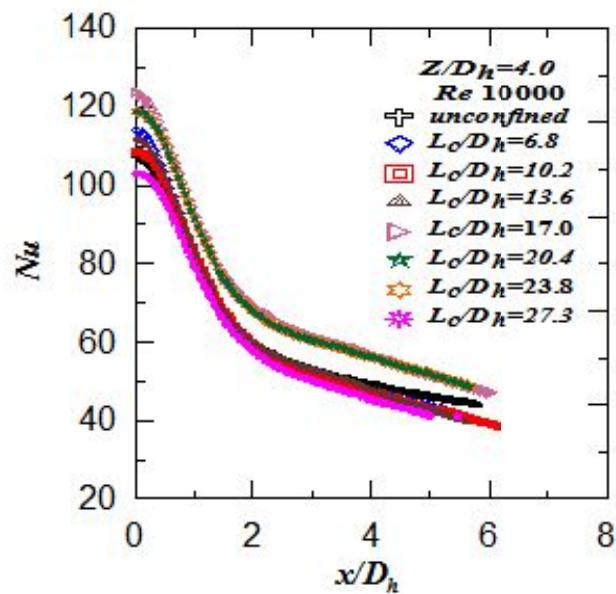


Fig 5.25. Effect of the L_c/D_h ratio on Local heat transfer distribution for Confined Slot air Jet at Re 10000 and Z/D_h at 4.0

Table 5.6 variation of Nu with the confinement (%) at $Z/D_h = 4.0$

Unconfined slot air jet $Nu_o = 107.07$ at $Z/D_h = 4.0$ for $Re = 10000$			
L_c/D_h	Nu_o	Percentage of Nu_o on Confined Slot Air Jet.	
06.8	113.95	+	06.03
10.2	108.45	+	01.28
13.6	111.69	+	04.30
17.0	123.33	+	15.10
20.6	118.81	+	10.90
23.8	100.26	-	06.40
27.2	102.97	-	03.80

By comparing the data from the table 5.7, it can be concluded that for the given $Z/D_h = 6.0$ at $Re = 10000$, confinement ratio L_c/D_h of 20.6 gives +16.16% better thermal efficiency, L_c/D_h of 6.8, 10.2, 13.6, & 17.0 has good preferences.

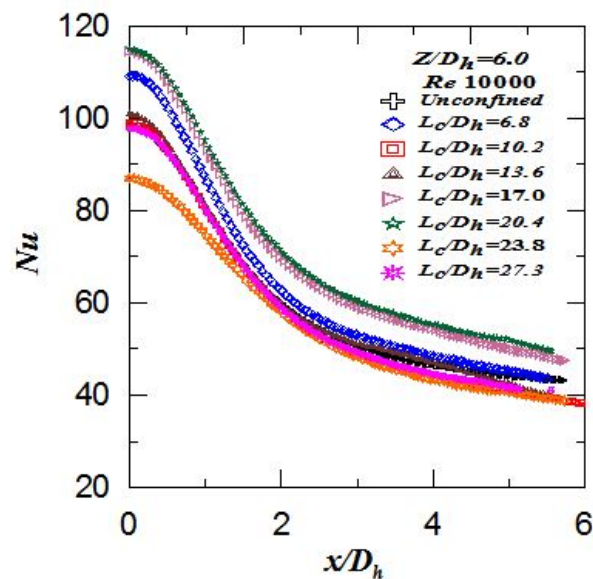


Fig 5.26. Effect of the L_c/D_h ratio on Local heat transfer distribution for Confined Slot air Jet at Re 10000 and Z/D_h at 6.0

Table 5.7 variation of Nu with the confinement (%) at $Z/D_h = 6.0$

Unconfined slot air jet $Nu_o = 98.67$ at $Z/D_h = 6.0$ for $Re = 10000$			
L_c/D_h	Nu_o	% change in Nu_o on Confinement.	
6.8	109.00	+	10.47
10.2	98.87	+	00.20
13.6	100.85	+	02.20
17.0	114.42	+	15.96
20.6	114.61	+	16.16
23.8	86.93	-	11.80
27.2	97.68	-	01.00

By comparing the data from the table 4.07, it can be concluded that for the given $Z/D_h = 8.0$ at $Re = 10000$, confinement ratio L_c/D_h of 20.6 gives +16.86% better thermal efficiency, L_c/D_h of 6.8, 13.6, & 17.0 has good preferences. L_c/D_h of 10.2, 23.8 & 27.2 gives a reduction in Nusselt number in comparisons with the unconfined jet and are not preferable.

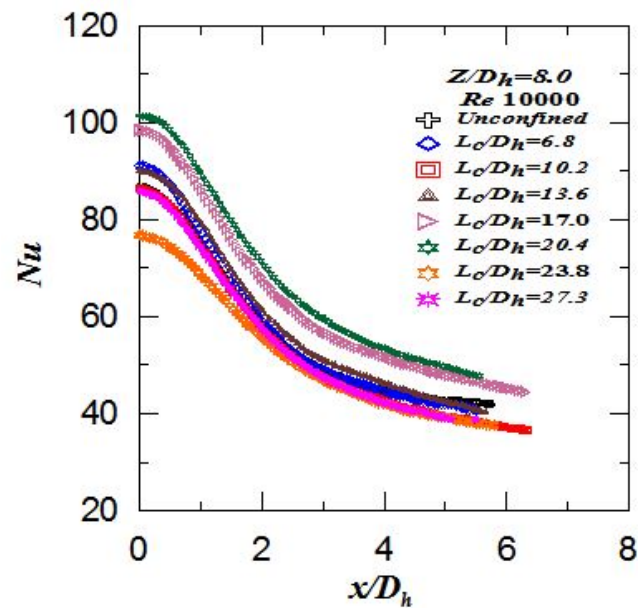


Fig 5.27. Effect of the L_c/D_h ratio on Local heat transfer distribution for Confined Slot air Jet at Re 10000 and Z/D_h at 8.0

Table 5.8 variation of Nu with the confinement (%) at $Z/D_h = 8.0$

Unconfined slot air jet $Nu_o = 86.79$ at $Z/D_h = 8.0$ for $Re = 10000$			
L_c/D_h	Nu_o	% change in Nu_o on Confinement	
6.8	90.95	+	04.79
10.2	86.33	-	00.53
13.6	90.09	+	03.80
17.0	98.42	+	13.92
20.6	101.44	+	16.86
23.8	76.81	-	11.50
27.2	85.79	-	01.12

By observation from, Fig 5.28 & Fig 5.29 we can conclude that:

- The flow pattern for varying of different Z/D_h with Cp_o and Nu_o way of the pattern will same for different L_c/D_h 's. This proves that for confined slot air jet the pressure and temperature are directly proportional to each other for different L_c/D_h 's
- The flow pattern for varying of different L_c/D_h with Cp_o and Nu_o way of the pattern will same for different Z/D_h 's. This proves that for confined slot air jet the pressure and temperature are directly proportional to each other for different Z/D_h 's.

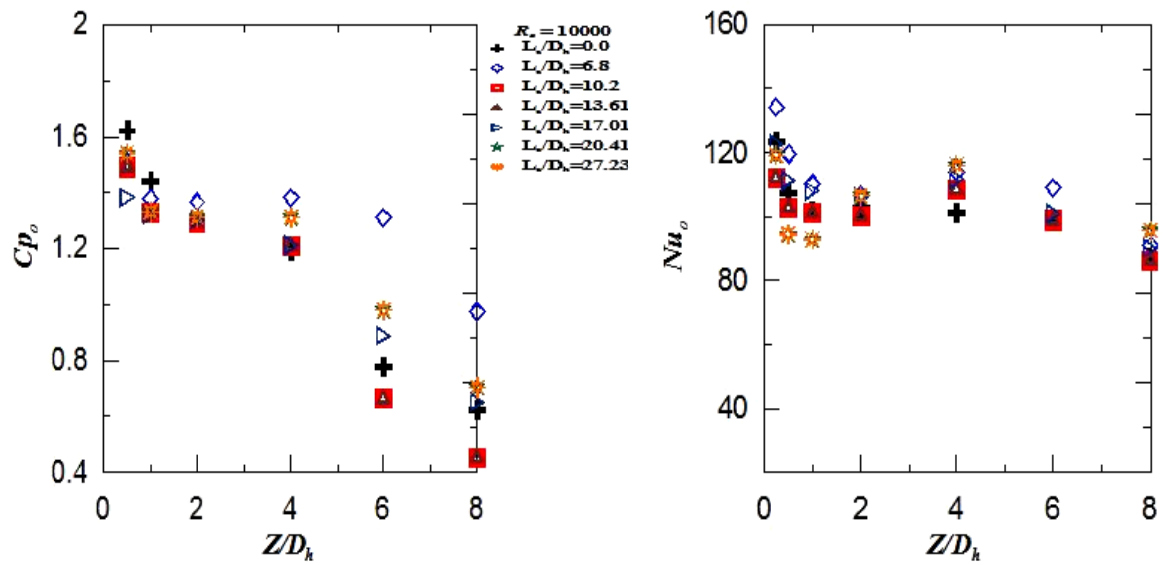


Fig 5.28 Variation of Stagnation Point Pressure and Nusselt Number with Confinement ratio and jet to plate distance at $Re = 10000$

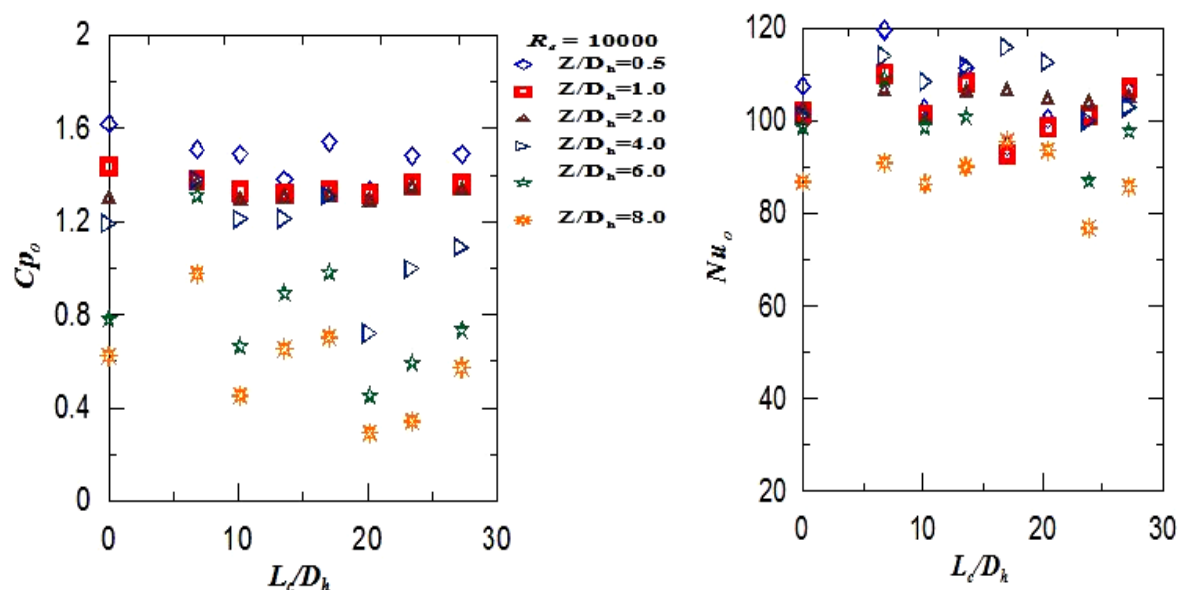


Fig 5.29 Variation of Stagnation Point Pressure and Nusselt Number with Confinement ratio and jet to plate distance at $Re = 10000$

5.8 Conclusions

Wall static pressure (C_p) and heat transfer coefficient distribution on a flat surface impinged by a confined slot air jet are experimentally analyzed for the confinement ratios, $L_c/D_h=0.0$ to 27.2 and nozzle slot jet to plate spacing ($Z/D_h=0.25-10.0$) at $Re= 10000$. Following conclusions elaborated from the present study:

- The Stagnation point wall static pressure coefficient is observed to be independent of Reynolds numbers for a given Z/D_h for an unconfined slot jet impingement on a flat surface.
- With the increase in the $J2P$ spacing the subatmospheric region moves outward from the stagnation point.
- It is observed that the highest value for the wall static pressure coefficient for a slot jet is at stagnation point for both confined and unconfined configurations at a given Reynolds number
- The maximum pressure is observed at the stagnation point for all confinements and nozzle to plate spaces under study.
- Subatmospheric pressure region is more significant for the $J2P$ spacing below 1.0 for all confinements studied.
- The Nusselt number at the stagnation is highest for the all the confinement ratios ($L_c/D_h=0.0$ to 27.3) studied.

CHAPTER 06

6.0 Influence of confinement on local “wall static pressure” and “heat transfer” between a rough flat surface and a “slot-air jet”

6.1 Introduction:

The fluid flow with tangential separation is known as jet; if fluid jet and the surrounding medium is same then it is called as submerged jet. If the temperature of the fluid at nozzle exits same as ambient is known as isothermal jets. Generally, jets are classified as free jet and impinging jet.

Jet impingement heat transfer has received noticeable research attention because of its inherent nature of high rates of heat transfer. Impinging jets allow for short flow paths with relatively higher heat transfer rate. The industrial processes like drying of textiles, film, paper; the processing of metals and glass; cooling of gas turbine blades and the outer wall of combustors; cooling of electronic equipment employ the impinging jets. [Visakanta 1993]”.

“Single jet is used where a highly localized cooling or heating is desired. The heat transfer characteristics are influenced by J2P spacing, type of confinement and directions of cross flow of spent fluid. After the impact the jet fluid, may exit the confined passage either in one direction, two opposite directions or all directions.

6.2 Literature review

The work done by the various researchers viz. Gardon and Akfirat [1965], Beitelmal *et al* [2000], Gau and Lee [2000] , Chirac and Ortega [2002], Gao and Sunden [2003] , Narayan *et al* [2004], Baydar and Ozmen [2005], Lou *et al* [2005], Gao and Ewing [2006] , Zhou and Lee [2007], Akansu *et al* [2008], Gulati *et al* [2009], Chao and Kim [2010], Ozmen [2011], Nirmalkumar *et al* [2011], Katti, *et al* [2014], etc., has been discussed already in the chapter LITERATURE REVIEW separately.

6.2.1 Objectives of the work

From the review of published and available literature it is identified that there is an ample scope for the study on the local distribution of WSP and HTC on a rough surface with confinement under the interaction of “slot jet”. The confined and rough surfaces are very common in most of the applications like electronic packaging, food industry etc. Based on the background the following objectives are considered in our present study.

- “To know the effect of Reynolds number and J2P spacing on the local distribution of WSP coefficient under the influence of a confined slot air-jet on a rough surface.
- To understand the effect of Reynolds number and J2P spacing on the local distribution of HTC due to the impact of a confined slot air-jet on a rough surface.

6.3 Experimental Setup

The experimental set-up for wall static pressure distribution and “heat transfer” studies explained in detail in the chapter 03 is used for the current experimentation also.

The experiment is conducted for different J2P spacing ($Z/D_h = 0.5, 1.2, 4, 6, 8, 10$) and for a range of “Reynolds numbers” ($Re = 2500, 5000, 10000, 15000, 20000$) chosen. The roughness is provided on the surface using the detachable ribs whose constructional details are discussed in chapter 04 while discussing the fluid flow and heat transfer characteristics of a rib-roughened surface impinged by an unconfined single slot jet. The confinement plates made of 10mm thick acrylic sheet having different lengths of 50, 75, 100, 125, 150, 175 and 200 mm are used to confine the jet. The confinement plate will be mounted on the nozzle flushing with nozzle exit. The mounting details of confinement plates on the nozzle exit is given in detail in the chapter 05 while discussing the fluid flow and heat transfer characteristics of a smooth surface impinged by a confined single slot jet.

The experiment methodology is exactly similar to that mentioned for smooth surface and rough surface flow and “heat transfer” studies in the earlier chapters 03 and chapter 04.

6.3.1 DATA REDUCTION:

The equations used to find the wall static pressure coefficient and “heat transfer” coefficients and related parameters are same as the data reduction equations explained the chapter 03, section 3.3 for the smooth surface and unconfined single slot jet

6.3.2 VALIDATION OF EXPERIMENTAL SET-UP

Figure 6.1 (a) and (b) compares the local “Nusselt number” distribution (Nu_b) and “stagnation point” “Nusselt number” distribution (Nu_0) from the present experimental set-up with Akansu(2008) at “Reynolds number” of 5000 and Z/D_h of 2.0 and Nirmal *et al* (2011) at “Reynolds number” 5200, we observed that the present results compare well with a standard deviation of 7% for Nu . This deviation in the values is mainly due to the change in the operating “Reynolds number” by 200 otherwise the values are almost

similar with the published results of Akansu(2008) and Nirmal *et al* (2011). Hence, the experiment setup used for subsequent experiments with “slot jet” is validated.

6.4 RESULTS AND DISCUSSION

These results of the investigation to determine the local WSP and HTC distribution of normally impinging confined slot air jet on the flat rough surface for “Reynolds number” ranging from 2500 to 20000. Wall static pressure and “heat transfer” distribution are estimated for the J2Pspacing (Z/D_h) of 0.5 to 10. Temperatures on the surface are measured using IR Thermal camera – FLUKE Ti-55 and pressure distribution are measured using Differential Pressure (DP) transducer of make FURNESS CONTROLS.

6.4.1 ROUGH SURFACE FLOW STUDY:

Influence of Z/D_h on WSP distribution for various “Reynolds number” along the “streamwise direction” for 4mm rib and confinement ratio (L_c/D_h) of 6.8.

Fig 6.2 (a) to (d) shows that local WSP on a “Target plate” for the J2P spaces ($Z/D_h=0.5$ to 10) studied at a range of “Reynolds number” 2500 to 20000 with a 4mm rib and confinement plate with a ratio (L_c/D_h) =6.8. The WSP is maximum at “stagnation point” ($x/D_h=0$) due to

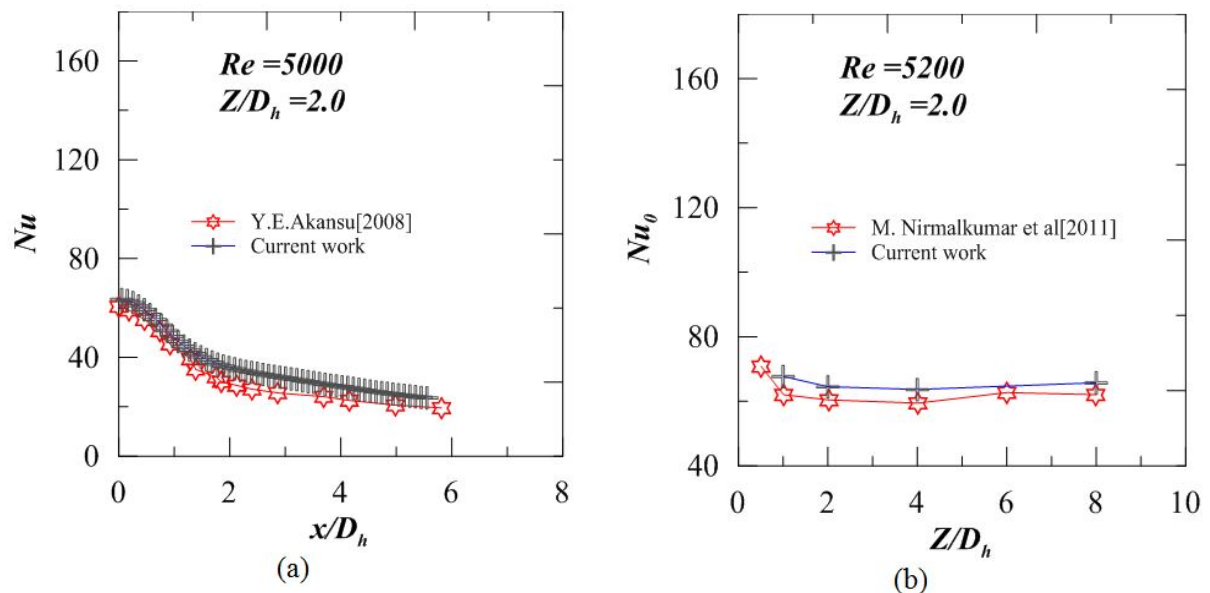


Figure 6.1 Comparison of current results with the results of (a) Akansu (2008), (b) Nirmal *et al* (2011)

translation of the entire velocity of the jet into static pressure, when the fluid hits the target surface. The maximum WSP is observed at the “stagnation point” of $Z/D_h=0.5$ of

all “Reynolds number” studied. Stagnation wall static pressure decreases with an increase in the J2P spacing due spreading of the jet. The negative pressure region occurs at $x/D_h=0.28$ i.e., at the opening of rib due flow acceleration that creates a negative pressure gradient. The subatmospheric region occurs due to the combined effect of rib and confinement.

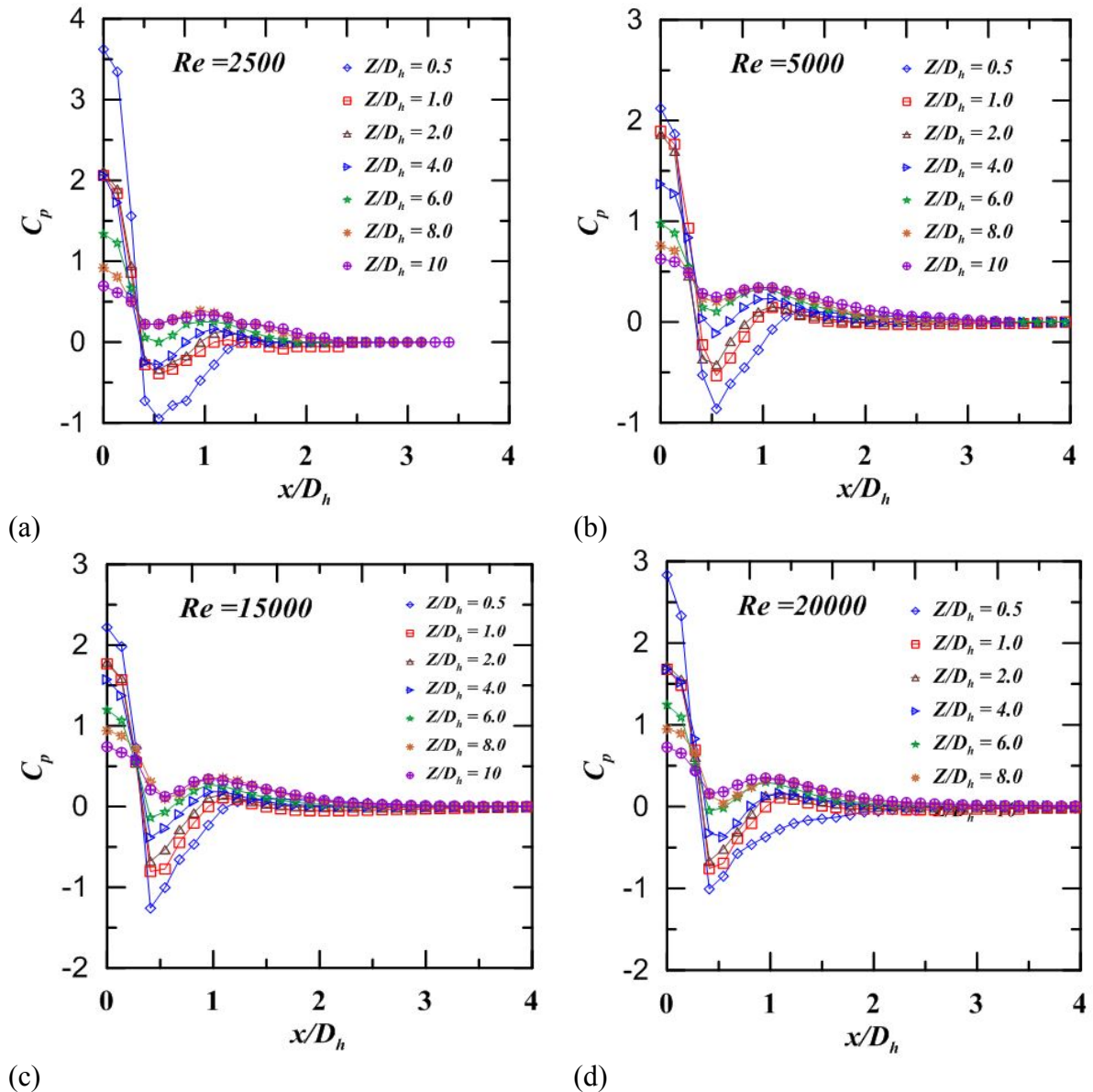


Fig 6.2 Variation of “wall static pressure” along “streamwise direction” for various Z/D_h at “Reynolds number” 2500 to 20000

The subatmospheric region occurred up to $Z/D_h=4$ (finish point of PCR), the secondary peak of “wall static pressure” observed for all J2P placing of all “Reynolds number”, increase in the J2P spacing peaks height increases. The “wall static pressure” diminishes in the stream-wise direction due to the increase in the spread of the jet reducing the core strength.

6.4.2 Influence of Z/D_h on “wall static pressure” distribution for various “Reynolds number” along the “streamwise direction” for 4mm rib and confinement ratio (L_c/D_h) of 10.2

Figures 6.3 (a) to (d) show the variation in the local WSP along the stream-wise direction for different J2P spacing (Z/D_h) of 0.5 to 10 at “Reynolds number” ranging from 2500 to 20000 for 4mm rib and confinement ratio 10.2. The maximum WSP occurs at the “stagnation point”

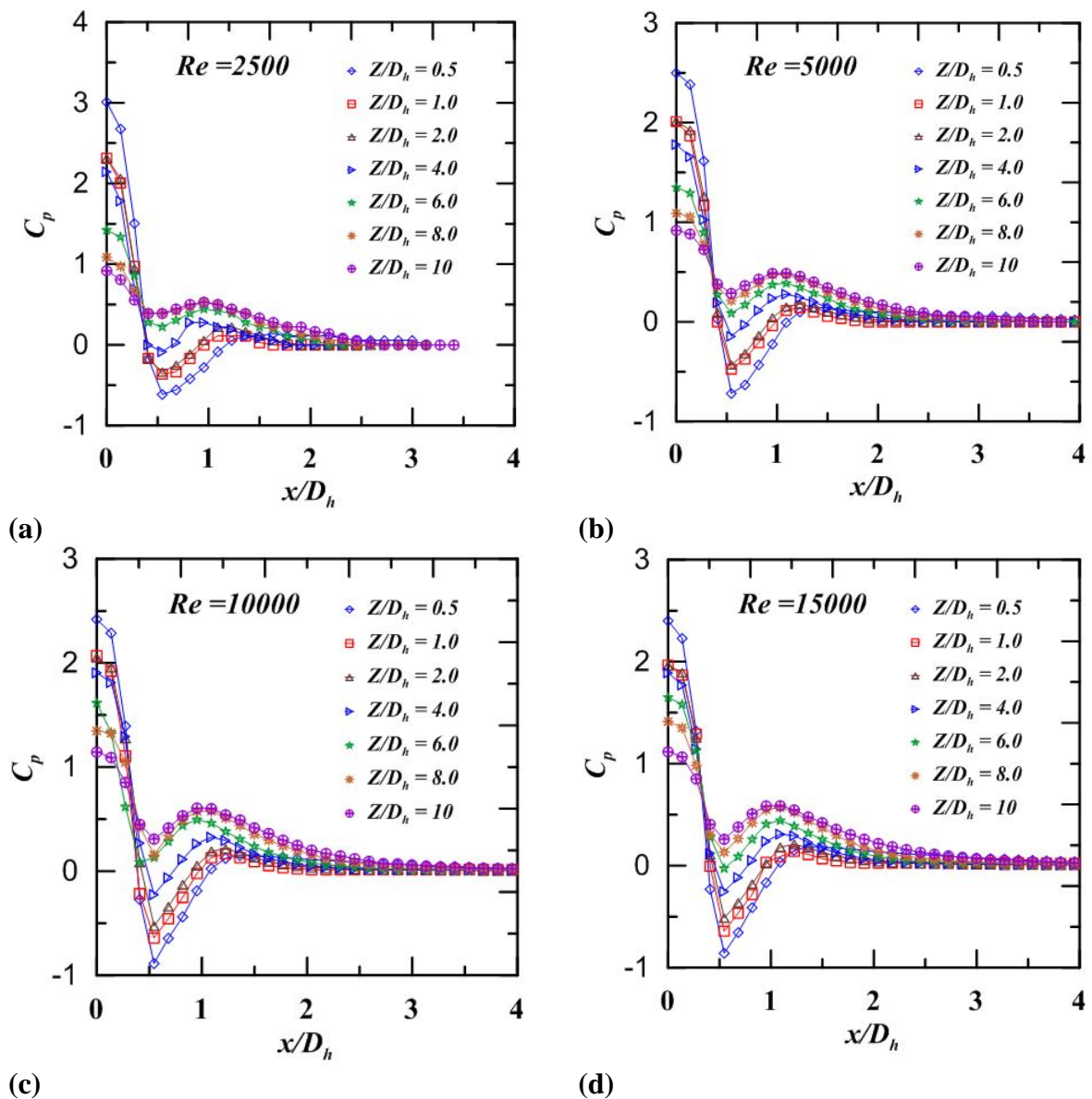


Fig 6.3 Variation of “wall static pressure” along the “streamwise direction” of various Z/D_h at “Reynolds number” 2500 to 20000 for 4mm rib and $L_c/D_h=10.2$.

at all J2P spacing. Stagnation wall static pressure decreases with an increase in Z/D_h because of entrainment of the quiescent air and increase in the spread of the jet leading to the weak core of the jet.

The negative pressure region is occurs at $x/D_h=0.28$ due to flow acceleration below the rib and flow recirculation from confinement plate. The negative pressure region vanishes at $Z/D_h>4$ due to the passing of jet at the outer periphery of rib, the secondary peaks of wall static pressure is observed for all “Reynolds number”, the height the secondary peaks rises with the rise in Z/D_h distance. The positive pressure gradient (secondary peak) shows the separation of the jet from the wall surface.

There is an increase in the values of the negative pressure region and secondary peaks compared to confinement ratio of 6.8. The reason may be the increase flow recirculation due increase length of confinement, which plays a significant role in the formation of negative pressure region.

6.4.3 Influence of Z/D_h on “wall static pressure” distribution for various “Reynolds number” along the “streamwise direction” for 4mm rib and confinement ratio (L_c/D_h) of 13.6

Figures 6.4(a) to (b) show the variation of local WSP, along the stream-wise direction for the J2P spacing (Z/D_h) 0.5-10 and at the “Reynolds number” varying from 2500 to 20000 with 4mm rib and confinement ratio (l_c/D_h) =13.6. The maximum WSP occurred at “stagnation point” for all “Reynolds number” at the J2P spacing. Stagnation WSP decreases with an increase in the J2P spacing. The negative pressure region occurs up to $Z/D_h=2$ due to increase in confinement length more amount of fluid re-circulates and breaks down the potential core and weakens the strength of jet. The lower secondary peaks of WSP observed compare to 6.8 and 10.2 confinement ratios due to flow restriction by increase length of confinement

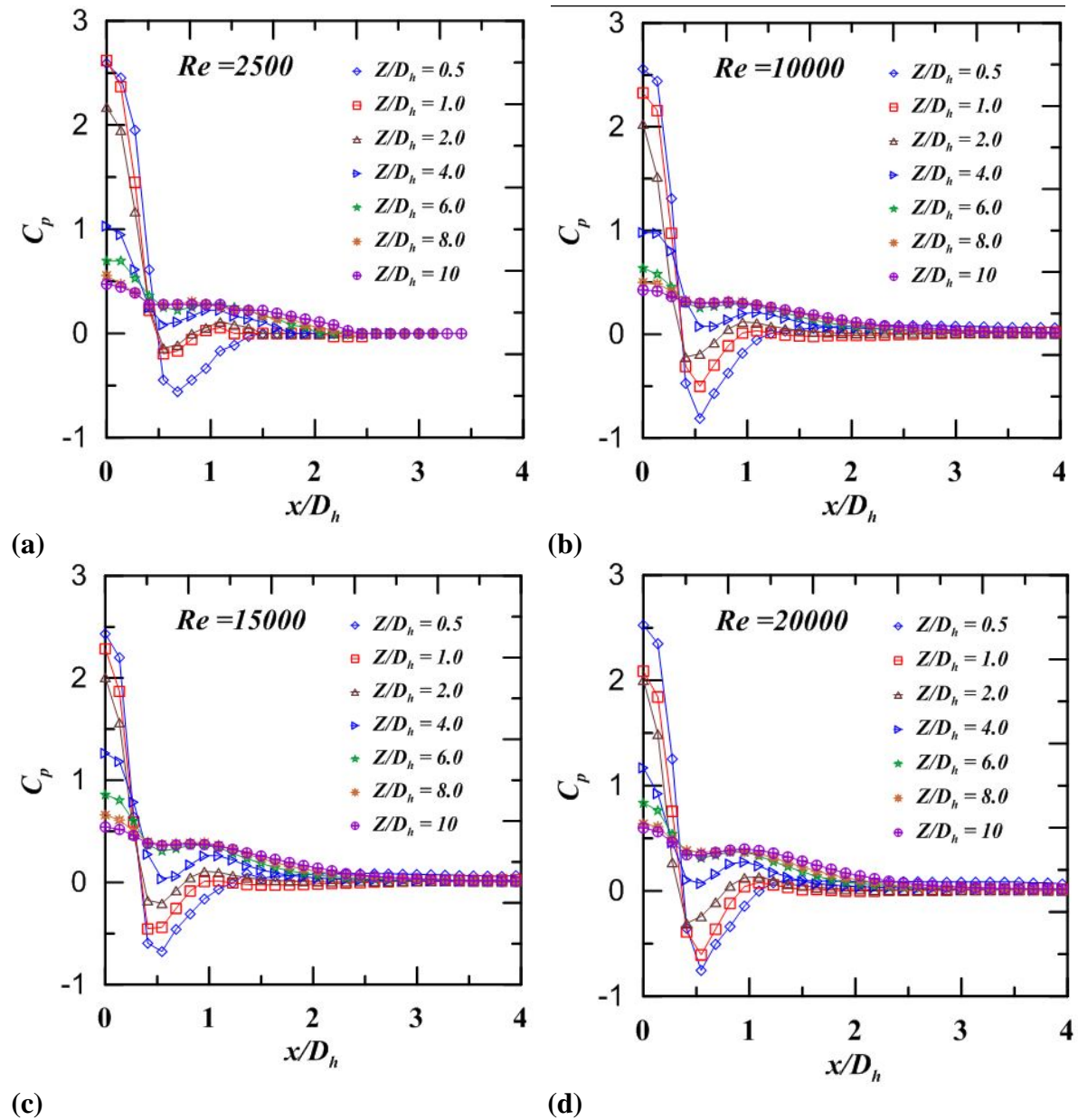


Fig 6.4 Variation of “wall static pressure” along the “streamwise direction” of various Z/D_h at “Reynolds number” 2500 to 20000 for 4mm rib and $L_c/D_h=13.6$.

6.4.4 Influence of Z/D_h on “wall static pressure” distribution for various “Reynolds number” along the “streamwise direction” for 6mm rib and confinement ratio (L_c/D_h) of 6.8

Figures 6.5 (a) to (d) shows a variation of the local WSP along the stream-wise direction for the J2P spacing of 0.5-10 at “Reynolds numbers” 2500 to 20000 with 6mm rib and confinement ratio 6.8. The negative pressure region increases with “Reynolds number” at lower Z/D_h values and the secondary peaks observed for all Z/D_h values and all the “Reynolds numbers”

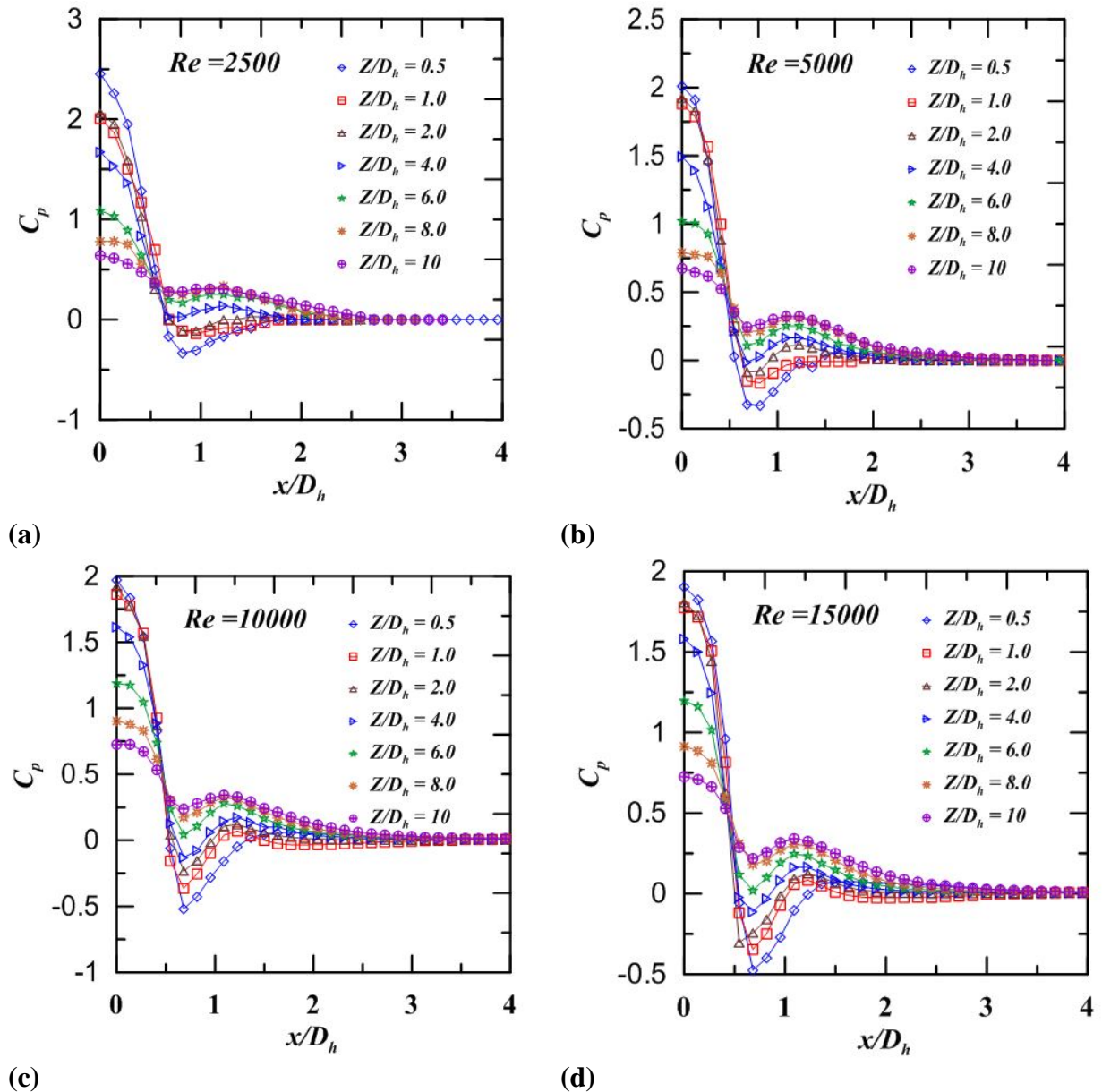


Fig 6.5 Variation of “wall static pressure” along the “streamwise direction” of various Z/D_h at “Reynolds number” 2500 to 20000 for 6mm rib and $L_c/D_h=6.8$

6.4.5 Influence of Z/D_h on “wall static pressure” distribution for various “Reynolds number” along the “streamwise direction” for 6mm rib and confinement ratio (L_c/D_h) of 10.2

Fig 6.6 (a) to (d) shows a variation of the local WSP along the stream-wise direction for the J2P spacing of 0.5-10 at “Reynolds numbers” 2500 to 20000 with 6mm rib and confinement ratio 10.2. The maximum WSP occurred at centerline of the jet at all Z/D_h values for all “Reynolds number”. The negative pressure region begins at $x/D_h = 0.28$. The secondary peaks occurred at all Z/D_h values and increase with an increase in Z/D_h .

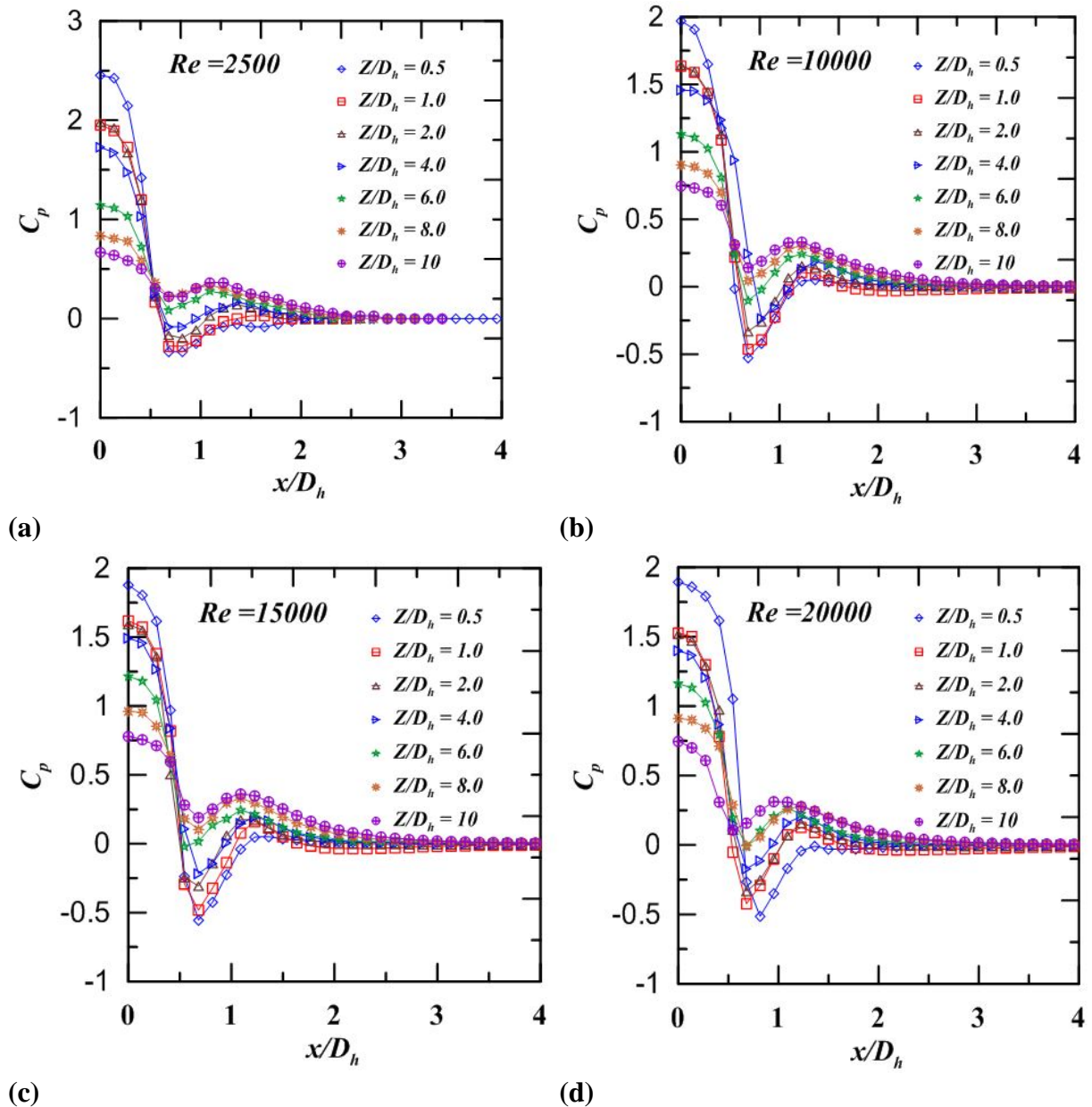


Fig 6.6 Variation of “wall static pressure” in the “streamwise direction” of various Z/D_h at “Reynolds number” 2500 to 20000 for 6mm rib and $L_c/D_h=10.2$.

6.4.6 Influence of Z/D_h on “wall static pressure” distribution for various “Reynolds number” along the “streamwise direction” for 6mm rib and confinement ratio (L_c/D_h) of 13.6

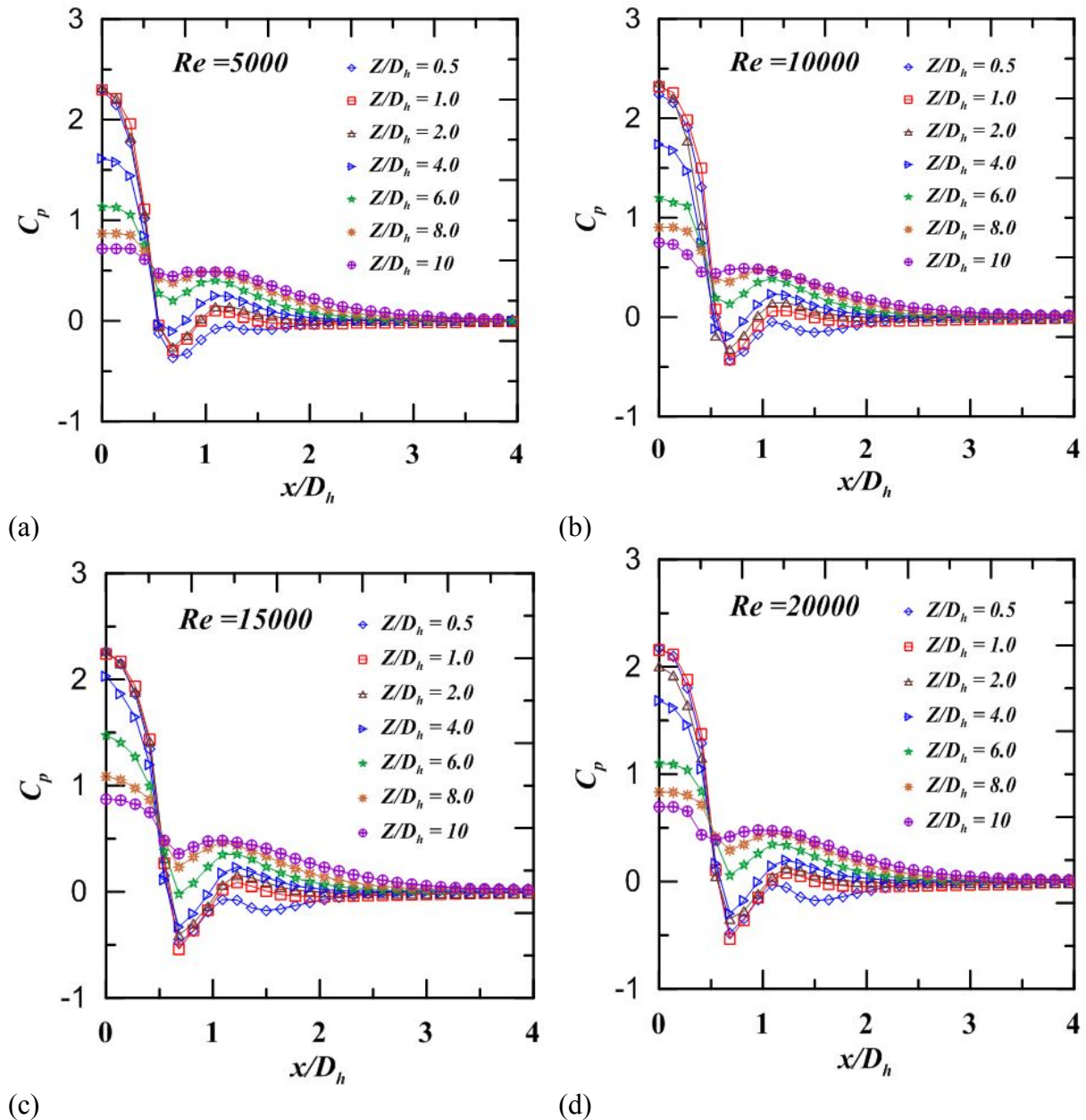


Fig 6.7 Variation of “wall static pressure” along the “streamwise direction” of various Z/D_h at “Reynolds number” 2500 to 20000 for 6mm rib and $L_c/D_h=13.6$.

Fig 6.7 (a) to (d) shows the distribution of local WSP along the stream-wise direction of Z/D_h 0.5 to 10 at “Reynolds number” 2500 to 20000 for 6mm rib and confinement ratio 13.6. The strength of the negative pressure region and secondary peaks decreases due increase length of confinement plate that increases the rate of recirculation of fluid that breaks down the potential core.

6.4.7 Influence of J2P spacing on “stagnation point wall static pressure” for different Rib and confinement configurations.

From Fig 6.8 (a) to (f) shows the variation of stagnation WSP (C_{p0}) with J2P spaces of all “Reynolds number” for different rib widths and confinement ratios.

The laminar flow ($Re = 2500$) exhibits higher Cp_0 values up to potential core compare to turbulent flows ($Re = 5000$ to 20000). behind potential core $Re = 15000$ shows the better value of Cp_0 for all configuration studied.

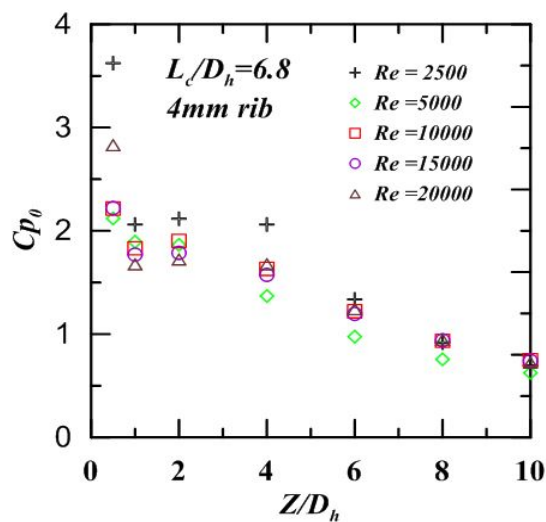
From figures, it is observed that stagnation WSP (Cp_0) increases with “Reynolds number” along with an increase in confinement length beyond the potential core.

It is observed that at lower $Re = 2500$, $L_c/D_h = 6.8$ show higher values of “stagnation point” WSP.

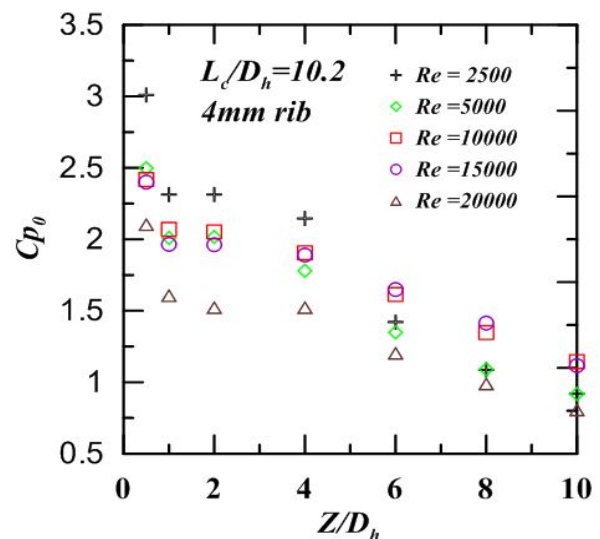
At $Re = 5000$ to 20000 The $L_c/D_h = 13.6$ shows higher value for Cp_0 within the PCR and confinement ratio $L_c/D_h = 10.2$ provides better values beyond potential core region.

The maximum stagnation WSP occurred for confined ribbed surface compare confined smooth surface. The negative pressure region occurred up to $Z/D_h = 4$ for the confined ribbed surface, $Z/D_h = 0.5$ for the confined smooth surface.

It clear that the strength of negative pressure region depends on the ribbed configuration at $Z/D_h > 0.5$, and secondary peaks observed for confined ribbed configuration and peaks height increases with the increment in Z/D_h . The spreading rate of a confined smooth jet is relatively larger than ribbed and confined.



(a)



(b)

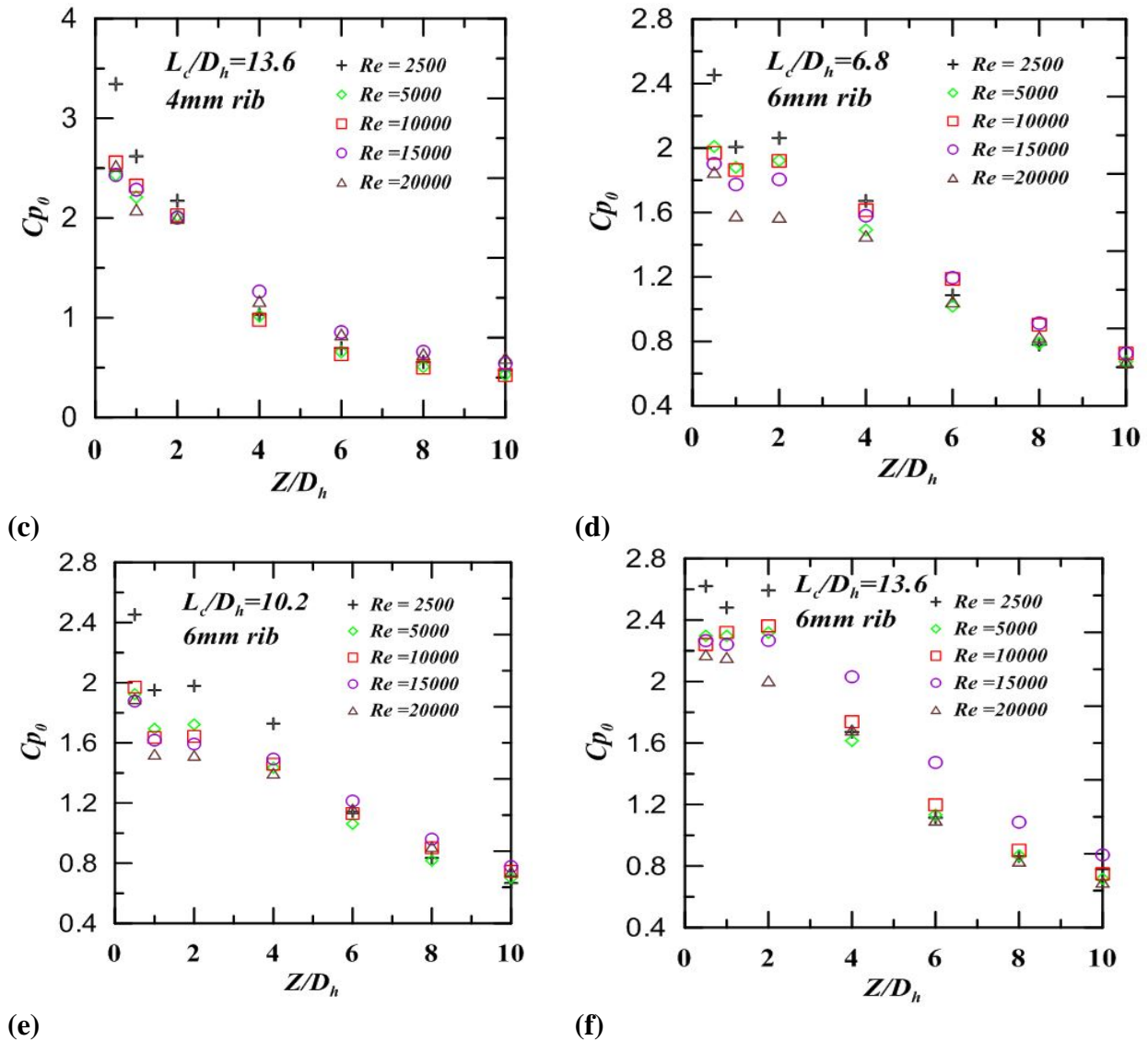


Figure 6.8 Variation of Cp_0 for the different J2P spacing at various “Reynolds number” for a rough surface.

6.5 COMPARISON OF FLUID FLOW CHARACTERISTICS OF CONFINED SMOOTH AND CONFINED ROUGH SURFACE

6.5.1 Influence surface roughness and confinement on wall static pressure distribution at $Re=2500$

Figures 6.9 (a) to (f) show the variation of local WSP along the “streamwise direction” for a given Z/D_h value at $Re=2500$ with different confinement ratios and with the ribs of 4mm and 6mm. From the various observations, it is found that 4mm rib with confinement ratio of 6.8 shows maximum SP WSP and the subatmospheric region at $Z/D_h=0.5$, subatmospheric region, and secondary peaks are dependent on the Z/D_h value.

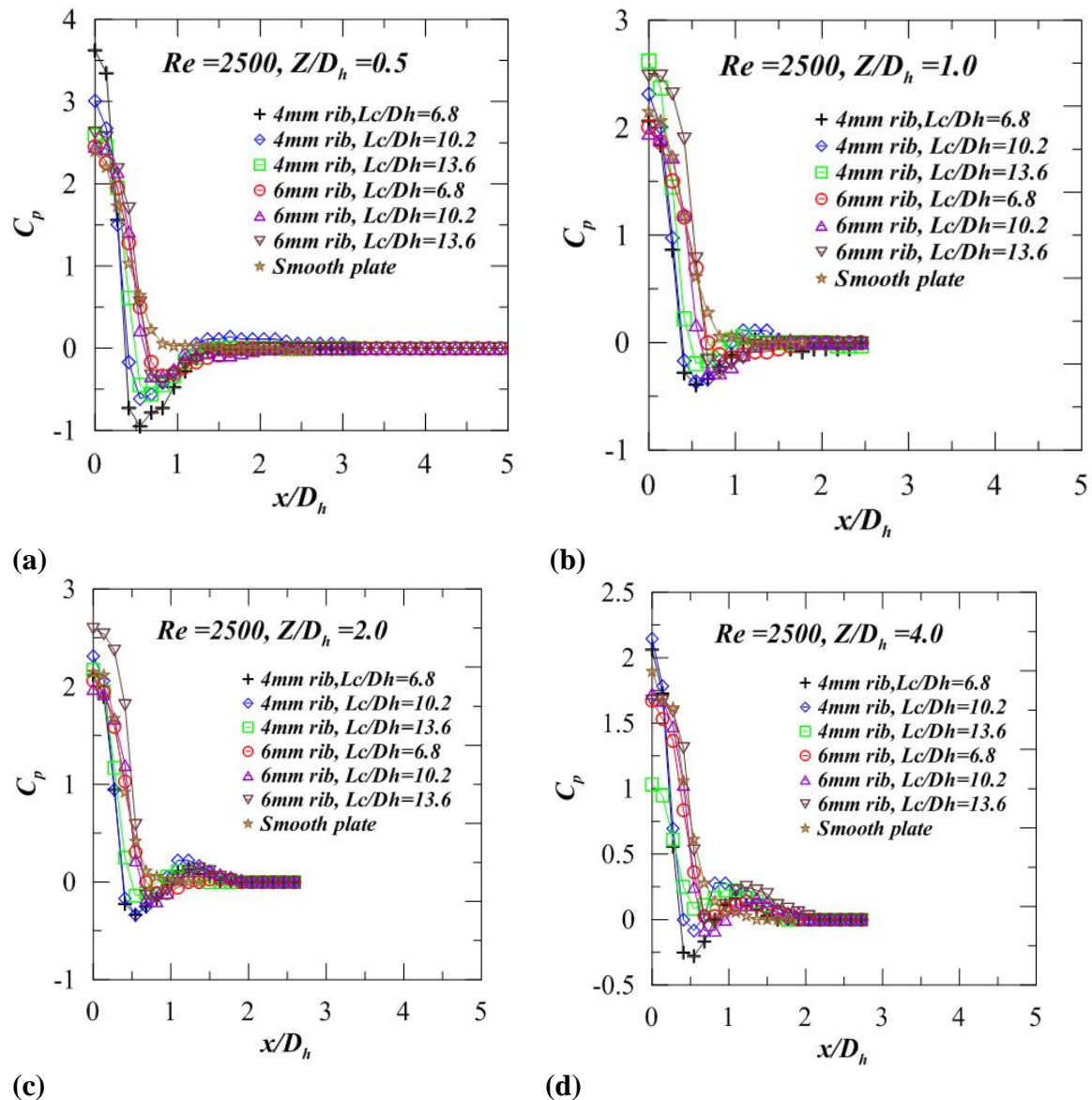


Fig 6.9 Comparison of “wall static pressure” of different width and confinement ratios

Influence of Confinement on the smooth and rough surface (4mm rib)

Figures 6.10 (a) to (f) show the effect of confinement ratios on variations of local WSP along the stream-wise direction of the smooth surface and rough surface (4mm rib) for various $J2P$ spacing. It can be observed from the graphs that confined and ribbed surface records the maximum value for C_{p0} in comparison to a confined smooth surface. The negative pressure region occurs up to $Z/D_h = 4$ for the confined ribbed surface and only at $Z/D_h = 0.5$ for the confined smooth surface.

From the results we can understand that the strength of the negative pressure region depends on the rib configuration at $Z/D_h > 0.5$, and secondary peaks observed for confined ribbed configuration and C_{p0} peaks with an increase in L_c/D_h . The spreading rate of the confined smooth jet is greater than the ribbed and confined.

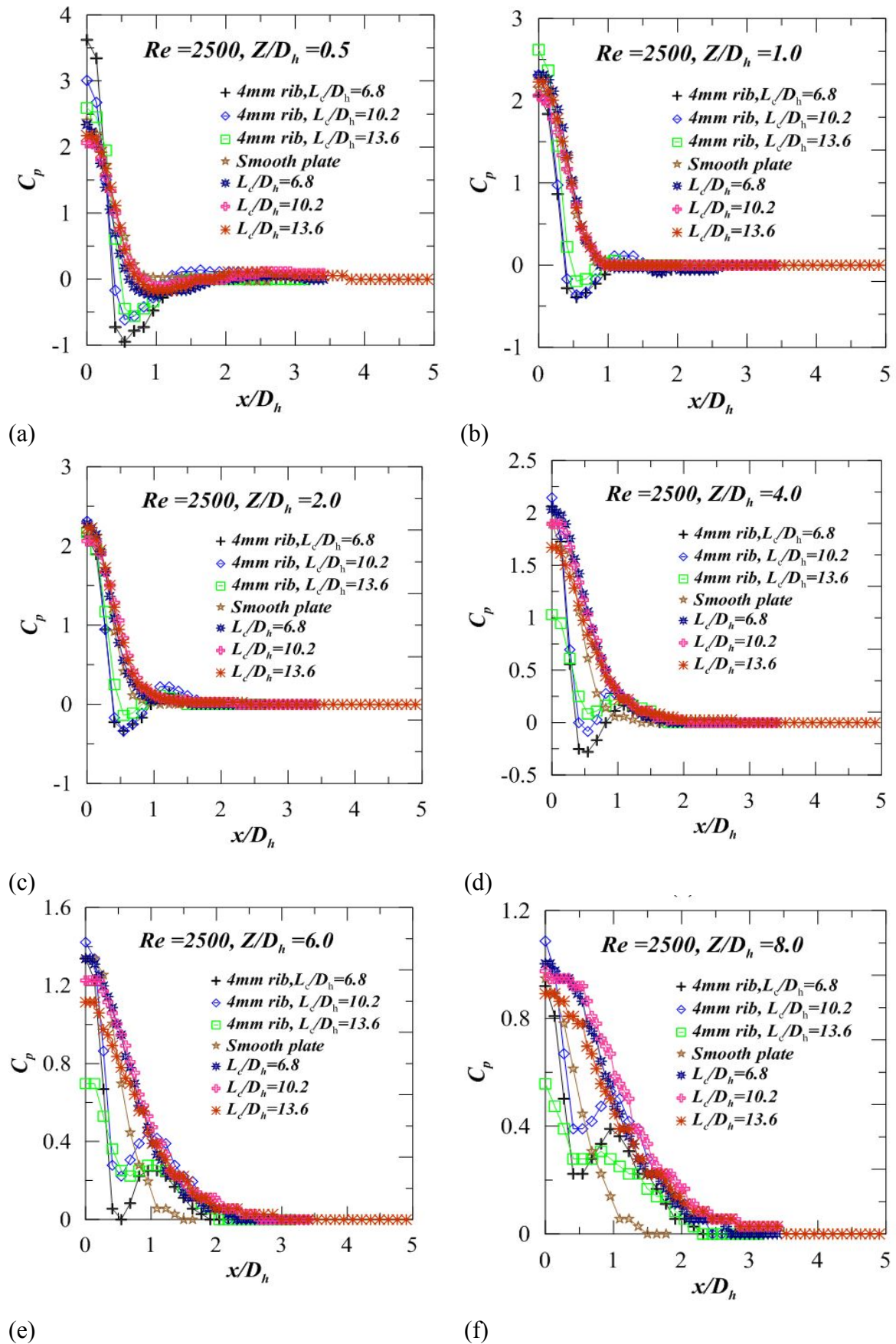


Fig 6.10 Effect of confinement on the wall static pressure coefficient over the smooth and rough surface (4mm rib) at $Re = 2500$ for various J2P distances

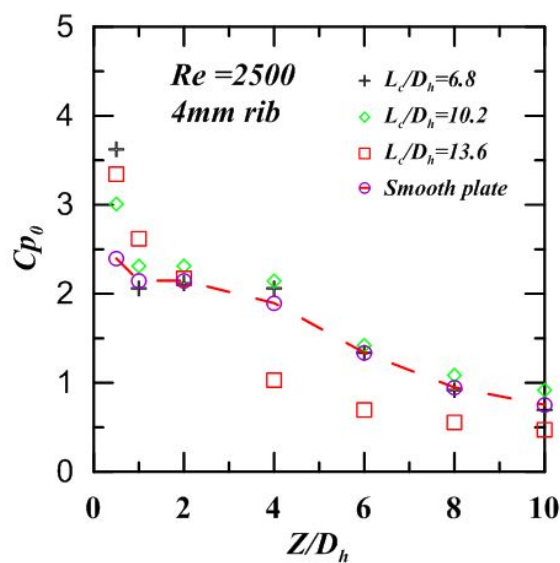
6.5.2 Influence of confinement ratio on “stagnation point wall static pressure”

Figures 6.11(a) to 6.11(e) show the variation of “stagnation point” WSP with Z/D_h for different confinement ratios for 4mm rib. At lower Reynolds, number $L_c/D_h=6.8$ shows better values. It is observed that at lower $Re=2500$, $L_c/D_h=6.8$ show higher values of “stagnation point” WSP.

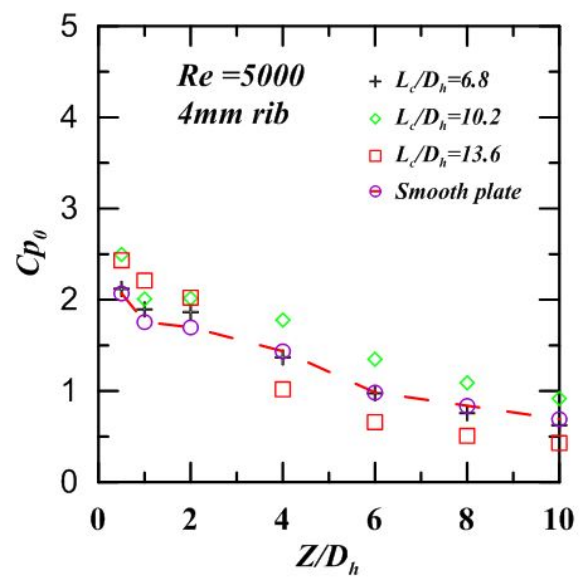
At $Re = 5000$ to 20000 The $L_c/D_h=13.6$ shows higher value for Cp_0 within the PCR and confinement ratio $L_c/D_h=10.2$ provides better values beyond potential core region.

The maximum stagnation WSP occurred for confined ribbed surface compare confined smooth surface. The negative pressure region occurred up to $Z/D_h=4$ for the confined ribbed surface, $Z/D_h=0.5$ for the confined smooth surface.

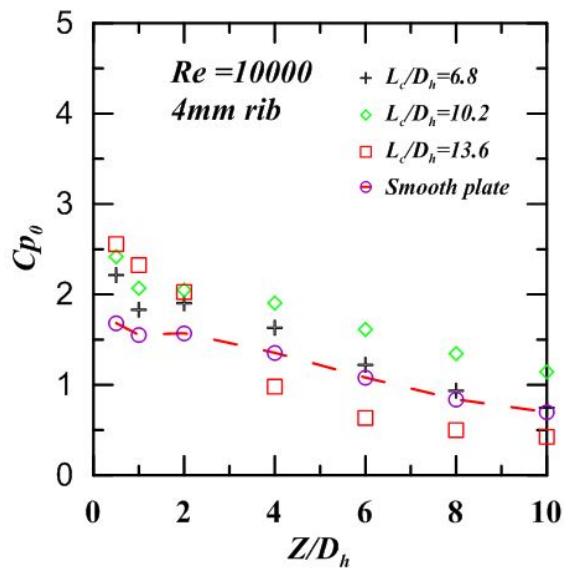
It clear that the strength of negative pressure region depends on the ribbed configuration at $Z/D_h > 0.5$, and secondary peaks observed for confined ribbed configuration and peaks height increases with the increment in Z/D_h . The spreading rate of a confined smooth jet is relatively larger than ribbed and confined.



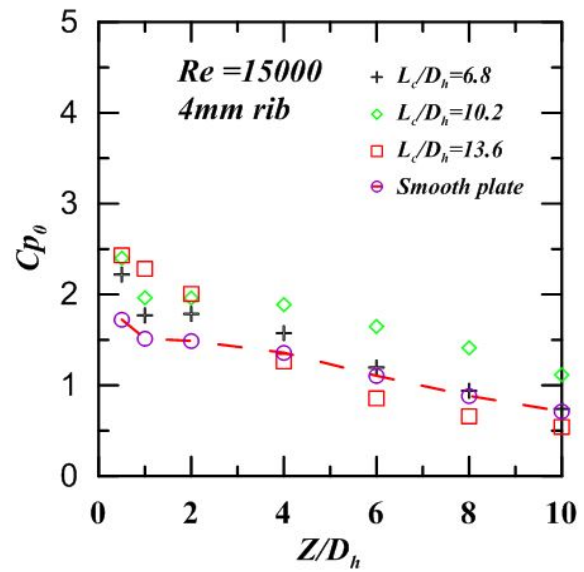
(a)



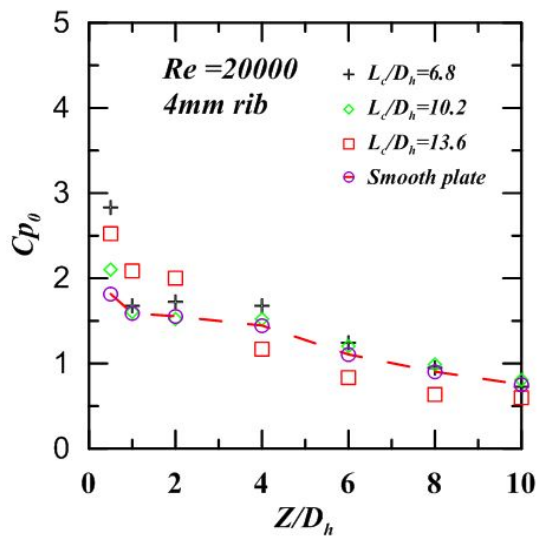
(b)



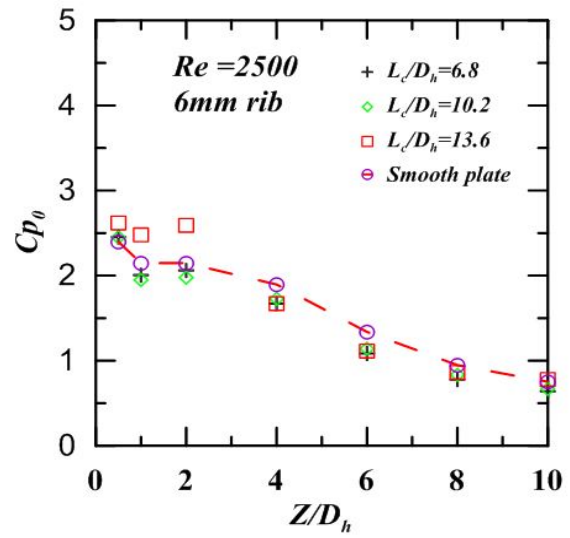
(c)



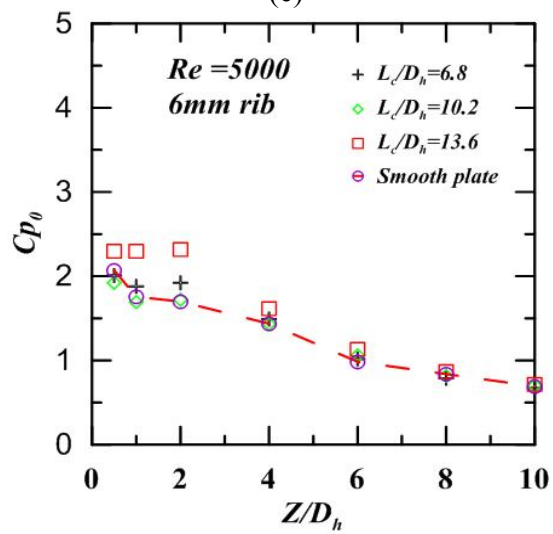
(d)



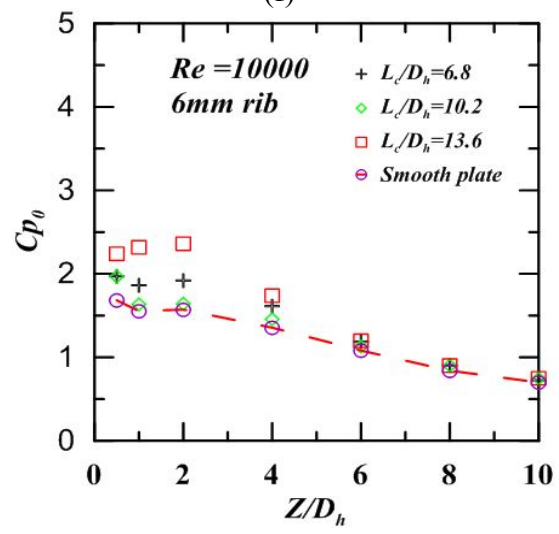
(e)



(f)



(g)



(h)

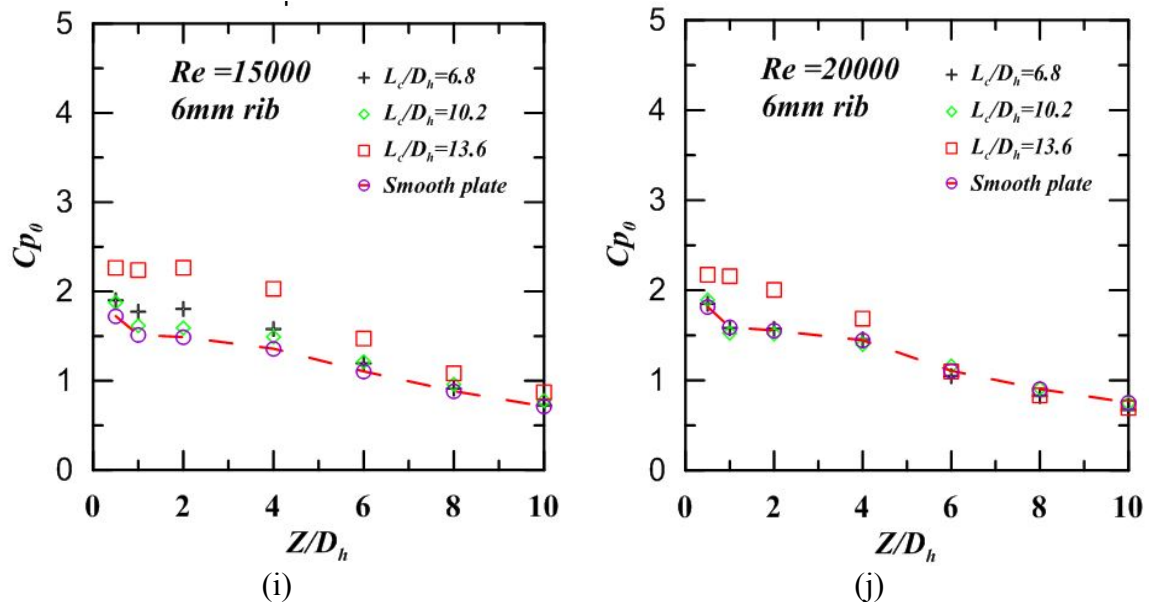


Fig 6.11 Influence of confinement ratio on stagnation point wall static pressure with 4 mm rib at various Reynolds numbers

At $Re = 5000$ to 20000 The $L_c/D_h = 13.6$ shows higher stagnation WSP within the PCR and $L_c/D_h = 10.2$ shows better values behind potential core region.

Figures 6.11(f) to 6.11(j) show the variation of Cp_0 with Z/D_h for different confinement ratio (L_c/D_h) for the surface with 6mm rib. The $L_c/D_h = 13.6$ gives better Cp_0 values at $Z/D_h < 4$ i.e. in the PCR region. After potential core ($Z/D_h > 4$), the Cp_0 values of all configurations is almost comparable with the smooth surface.

6.6 “Heat transfer” study on a Confined rough surface

Heat transfer characteristics of an impinging jet can be understood better if the regions on the “Target plate” i.e., Stagnation region, Transition region, and wall jet region are properly identified. The centerline velocity of the impinging jet is highest at the nozzle exit and reduces to zero at the point of impact on the target surface which is the stagnation point. At the stagnation point, the WSP is maximum and higher than the atmospheric pressure. This results in a favorable pressure gradient along the direction parallel to the target surface in the stagnation region. Finally, the flow over the target surface forms the wall jet region the wall jet adheres to the surface and flows over the plate interacting with the surrounding air. The jet flows from the stagnation region to wall jet region through the transition region where the boundary layer changes from laminar to turbulent.

6.6.1 Influence of “Reynolds number” on the local distribution of “Nusselt number” with 4mm rib and $L_c/D_h = 6.8$

Figures 6.12 (a) to 6.12 (h) show the lateral variation of “Nusselt number” for the various J2P spacing with rib of width 4mm rib and confinement ratio 6.8.

The graph indicates that the Nu is a function of Z/D_h at a given “Reynolds number”. For any given Z/D_h the “Nusselt number” is higher at the “stagnation point” and gradually decreases in the “streamwise direction”. The “Nusselt number” is high for the J2P spacing of Z/D_h 4.0 since at end of the PCR the increase in turbulence enhances the “heat transfer” rate and it is observed for all range of “Reynolds numbers” studied.

A secondary peak can be noticed for all J2P spaces due to the flow acceleration under the rib and the influence of confinement over the flow behaviour of the jet.

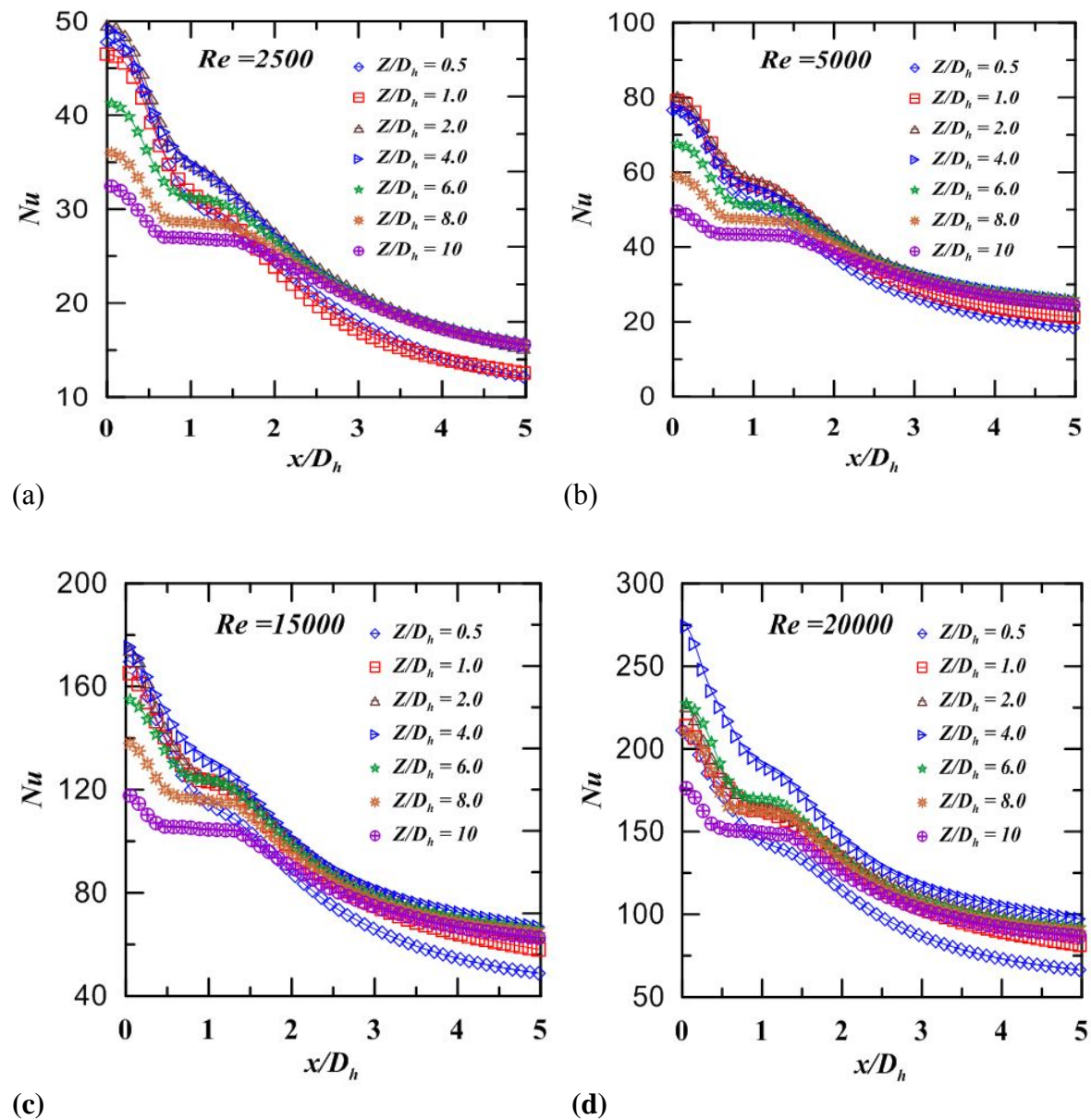


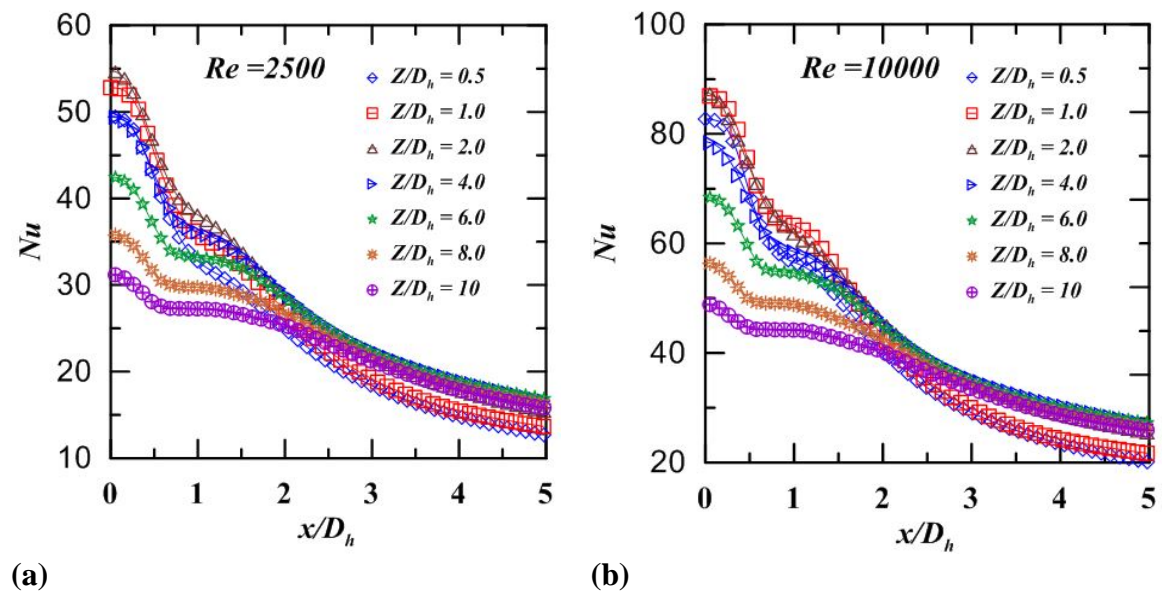
Figure 6.12 Lateral variation of “Nusselt number” for the different J2P spacing (Z/D_h) at $Re = 2500$ to 20000 for confined rough surface (4mm rib, $L_c/D_h = 6.8$)

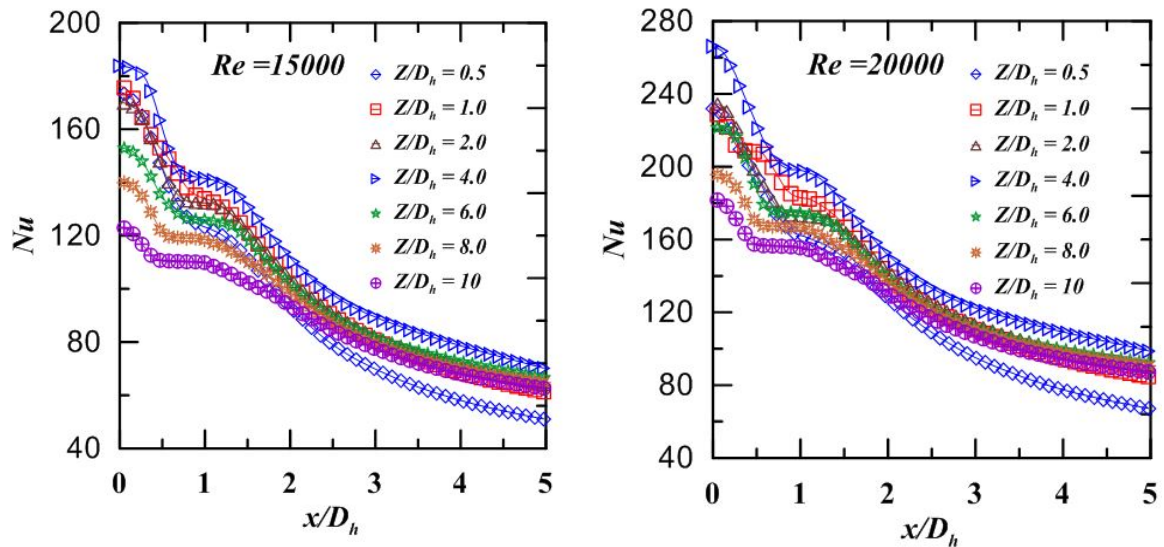
6.6.2 Effect of “Reynolds number” on the local distribution of the “Nusselt number” of 4mm rib and $L_c/D_h=10.2$ configuration

Figures 6.13(a) to (d) show the lateral variation of “Nusselt number” for the different J2P spacing for “Reynolds number” ranging from 2500 to 20000 for 4mm rib and confinement ratio 10.2.

From figures, the maximum “Nusselt number” is visible up to $Z/D_h=2$ for “Reynolds number” 10000 and increases in “Reynolds number” maximum point of “Nusselt number” shift to $Z/D_h=4$ (end of the potential core). The secondary peaks observed for all Z/D_h values of “Reynolds number” because of the acceleration of the flow under the rib. The strength of secondary peaks increases with Z/D_h and decreases with increase in “Reynolds number”.

The “Nusselt number” increases with the “Reynolds number” due to increase in the momentum of the jet with Re and the peak value of “Nusselt number” is recorded at “Reynolds number” of 20000.

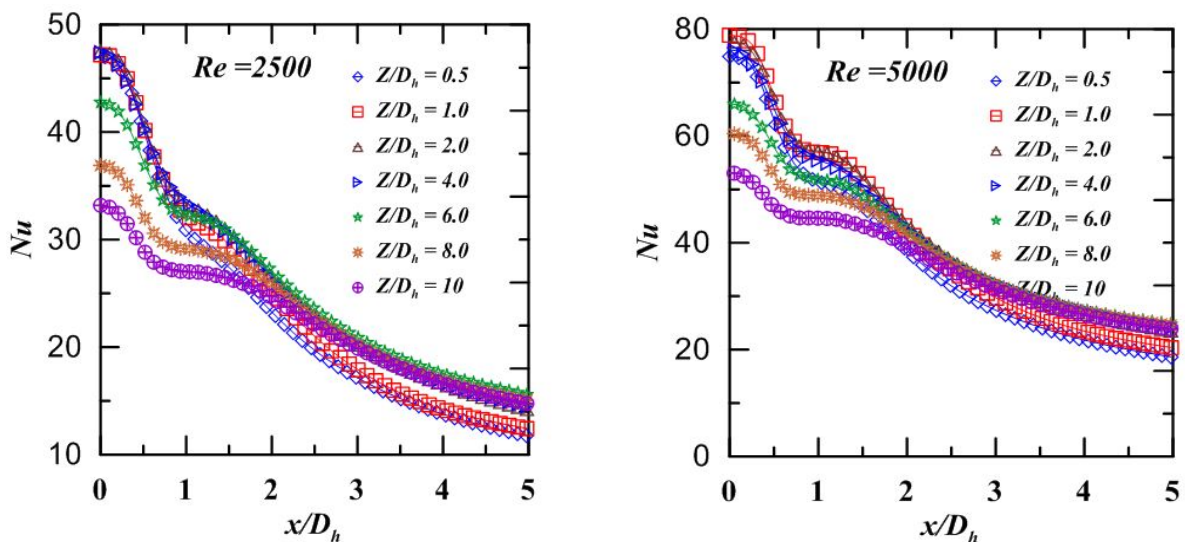


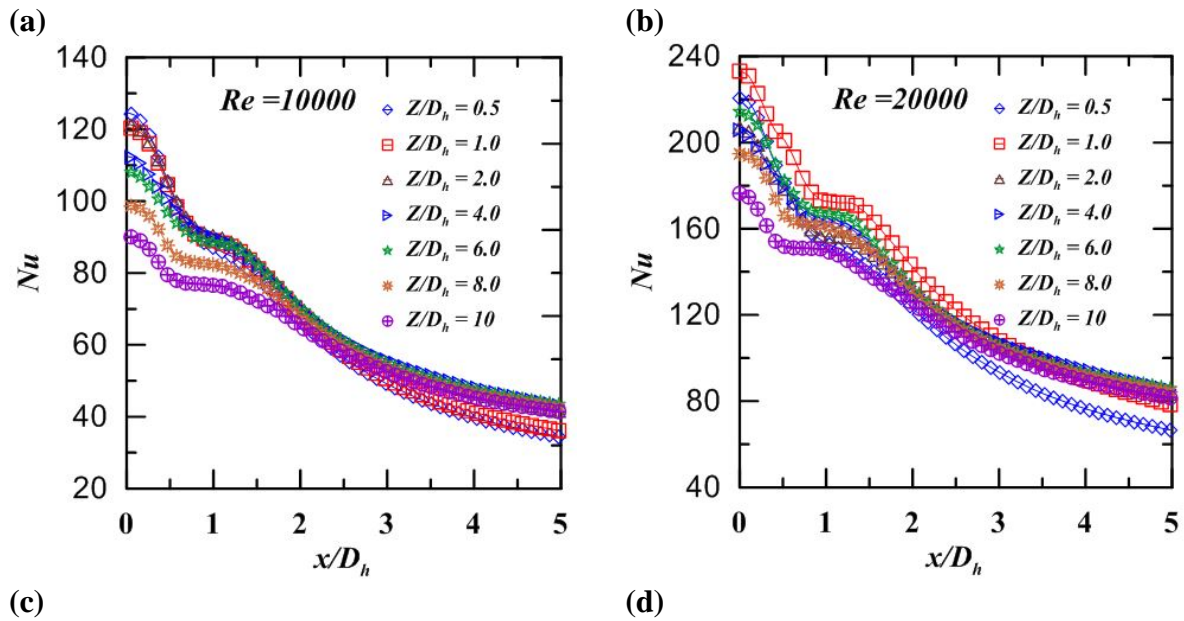


(c) (d)
Figure 6.13 Lateral distribution of “Nusselt number” for the different J2Pspacing (Z/D_h) at $Re = 2500$ to 20000 for confined rough surface (4mm rib, $L_c/D_h = 10.2$)

6.6.3 Influence of “Reynolds number” on the local distribution of the “Nusselt number” of 4mm rib and $L_c/D_h = 13.6$ configuration

Figures 6.14(a) to (d) show the lateral distribution of local Nu for different Z/D_h at “Reynolds numbers” 2500 to 20000 for 4mm rib and confinement ratio of 13.6. The maximum “Nusselt number” is observed for $Z/D_h = 0.5$ and 1.0 for all “Reynolds number” except 20000, Figure 4.3.3(d) reveals that increase in confinement ratio increases the length of PCR with an increase in the “Reynolds number”. The “Nusselt number” values at $Z/D_h = 6.0$ same Z/D_h of 0.5, 2.0 and 4.0.

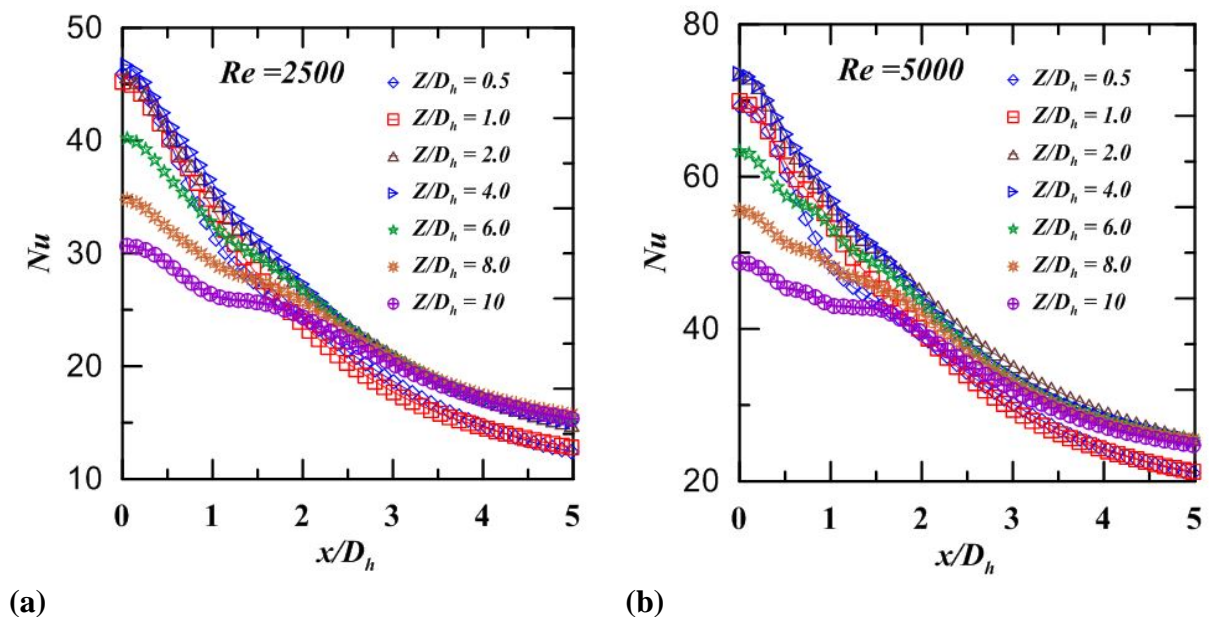




(c) (d)
Fig 6.14 Lateral distribution of “Nusselt number” for the different J2P spacing (Z/D_h) at $Re = 2500$ to 20000 for confined rough surface (4mm rib, $L_c/D_h = 13.6$)

6.7.1 Influence of “Reynolds number” on the local distribution of the “Nusselt number” of 6mm rib and $L_c/D_h = 6.8$ configuration

Figures 6.15(a) to (d) show the lateral distribution of “Nusselt number” for the different J2P placing at “Reynolds numbers” 2500 to 20000 for 6mm rib and confinement ratio 6.8. From the figure, the maximum “Nusselt number” occurs at $Z/D_h = 0.5$ invariably at all “Reynolds numbers” studied. Due to the increase in width of rib its presence not observed up to $Z/D_h = 6.0$ for “Reynolds number” up to 5000. The monotonic decreases of “Nusselt number” observed in potential core region for “Reynolds number” up to 5000.



(a)

(b)

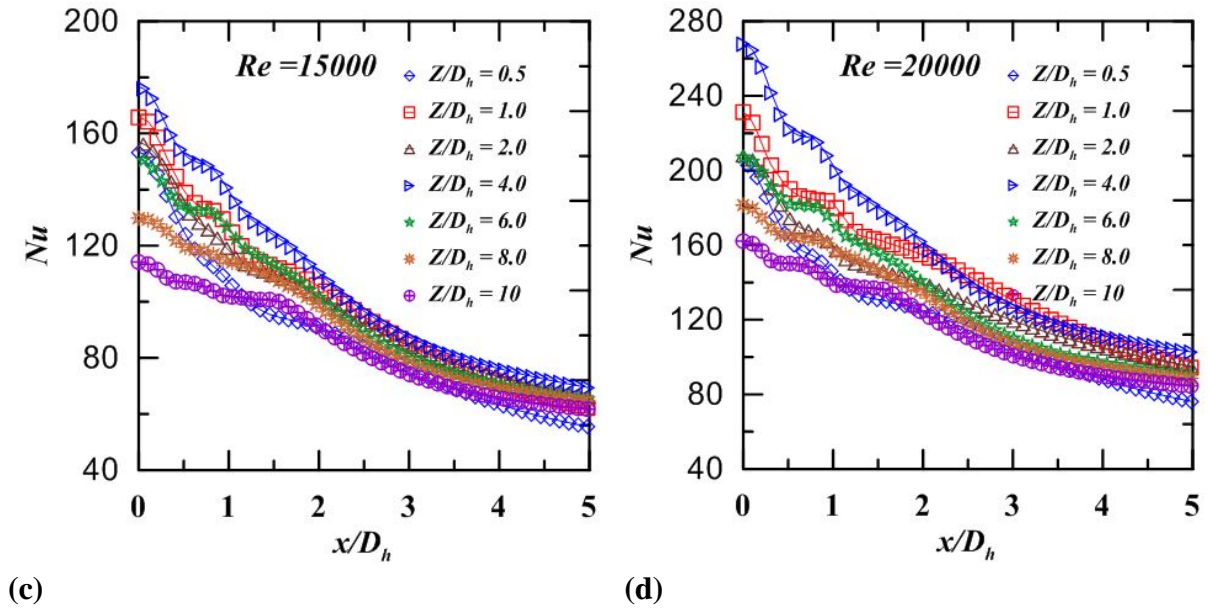
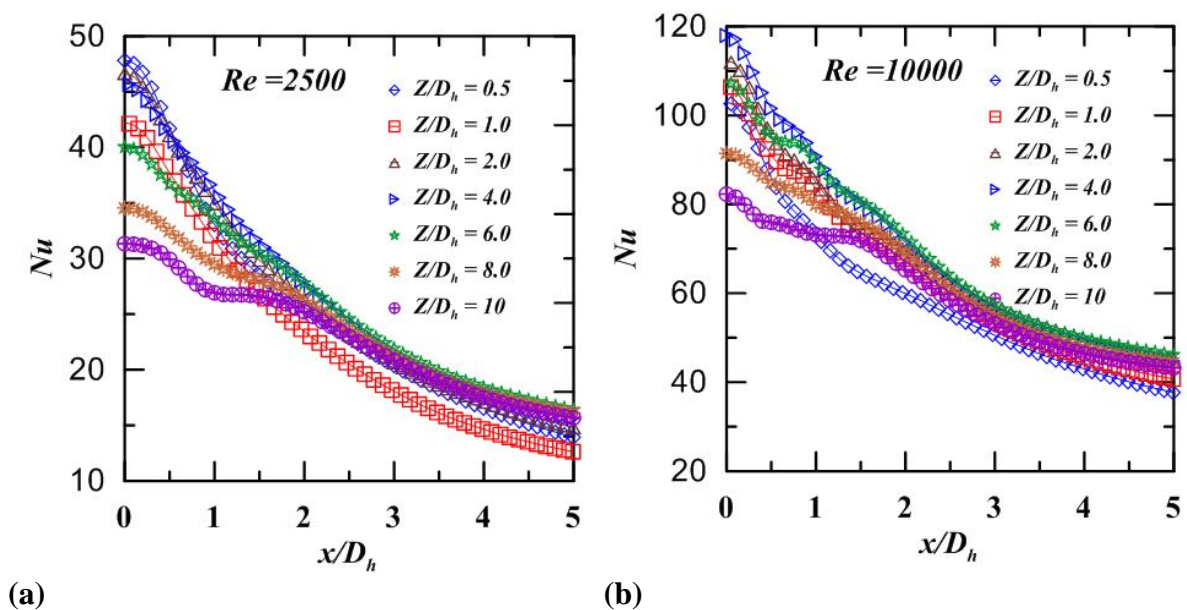


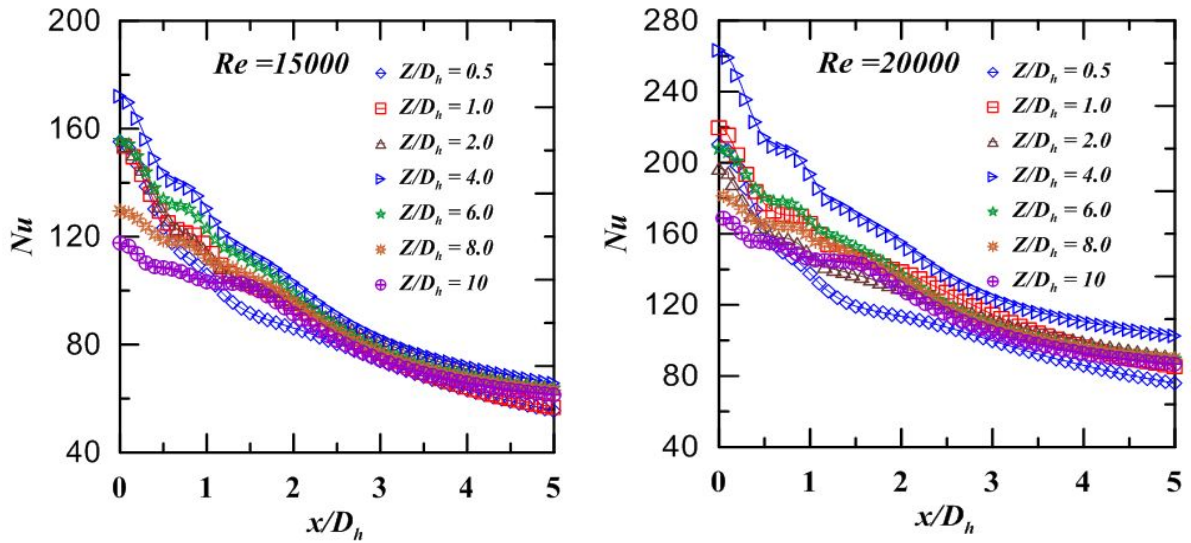
Figure 6.15 Lateral variation of “Nusselt number” for the different J2P spacing (Z/D_h) at $Re = 2500$ to 20000 for confined rough surface (6mm rib, $L_c/D_h = 6.8$)

6.7.2 Influence of “Reynolds number” on the local distribution of the “Nusselt number” of 6mm rib and $L_c/D_h = 10.2$ configuration

Fig 6.16(a) to (d) show a lateral variation of “Nusselt number” for different Z/D_h values at “Reynolds number” 2500 to 20000 for 6mm rib and confinement ratio 10.2 configurations. The maximum “Nusselt number” is recorded for $Z/D_h = 4.0$ (end of the potential core) for all “Reynolds number” studied.

The effect rib is not visible up to $Z/D_h = 6.0$ for $Re = 2500$. And potential core length increases due to the increase in confinement ratio along with an increase in “Reynolds number”. Secondary peaks observed for all Z/D_h values for $Re = 10000$ to 20000 .

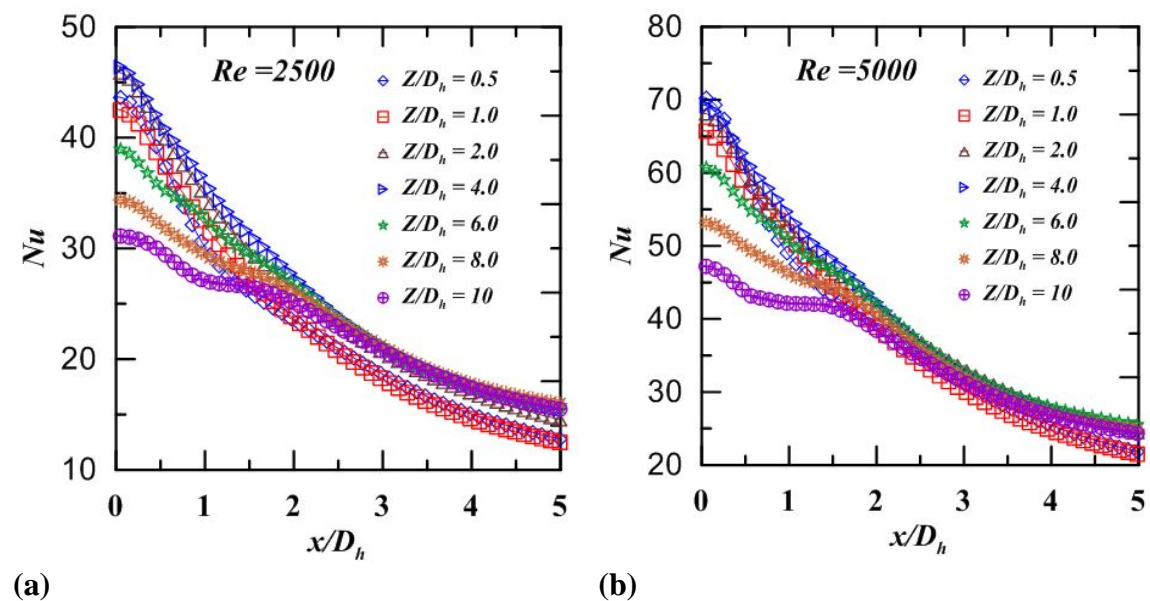




(c) (d)
Figure 6.16 Lateral variation of “Nusselt number” for the different J2P spacing (Z/D_h) at $Re = 2500$ to 20000 for confined rough surface (6mm rib, $L_c/D_h = 10.2$)

6.7.3 Influence of “Reynolds number” on the local distribution of the “Nusselt number” of 6mm rib and $L_c/D_h = 13.6$ configuration

Figures 6.17(a) to (d) show the variation of the local “Nusselt number” in the stream-wise direction for various Z/D_h values for 6mm rib and confinement ratio 13.6 configuration. The maximum “Nusselt number” can be seen for $Z/D_h = 4.0$ for all “Reynolds number”. Secondary peaks are visible at $Z/D_h = 8.0$ for $Re = 5000$. The potential core length increases with increase in “Reynolds number” and confinement ratio [Baydar and Ozmen.2006].



(a) (b)

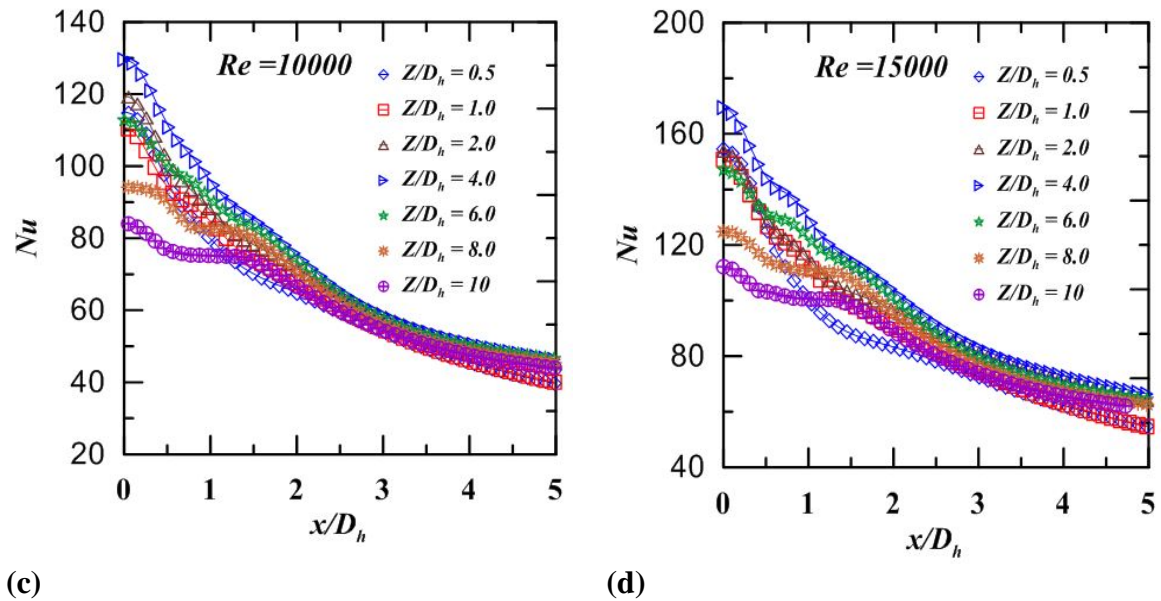
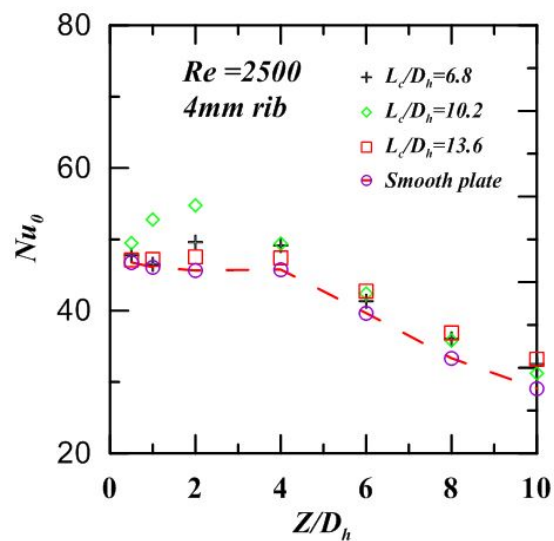


Fig. 6.17 Lateral variation of “Nusselt number” for the different J2P spacing (Z/D_h) at $Re = 2500$ to 20000 for confined rough surface (6mm rib, $L_c/D_h = 13.6$)

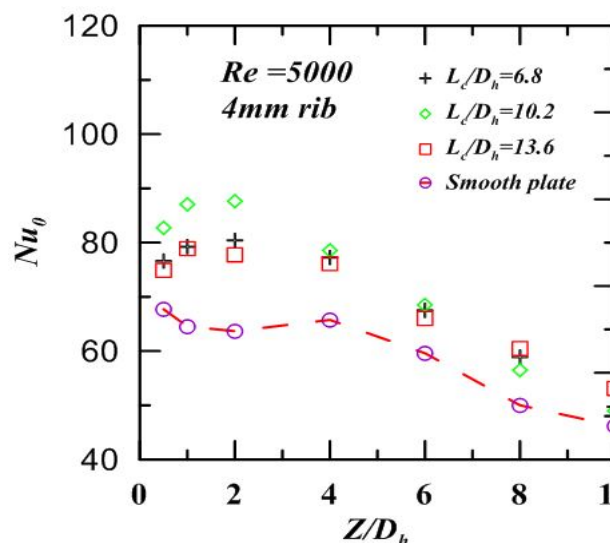
6.8 Influence of confinement ratio on stagnation “Nusselt number”

Figures 6.18(a) to (e) show the variation of $SP Nu$ with variation of Z/D_h and confinement ratio with 4mm rib mounted on the target surface. $L_c/D_h = 10.2$ shows higher values of Nu_{0up} to $Z/D_h = 6.0$ for all Reynolds numbers. All configurations show higher values of Nu_0 compare to a smooth surface.

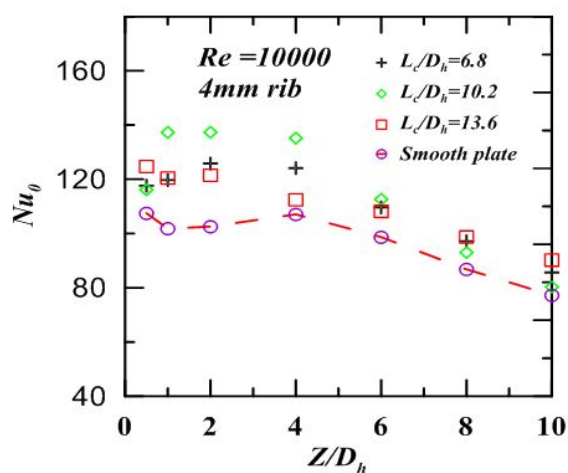
Figures 4.3.7(f) to (j) show the variation of $SP Nu$ with variation of Z/D_h and confinement ratio with 6mm rib mounted on the target surface. At $Re 2500$, $L_c/D_h = 10$ shows higher values for the Nu_0 in the potential core region and maximum value is recorded for $Z/D_h = 2$ and there is no considerable variation beyond the potential core region for all configuration in comparison with the smooth surface. Confinement ratios $L_c/D_h = 6.8$ and 13.6 shows better Nu_o values all J2P spaces.



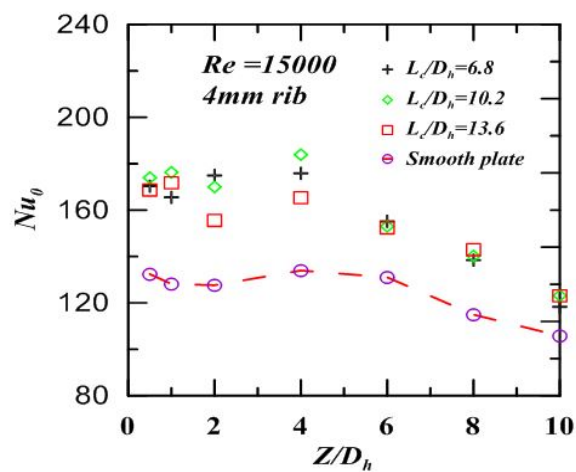
(a)



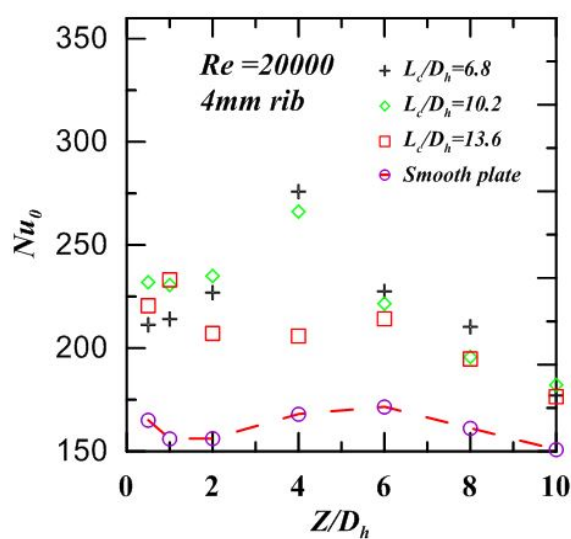
(b)



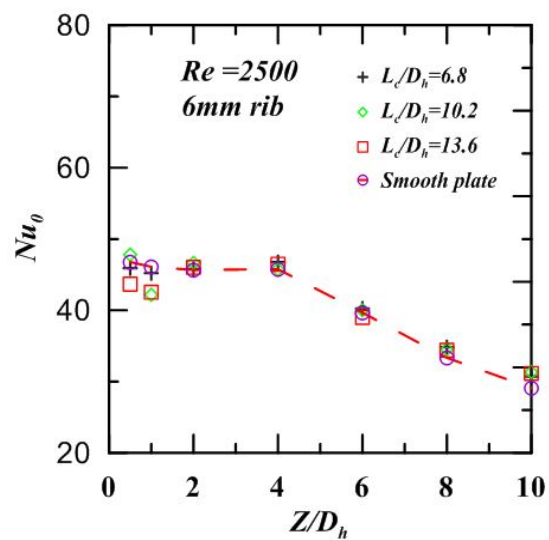
(c)



(d)



(e)



(f)

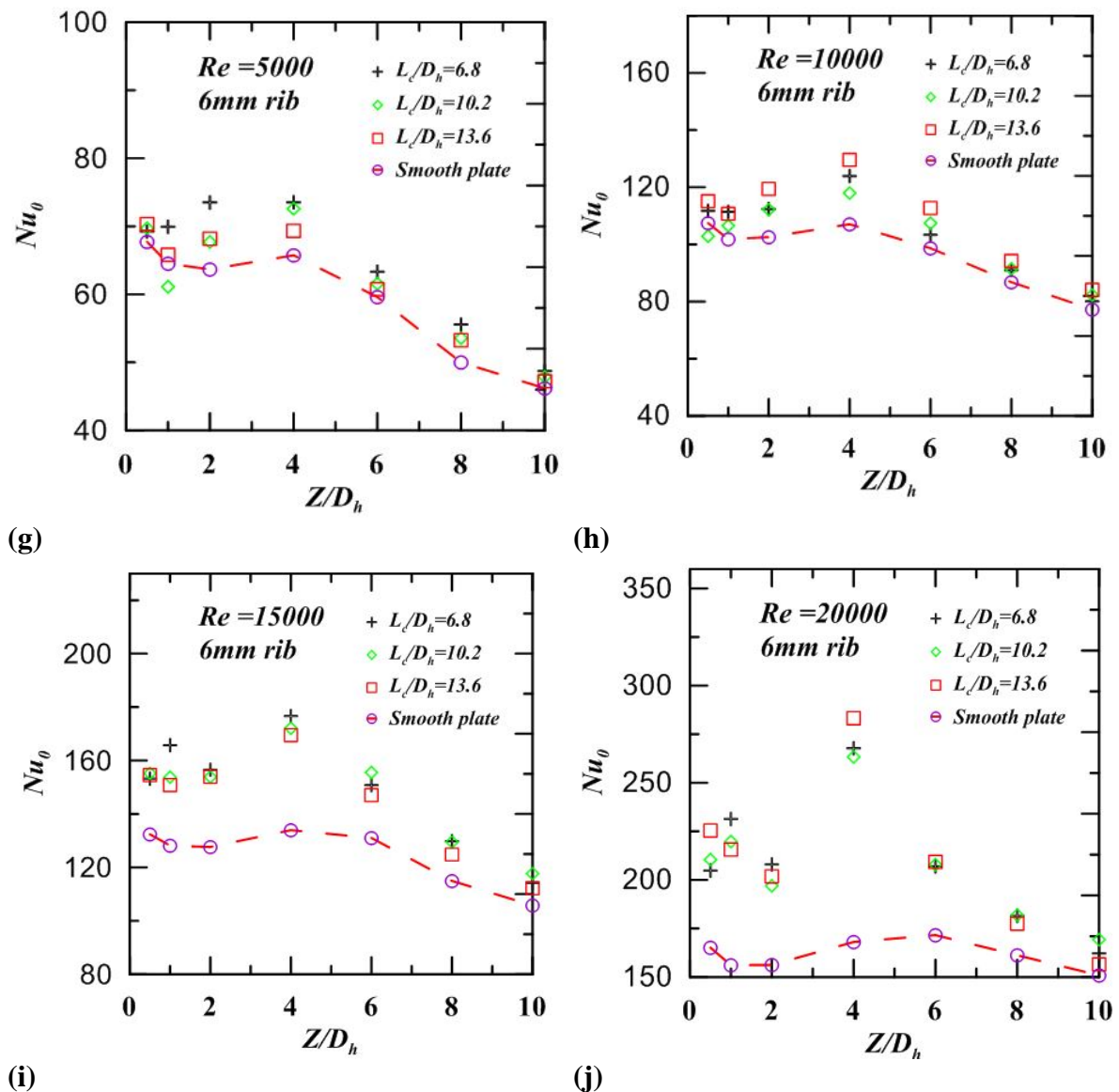


Fig 6.18 Influence of confinement ratio on “stagnation point Nusselt number” at various “Reynolds numbers” with 4mm rib and 6mm rib

6.8.1 Comparison of “Nusselt number” for different configuration at $Re=5000$

Fig. 6.19 (a to d) shows a variation in the Nu along the “streamwise direction” for various configurations for “Reynolds number” 5000. 4mm rib with 10.2 confinement ratio shows the higher value of the Nu in the stagnation region compared to all other configurations. The confined rough surface shows higher values than the unconfined smooth surface for all J2P spaces studied. Increase in the J2P spacing all confined ribbed configuration shows nearly the same results.

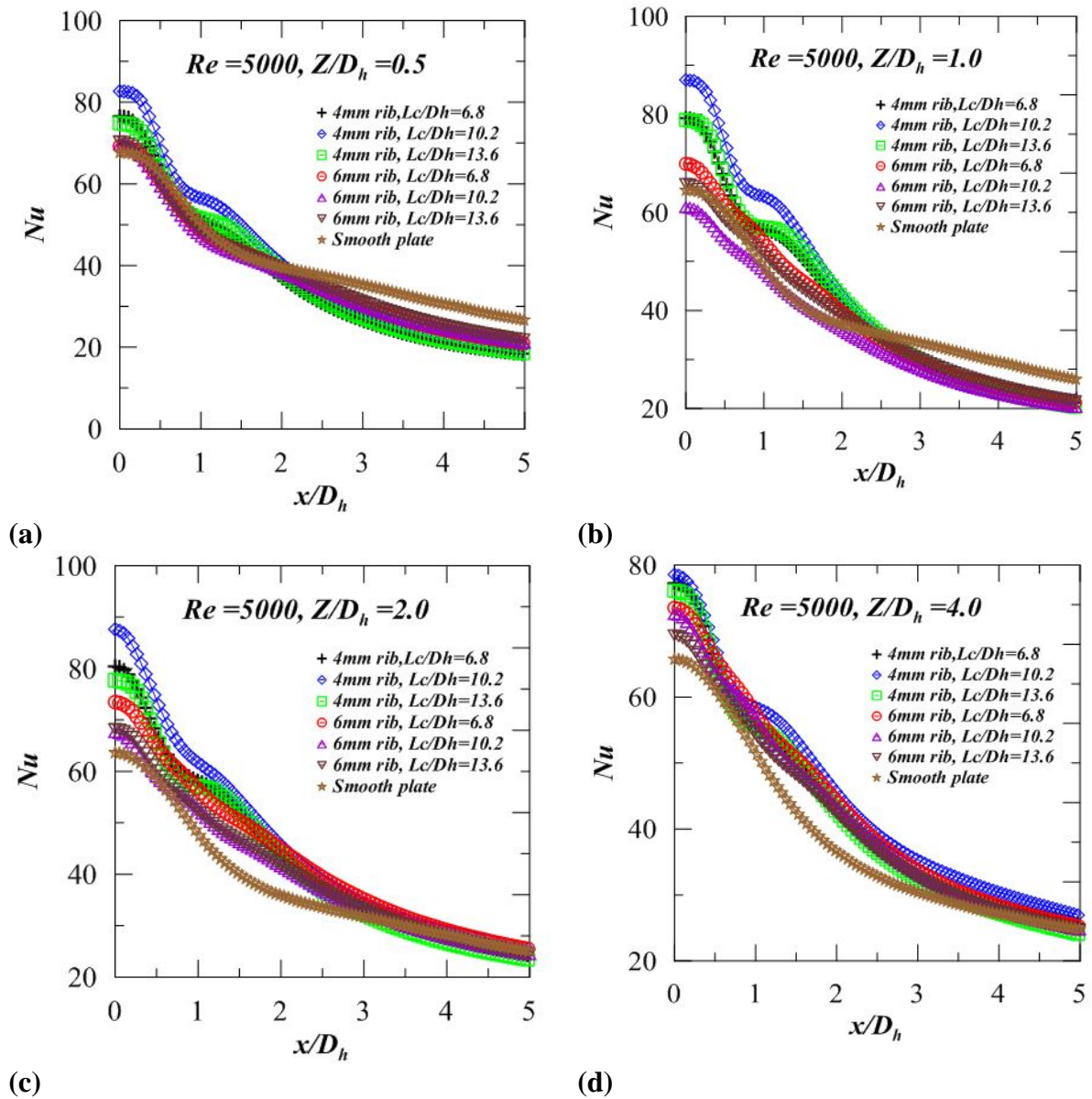


Fig. 6.19 Comparison of the lateral variation of “Nusselt number” for different rib and confinement combinations at $Re=5000$

6.8.2 Comparison of the “Nusselt number” of different configuration at $Re=10000$

Fig.6.20 (a-d) shows the variation in the Nu along the “streamwise direction” for various configurations compared at “Reynolds number” 10000. 4mm rib with 13.6 confinement ratio shows higher Nu at $Z/D_h=0.5$ and 4mm rib with 10.2 confinement ratio shows higher values at all other Z/D_h values in the stagnation region.

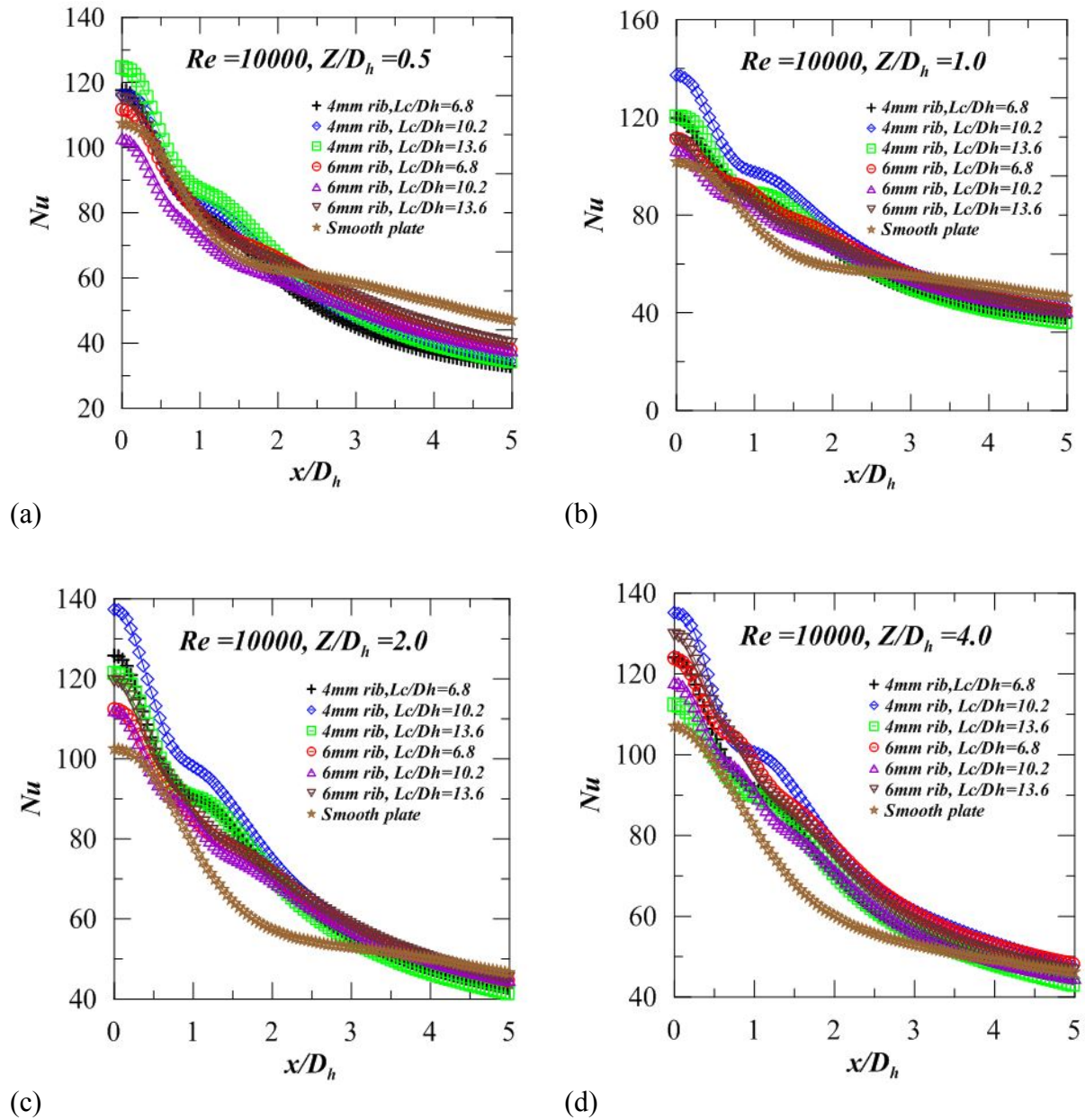


Fig. 6.20 Comparison of the lateral variation of “Nusselt number” for different rib and confinement combinations at $Re=10000$

6.8.3 Comparison of the “Nusselt number” of different configuration at $Re=15000$

Fig. 6.21(a-d) shows a variation of the Nu along “streamwise direction” for different configurations at “Reynolds number” =15000. 4mm rib with 10.2 confinement ratio provides higher values of the “Nusselt number” at all J2P spacing’s and at $Z/D_h=0.5, 1.0,$

2.0 and 4.0 there is an enhancement in the “Nusselt number” of 31.8%, 37.5%, 33.8%, and 37.5% respectively compared to the smooth plate.

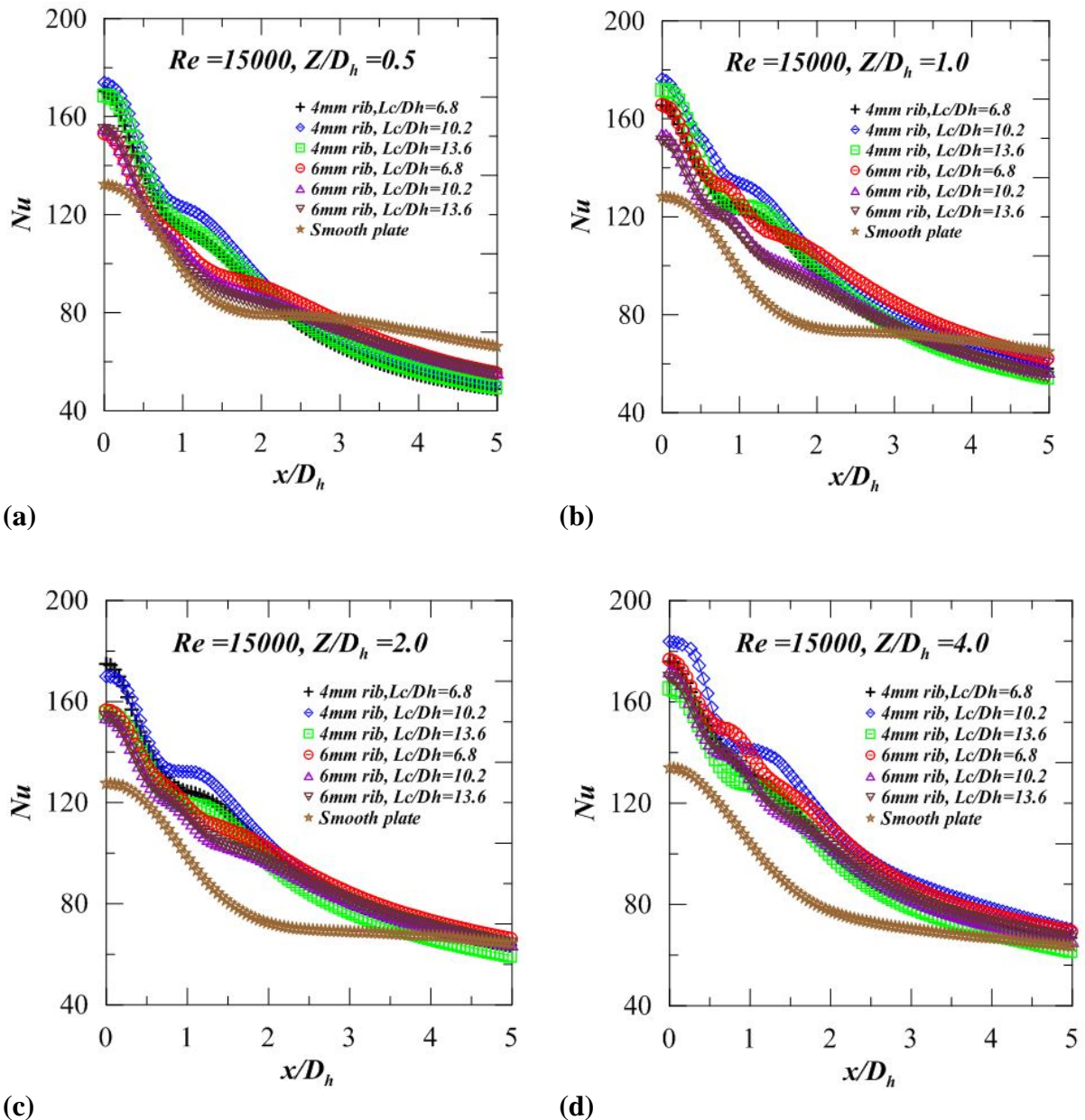


Fig. 6.21 Comparison of the lateral variation of “Nusselt number” for different rib and confinement combinations at $Re=15000$

6.8.4 Comparison of the “Nusselt number” of different configuration at $Re=20000$

Fig.6.22 (a-d) shows a variation of the Nu along with the “streamwise direction” for all configurations at “Reynolds number” 20000. 4mm rib with 10.2 confinement ratio shows higher values of the Nu at $Z/D_h=0.5$ and 2.0, 4mm rib with 13.6 confinement ratio at

$Z/D_h=1.0$ and 6mm rib with 13.6 confinement ratio at $Z/D_h=4.0$ in the stagnation region. 4mm rib with 10.2 confinement ratio shows enhancement in “Nusselt number” 40.5%, 47.8%, 50.24% and 58.46% at $Z/D_h=0.5, 1.0, 2.0$ and 4.0 respectively compared to smooth surface.

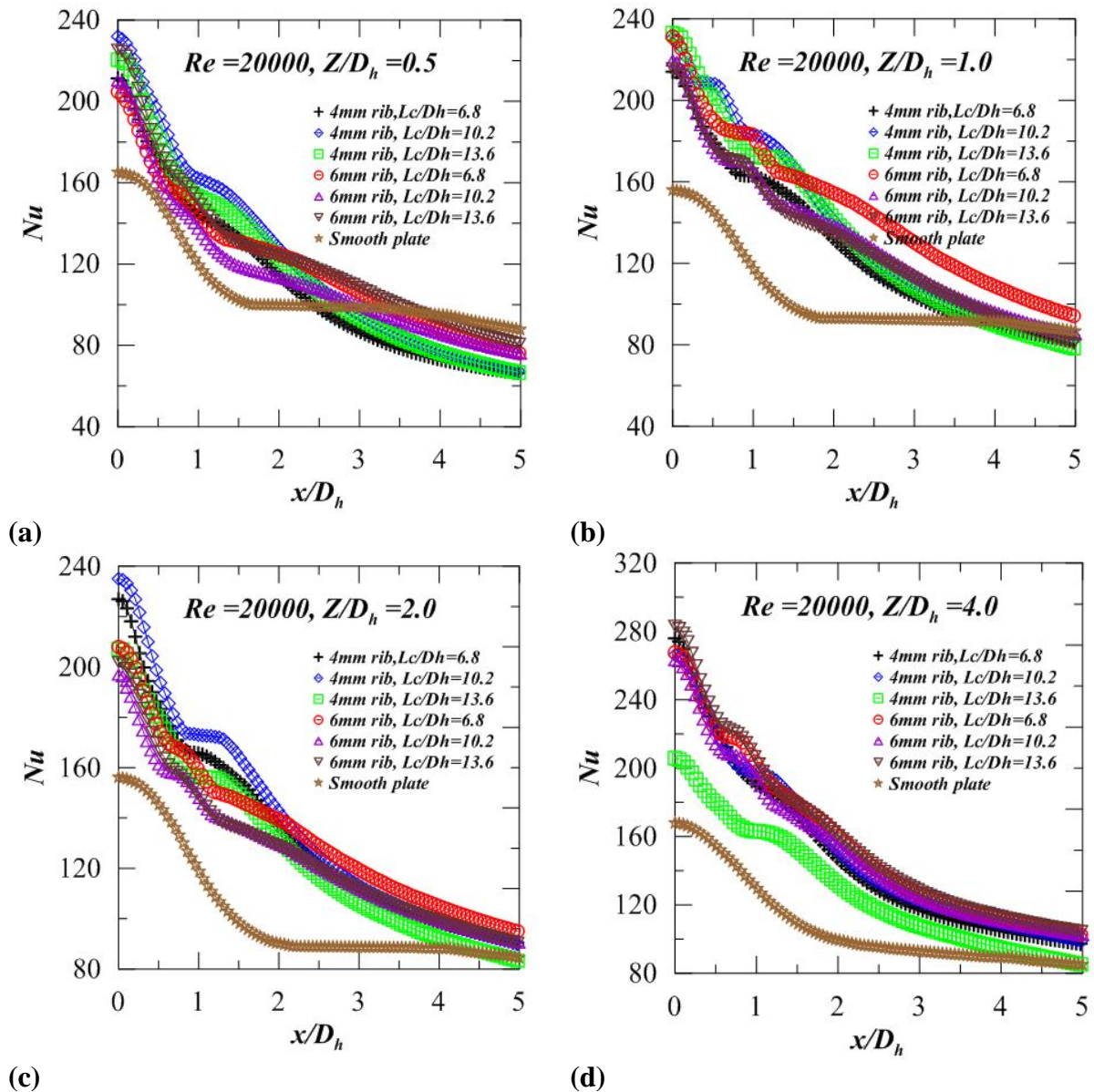


Fig. 6.22 Comparison of the lateral variation of “Nusselt number” for different rib and confinement combinations at $Re=20000$

6.9 Correlations developed from the results for the estimation of stagnation point “Nusselt number” at $Re=2500$

An attempt is made to formulate the correlations to estimate the “stagnation point” “Nusselt number” as a function of J2P distance for the potential core region and the remaining regions separately for a laminar flow at a “Reynolds number” 2500.

“Stagnation point” “Nusselt number” (Nu_0) can be determined as a function of the J2P spacing (Z/D_h) without the ratio of confinement for laminar flow at $Re=2500$.

a) For $0.5 \leq Z/D_h < 4$ (potential core region)

$$Nu_{0=} c_1[-3.085(Z/D_h)^2 + 11.23(Z/D_h) + 44.66] \dots\dots(6.1)$$

Where ‘ c_1 ’ is a correction factor

Table 6.1 Values of c_1

L_c/D_h	6.8	10.2	13.6
4mm rib	0.92	1.0	0.90
6mm rib	0.87	0.65	0.84

The maximum deviation is 7.2% and compares well with experimental results.

b) For $4 \leq Z/D_h \leq 10$ (behind potential core region)

$$Nu_o = c_2[-3.055(Z/D_h) + 61.13] \dots\dots (6.2)$$

Where ‘ c_2 ’ is a correction factor

Table 6.2 Values of c_2 for different ribs

L_c/D_h	6.8	10.2	13.6
4mm rib	1.0	1.0	1.01
6mm rib	0.98	0.95	0.95

The maximum deviation is 4.6% and compares well with experimental results.

6.10 CONCLUSIONS

The local wall static pressure distribution and local “heat transfer” distribution between a confined “slot air-jet” and a rough surface are studied experimentally. A single fully developed jet issued from a “slot jet” having and L/D_h ratio of about 24 is chosen. “Reynolds number” based on nozzle exit is altered from 2500 to 20000. Various widths

of detached ribs and confinement plates are chosen. Different parameters are sequentially studied to know the influence of confinement on the local WSP and local HTC distributions on a rough surface. The J2P distance is varied from 0.5 to 10 times the Hydraulic diameter of the jet.

The following conclusions are derived from the experimental investigations made with the confined jet and the ribbed surface for flow and heat exchange behaviors.

- Maximum WSP records at the “stagnation point” invariably for all the configurations studied and its value diminishes with increasing J2P distances.
- Negative pressure region is observed only up to $Z/D_h=4$ for all rough surface configurations investigated.
- The effect of confinement is pronounced at $Z/D_h=0.5$ for all configurations. This can be accredited to the higher recirculation of the jet fluid happening at lower Z/D_h distances.
- Secondary peaks in C_p are common with all J2P spacing and “Reynolds numbers” for rough surface. This may be due to the effect of flow acceleration under the detached ribs.
- An increase in confinement ratio increases the potential core length with an increase in the “Reynolds number”. The similar behavior of the jet is reported by Baydar and Ozmen [2006].
- The maximum Nu occurs at the SP for all the configurations studied.
- For laminar flow ($Re=2500$) maximum Nu occurs at the lower J2P spacing of 0.5 to 1.0.
- For turbulent flow ($Re=5000$ to 20000) maximum Nu occurs at the end of potential core region (PCR) i.e., $Z/D_h = 4.0$
- 4mm rib with confinement ratio 10.2 gives a better heat transfer coefficient comparatively.
- The correlation for $SP Nu$ as a function of Z/D_h for laminar flow ($Re=2500$) is presented. The results from the correlation compares well with the experimental results within a maximum deviation of 5.2 %.

CHAPTER 07

CONCLUSIONS

7.1 Introduction:

Jet impingement has the most significant potential to increase the local heat transfer coefficient among all heat transfer enhancement techniques. The geometric parameters,

namely nozzle- plate spacing, radial distance from the stagnation point, confinement of jets, nozzle geometry, turbulence intensity, surface roughness, etc. influence the local heat transfer and fluid flow characteristics. Hence, the objective of the present study is to experimentally investigate the local heat transfer and fluid flow distribution on smooth flat and ribbed surfaces due to impinging slot air jets. Based on the investigations carried out, the conclusions from each of the configurations studied during the present work are outlined in this chapter.

7.2 Conclusions from the study of local heat transfer distribution between smooth flat surface and impinging slot air:

An experimental investigation is performed to study the distribution of heat transfer coefficients between the submerged slot impinging jet and a flat smooth surface. In this study the Reynolds number based on hydraulic diameter is varied from 2500 to 15000 and the Z/D_h is varied from 0.25 to 10. Experiments are also conducted to measure the static wall pressure distribution in the “Target plate” from the stagnation point to x/D_h of 10.

- Heat transfer coefficients are highest at the stagnation point for all jet-to-plate distances and Reynolds numbers investigated.
- For lower jet-to-plate distances and higher Reynolds number, secondary peaks are observed in the heat transfer distributions. These secondary peaks may be due to fluid transiting from laminar to turbulent flow on the target plate. However, existence of secondary peaks is not prominently observed at lower Reynolds number.
- Wall static pressure coefficients are seen to be independent of Reynolds number in the range between 5000 and 15000 for a given jet-to-plate distance. This may indicate self-similar behavior of the turbulent submerged jet.
- Sub atmospheric pressure region is identified for the Z/D_h of 0.25 for all the Reynolds numbers investigated. However, Sub atmospheric pressure region vanishes at higher jet-to-plate distance.
- The correlation for estimation of normalized value of Nusselt number for stagnation region is: $Nu/Nu_0 = 1 - 0.36 * (x/D_h)^2$

The correlation holds good for any “jet to plate distance” in the “potential core region” and independent of the Reynolds number.

7.3 Conclusions from the study of heat transfer enhancement on a flat surface with Detached ribs by normal impingement of single slot air jet:

An experimental study is carried out to investigate local distribution of wall static pressure and heat transfer between the normally impinging slot air jet and flat smooth surface and also with a rough surface. The roughness is introduced on the plate by mounting detached rib-rougher. A single fully developed jet issued from a nozzle of slot configuration is chosen for the study. Reynolds number based on nozzle exit condition is varied between 2500 and 20000. Different configurations of detached ribs are arranged on the target plate. Sequential parametric study is carried out to investigate the influence of different ribs on the local wall static pressure and local heat transfer distributions. The jet to plate distance is varied from 0.5 to 10. The conclusions from this investigation can be summarized as bellow:

- Wall static pressure co-efficient are seen to be independent of Reynolds number in the range of 5000 to 20000 for a given jet to plate distance for smooth surface.
- Wall static pressure co-efficient decreases with increase in $J2P$ distance due to mixing of surrounding air.
- Ribbed surface gives the maximum coefficient of stagnation wall static pressure than the smooth surface at all Reynolds numbers studied. This may be attributed to fluid accelerations under the rib.
- The Ribs are effective up to the Z/D_h of 6.0 and later it is comparable with smooth surface.
- From the heat transfer study, it is observed that, for a given jet to plate spacing (Z/D_h), increase in Reynolds number increases the heat transfer coefficient at all the points in the stream wise direction for both smooth and rough surface.
- Rib of 4mm width gives the maximum heat transfer coefficient compared with the other rib sizes (6mm, 8mm, and 12mm) and smooth surface. Higher rib widths lead to drop in Nusselt numbers in the downstream. This may be due to major jet flow at its periphery miss to impact the target surface.
- Enhancement up to 19% in the average $Nu_{2,0}$ can be achieved by 4 mm rib with turbulent slot air jet in the stagnation region with no additional pumping power.
- Enhancement up to 15% in the average $Nu_{2,0}$ can be achieved by 6 mm rib with laminar slot air jet in the stagnation region with no additional pumping power.

- For a given Reynolds number, Nusselt number at stagnation point increases with increase in Z/D_h from 1.0 to still around Z/D_h of 6.0. This may be due to increase in near wall turbulence intensities with increase in jet to plate spacing.

7.4 Conclusions from the study of heat transfer and fluid flow behavior of a flat surface impinged by a confined slot jet

Wall static pressure (C_p) and heat transfer co-efficient distribution on a flat surface impinged by a confined slot air jet are experimentally analyzed for the confinement ratios, $L_c/D_h=0.0$ to 27.2 and nozzle slot jet to plate spacing ($Z/D_h=0.25-10.0$) at $Re= 10000$. Following conclusions elaborated from the present study:

- The peak pressure co-efficient is observed to be independent of Reynolds numbers for a given Z/D_h for an unconfined slot jet impingement on a flat surface.
- With increase in $J2P$ spacing the sub atmospheric region moves outward from the stagnation point.
- It is observed that the highest static coefficient of pressure for a slot jet is at stagnation point for both confined and unconfined at $Re =10000$.
- The maximum pressure is observed at the stagnation point for all confinements and nozzle to plate spacing under study.
- Sub atmospheric pressure region is more significant for $J2P$ spacing below 1.0 for all confinements studied.
- Nusselt number at the stagnation point is highest for the all the confinement ratios ($L_c/D_h =0.0-27.3$) studied.
- It is observed in general that the Nusselt number is a function of Coefficient of Pressure at any given point on the target surface and closely follows the flow pattern.

7.5 Conclusions from the study of heat transfer and fluid flow behavior of a flat rough(ribbed) surface impinged by a confined slot jet

In this study a single fully developed jet issued from a confined slot jet is made to impinge over a ribbed surface and Reynolds number based on nozzle exit condition is

varied from 2500 to 20000. Different configurations of detached ribs and confinement plates are chosen. Sequential parametric study is carried out to investigate the influence of confinement on the local wall static pressure and local heat transfer distributions on rough surface. The jet to plate distance is varied from 0.5 to 10 times the hydraulic diameter of the jet.

The conclusions drawn from the investigation are as follows:

- Maximum wall static pressure occurs at stagnation point and its value decreases with increase in nozzle to plate spacing for all the configurations investigated.
- Sub-atmospheric region is observed up to $Z/D_h=4$ for all rough surface configurations studied.
- Effect of confinement is pronounced more at $Z/D_h=0.5$ for all configurations since at lower jet to plate spacing, more recirculation of the jet happens.
- Secondary peaks in wall static pressure are visible invariably at all jet to plate spaces and Reynolds numbers for rough surface due to the effect of flow acceleration under the detached ribs.
- Increase in confinement ratio increases the potential core length with increasing Reynolds number. It is also reported by Baydar and Ozmen(2006).
- For laminar flow ($Re=2500$) maximum Nusselt number occurs at lower jet to plate spacing of 0.5 to 1.0.
- For turbulent flow ($Re=5000$ to 20000) maximum Nusselt number occurs at end of potential core region i.e. $Z/D_h = 4.0$
- 4mm rib with confinement ratio 10.2 give better heat transfer coefficient comparatively.
- Correlation for stagnation Nusselt number with function of Z/D_h for laminar flow ($Re=2500$) presented. All correlations give the Nu_0 values within 7.2% deviation.

7.6 Scope for future work:

The experimental technique and procedure developed during the present work finds further scope of its application in some of the following areas.

- The influence of inclination of the jet with reference to the target surface can be considered for the study, as necessitated in some of the electronic packages, food processing etc.
- Array of slot jets can be considered for the study which may be useful in cooling/heating larger surface areas as required in paper, metal and glass industry to name a few.
- Combination of orthogonal and inclined jets can also be a matter of significance for the study.
- Numerical modeling can be developed for the configurations considered in our study to avoid further experimentations.

APPENDIX A1

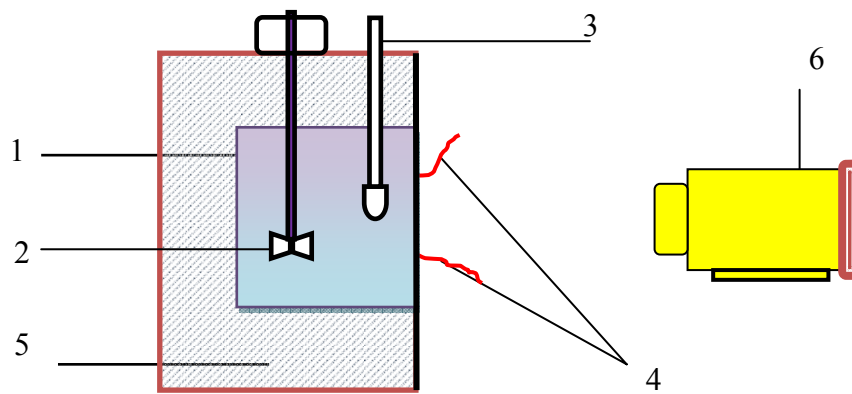
Calibration of emissivity of the painted surface of target plate

'FLUKE Ti 55' infrared (IR) thermal imaging camera is used to collect the local temperatures from the target plate. The thermal images, shows the temperatures on various points over the target surface. The infrared camera is placed on the side of the stain steel heater cum "Target plate" opposite the impinging nozzle. The target surface facing the camera is painted with black color Asian paint having 'Matt' finish and high emissivity surface. "IR camera reads the temperature of the plate depending on the emissivity value of the surface of the plate. Therefore, it is necessary to calibrate the emissivity of the surface".

The methodology for estimation of emissivity:

A cubical tank of 100 mm is made from the material used for the target cum heater plate. The Tank surface is painted with a thin uniform coat of black color Asian paint having 'Matt' finish and high emissivity. Insulation is provided to the five sides of the tank and one side is opened to the atmosphere. "The tank filled with water is heated with an immersion heater of 500 W which is immersed from the top. To maintain the uniform temperature of the water bath, a small capacity motor driven stirrer is also immersed in the water. Two calibrated thermocouples are soldered on the surface of the tank exposed to the atmosphere, at two different locations. Initially, water in the tank is heated to the temperature of about 80°C (*i. e.*, the temperature more than the maximum temperature obtained during the experimentation). Then, the electrical power to the heater is switched off and temperature of surface is allowed to drop. During cooling of the surface, the time constant of the temperature drop is about 3 minutes per 0.24⁰ C. This time is sufficient to take 4 to 5 images of the surface with the infrared camera and to read the thermocouple readings. The emissivity input to the images is then adjusted till the temperature read by the image is the same as that read by the thermocouples. This procedure is repeated for different temperatures of the exposed surface in the range of the temperature of the impinging surface at an interval of 5⁰ C.

In the set of measurement, minimum deviation between thermocouple reading and temperature read by IR camera is observed at $\varepsilon_b = 0.92$, therefore, emissivity of the surface is assumed 0.92. The maximum difference between thermocouple reading and temperature read by IR camera corresponding to $\varepsilon_b = 0.92$ is observed to be 0.5°C. The uncertainty in the measurement of local surface temperatures with the calibrated value of emissivity was estimated to be less than $\pm 0.5^\circ\text{C}$.



1. SS tank filled with water 2. Stirrer 3. Heater 4. Thermocouples soldered to the black painted surface exposed to IR camera 5. Insulation surrounding the tank 6. Infrared Camera

Fig. A1.1 Experimental set-up for surface emissivity calibration

Estimation of energy loss from the target surface with jet impingement on one side of the target surface

The “Target plate” cum heater is made from SS foil having a very small thickness of 60 microns. The foil heater is stretched well and firmly held between the bus bars to form a flat surface which acts as a target surface for jet impingement cooling. As the SS foil is very thin the lateral conduction of heat is highly negligible and surface assumes a constant heat flux situation as reported by Lytle and Webb (1994). “The jet impinges on one side of the surface. One dimensional energy balance across the heated plate shows that the temperature difference across it is negligibly small. Hence, the local temperature measured on the back surface is considered the same as that on the impingement plane. The thermal images, showing the temperature distribution over the target surface are obtained using an infrared camera positioned on the side of the heater opposite the impinging nozzle.” The target surface facing the camera is painted with black color Asian paint having ‘Matt’ finish and high emissivity (0.92) surface for the temperature range between 35° C and 80° C. The detailed procedure is explained in Appendix A1.

During the experiments, the target surface is exposed to the laboratory environment. “Hence a part of the heat energy supplied to the “Target plate” is lost to the surroundings. It is imperative to estimate this loss and account for it while computing heat transfer coefficients due to impinging jet on the target surface. In the present investigations, the loss of energy is evaluated experimentally”.

The energy balance on the target surface during jet impingement is as given below,

$$(\text{Energy supplied as Ohmic dissipation}) = (\text{Energy convected by impinging jet from the Front surface}) + (\text{Energy lost})$$

The energy loss, assuming negligible natural convection from the front surface during impingement, is because of,

- Natural convection from the back surface of target plate
- Thermal radiation from front and back surfaces of target plate.

The methodology for Energy loss estimation:

The foil is heated by supplying electric power in the absence of air jet and a steady state is maintained. The power supplied to the heater and the room temperature is recorded. Image of the heated surface is captured with IR camera. The temperatures on the surface image are extracted using dedicated software SMART VIEW. The average surface temperature is determined for a selected portion of the hot surface. This is repeated for different power inputs to the heater surface. “For each power input, one has a corresponding temperature difference between heated plate surface and surroundings. As the surface provides constant heat flux situation, the energy balance for the chosen area on the heater surface can be re-written as”,

Supplied heat flux = Heat flux due to natural convection + Heat flux due to radiation

$$q'' = q''_{convb} + q''_{convf} + q''_{radb} + q''_{radf} \quad (A2.1)$$

$$q''_{radb} + q''_{radf} = \sigma(\varepsilon_f + \varepsilon_b)(T_w^4 - T_{amb}^4) \quad (A2.2)$$

“The emissivity of the back surface, $\varepsilon_b = 0.92$ for the front surface, and $\varepsilon_f = 0.2$ (chosen for stainless steel surface)”

The heater surface is very thin with only 60 microns thickness it is considered that there will be no lateral conduction and the convection losses from the front side and rear side of the heater can be equal. The heat energy dissipated due to radiation and convective losses from both the surfaces are estimated using equations A2.1 and A2.2. “This heat flux should correspond to energy flux lost from the target surface during jet impingement for the corresponding ambient temperature and surface temperature. Tests are conducted for different power inputs to obtain losses at different surface temperatures of target plate”.

Figure A2.1 shows “the distribution of energy loss from the target surface due to combined natural convection and radiation (Q_{loss}) and corresponding effective heat transfer coefficients for different temperature differences between ambient and target surface. A linear fit to the distribution for temperature differences” for h_{loss} from 5°C to 65°C is

$$h_{Loss} = 0.1 (T_w - T_{amb}) + 12.953 \quad (A2.3)$$

This correction is included in the determination of “local Nusselt numbers” from the target surface.

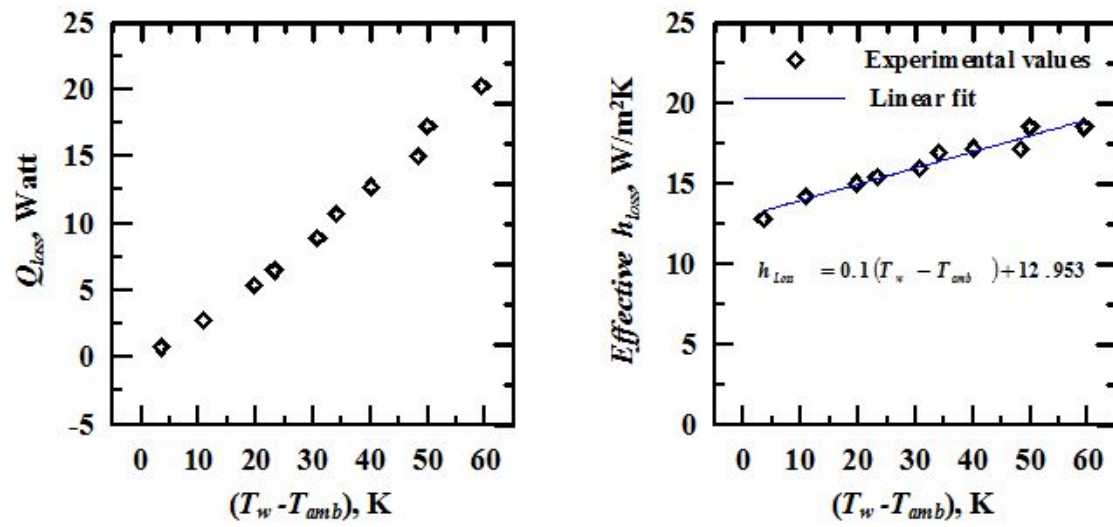


Fig A2.1 Distribution of Q_{loss} and h_{loss} from the target plate

APPENDIX A3

Uncertainty analysis of heat transfer and flow parameters

The uncertainty analysis of the heat transfer and fluid flow parameters is based on the method of Moffat (1988) and is explained as follows.

A.3.1 Uncertainty of coefficient of discharge (C_d) of orifice meter / venturi meter:

“The coefficient of discharge (C_d) of orifice meter and venturi meter is defined as the ratio of actual mass flow rate to theoretical mass flow rate of fluid flowing through them”.

Mathematically, C_d is expressed as in Equation A3.1

$$C_d = m_{act}/m_{Theo} \quad (A3.1)$$

Uncertainty in the estimation of C_d may be computed using Equation (A3.2).

$$\frac{\delta C_d}{C_d} = \left[\left(\frac{\delta m_{act}}{m_{act}} \right)^2 + \left(\frac{\delta t}{t} \right)^2 + \left(\frac{\delta A_o}{A_o} \right)^2 + 4 \left(\frac{\delta \beta}{\beta} \right)^2 + \frac{1}{4} \left(\frac{\Delta p}{p} \right)^2 \right]^{0.5} \quad (A3.2)$$

A_o is the throat area of orifice meter / venturi meter and β is the ratio of the diameters at the orifice meter / venturi throat and inlet. Uncertainties in the measurement of A_o and β are estimated as follows:

Orifice meter / venturi meter throat area, A_o , is evaluated using Equation (A3.3)

$$A_o = \frac{\pi}{4} D_o^2 \quad (A3.3)$$

The uncertainty of A_o is estimated using the Equation (A3.4)

$$\frac{\delta A_o}{A_o} = \sqrt{4 \left(\frac{\delta D_o}{D_o} \right)^2} \quad (A3.4)$$

Sample uncertainty calculation in estimation of A_o of venturi meter is as shown in Equation (A3.5).

$$\frac{\delta A_o}{A_o} = \sqrt{4 \left(\frac{0.1}{15.0} \right)^2} \Rightarrow \frac{\delta A_o}{A_o} = 0.0133 \quad (A3.5)$$

The ratio of diameters of orifice meter / venturi meter, β , is evaluated using Equation (A3.6)

$$\beta = \frac{D_o}{D} \quad (A3.6)$$

The uncertainty of β is estimated using the Equation (A3.7)

$$\frac{\delta\beta}{\beta} = \sqrt{\left(\frac{\delta D_o}{D_o}\right)^2 + \left(\frac{\delta D}{D}\right)^2} \quad (\text{A3.7})$$

Sample uncertainty calculation in estimation of β of venturi meter is as shown in Equation (A3.8).

$$\frac{\delta\beta}{\beta} = \sqrt{\left(\frac{0.1}{15.0}\right)^2 + \left(\frac{0.1}{25.0}\right)^2} \Rightarrow \frac{\delta\beta}{\beta} = 0.00778 \quad (\text{A3.8})$$

Hence, sample uncertainty calculation in estimation of C_d of venturi meter is as shown in Equation (A3.9).

$$\frac{\delta C_d}{C_d} = \left[\left(\frac{1.0}{250}\right)^2 + \left(\frac{0.1}{124.4}\right)^2 + (0.0133)^2 + 4(0.00778)^2 + \frac{1}{4}(0.001)^2 \right]^{0.5}$$

$$\frac{\delta C_d}{C_d} = 0.0208 \quad (\text{A3.9})$$

A.3.2 Uncertainty analysis of mass flow rate:

The mass flow rates are measured using calibrated orifice meter / venturi meter and water tube differential manometer. Mass flow rates are estimated using Equation (A3.10).

$$\dot{m} = \frac{\rho C_d A_2 \sqrt{2g \left(\frac{\rho_w}{\rho} - 1 \right) h_w}}{\sqrt{1 - \beta^4}} \quad (\text{A3.10})$$

Fluid properties are considered as constants. Thus, uncertainty in the mass flow measurement may be evaluated using Equation (A3.11).

$$\frac{\delta \dot{m}}{\dot{m}} = \left[\left(\frac{\delta A_o}{A_o}\right)^2 + \left(\frac{\delta C_d}{C_d}\right)^2 + \left(2 \frac{\delta \beta}{\beta}\right)^2 + \left(\frac{0.5 h_w}{h_w}\right)^2 \right]^{0.5} \quad (\text{A3.11})$$

Thus, sample uncertainty calculation in estimation of mass flow rate through venturi meter is as shown in Equation (A3.12).

$$\frac{\delta \dot{m}}{\dot{m}} = \left[(0.0133)^2 + (0.0208)^2 + 4(0.00778)^2 + 0.25 \left(\frac{0.5}{615}\right)^2 \right]^{0.5} \quad (\text{A3.12})$$

$$\Rightarrow \frac{\delta \dot{m}}{\dot{m}} = 0.0292$$

A.3.3 Uncertainty of Reynolds number estimation

Reynolds number is computed using Equation (A3.13).

$$Re = \frac{4 \dot{m}}{\pi d \mu} \quad (\text{A3.13})$$

Hence, uncertainty in the computation of Reynolds number is done using Equation (A3.14) considering fluid properties as constants.

$$\frac{\delta Re}{Re} = \left[\left(\frac{\delta \dot{m}}{\dot{m}} \right)^2 + \left(\frac{\delta d}{d} \right)^2 \right]^{0.5} \quad (\text{A3.14})$$

Sample uncertainty calculation in estimation of jet Reynolds number of is as shown in Equation (A3.15).

$$\begin{aligned} \frac{\delta Re}{Re} &= \left[(0.0292)^2 + \left(\frac{0.1}{5.0} \right)^2 \right]^{0.5} \\ \Rightarrow \frac{\delta Re}{Re} &= 0.0354 \end{aligned} \quad (\text{A3.15})$$

A.3.4 Uncertainty of temperature estimation:

“Target plate” surface temperatures are obtained from the thermal images of IR Camera. The emissivity of the surface along with calibration of the camera is explained in Appendix A1 and the accuracy in the temperature measurement from IR Camera is found to be 0.5°C. Minimum temperature difference between the “Target plate” and the ambient is generally kept above 15°C and at least 10°C under worst conditions. Hence, maximum uncertainty in the measurement of temperature is 5.0. However, the resolution of the temperature measured from the camera is 0.1°C.

A.3.5 Uncertainty of Nusselt number estimation:

Nusselt number is calculated using Equation (A3.16).

$$Nu = \frac{hd}{k} = \frac{V \times I \times d}{A(T_w - T_j) k} \quad (\text{A3.16})$$

Uncertainty in the Nusselt number is estimated using Equation (A3.17) considering fluid properties as constants.

$$\frac{\delta Nu}{Nu} = \left[\left(\frac{\delta V}{V} \right)^2 + \left(\frac{\delta I}{I} \right)^2 + \left(\frac{\delta W}{W} \right)^2 + \left(\frac{\delta B}{B} \right)^2 + \left(\frac{\delta T_w}{T_w} \right)^2 + \left(\frac{\delta d}{d} \right)^2 \right]^{0.5} \quad (\text{A3.17})$$

Sample uncertainty calculation in estimation of Nusselt number of the surface is as shown in Equation (A3.18).

$$\frac{\delta Nu}{Nu} = \left[\left(\frac{0.05}{2.583} \right)^2 + \left(\frac{0.1}{58.8} \right)^2 + \left(\frac{0.1}{250} \right)^2 + \left(\frac{0.1}{65} \right)^2 + \left(\frac{0.5}{10} \right)^2 + \left(\frac{0.1}{5.0} \right)^2 \right]^{0.5}$$

$$\frac{\delta Nu}{Nu} = 0.0576 \quad (\text{A3.18})$$

A.3.5 Uncertainty of “wall static pressure coefficient (C_p)” estimation:

“Wall static pressure coefficient” is calculated using Equation (A3.19)

$$C_p = \frac{\Delta P}{0.5 \rho \bar{V}^2} \quad (\text{A3.19})$$

Uncertainty in the “wall static pressure coefficient” is estimated using Equation (A3.20) considering fluid properties as constants.

$$\frac{\delta C_p}{C_p} = \left[\left(\frac{\delta(\Delta P)}{\Delta P} \right)^2 + 4 \left(\frac{\delta \bar{V}}{\bar{V}} \right)^2 \right]^{0.5} \quad (\text{A3.20})$$

The jet exit velocity \bar{V} can be evaluated using Equation (A3.21).

$$\bar{V} = \frac{\left(\frac{\dot{m}}{\text{Number of jets}} \right)}{\rho \left(\frac{\pi}{4} d^2 \right)} \quad (\text{A3.21})$$

Uncertainty in the jet exit velocity is estimated using Equation (A3.22) considering fluid properties as constants.

$$\frac{\delta \bar{V}}{\bar{V}} = \left[\left(\frac{\delta \dot{m}}{\dot{m}} \right)^2 + 4 \left(\frac{\delta d}{d} \right)^2 \right]^{0.5} \quad (\text{A3.22})$$

Sample uncertainty in the jet exit velocity is estimated using Equation (A3.23).

$$\frac{\delta \bar{V}}{\bar{V}} = \left[(0.029)^2 + 4 \left(\frac{0.01}{20.0} \right)^2 \right]^{0.5}$$

$$\frac{\delta \bar{V}}{\bar{V}} = 0.029 \quad (\text{A3.23})$$

Hence, sample uncertainty calculation in estimation of “wall static pressure coefficient” is as shown in Equation (A3.24).

$$\frac{\delta C_p}{C_p} = \left[(0.005)^2 + 4 (0.029)^2 \right]^{0.5}, \quad (\text{A3.24})$$

$$\frac{\delta C_p}{C_p} = 0.0582$$

BIBLIOGRAPHY

- [1] A.K. Shukla and A. Dewan (2018) and (2019): Heat transfer and flow characteristics of turbulent slot jet impingement on plane and ribbed surfaces, *Thermophysics and Aeromechanics*, 2018, Vol. 25, No. 5, Journal of Physics: Conf. Series 1240 (2019) 012126 IOP Publishing
- [2] Abdulrahman H. Alenezi, Abdulrahman Almutairi, Hamad M. Alhajeri, Abdulmajid Addali and Abdelaziz A. A. Gamil (2018), Flow Structure and Heat Transfer of Jet Impingement on a Rib-Roughened Flat Plate, *Energies* 2018, 11, 1550; doi:10.3390/en11061550, www.mdpi.com/journal/energies.
- [3] Akansu, Yahya Erkan, *et al.* "Flow field and heat transfer characteristics in an oblique slot jet impinging on a flat plate." *International Communications in Heat and Mass Transfer* 35.7 (2008): 873-880.
- [4] Baughn J. W. and Shimizu S., "Heat Transfer Measurements from a Surface with Uniform Heat Flux and Impinging Jet", *J. of Heat Transfer*, 111, (1989), pp. 1096-1098.
- [5] Baydar, E., and Y. Ozmen. "An experimental and numerical investigation on a confined impinging air jet at high Reynolds numbers." *Applied thermal engineering* 25.2 (2005): 409-421.
- [6] Beitelmal, A.H., Shah, A.H., Saad, M.A., Analysis of an impinging two-dimensional jet, *Journal of Heat Transfer*, 128 (2006) 307-310.
- [7] Beitelmal, Abdmonem H., Michel A. Saad, and Chandrakant D. Patel. "Effects of surface roughness on the average heat transfer of an impinging air jet." *International Communications in Heat and Mass Transfer* 27.1 (2000): 1-12.
- [8] Brahma R. K. Prediction of stagnation point heat transfer for a slot jet impinging on a flat surface, *Warme- and Stofffibertragung* 27, 61 66 (1992), © Springer-Verlag 1992.
- [9] Carlo Carcasci "An Experimental Investigation on Air Impinging Jets using Visualization Methods". *International Journal Thermal Science* (1999).38, 808-818.

- [10] Chakroun W.M Abdel-Rahman A.A and Al-Fahed S.F., "Heat transfer augmentation for air jet impinged on a rough surface", *Applied Thermal Engineering* 18, (1998), pp. 1225-1241.
- [11] Chang, Shyy Woei, Shyr Fuu Chiou, and Shuen Fei Chang. "Heat transfer of impinging jet array over concave-dimpled surface with applications to cooling of electronic chipsets." *Experimental thermal and fluid science* 31.7 (2007): 625-640.
- [12] Chiriac, Victor A., and Alfonso Ortega. "A numerical study of the unsteady flow and heat transfer in a transitional confined slot jet impinging on an isothermal surface." *International Journal of Heat and Mass Transfer* 45.6 (2002): 1237-1248.
- [13] Choo, Kyo Sung, and Sung Jin Kim. "Comparison of thermal characteristics of confined and unconfined impinging jets." *International Journal of Heat and Mass Transfer* 53.15 (2010): 3366-3371.
- [14] D Cooper, D.C. Jackson, B.E. Launder & G.X. Liao, "Impinging Jet studies for Turbulence model assessment – Flow – Field Experiments". *International Journal Heat Mass Transfer*, Vol 36 No 10 PP 2675-2684(1993) .
- [15] Dae Hee Lee, Hyun Jin Park, & Phil Ligrani, "Milli scale Confined Impinging Slot Jets: Laminar Heat Transfer Characteristics for an Isothermal Flat Plate". *International Journal of Heat and Mass Transfer* 55(2012): 2249-2260.
- [16] Danielle R.S. Guerra, Jian Su, Atila P. Silva Freire, "The Near Wall Behavior of an Impinging Jet". *International Journal of Heat and Mass Transfer* 48(2005):2829-2840.
- [17] Dandan Qiu, Lei Luo, Songtao Wang, Bengt Ake Sunden and Xinhong Zhang (2019) Analysis of heat transfer and fluid flow of a slot jet impinging on a confined concave surface with various curvature and small jet to target spacing, *International Journal of Numerical Methods for Heat and Fluid Flow*, Volume 29, Issue 8, pp 2885-2910, <http://dx.doi.org/10.1108/HFF-07-2018-0354>
- [18] David T Dader, F P Incropera, R. Viskanta. "A method for measuring steady local heat transfer to an impinging liquid jet". *Experimental Thermal and Fluid Science* 4:1-11. (1991).

- [19] Dipankar Sahoo, Sharif M.A.R., Numerical modeling of slot-jet impingement cooling of a constant heat flux surface confined by a parallel wall, *International Journal of Thermal Sciences* 43 (2004) 877–887.
- [20] Dogan Engin Alnak and Koray Karabulut (2018): Analysis of Heat and Mass Transfer of The Different Moist Object Geometries with Air Slot Jet Impinging for Forced Convection Drying, *thermal science: year 2018, vol. 22, no. 6b*, pp. 2943-2953 2943.
DOI: 10.1080/07373937.2020.1729173
- [21] E. Baydar, Y. Ozmen “Confined impinging air jet at lower Reynolds numbers”. *Experimental Thermal and Fluid Science* (1999), 19, 27-33
- [22] E. Baydar, Y. Ozmen. “An experimental and numerical investigation on a confined impinging air jet at Higher Reynolds numbers”. (*Applied Thermal Engineering* 25 (2005): 409–421.
- [23] Florschuetz, L. W., C. R. Truman, and D. E. Metzger. "Streamwise flow and heat transfer distributions for jet array impingement with crossflow." ASME 1981 International Gas Turbine Conference and Products Show. American Society of Mechanical Engineers, (1981).
- [24] Gao Xiufang and Sundén Bengt, Experimental investigation of the heat transfer characteristics of confined impinging slot jets, *Experimental Heat Transfer*, 16:1–18, 2003, Taylor and Francis.
- [25] Gao N and D. Ewing. "Investigation of the effect of confinement on the heat transfer to round impinging jets exiting a long pipe." *International journal of heat and fluid flow* 27.1 (2006): 33-41.
- [26] Gardon R and Akfirat C. “Heat Transfer Characteristics of Impinging Two-Dimensional Air Jets”, *J. of Heat Transfer*, 88, February (1966), pp. 101-108.
- [27] Gardon R and Akfirat C., “The Role of Turbulence in Determining the Heat Transfer Characteristics of Impinging Jets”, *Int. J. Heat Mass Transfer*, 8, (1965), pp. 1261-1272.
- [28] Gardon R. and Cobonpue J., “Heat Transfer Between a Flat Plate and Jets of Air Impinging on It”, *Int. Journal of Developments in Heat Transfer*, ASME, (1962), pp. 454-460.

- [29] Gau C and Lee J.C., "Flow and impingement cooling heat transfer along triangular rib-roughened walls", Elsevier Science Ltd. International Journal of Heat and Mass Transfer 43, (2000), pp. 4405-4418.
- [30] Gau C and Lee J.C., "Impingement cooling flow structure and heat transfer along rib-roughened walls", Int. J. Heat and Mass transfer Vol. 35,11, (1992), pp. 3009-3020, Elsevier Science Ltd. Pergamon Press Ltd.
- [31] Gau, Chie, and I. C. Lee. "Flow and impingement cooling heat transfer along triangular rib-roughened walls." International journal of heat and mass transfer 43.24 (2000): 4405-4418.
- [32] Gulati, Puneet, Vadiraj Katti, and S. V. Prabhu. "Influence of the shape of the nozzle on local heat transfer distribution between smooth flat surface and impinging air jet." International Journal of Thermal Sciences 48.3 (2009): 602-617.
- [33] Han J.C, Glicksman L.R and Rohsenow., "An investigation of heat transfer and friction for rib-roughened surfaces", Int. J. Heat and Mass transfer Vol. 21, (1978), pp. 1143-1156, Pergamon Press Ltd.
- [34] Hansen L.G and Webb B.W, "Air jet impingement heat transfer from modified surfaces", Int. J. Heat and Mass transfer Vol. 36, No.04, (1993), pp. 989-997, Elsevier Science Ltd. Pergamon Press Ltd.
- [35] Haydar Eren, Nevin Celik, Cooling of a heated flat plate by an obliquely impinging slot jet, International Communications in Heat and Mass Transfer 33 (2006) 372–380.
- [36] Hrycak P., "Heat transfer from impinging jets to a flat plate with conical and ring protuberances", Int. J. Heat and Mass Transfer. Vol. 27, (1984), pp. 2145-2154, Elsevier Science Ltd. Pergamon Press Ltd.
- [37] Hrycak P., "Heat Transfer from Round Impinging Jets to a Flat Plate", Int. J. Heat Mass Transfer, 26, (1983), pp. 1857-1865.
- [38] Jambunathan K, Lai E., Moss M. A., Button B.L., "A Review of Heat Transfer Data for Single Circular Jet Impingement", Int. J. Heat Fluid Flow, 13, 2, June (1992), pp.106- 115.

- [39] James. W. Gauntner, John. B.Livingood & Peter Hrycak, “Survey of literature on flow characteristics of a single turbulent jet impinging on a flat plate”. National aeronautics and Space Administration, Washington, D.C 4 56-81. (1970).
- [40] JinqiZhua, RuifengDoua,b, Ye Hua, ShixingZhanga, Xuyun Wanga, Heat transfer of multi-slot nozzles air jet impingement with different Reynolds number, Applied Thermal Engineering186,116470(2021)
- [41] K.Jambunathan, E.Lai,M. A. Moss & B.L.Button. “A review of heat transfer data for single circular jet impingement”. Department of Mechanical Engineering Nottingham, U.K 69-85(1992).
- [42] Katti V. V and Prabhu S. V, “Experimental Study and Theoretical Analysis of Local Heat Transfer Distribution between Smooth Flat Surface and Impinging Air Jet from a Circular Straight Pipe Nozzle”, Int. J. Heat Mass Transfer. 51, (2008), pp. 4480-4495 doi:10.1016/j.ijheatmasstransfer.2007.12.024
- [43] Katti, Vadiraj, and S. V. Prabhu. "Heat transfer enhancement on a flat surface with axisymmetric detached ribs by normal impingement of circular air jet." International Journal of Heat and Fluid Flow 29.5 (2008): 1279-1294.
- [44] Koichi Inchimiya & Nobuo Hosaka, “Experimental Study of Heat Transfer Characteristics due to Confined Impinging Two- Dimensional Jets”. Experimental Thermal and Fluid Science, Vol5; 803-807 (1992).
- [45] Kyo Sung Choo, Sung Jin Kim, “Comparison of thermal characteristics of confined and unconfined impinging jets”, International Journal of Heat and Mass Transfer 53 (2010): 3366–3371.
- [46] Lee D. H., Song J., Myeong Chan Jo., “The Effect of Nozzle Diameter on Impinging Jet Heat Transfer and Fluid Flow”, Int. J. Of Heat Transfer, 126, (2004), pp. 554-557.
- [47] LinglingChen, Robin G.A.Brakmann, BernhardWeigand, RicoPoser, and QingzhenYang ., Detailed investigation of staggered jet impingement array cooling performance with cubic micro pin fin roughened target plate, Applied Thermal Engineering, Volume 171, 5 May (2020), 115095, <https://doi.org/10.1016/j.applthermaleng.2020.115095>

- [48] Liou T and Wang W., "Laser holographic interferometry study of developing heat transfer in a duct with a detached rib array", *Int. J. Heat and Mass transfer*. Vol.38, No.1, (1995), pp. 91- 100, Elsevier Science Ltd.
- [49] Liou Tong-Miin and Chen Shih-Hui., "Turbulent heat and fluid flow in a passage disturbed by detached perforated ribs of different heights", *Int. J. Heat and Mass transfer*. Elsevier Science Ltd. Vol. 41, No.12, (1998), pp. 1795-1806,
- [50] Livingood J.N.B. and Hrycak P., "Impingement heat transfer from turbulent air jets to flat plates – A literature survey", *NASA Technical Memorandum (NASA TM X-2778)*, (1970).
- [51] Lou, Z. Q., A. S. Mujumdar, and C. Yap. "Effects of geometric parameters on confined impinging jet heat transfer." *Applied Thermal Engineering* 25.17 (2005): 2687-2697.
- [52] Lytle D., Webb B. W., "Air Jet Impingement Heat Transfer at Low Nozzle Plate Spaces", *Int. J. Heat and Mass Transfer*, 37 (1994) 1687-1697.
- [53] M. Nirmalkumar, Vadiraj V Katti, S.V. Prabhu. "Local heat transfer distribution on a smooth flat plate impinged by a slot jet". *International Journal of Heat and Mass Transfer* 54 (2011): 727–738.
- [54] Martin H., *Heat and Mass transfer between impinging gas jet and solid surface*, *Adv. Heat Transfer*, 13 (1977) 1-60.
- [55] Milad Farzad & Jamal Yagoobi., *Drying of moist cookie doughs with innovative slot jet reattachment nozzle*, *Drying Technology*, (2020)
- [56] Moffat R. J., "Describing the uncertainties in experimental results", *Experimental Thermal and Fluid Science*, 1, (1988), pp. 3-17.
- [57] Narayanan, V., J. Seyed-Yagoobi, and R. H. Page. "An experimental study of fluid mechanics and heat transfer in an impinging slot jet flow." *International Journal of Heat and Mass Transfer* 47.8 (2004): 1827-1845.
- [58] Nirmalkumar M., Vadiraj Katti, S.V. Prabhu, *Local heat transfer distribution on a smooth flat plate impinged by a slot jet*, *International Journal of Heat and Mass Transfer* 54 (2011) 727–738.

- [59] Nevin Celik (2020), Effects of dimples' arrangement style of rough surface and jet geometry on impinging jet heat transfer, *Heat and Mass Transfer* (2020) 56:339–354, <https://doi.org/10.1007/s00231-019-02714-x>
- [60] Ozmen, Y. "Confined impinging twin air jets at high Reynolds numbers." *Experimental Thermal and Fluid Science* 35.2 (2011): 355-363.
- [61] Patil Deogounda, Vijaykumar N Chawla, Muruges .M.C, Vinod Dixit, "Wall Static Pressure Distribution due to Confined Impinging Circular Air Jet". *International Journal of Research in Engineering and Technology*. VOLUME 03pISSN:2321-7308 May -(2014).
- [62] Puneet Gulati, Vadiraj Katti, S.V. Prabhu, Influence of the shape of the nozzle on local heat transfer distribution between smooth flat surface and impinging air jet, *International Journal of Thermal Sciences* 48 (2009) 602–617.
- [63] R K Brahma, "Prediction of stagnation point heat transfer for a slot jet impinging on a flat surface", *Warme-and Stoffubertragung Springer- Verlag* 27, 61-66(1992).
- [64] RobinBrakmann, LinglingChen, RicoPoser, JoseRodriguez, MichaelCrawford, and BernhardWeigand, Heat transfer investigation of an array of jets impinging on a "Target plate" with detached ribs, *International Journal of Heat and Fluid Flow*, Volume 78, August (2019), 108420, <https://doi.org/10.1016/j.ijheatfluidflow.2019.05.009>
- [65] Shariff Muhammad A R, Heat Transfer from an Isothermally heated flat surface due to twin oblique jet impingement, 5th BSME International Conference on Thermal Engineering, *Procedia Engineering* 56 (2013) 544 – 550.
- [66] Slayzak S. J., Viskanta R. and Incropera F. P., Effects of interaction between adjacent free surface planar jets on local heat transfer from the impingement surface, *International Journal of Heat and Mass Transfer*, vol. 37, No. 2, pp.269-282,1994.
- [67] Suresh P. R., Sarit K. Das, T. Sundararajan, Influence of Reynolds number on the evolution of a plane air jet issuing from a slit, *Transactions of the ASME*, Vol. 129, (2007) 1288-1296.
- [68] Sushil Kumar Rathore., Sanjay Singh Rathore and Sudarshan Singh., (2019): Computational investigation of slot jet impinging on a heated flat plate using low-Reynold number modeling. *NFEST, IOP Conf. Series: Journal of Physics: Conf.*

- Series, 1240 (2019) 012126, doi: 10.1088/1742-6596/1240/1/012126, IOP Publishing.
- [69] T L Lupton, D B Murray and A J Robinson. "The effect of varying confinement levels on the heat transfer to a miniature impinging air jet". 5th European thermal sciences conference, Netherlands (2008).
- [70] Tu, C.V. and Wood, D.H, Wall Pressure and Shear Stress Measurements Beneath an Impinging Jet, *Experimental Thermal and Fluid Science*, 13 (1996) 364-373.
- [71] V Narayanan, J Seyed Yagoobi, R H Page, "An experimental study of fluid mechanics and heat transfer in an impinging slot jet flow", *International Journal of Heat and Mass transfer* 47(2004):1827-1845.
- [72] VVKatti, AdimurthyM & AshwiniMTamagond, "Experimental Investigation on Local Distribution of Wall Static Pressure Coefficient due to Impinging Slot Air Jet on Smooth and Rough Surface". *Journal of Mechanical Engineering Research and Technology*, Volume2, Number 1, (2014):500-508.
- [73] Viskanta, R. "Heat transfer to impinging isothermal gas and flame jets. "Experimental thermal and fluid science 6.2 (1993): 111-134.
- [74] Wen –Lih Chen "Estimation of Heat Flux on the Surface of an Initially Hot Cylinder Cooled by a Laminar Confined Impinging Jet". *International Journal of Heat and Mass Transfer* 55 (2012):597-606.
- [75] Yan W.M, Liu H.C, Soong C.Y, and Yang W.J., "Experimental study of impinging heat transfer along rib-roughened walls by using transient liquid crystal technique". Elsevier Science Ltd. *International Journal of Heat and Mass Transfer* 48, (2005), pp. 2420–2428.
- [76] Z H Lin, YJChou and Y H Hung "Heat transfer behaviors of a confined slot jet impingement", *Pergamon International Journal Heat Mass Transfer* (1997). 40 NO 5 PP 1095-1107
- [77] Zhou D.W., Sang-Joon Lee, Forced convective heat transfer with impinging rectangular jets, *International Journal of Heat and Mass Transfer* 50 (2007) 1916–1926.

- [78] Zhou, D. W., and Sang-Joon Lee. "Forced convective heat transfer with impinging rectangular jets." *International Journal of heat and mass transfer* 50.9 (2007): 1916-1926.

PUBLICATIONS

International conference proceedings:

- 1) V V Katti Adimurthy M Ashok P Ganganavar. "Local Heat Transfer and wall static pressure characteristics due to impinging slot air jet on a Flat Surface", proceedings of National conference on Fluid Mechanics and Fluid Power (FMFP-2013) November 2013.
- 2) V.V. Katti, Adimurthy. M, Ashwini. M. Tamagond," Experimental Investigations on local distribution of wall static pressure coefficient due to impinging slot air jet on smooth and rough surface" International Conference on Recent Advances in Engineering Sciences 2014 ICRAES 2014, 4 - 5 September 2014,
- 3) M. Adimurthy and V V Katti Experimental investigation of wall static pressure Distribution due to impinging slot air jet on a flat surface with detached rib. International Conference on Engineering and Material Sciences 2016, ICEMS 2016, JNU, Jaipur
- 4) M.Adimurthy and V V Katti, Experimental Investigations of the Fluid Flow and Heat Transfer Characteristics of a Rough Surface, impinged by a Confined Turbulent Slot Air Jet, HEFAT-ATE International conference-July-2021-Accepted for publication.

International journal papers:

- 1) **Adimurthy. M** and Pavankumar M Sureban the Influence of Confinement on Local Heat Transfer Distribution Due to Impingement of Slot Air Jet on a Flat Surface. June 2015 | IJIRT | Volume 2 Issue 1 | ISSN: 2349-6002
- 2) **Adimurthy M**, Venkatesha, and Vadiraj V Katti Experimental study of fluid flow and heat transfer characteristics of rough surface, impinged by a confined laminar slot air jet, *International Journal of Engineering Research & Technology*, Vol.5 Issue 06, June-2016. e-ISSN: 2278-0181, DOI: <http://dx.doi.org/10.17577/IJERTV5IS060418>
- 3) **Adimurthy M & Vadiraj V. Katti**, Experimental Investigations on the Local Distribution of wall static pressure coefficient Due to an Impinging Slot Air Jet on a Confined Rough Surface, *International Journal of Engineering Technology, Management and Applied Sciences (IJETMAS)*, December 2016, Volume 4, Issue 12, ISSN 2349-4476

- 4) **Adimurthy M & Vadiraj V. Katti**, Local distribution of wall static pressure and heat transfer on a smooth flat plate impinged by a slot air jet, Heat Mass Transfer (2016), DOI 10.1007/s00231-016-1847-9
- 5) **Adimurthy M & Vadiraj V. Katti** Local distribution of wall static pressure and heat Transfer on a rough flat plate impinged by a slot air jet, Heat Mass Transfer (2017), DOI 10.1007/s00231-017-1999-2